Universitat Autònoma de Barcelona

Exploring the Flavour Anomalies in B decays: A path towards New Physics

Marcel Algueró Casas

Universitat Autònoma de Barcelona (UAB)

Doctoral Thesis

Exploring the Flavour Anomalies in B decays: A path towards New Physics

---

Author:
Marcel Algueró Casas

Supervisors:
Dr. Joaquim Matias Espona
Dr. Pere Masjuan Queralt

A thesis submitted in fulfillment of the requirements for the degree of Philosophae Doctor (PhD)

in the

Institut de Física d'Altes Energies (IFAE)
Departament de Física

May 27, 2022

UNIVERSITAT AUTÒNOMA DE BARCELONA (UAB)

Abstract

Facultat de Ciències
Departament de Física

Philosophae Doctor (PhD)

Exploring the Flavour Anomalies in B decays: A path towards New Physics

by Marcel Algueró Casas

The field of Flavour Physics has been actively challenging the Standard Model in recent years, in particular in transitions involving a b quark. These are the so-called B-anomalies, and discrepancies between experimental measurements and theoretical predictions have been found in different channels related to a B-meson decay: semileptonic currents, both charged and neutral, fully leptonic and also nonleptonic processes. Concerning the former, global analyses including all available experimental data on $b \to s\ell^+\ell^-$ observables reach global tensions of more than 7σ. In other channels, individual observables already show discrepancies at the level of $2-3\sigma$. While this alone could make a compelling case for the need of New Physics to explain the current experimental data, what is most remarkable is the fact that one can establish coherent patterns linking all these apparently independent deviations.

In this Thesis we present an introduction to the different theoretical elements needed to describe the aforementioned B-anomalies within the framework of an Effective Field Theory, as well as the state-of-the-art results of our Global Fit to $b \to s\ell^+\ell^-$ observables. We also discuss individual tensions in observables of the charged semileptonic current $B \to D^*\ell\nu$ and also the nonleptonic $B_{d,s} \to K^{*0}\bar{K}^{*0}$ transition. On top of that, we also propose possible New Physics models that could bridge the gap between these different kinds of processes.

Acknowledgements

First of all, I want to express my most sincere (and endless) gratitude to my supervisor, guide, mentor, boss and also colleague, Joaquim Matias. We are often told that it's difficult to realize how good times are when they are good, but I feel I've been lucky enough to actually be aware of what an amazing opportunity working with you has been. Wow, have I learned! This journey started not really four years ago but six, when I was only a project of a physicist (this I'm not sure has changed that much to be honest, but well, now I can pretend I'm a mature physicist thanks to that "Dr." in front of my name) and I wouldn't change a single thing. Well, maybe one thing, this nightmare of the pandemics that robbed us of many fun meetings at either office to discuss our projects. This I would definitely change. But in all seriousness, I've enjoyed every step of the way. You've cared for me and my career, providing opportunities for me to make myself known in the community, giving insight and advice by sharing your experience, and most importantly showing an absolute trust in me and the contributions I could possibly make. I've always felt listened to and respected, and for this I thank you.

Second, I want to also thank Pere Masjuan from the bottom of my heart. Even if your "official" title was supervisor, you've been much more than that. You are kinda like my academic cool uncle, bearing with me and my infinite questions and helping me out whenever I had some trouble understanding some of the physics we do, or offering a helping hand when I was doubting myself and everything. I mean, I learnt more physics from discussions with you than in some lectures I took (though here maybe it'd be more appropriate to say listening to you explaining something, more than discussions haha). Really, it has been fantastic working with you and learning from you and your enthusiasm for everything you do. I hope one day I'm able to explain anything I'm passionate about with the same passion as you do. Thanks a lot!

I would also like to mention Sébastien Descotes-Genon who, despite not being directly my supervisor, I somewhat feel like he was. It was truly a pleasure working with you and learning from you. I cherish the countless meetings on Skype, the discussions we had, the fact that you were always open to hearing opinions or suggestions from the younglings, and maybe specially that they never felt like work meetings. I mean, we've worked, and worked hard, but with a joke here and there it's always been fun having meetings. I remember how you spent like half an hour in Lyon when I did my first ever talk in a workshop, going together through my slides and helping me minimize my nerves a bit. The only regret I have is that I could never come stay in Paris for a while because of the damn pandemics. In any case, I'm very very grateful that we shared so many projects. Thank you very much, Sébastien.

Even if it may seem the researcher's life, and by extension, the life of a PhD student can be a lonely enterprise, I must admit fortunately it was not. I feel very lucky to have shared so many moments with all the beautiful PhDs that were at IFAE at the same time I was. Even before I officially started my PhD I was already included in PhD lunches at Lletres, and at Thesis' Defences and their aftermath (which is the coolest part, of course). For that, Quim, Leyre, Dani, Carles, Judit, Marco, Daniele, Giulia, Elia, Xabi, Chai: thank you, thank you, thank you. You made this so much fun. Menció a banda mereixen la Laura i el Jan, que tot i que evidentment formen part d'aquest grup de gent, com que som companys de promoció la nostra història ve des que vam començar la carrera. Quin camí, companys! El Jan, de fet, ja és Dr. Ollé, vull dir que diria moltes coses aquí però tampoc voldria arruinar carreres jeje.

Evidentment, a tu Bernat et dedico un paràgraf (i honestament t'hauria de dedicar un capítol sencer). Només vull fer un sol comentari sobre feina, però és que quin plaer haver pogut fer gairebé tots els projectes amb tu, perquè sense la teva ajuda el meu PhD hagués durat aproximadament 42 anys. Collons, nen, quina sort! De veritat que ni somiant, ni extremadament borratxo (com un periodista de l'As un dimarts qualsevol) hagués pogut aventurar un company com tu. Ni, sobretot, un amic com tu. I dic aventurar totalment expressament, perquè hem viscut unes

aventures de la hòstia. Crec que "Puerto Rico me lo regaló" podria resumir moltes coses, i ho aprofitaré perquè això segurament ho llegirà més gent jajaja Dit això, espero que algun dia puguis perdonar tots els meus outfits (i cabells) que sé que et regiraven (i et regiren) l'estómac, però recorda que si m'ho retreus, tinc fotos teves del després de la teva Tesi :) Gràcies per tot nen! Tinc moltes ganes de convidar-te a un Old Fashioned i brindar com dos Doctors.

A ti, Martín, también podría escribirte más de un párrafo. Qué suerte poder trabajar codo con codo contigo, nene! Aunque mucho mejor que trabajar, poder tomar cervezas en Lyon y en Trento (aunque pueda parecer todo lo contrario, me gusta mucho más tomar cerveza que trabajar). Como dije antes, fue una pena no poder ir a Paris un tiempo para trabajar juntos, pero estoy tranquilo porque sé que en algún momento iré a Bari o a Santiago (mejor) con cualquier excusa. Además, gracias a ti ahora no digo casi nunca "utilizar" o "qué palo" porque me gusta muchísimo más poder decir "ocupar" o "qué paja" jeje viva Chile! Por haber compartido todo ese camino a la vez, quiero darte las gracias.

Claudia, Marc, César, Sergi, no sé com es dóna les gràcies a algú tan important, però espero que ja sabreu, d'alguna manera o una altra, el que de veritat sento per vosaltres. Deu (10!!) anys fent-nos costat. Apunts, entregues, laboratoris, exàmens, braves a la Cívica, birres, Pots, Maxwells, sopars, dinars, Menorca, viatges, cançons, Dresden, Comunio, una boda i molt d'amor. Sobretot això últim, que és el més important. Si només us heu de creure una cosa de les que pugui haver dit mai, creieu-vos aquesta: sense vosaltres el meu camí en el món de la Física hagués estat molt més curt, i sens dubte la millor part d'acabar sent doctor és haver-ho fet al vostre costat. Us estimo molt (i estaria bé que ens féssim (més) vellets vivint a prop perquè el Carcassone-1300-extensions-alhora no es juga sol).

També vull donar les gràcies als meus amics de tota (i gairebé tota, encara que tinc la sort que és com si fos tota) la vida. Començaré per Sabadell. Oscar, Arnau, Arnau, Clara, Adri, Maria, Laura, Marc, Ricard, Laura i Marc: som el Sol, i vosaltres sou uns sols per escoltar les meves xapes físiques. Us estimo encara que haguem quedat un total de 0 vegades a Terrassa i 1 a Barcelona (es broma pero tampoco mucho), perquè també formeu part del meu viatge fins aquí. Gràcies de tot sol. I ara me'n vaig a Terrassa, i una mica a Barcelona. Sergi, Adri, Gerard, Arnau, Pau, Albert (se'm fa estrany escriure Albert i no Xiku, Xiku) i Marc: hòstia nens, com us necessito. Potser sovint no ho sembla, o sí, no ho sé, perquè jo sóc com sóc i duc moltes coses sota la pell, però us estimo amb la certesa del qui no s'equivoca, i amb la tranquil·litat de saber que gaudirem junts de totes les coses emocionants que ens esperen. Tan de bo creieu que de tant en tant us torno la meitat de les coses que feu per demostrar-me el que represento per vosaltres. Vull fer un petit apèndix per parlar dels dinars+Clash amb tu, Arnau. Ja sé que ho saps, però ho diré igualment així: aquest últim any t'he trobat molt a faltar. També, per motius evidents, vull fer una menció al Sergi, a l'Adri i al Pau. Ningú, però absolutament ningú, ha viscut mai compartint pis millor que jo.

Per últim, i més important, vull donar les gràcies a la meva família sencera: àvies, avis, tietes, tiets i cosines i cosins, sóc qui sóc gràcies a tots vosaltres. Especialment gràcies a tu, padrí, que des de petit has estat un referent i una mena de germà gran per a mi. Tinc molts records molt bonics de totes les coses que hem fet des que tinc records, i són dels que, quan fa fred, escalfen. Gràcies a tots per creure sempre que sóc millor del que sóc.

Però sobretot vull agrair als meus pares i a la meva germana que siguin els meus pares i la meva germana. Papa, Mama, Helena, ja sabeu que sovint em surt millor quan em llegiu que quan ens tenim al davant, però aquest cop també em costa fins i tot escriure tot el que em passa pel cap mentre escric. Sense vosaltres jo no seria. En general, no seria, no seria res. Totes les coses bones que pugui tenir són, en part o del tot, gràcies a vosaltres. Sou una xarxa i sou un caliu que últimament m'he anat adonant que són rars, que no es troben, i per sort vaig comprenent poc a poc la sort que tinc jo de tenir-vos a vosaltres. Gràcies per tenir cura de mi, de tantes i tantes maneres diferents que (i potser fer-se gran vol dir això) vaig aprenent a descobrir. Molts

cops m'emociono quan em ve al cap el contorn, gairebé de passada, de les vostres idees, del que representeu per a mi i de com us estimo. Us estimo molt més del que mai he sigut capaç d'expressar, però n'aprendré. Gràcies per ensenyar-me tantes coses, i per estimar-me com ho feu. Aquest doctorat és tant meu com vostre.

Contents

Acknowledgements v

Introduction 1

I Semileptonic B decays 5

1 Global analysis of semileptonic $b \to s\ell^+\ell^-$ Decays 7
1.1 Theoretical Framework . . . 7
1.1.1 The Weak Effective Hamiltonian . . . 7
1.1.2 $B \to K^*(K\pi)\ell^+\ell^-$ angular distribution . . . 10
1.1.3 Transversity amplitudes and $B \to K^*$ form factors . . . 12
1.2 Semileptonic, purely leptonic and radiative $b \to s$ observables . . . 16
1.2.1 $B \to K^*\ell^+\ell^-$ . . . 16
1.2.2 $B_s \to \phi\ell^+\ell^-$ . . . 18
1.2.3 $B \to K\ell^+\ell^-$ . . . 19
1.2.4 $B_s \to \mu^+\mu^-$ . . . 21
1.2.5 Lepton Flavour Universality Violating observables . . . 22
1.2.6 $B \to X_s\ell^+\ell^-$ . . . 22
1.2.7 Radiative modes . . . 23
1.3 Global Fits after R_{K_S} and $R_{K^{*+}}$ . . . 24
1.3.1 Observables . . . 26
1.3.2 Fit approach . . . 26
1.3.3 Fit Results . . . 28
1.3.4 Favoured scenarios and connection with other observables . . . 30
1.4 Summary and Conclusions . . . 32

2 P- and S-wave contributions to the $B^0 \to K^{*0}(\to K^+\pi^-)\ell^+\ell^-$ decay 35
2.1 Structure of the differential decay rate: P and S waves . . . 36
2.1.1 P-wave massive observables . . . 38
2.1.2 Definition of S-wave observables: massless and massive case . . . 40
2.2 Symmetries of the distribution . . . 43
2.2.1 Counting degrees of freedom: massive and massless cases . . . 44
2.2.2 P-wave and S-wave symmetry relations among observables . . . 46
2.3 Bounds on S-wave observables and $W_{1,2}$ observables . . . 48
2.4 Common zeroes of P- and S-wave observables . . . 52
2.4.1 A closer look at the observable X_2: from New Physics to hadronic contributions . . . 54
2.5 Experimental prospects and precision . . . 57
2.5.1 Experimental test of symmetry relations . . . 58
2.5.2 S wave in the global fits . . . 58
2.6 Summary and Conclusions . . . 60

3 Symmetries in $B \to D^* \ell \nu$ angular observables **61**
3.1 $\bar{B} \to D^* \ell \bar{\nu}$ angular distribution . . . 62
3.1.1 Effective Hamiltonian and angular observables . . . 62
3.1.2 Observables . . . 64
3.1.3 Global fits . . . 65
3.2 Relations among angular coefficients . . . 66
3.2.1 Symmetries and dependencies . . . 66
3.2.2 Massless case with no pseudoscalar operator and no tensor operators . . . 67
3.2.3 Massless case with pseudoscalar operator but no tensor operators . . . 68
3.2.4 Massive case with pseudoscalar operator but no tensor operators . . . 68
3.2.5 Cases with tensor operators . . . 69
3.3 Expressions of the D^* polarisation . . . 69
3.3.1 Massless case without pseudoscalar operator . . . 69
3.3.2 Massless case without imaginary contributions . . . 70
3.3.3 Massive case with pseudoscalar operator but without imaginary contributions 70
3.3.4 Cases with pseudoscalar operator and imaginary contributions . . . 71
3.3.5 Binning . . . 71
3.3.6 Decision Tree . . . 74
3.4 Impact of the presence of light right-handed neutrinos . . . 77
3.5 Experimental sensitivity . . . 79
3.6 Summary and Conclusions . . . 79

II Nonleptonic B decays **81**

4 A new B-flavour anomaly in $B_{d,s} \to K^{*0} \bar{K}^{*0}$: anatomy and interpretation **83**
4.1 Theoretical framework . . . 84
4.1.1 Helicity amplitudes . . . 84
4.1.2 Hadronic matrix elements . . . 84
4.2 The L-observable for $B_Q \to K^{*0} \bar{K}^{*0}$ . . . 85
4.2.1 Definition and experimental determination . . . 85
4.2.2 Theoretical prediction in the SM and comparison with data . . . 86
4.3 Model-independent NP analysis . . . 89
4.4 Simplified NP models . . . 90
4.5 Summary and Conclusions . . . 93

III Connecting Different Sectors of Flavour Physics **95**

5 Importance of $Z - Z'$ Mixing in $b \to s \ell^+ \ell^-$ and the W mass **97**
5.1 Setup . . . 98
5.2 Observables . . . 99
5.2.1 $b \to s \ell^+ \ell^-$ . . . 99
5.2.2 $B_s - \bar{B}_s$ Mixing . . . 100
5.2.3 LFUV in tau decays . . . 100
5.2.4 Electroweak fit . . . 100
5.2.5 Neutrino Trident Production . . . 101
5.2.6 Direct searches . . . 101
5.3 Phenomenology . . . 101
5.4 Implications of the new measurement of m_W . . . 103
5.5 Summary and Conclusions . . . 104

Conclusions and Outlook **105**

A Angular conventions **107**

B Predictions for the observables in the Standard Model **109**

C The 7th massive relation **117**

D A hitchhiker's guide to the symmetry relations in $B \to D^* \ell \nu$ **121**
D.1 Massive relations among angular coefficients of $B \to D^* \ell \nu$ 121
D.2 Comparison of binned expressions for $\tilde{F}_T^{D^*}$ in benchmark NP scenarios 122

E Theoretical framework for $B_{d,s} \to K^{*0} \bar{K}^{*0}$ decays **131**
E.1 Weak effective theory and QCD factorization framework 131
E.2 Semi-analytical expressions 133
E.3 Sensitivity to New Physics 134

F Electroweak observables and interaction Lagrangian **137**

Bibliography **139**

Aquesta va per tu, P

Introduction

The Standard Model of particle physics (SM) is considered the most complete theory of particle physics to the present day. It successfully unifies three of the four fundamental interactions in nature, namely the Electromagnetic, the Weak and the Strong interactions, within a rather simple framework. All elemental constituents of matter and their interactions are described in terms of a Quantum Field Theory and the symmetries derived from that. However, despite the enormous success that the SM represents, there exist several reasons to be certain that it cannot be the final answer. For once, and maybe this could be considered the main problematic issue, it is unable to reconcile the fourth fundamental force, i.e. Gravity, with a Quantum Field Theory. More examples of phenomena that cannot be explained within the framework of the SM are the existence of neutrino masses, the origin of the matter-antimatter asymmetry, or the mass hierarchy among the quark and the lepton families, among others.

For that reason, for many years the physics community expected to keep unfolding continually new particles and interactions embedded in the SM, with the use of the plethora of accelerators and colliders built along the second half of the 20th century and until the present day. However, since the discovery of the Higgs boson in 2012 at the Large Hadron Collider (LHC), no new particles have been found by direct searches, leading us to declare the SM "complete". This indicates that the masses/energy of the possible new particles that could be behind the phenomena that the SM cannot account for are too large to be observed at present-day colliders. Alternatively, it can also imply that the interactions between these undiscovered particles and SM constituents are too weak to be detected by current experiments. Fortunately, this technological impediment is not the end of the road. We know that these heavy new particles might generate indirect effects through higher order quantum corrections to several processes that can be effectively described within the SM. Therefore, it is worth exploring decays and transitions that currently show tensions with respect to the SM predictions.

In recent years, the paradigm of such promising processes are the so-called flavour anomalies, or b-anomalies, since several deviations from the SM have been consistently popping up in both the Flavour Charged Current (FCC) transitions $b \to c\ell\bar{\nu}$ and the Flavour Changing Neutral Current (FCNC) modes $b \to s\ell^+\ell^-$. Since the former involve a quark flavour change through a charged interaction, they are thus processes that take place at tree-level. Instead, the latter consist of a quark flavour change via a neutral current, hence they are CKM-suppressed transitions and therefore occur at loop-level in the SM. This allows possible new particles to generate contributions through quantum corrections that are on the same footing as the SM corrections, making these $b \to s\ell^+\ell^-$ transitions highly sensitive to potential NP effects.

Nowadays, a good deal of observables related to this type of transitions have been measured by different experiments and collaborations such as the LHCb, Belle, ATLAS or CMS. Remarkably, deviations with respect to what the SM predicts have been found in independent analyses from different experiments. Even more outstanding is the fact that all these phenomenological global analyses find coherent patterns behind the observed anomalies. Here a pattern of NP refers to a rather simple explanation that reduces the tensions between theory and experiment in many different observables at the same time. In principle, there is no apparently evident reason for this to happen, as observables measuring different properties of a $b \to s$ transition could need different kinds and structures of NP contributions to alleviate their tension. However, it turns

out that once the SM is treated as an Effective Field Theory (EFT) of a more general framework, which allows us to include possible NP contributions in a very surgical way, only a handful of extra degrees of freedom are needed to drastically reduce the tensions across the many different observables studied.

Thereby, assessing the type and nature of the NP contributions that successfully adjust the theoretical predictions to match the experimental results in the B-meson sector of Flavour Physics is of paramount importance in order to set the next steps in our ultimate goal of building a Beyond the Standard Model (BSM) theory.

In this Thesis we will discuss and detail the methodology followed in the Global Analyses of the B-anomalies. We aim at providing a general framework with the tools needed to understand how these global analyses are performed and how they should be interpreted, as well as the implications that their results may have in terms of building models of NP with particles and interactions currently not present in the SM. To this end, it is structured in three parts.

First, in Part I, we focus on the semileptonic B transitions. In Chapter 1 we review the tools and elements required to perform a Global analysis of the different anomalies measured concerning the $b \to s\ell^+\ell^-$ transition. Starting from the EFT that allows us to treat these processes as local interactions, we introduce the key ingredients to understand the theoretical computation of the observables included in the so-called Global Fits, following a top-bottom approach. We then define the whole set of quantities and give their expressions in terms of NP contributions. Later on we present one of the most important outcomes of the present Thesis: the state-of-the-art of our Global Analyses, including the most updated results and a discussion of the implications for preferred scenarios of New Physics. We also establish a model-independent connection between the neutral anomalies and the ones seen in the charged $b \to c\ell\nu$ transition.

Chapter 2 is devoted to the study of the impact of including higher partial waves in the $B \to K^{*0}(\to K^+\pi^-)\ell^+\ell^-$ decay, in particular the S-wave pollution from the $B \to K_0^*$ system. From the symmetries of the angular distribution we find relations between the angular coefficients of the decay, which in turn give us access to new observables that were not considered until now. We also place bounds on these new observables, which can be used as crosschecks for the experimental analyses. On top of that, we define two new quantities that allow us to extract information on the S-wave contribution to the decay without having to rely on poorly known S-wave form factors.

We conclude the first part of this Thesis in Chapter 3, dedicated to the analysis of the charged current $b \to c\ell\nu$ process. There we schematically provide the theoretical framework needed. Following an analogous methodology to the one in Chapter 2, we make use of the symmetries of the decay distribution of these processes to establish the exact number of independent degrees of freedom of the distribution and subsequently define an alternative way of measuring the longitudinal polarisation $F_L^{D^*}$, which shows an interesting tension with respect to the SM prediction. Consequently, this alternative strategy could potentially confirm or dismiss the deviation measured in the polarization observable.

Next, in Part II we shift our attention to a different kind of B decays with no leptons in the final state. Chapter 4 serves as a study of the $B_{d,s} \to \bar{K}^{*0}K^{*0}$ transition, which has not undergone as much scrutiny as the partner semileptonic decays. Nonetheless, these decays exhibit a striking tension with respect to the SM in one particular observable. Moreover, following the coherent pattern behind the many different $b \to s$ anomalies, we tried also to establish a parallelism between the semileptonic and nonleptonic anomalies and explored the possibility of a link among them.

Finally, Part III consists in a study of possible connections between different sectors of Flavour Physics through simple models of NP. In particular, in Chapter 5 we discuss the implications of the existence of an additional vector gauge boson Z' for the $b \to s\ell^+\ell^-$ anomalies and the shift

that would induce on the mass of the SM W boson. This turns out to be particularly relevant after the recent analysis of the mass of the W boson by the CDF collaboration.

Part I

Semileptonic B decays

Chapter 1

Global analysis of semileptonic $b \to s\ell^+\ell^-$ Decays

In recent years, indirect searches at the LHC and at B-factories have led to a large set of deviations with respect to the SM (or anomalies) in both $b \to c\ell\bar{\nu}$ and in $b \to s\ell^+\ell^-$ decays [1–3]. We can classify the latter (which we focus on in this chapter) in two sets: $b \to s\mu^+\mu^-$ anomalies related to observables testing only muonic transitions, which we call Lepton Flavour Dependent (LFD), and Lepton-Flavour Universality Violating (LFUV) anomalies that correspond to deviations in observables comparing muonic and electronic transitions.

This chapter is organized in three main sections. In Section 1.1, we will discuss the basic features of the theoretical framework needed to study the flavour anomalies in the neutral B sector. We will detail in Section 1.2 the different observables and quantities included in the analyses. Finally, we will review in Section 1.3 the most up to date results of the global fits to $b \to s\ell^+\ell^-$ data presented in [4].

1.1 Theoretical Framework

1.1.1 The Weak Effective Hamiltonian

The $b \to s\ell^+\ell^-$ processes can be described in the context of an Effective Field Theory approach, namely the Weak Effective Hamiltonian (WEH) [5–7], by virtue of the existing scale hierarchy for weak decays of B mesons, $\Lambda_{\rm QCD} \ll m_Q \ll M_W$. In this effective framework, the heavy degrees of freedom (the top quark, the W and Z bosons, the Higgs boson and any potential heavy new particles) have been integrated out in short-distance Wilson coefficients $\mathcal{C}_i$, leaving only a set of local effective operators $\mathcal{O}_i$ describing the physics at long distances[1]:

$$\mathcal{H}_{\rm eff} = -\frac{4G_F}{\sqrt{2}} \sum_i \mathcal{C}_i(\mu)\mathcal{O}_i \tag{1.1}$$

Here μ is a renormalization scale to run down the Wilson coefficients from the heavy scale (typically the Electroweak scale, M_W) where they are matched to the computation from the whole theory, to the low scale μ, which is generally chosen to be of the order of the b quark mass, $\mu = \mu_b = m_b$. More specifically, the structure of the WEH for a $b \to s$ transition is:

$$\mathcal{H}_{\rm eff} = -\frac{4G_F}{\sqrt{2}} \left(\lambda_t^{(s)} \mathcal{H}_{\rm eff}^{(t)} + \lambda_u^{(s)} \mathcal{H}_{\rm eff}^{(u)} \right) + h.c. \tag{1.2}$$

[1] Formally, the Weak Effective Hamiltonian has the structure of an Operator Product Expansion (OPE), encoding the perturbatively calculable elements inside the Wilson coefficients $\mathcal{C}_i(\mu)$ and all the non-perturbative pieces are written in terms of the matrix elements of the effective operators $\mathcal{O}_i$.

where $\lambda_q^{(s)} \equiv V_{qb}V_{qs}^*$ are combinations of CKM parameters. One would also expect a contribution proportional to $\lambda_c^{(s)}$, but assuming that the CKM matrix remains unitary even in presence of NP, one can always reexpress this contribution by absorbing it inside the other two. The two structures $\mathcal{H}_{\rm eff}^{(u)}$ and $\mathcal{H}_{\rm eff}^{(t)}$ read [8–10]

$$\begin{aligned}\mathcal{H}_{\rm eff}^{(t)} = \mathcal{C}_1(\mu)\mathcal{O}_1^c + \mathcal{C}_2(\mu)\mathcal{O}_2^c + \sum_{i=3}^{6}\mathcal{C}_i(\mu)\mathcal{O}_i + \sum_{i=7}^{10}\Big(\mathcal{C}_i(\mu)\mathcal{O}_i + \mathcal{C}_{i'}(\mu)\mathcal{O}_{i'}\Big) \\ + \sum_{i=S,PS}\Big(\mathcal{C}_i(\mu)\mathcal{O}_i + \mathcal{C}_{i'}(\mu)\mathcal{O}_{i'}\Big) + \sum_{i=T,PT}\mathcal{C}_i(\mu)\mathcal{O}_i,\end{aligned} \tag{1.3}$$

$$\mathcal{H}_{\rm eff}^{(u)} = \mathcal{C}_1(\mu)(\mathcal{O}_1^c - \mathcal{O}_1^u) + \mathcal{C}_2(\mu)(\mathcal{O}_2^c - \mathcal{O}_2^u). \tag{1.4}$$

Notice that even if $\lambda_u^{(s)}$ is doubly Cabibbo-suppressed relative to $\lambda_t^{(s)}$, we will keep the contributions from $\mathcal{H}_{\rm eff}^{(u)}$ as they are an important source of weak phases in the SM and are included in our analysis.

In the SM, the Hamiltonian in Eq. (1.2) contains 10 main operators with specific chiralities due to the $V-A$ structure of the weak interactions. This basis of operators constitutes an irreducible set of all dimension-six operators with the quantum numbers associated to a $b \to s\ell^+\ell^-$ transition that fulfill Lorentz invariance and respect the gauge symmetries of the SM:

$$\begin{aligned}
\mathcal{O}_1^u &= (\bar{s}\gamma_\mu T^a P_L u)\,(\bar{u}\gamma^\mu T^a P_L b) & \mathcal{O}_5 &= (\bar{s}\gamma_\mu\gamma_\nu\gamma_\rho P_L b)\sum_q (\bar{q}\gamma^\mu\gamma^\nu\gamma^\rho q)\\
\mathcal{O}_2^u &= (\bar{s}\gamma_\mu P_L u)\,(\bar{u}\gamma^\mu P_L b) & \mathcal{O}_6 &= (\bar{s}\gamma_\mu\gamma_\nu\gamma_\rho T^a P_L b)\sum_q (\bar{q}\gamma^\mu\gamma^\nu\gamma^\rho T^a q)\\
\mathcal{O}_1^c &= (\bar{s}\gamma_\mu T^a P_L c)\,(\bar{c}\gamma^\mu T^a P_L b) & \mathcal{O}_7 &= \frac{e}{16\pi^2} m_b(\bar{s}\sigma_{\mu\nu}P_R b)F^{\mu\nu}\\
\mathcal{O}_2^c &= (\bar{s}\gamma_\mu P_L c)\,(\bar{c}\gamma^\mu P_L b) & \mathcal{O}_8 &= \frac{g_s}{16\pi^2} m_b(\bar{s}\,T^a\sigma_{\mu\nu}P_R b)G^{a\mu\nu}\\
\mathcal{O}_3 &= (\bar{s}\gamma_\mu P_L b)\sum_q (\bar{q}\gamma^\mu q) & \mathcal{O}_9 &= \frac{e^2}{16\pi^2}(\bar{s}\gamma_\mu P_L b)(\bar{\ell}\gamma^\mu \ell)\\
\mathcal{O}_4 &= (\bar{s}\gamma_\mu T^a P_L b)\sum_q (\bar{q}\gamma^\mu T^a q) & \mathcal{O}_{10} &= \frac{e^2}{16\pi^2}(\bar{s}\gamma_\mu P_L b)(\bar{\ell}\gamma^\mu\gamma_5 \ell)
\end{aligned} \tag{1.5}$$

where $P_{L,R} = \frac{1}{2}(1\mp\gamma_5)$ are the chirality projection operators (γ_5 is taken as fully anticommuting), $F^{\mu\nu}$ is the electromagnetic-field strength tensor, $G^{a\mu\nu}$ is the gluon-field strength tensor (with the color index a, omitted in the rest of operators) and $\sigma^{\mu\nu} = \frac{i}{2}[\gamma_\mu, \gamma_\nu]$.

In presence of NP, additional operators may become important, either with opposite chirality (the so-called chirally-flipped operators or Right-Handed Currents):

$$\mathcal{O}_{7'} = \frac{e}{16\pi^2} m_b (\bar{s}\sigma_{\mu\nu} P_L b) F^{\mu\nu} \qquad \mathcal{O}_{8'} = \frac{g_s}{16\pi^2} m_b (\bar{s} T^a \sigma^{\mu\nu} P_L b) G^a_{\mu\nu}$$

$$\mathcal{O}_{9'} = \frac{e^2}{16\pi^2} (\bar{s}\gamma_\mu P_R b)(\bar{\ell}\gamma^\mu \ell) \qquad \mathcal{O}_{10'} = \frac{e^2}{16\pi^2} (\bar{s}\gamma_\mu P_R b)(\bar{\ell}\gamma^\mu \gamma_5 \ell) \tag{1.6}$$

or with different structures, such as the Scalar, Pseudoscalar or Tensor operators:

$$\mathcal{O}_S = \frac{e^2}{16\pi^2} m_b (\bar{s} P_R b)(\bar{\ell}\ell) \qquad \mathcal{O}_{S'} = \frac{e^2}{16\pi^2} m_b (\bar{s} P_L b)(\bar{\ell}\ell)$$

$$\mathcal{O}_{PS} = \frac{e^2}{16\pi^2} m_b (\bar{s} P_R b)(\bar{\ell}\gamma_5 \ell) \qquad \mathcal{O}_{PS'} = \frac{e^2}{16\pi^2} m_b (\bar{s} P_L b)(\bar{\ell}\gamma_5 \ell)$$

$$\mathcal{O}_T = \frac{e}{16\pi^2} (\bar{s}\sigma_{\mu\nu} b)(\bar{\ell}\sigma^{\mu\nu} \ell) \qquad \mathcal{O}_{PT} = \frac{e^2}{16\pi^2} \epsilon^{\mu\nu\rho\sigma} (\bar{s}\sigma_{\mu\nu} b)(\bar{\ell}\sigma_{\rho\sigma} \ell) \tag{1.7}$$

From the expressions above, it follows that the observables for exclusive decays can be written in terms of helicity amplitudes given as Wilson coefficients multiplying hadronic matrix elements [9, 11, 12]:

$$\mathcal{A}(M_1 \to M_2) = \langle M_2 | \mathcal{H}_{\text{eff}} | M_1 \rangle = \frac{G_F}{\sqrt{2}} \sum_i \mathcal{C}_i(\mu) \langle M_2 | \mathcal{O}_i | M_1 \rangle(\mu) \equiv \frac{G_F}{\sqrt{2}} \sum_i \mathcal{C}_i(\mu) \langle \mathcal{O}_i(\mu) \rangle \tag{1.8}$$

Notice that since the square of the amplitude of a physical process is an observable quantity, it has to be independent of the renormalization scale, thus the matrix elements of the operators have a dependence on the scale μ such that it cancels with the scale dependence of the Wilson coefficients.

The relevant operators for the processes considered here, that is $b \to s\ell^+\ell^-$, are the operators $\mathcal{O}_{7^{(\prime)},9^{(\prime)}\ell,10^{(\prime)}\ell}$ and their associated Wilson coefficients $\mathcal{C}_{7^{(\prime)}}, \mathcal{C}_{9^{(\prime)}\ell}, \mathcal{C}_{10^{(\prime)}\ell}$ where $\ell = e$ or μ. $\mathcal{C}_{7^{(\prime)}}$ describe the interaction strength of bottom (b) and strange (s) quarks with the photon while $\mathcal{C}_{9\ell,10\ell}$ and $\mathcal{C}_{9'\ell,10'\ell}$ encode the interaction strength of b and s quarks with charged leptons.

$\mathcal{C}_{9\ell,10\ell}$ and $\mathcal{C}_{9'\ell,10'\ell}$[2] are equal for muons and electrons in the SM but NP can add different contributions to muon operators compared to the electron ones. For $\mathcal{C}_7$ and $\mathcal{C}_{9\ell,10\ell}$ we split SM and NP contributions like

$$\mathcal{C}_{i\ell} = \mathcal{C}^{\text{SM}}_{i\ell} + \mathcal{C}^{\text{NP}}_{i\ell} \tag{1.9}$$

One can use the fact that m_b is significantly larger than the typical QCD scale ($\Lambda_{\text{QCD}} \sim 0.2\,\text{GeV}$) in order to isolate, in Eq. (1.8), perturbatively computable contributions to the hadronic matrix elements (using effective approaches like QCD factorization [13]). These perturbative contributions of hadronic origin can be lumped together with the purely short-distance contribution into effective Wilson coefficients (that will multiply non-perturbative hadronic form factors) with the following structure in the case of $B \to K^{(*)}\ell^+\ell^-$ [14]:

$$\mathcal{C}_{9\ell}(q^2) = \mathcal{C}^{\text{SM}}_{9\,\text{pert}}(q^2) + \mathcal{C}^{c\bar{c}}_9(q^2) + \mathcal{C}^{\text{NP}}_{9\ell} \tag{1.10}$$

[2] The Wilson coefficients of the chirally-flipped operators are zero in the SM, apart from $\mathcal{C}_{7'}$ which features a small SM contribution of $O(m_s/m_b)$, $\mathcal{C}_{7'} = \frac{m_s}{m_b}\mathcal{C}_7 + \mathcal{C}^{\text{NP}}_{7'}$.

where $\ell = e, \mu$. Concerning the different elements in $\mathcal{C}_{9\ell}(q^2)$, we have $\mathcal{C}_{9\,\text{pert}}^{\text{SM}} = \mathcal{C}_9^{\text{SM}} + Y(q^2)$, where the function $Y(q^2)$ stems from one-loop matrix elements of four-quark operators $\mathcal{O}_{1-6}$, corresponding to the $c\bar{c}$ continuum. It can be evaluated within perturbation theory at LO, and corrections at $O(\alpha_s)$ to $\mathcal{C}_{9\ell}$ to this function are known [14–16]. In addition to this continuum, there is a long-distance contribution, which corresponds in particular to charmonium resonances $\mathcal{C}_9^{c\bar{c}}$ and depends on the external hadron state. Moreover, this long-distance contribution is both q^2- and helicity-dependent. Several approaches are available to estimate this contribution [17–19], all with similar outcomes [20, 21]. We follow here [20, 22], using the light-cone sum rule computation with one soft-gluon exchange [23] to get an order of magnitude estimate of this contribution, without making any assumption about its sign and thus allowing for constructive or destructive interference with the other contributions to $\mathcal{C}_{9\mu}$, as we will show below.

Including electromagnetic corrections introduces mixing among the operators in Eq. (1.5) that share the same quantum numbers. Therefore, since the Wilson coefficients $\mathcal{C}_7$ and $\mathcal{C}_8$ always appear in matrix elements in certain combinations, it is useful to define the following effective coefficients [24]:

$$\mathcal{C}_7^{\text{eff}} \equiv \mathcal{C}_7 - \frac{1}{3}\mathcal{C}_3 - \frac{4}{9}\mathcal{C}_4 - \frac{20}{3}\mathcal{C}_5 - \frac{80}{9}\mathcal{C}_6 \tag{1.11}$$

$$\mathcal{C}_8^{\text{eff}} \equiv \mathcal{C}_8 - \frac{1}{6}\mathcal{C}_4 + 20\mathcal{C}_5 - \frac{10}{3}\mathcal{C}_6 \tag{1.12}$$

The next-to-next-to-leading logarithmic order value of the Wilson coefficients in the SM at the scale $\mu_b = 4.8\,\text{GeV}$ [25] can be found in Table 1.1.

$\mathcal{C}_1(\mu_b)$	$\mathcal{C}_2(\mu_b)$	$\mathcal{C}_3(\mu_b)$	$\mathcal{C}_4(\mu_b)$	$\mathcal{C}_5(\mu_b)$	$\mathcal{C}_6(\mu_b)$	$\mathcal{C}_7^{\text{eff}}(\mu_b)$	$\mathcal{C}_8^{\text{eff}}(\mu_b)$	$\mathcal{C}_9(\mu_b)$	$\mathcal{C}_{10}(\mu_b)$
-0.2632	1.0111	-0.0055	-0.0806	0.0004	0.0009	-0.2923	-0.1663	4.0749	-4.3085

Table 1.1: NNLO Wilson coefficients in the SM and at the scale $\mu_b = 4.8\,\text{GeV}$ [25].

1.1.2 $B \to K^*(K\pi)\ell^+\ell^-$ angular distribution

The full angular distribution of the $B \to K^*(K\pi)\ell^+\ell^-$ decay is obtained by squaring the matrix element of the Hamiltonian in Eq. (1.2):

$$\begin{aligned}
\mathcal{M} = \frac{G_F\alpha}{\sqrt{2}\pi}\lambda_t^{(s)}\Bigg\{ & \Bigg[\langle K\pi|\bar{s}\gamma^\mu(\mathcal{C}_9^{\text{eff}}P_L + \mathcal{C}_{9'}^{\text{eff}}P_R)b|\bar{B}\rangle \\
& - \frac{2m_b}{q^2}\langle K\pi|\bar{s}i\,\sigma^{\mu\nu}q_\nu\left[\left(\mathcal{C}_7^{\text{eff}} + \frac{m_s}{m_b}\mathcal{C}_{7'}^{\text{eff}}\right)P_R + \left(\frac{m_s}{m_b}\mathcal{C}_7^{\text{eff}} + \mathcal{C}_{7'}^{\text{eff}}\right)P_L\right]b|\bar{B}\rangle\Bigg]\langle\ell^+\ell^-|\bar{\ell}\gamma_\mu\ell|0\rangle \\
& + \langle K\pi|\bar{s}\gamma^\mu(\mathcal{C}_{10}P_L + \mathcal{C}_{10'}P_R)b|\bar{B}\rangle\langle\ell^+\ell^-|\bar{\ell}\gamma_\mu\gamma_5\ell|0\rangle \\
& + \langle K\pi|\bar{s}\left(\mathcal{C}_S P_R + \mathcal{C}_{S'}P_L\right)b|\bar{B}\rangle\langle\ell^+\ell^-|\bar{\ell}\ell|0\rangle \\
& + \langle K\pi|\bar{s}\left(\mathcal{C}_{PS}P_R + \mathcal{C}_{PS'}P_L\right)b|\bar{B}\rangle\langle\ell^+\ell^-|\bar{\ell}\gamma_5\ell|0\rangle + \mathcal{C}_T\langle K\pi|\bar{s}\sigma_{\mu\nu}b|\bar{B}\rangle\langle\ell^+\ell^-|\bar{\ell}\sigma^{\mu\nu}\ell|0\rangle \\
& + i\mathcal{C}_{PT}\epsilon^{\mu\nu\rho\sigma}\langle K\pi|\bar{s}\sigma_{\mu\nu}b|\bar{B}\rangle\langle\ell^+\ell^-|\bar{\ell}\sigma_{\rho\sigma}\ell|0\rangle\Bigg\} + \mathcal{M}_u
\end{aligned} \tag{1.13}$$

where $\mathcal{M}_u$ corresponds to the analogous contributions from $\mathcal{H}_{\text{eff}}^{(u)}$. Notice that the matrix elements above are expressed in terms of a $B \to K\pi$ transition. However, by virtue of the narrow width

approximation assuming the K^* to be produced resonantly, one can rewrite them in terms of the $B \to V$ form factors that we will show below[3].

After summing over spins of the final states and making use of some kinematical identities, one arrives at the following expression in terms of only four independent kinematical variables that suffice to describe all the quantities in the decay, namely the dilepton invariant mass q^2 and the three angles θ_{K^*}, θ_ℓ and ϕ (see Appendix A for our angle definitions [12], which differs from the usual LHCb convention [26, 27]):

$$\frac{d^4\Gamma}{dq^2 d\cos\theta_\ell d\cos\theta_{K^*} d\phi} = \frac{9}{32\pi} J(q^2, \theta_\ell, \theta_{K^*}, \phi) \tag{1.14}$$

where the function $J(q^2, \theta_\ell, \theta_{K^*}, \phi)$ can be factorized in such a way that the q^2 dependence is encoded inside the angular coefficients J_i:

$$\begin{aligned} J(q^2, \theta_\ell, \theta_{K^*}, \phi) = {} & J_{1s} \sin^2\theta_{K^*} + J_{1c} \cos^2\theta_{K^*} + (J_{2s} \sin^2\theta_{K^*} + J_{2c} \cos^2\theta_{K^*}) \cos 2\theta_\ell \\ & + J_3 \sin^2\theta_{K^*} \sin^2\theta_\ell \cos 2\phi + J_4 \sin 2\theta_{K^*} \sin 2\theta_\ell \cos\phi \\ & + J_5 \sin 2\theta_{K^*} \sin\theta_\ell \cos\phi \\ & + (J_{6s} \sin^2\theta_{K^*} + J_{6c} \cos^2\theta_{K^*}) \cos\theta_\ell + J_7 \sin 2\theta_{K^*} \sin\theta_\ell \sin\phi \\ & + J_8 \sin 2\theta_{K^*} \sin 2\theta_\ell \sin\phi + J_9 \sin^2\theta_{K^*} \sin^2\theta_\ell \sin 2\phi \end{aligned} \tag{1.15}$$

For the CP-conjugated mode one obtains a similar expression, but with the following replacements due to the angle convention:

$$J_{1s,1c,2s,2c,3,4,7} \to \bar{J}_{1s,1c,2s,2c,3,4,7}\,, \quad J_{5,6s,6c,8,9} \to -\bar{J}_{5,6s,6c,8,9} \tag{1.16}$$

where the $\bar{J}_i$ equal J_i but with all weak phases conjugated.

The angular coefficients $J_i(q^2)$ are in turn expressed in terms of eight transversity amplitudes by contracting the matrix element associated to the amplitude of the process with the different possible polarizations of the K^* and the vector boson mediating the transition. If one neglects (pseudo)tensor contributions, the angular coefficients have the following expressions [11, 28]:

$$J_{1s} = \frac{(2+\beta_\ell^2)}{4}\Big[|A_\perp^L|^2 + |A_\parallel^L|^2 + (L \to R)\Big] + \frac{4m_\ell^2}{q^2}\mathrm{Re}\Big(A_\perp^L A_\perp^{R*} + A_\parallel^L A_\parallel^{R*}\Big) \tag{1.17}$$

$$J_{1c} = |A_0^L|^2 + |A_0^R|^2 + \frac{4m_\ell^2}{q^2}\Big[|A_t|^2 + 2\mathrm{Re}(A_0^L A_0^{R*})\Big] + \beta_\ell^2 |A_S|^2 \tag{1.18}$$

$$J_{2s} = \frac{\beta_\ell^2}{4}\Big[|A_\perp^L|^2 + |A_\parallel^L|^2 + (L \to R)\Big] \qquad J_{2c} = -\beta_\ell^2\Big[|A_0^L|^2 + |A_0^R|^2\Big] \tag{1.19}$$

[3] Later on, in Chapter 2, we will review in more detail the implications of considering the full amplitude of the $K\pi$ system and the contributions of higher partial waves to the total decay rate of the $B^0 \to K^{*0}(K^+\pi^-)\ell^+\ell^-$ transition.

$$J_3 = \frac{\beta_\ell^2}{2}\Big[|A_\perp^L|^2 - |A_\parallel^L|^2 + |A_\perp^R|^2 - |A_\parallel^R|^2\Big] \qquad J_4 = \frac{1}{\sqrt{2}}\beta_\ell^2\Big[\mathrm{Re}(A_0^L A_\parallel^{L*} + A_0^R A_\parallel^{R*})\Big] \tag{1.20}$$

$$J_5 = \sqrt{2}\beta_\ell\Big[\mathrm{Re}(A_0^L A_\perp^{L*} - A_0^R A_\perp^{R*}) - \frac{m_\ell}{\sqrt{q^2}}\mathrm{Re}(A_\parallel^L A_S^* + A_\parallel^{R*} A_S)\Big] \tag{1.21}$$

$$J_{6s} = 2\beta_\ell\Big[\mathrm{Re}(A_\parallel^L A_\perp^{L*} - A_\parallel^R A_\perp^{R*})\Big] \qquad J_{6c} = 4\beta_\ell\frac{m_\ell}{\sqrt{q^2}}\mathrm{Re}(A_0^L A_S^* + A_\parallel^{R*}) \tag{1.22}$$

$$J_7 = \sqrt{2}\beta_\ell\Big[\mathrm{Im}(A_0^L A_\parallel^{L*} - A_0^R A_\parallel^{R*}) + \frac{m_\ell}{\sqrt{q^2}}\mathrm{Im}(A_\perp^L A_S^* - A_\perp^{R*} A_S)\Big] \tag{1.23}$$

$$J_8 = \frac{\beta_\ell^2}{\sqrt{2}}\Big[\mathrm{Im}(A_0^L A_\perp^{L*} + A_0^R A_\perp^{R*})\Big] \qquad J_9 = \beta_\ell^2\Big[\mathrm{Im}(A_\parallel^{L*} A_\perp^L + A_\parallel^{R*} A_\perp^R)\Big] \tag{1.24}$$

with

$$\beta_\ell = \sqrt{1 - 4\frac{m_\ell^2}{q^2}} \tag{1.25}$$

The amplitudes $A_0^{L,R}$ ($A_{\perp,\parallel}^{L,R}$) account for a longitudinal (transverse) polarization of the K^* meson, with L, R referring to the chirality of the leptonic current, and A_t is obtained by contracting the hadronic tensor associated to the matrix element of the decay with a K^* longitudinal polarization in the K^* rest frame and the extra timelike polarization (the gauge boson being virtual) of the gauge boson in its own rest frame. Since A_t can only couple to an axial-vector current [9], there is no separate left/right-handed part. Pseudoscalar contributions can always be absorbed into A_t for the same reason, while if scalar operators are included, an additional scalar amplitude A_S is required.

1.1.3 Transversity amplitudes and $B \to K^*$ form factors

The transversity amplitudes $A_{0,\perp,\parallel}^{L,R}, A_t, A_S$ in Eqs. (1.17)-(1.24) contain both factorizable and non-factorizable corrections of order $O(\alpha_s)$ and $O(\Lambda_{\mathrm{QCD}}/m_b)$, which can be computed within the framework of QCD factorization (QCDf) [13]:

$$\begin{aligned} A_\perp^{L,R} = N\sqrt{2}\lambda^{1/2}\Bigg\{ & \frac{2m_b}{q^2}\Big[\big(\mathcal{C}_7^{\mathrm{eff}} + \mathcal{C}_{7'}\big)\,T_1(q^2) + \big(1 + r_1(q^2)\big)\mathcal{T}_\perp(q^2)\Big] \\ & + \Big[(\mathcal{C}_9 + \mathcal{C}_{9'}) \mp (\mathcal{C}_{10} + \mathcal{C}_{10'}) + \big(1 + r_1(q^2)\big)Y_t(q^2) + \frac{\lambda_u}{\lambda_t}Y_u(q^2) + c_\perp^{\mathrm{long}}(q^2)s_\perp\Big]\frac{V(q^2)}{m_B + m_{K^*}}\Bigg\} \end{aligned} \tag{1.26}$$

$$\begin{aligned} A_\parallel^{L,R} = -N\sqrt{2}(m_B^2 - m_{K^*}^2)\Bigg\{ & \frac{2m_b}{q^2}\Big[\big(\mathcal{C}_7^{\mathrm{eff}} - \mathcal{C}_{7'}\big)\,T_2(q^2) + \big(1 + r_2(q^2)\big)\mathcal{T}_\perp(q^2)\frac{(m_B^2 - q^2)}{m_B^2}\Big] \\ & + \Big[(\mathcal{C}_9 - \mathcal{C}_{9'}) \mp (\mathcal{C}_{10} - \mathcal{C}_{10'}) + \big(1 + r_2(q^2)\big)Y_t(q^2) + \frac{\lambda_u}{\lambda_t}Y_u(q^2) + c_\parallel^{\mathrm{long}}(q^2)s_\parallel\Big]\frac{A_1(q^2)}{m_B - m_{K^*}}\Bigg\} \end{aligned} \tag{1.27}$$

$$A_0^{L,R} = -\frac{N}{2m_{K^*}\sqrt{q^2}}\Bigg\{2m_b\Bigg[\left(\left(\mathcal{C}_7^{\text{eff}} - \mathcal{C}_{7'}\right)T_2(q^2) + \left(1 + r_2(s)\right)\mathcal{T}_\perp(q^2)\frac{\left(m_B^2 - q^2\right)}{m_B^2}\right)\left(m_B^2 + 3m_{K^*}^2 - q^2\right)$$
$$- \left(\left(\mathcal{C}_7^{\text{eff}} - \mathcal{C}_{7'}\right)T_3(q^2) + \left(1 + r_3(q^2)\right)\mathcal{T}_\parallel(q^2) + \mathcal{T}_\perp(q^2)\right)\frac{\lambda}{m_B^2 - m_{K^*}^2}\Bigg]$$
$$+ \Bigg[\left(\mathcal{C}_9 - \mathcal{C}_{9'}\right) \mp \left(\mathcal{C}_{10} - \mathcal{C}_{10'}\right) + \left(1 + r_3(q^2)\right)Y_t(q^2) + \frac{\lambda_u}{\lambda_t}Y_u(q^2) + c_0^{\text{long}}(q^2)s_0\Bigg]\times$$
$$\times\Bigg[\left(m_B^2 - m_{K^*}^2 - q^2\right)\left(m_B + m_{K^*}\right)A_1(q^2) - \frac{\lambda A_2(q^2)}{m_B + m_{K^*}}\Bigg]\Bigg\} \tag{1.28}$$

$$A_t = \frac{N}{\sqrt{q^2}}\lambda^{1/2}\left[2(\mathcal{C}_{10} - \mathcal{C}_{10'}) + \frac{q^2}{m_\ell}(\mathcal{C}_{PS} - \mathcal{C}_{PS'})\right]A_0(q^2) \tag{1.29}$$

$$A_S = -2N\lambda^{1/2}(\mathcal{C}_S - \mathcal{C}_{S'})A_0(q^2) \tag{1.30}$$

with the normalization

$$N = \sqrt{\frac{G_F^2\alpha^2}{3\cdot 2^{10}\pi^5 m_B^3}\lambda_t^2 q^2\lambda^{1/2}\sqrt{1 - 4\frac{m_\ell^2}{q^2}}} \tag{1.31}$$

and λ is the Källén function:

$$\lambda = m_B^4 + m_{K^*}^4 + q^4 - 2(m_B^2 m_{K^*}^2 + q^2 m_{K^*}^2 + q^2 m_B^2) \tag{1.32}$$

The hadronic amplitudes $\mathcal{T}_{\parallel,\perp}(q^2)$ are functions containing all contributions calculable in QCDf, both factorizable and non-factorizable (see Refs. [14, 29] for explicit definitions). $r_{1,2,3}(q^2)$ correspond to the different types of non-factorizable power corrections and serve to single out the hadronic contribution that is not related to the radiative Wilson coefficients, which is included in $\mathcal{T}_{\parallel,\perp}(q^2)$. The parametrisation in terms of q^2 of such non-factorizable power corrections is the following [30]:

$$r_i(q^2) = r_i^a \mathrm{e}^{i\phi_i^a} + r_i^b \mathrm{e}^{i\phi_i^b}\frac{q^2}{m_B^2} + r_i^c \mathrm{e}^{i\phi_i^c}\left(\frac{q^2}{m_B^2}\right)^2 \tag{1.33}$$

with $i = 1, 2, 3$[4].

On the other hand, the parameters s_i and also $c_i^{\text{long}}(q^2)$, with $i = \perp, \parallel, 0$ correspond to long-distance charm-loop contributions to $B \to K^*$ at the Large-Recoil region, parametrised in the following way (see Refs. [20, 31] for the definition of the parameters):

$$c_{\perp,\parallel}^{\text{long}}(q^2) = \left(a_{\perp,\parallel}^{c\bar{c}} + b_{\perp,\parallel}^{c\bar{c}}(c_{\perp,\parallel}^{c\bar{c}} - q^2)q^2\right)\frac{1}{(c_{\perp,\parallel}^{c\bar{c}} - q^2)q^2}$$
$$c_0^{\text{long}}(q^2) = \left(a_0^{c\bar{c}} + b_0^{c\bar{c}}(c_0^{c\bar{c}} - q^2)(q^2 + 1)\right)\frac{1}{(c_0^{c\bar{c}} - q^2)(q^2 + 1)} \tag{1.34}$$

[4]The two contributions $\mathcal{T}_\perp, \mathcal{T}_\parallel$ that appear in the expressions of the transversity amplitudes are related to the T_i form factors (with $i = 1, 2, 3$) as in Ref. [14]. Since the non-factorizable power corrections need to be considered at the level of the matrix elements of the radiative decay, we include three independent power corrections $r_i(q^2)$, one for each form factor T_i.

Part of these $c\bar{c}$-loop contributions have been already included in the non-factorizable contributions from hard-gluon exchange. Here we parametrise the remaining long-distance contributions in a manner that it matches the non-perturbative computation from Ref. [23]. The contributions to the transverse amplitudes have the same structure and input values, being slightly different for the longitudinal amplitude. In Table 1.2 we provide the numerical values of the different theoretical inputs accounting for the different types of non-factorizable contributions that appear in Eqs. (1.33)-(1.34).

Non-factorizable Power Corrections								
r_1^a	ϕ_1^a	r_1^b	ϕ_1^b	r_1^c	ϕ_1^c	r_2^a	ϕ_2^a	r_2^b
0 ± 0.10	$0 \pm \pi$	0 ± 0.10	$0 \pm \pi$	0 ± 0.10	$0 \pm \pi$	0 ± 0.10	$0 \pm \pi$	0 ± 0.10
ϕ_2^b	r_2^c	ϕ_2^c	r_3^a	ϕ_3^a	r_3^b	ϕ_3^b	r_3^c	ϕ_3^c
$0 \pm \pi$	0 ± 0.10	$0 \pm \pi$	0 ± 0.10	$0 \pm \pi$	0 ± 0.10	$0 \pm \pi$	0 ± 0.10	$0 \pm \pi$

Long-distance charm loop					
$s_\perp$	$s_\parallel$	s_0	$a_\perp^{c\bar{c}}$	$b_\perp^{c\bar{c}}$	$c_\perp^{c\bar{c}}$
0 ± 1	0 ± 1	0 ± 1	9.25 ± 2.25	-0.5 ± 0.3	9.35 ± 0.25
$a_\parallel^{c\bar{c}}$	$b_\parallel^{c\bar{c}}$	$c_\parallel^{c\bar{c}}$	$a_0^{c\bar{c}}$	$b_0^{c\bar{c}}$	$c_0^{c\bar{c}}$
9.25 ± 2.25	-0.5 ± 0.3	9.35 ± 0.25	33 ± 7	-0.9 ± 0.5	10.35 ± 0.55

Table 1.2: Numerical value of the theoretical parameters accounting for the different non-factorizable contributions included in our analysis.

On top of that, one can see in Eqs. (1.28)-(1.30) the seven form factors $V, A_{0,1,2}, T_{1,2,3}$ that describe a $B \to K^*$ transition [29], defined through the matrix elements:

$$\langle K^*(p',\varepsilon^*)|\bar{s}\gamma_\mu b|\bar{B}(p)\rangle = \frac{2iV(q^2)}{m_B + m_{K^*}}\epsilon_{\mu\nu\rho\sigma}\varepsilon^{*\nu}p'^{\rho}p^{\sigma} \tag{1.35}$$

$$\begin{aligned}\langle K^*(p',\varepsilon^*)|\bar{s}\gamma_\mu\gamma_5 b|\bar{B}(p)\rangle = {} & 2m_{K^*}A_0(q^2)\frac{\varepsilon^*\cdot q}{q^2}q_\mu + (m_B + m_{K^*})A_1(q^2)\left[\varepsilon_\mu^* - \frac{\varepsilon^*\cdot q}{q^2}q_\mu\right] \\ & - A_2(q^2)\frac{\varepsilon^*\cdot q}{m_B + m_{K^*}}\left[(p+p')_\mu - \frac{m_B^2 - m_{K^*}^2}{q^2}q_\mu\right]\end{aligned} \tag{1.36}$$

$$\langle K^*(p',\varepsilon^*)|\bar{s}\sigma_{\mu\nu}q^\nu b|\bar{B}(p)\rangle = -2T_1(q^2)\epsilon_{\mu\nu\rho\sigma}\varepsilon^{*\nu}p'^{\rho}p^{\sigma} \tag{1.37}$$

$$\begin{aligned}\langle K^*(p',\varepsilon^*)|\bar{s}\sigma_{\mu\nu}q^\nu\gamma_5 b|\bar{B}(p)\rangle = {} & -iT_2(q^2)\left[(m_B^2 - m_{K^*}^2)\varepsilon_\mu^* - (\varepsilon^*\cdot q)(p+p')_\mu\right] \\ & - iT_3(q^2)(\varepsilon^*\cdot q)\left[q_\mu - \frac{q^2}{m_B^2 - m_{K^*}^2}(p+p')_\mu\right]\end{aligned} \tag{1.38}$$

where p'^μ and ε^μ are the 4-momentum and polarization of the K^* in the final state, p^μ is the 4-momentum of the B meson, and $q_\mu = p_\mu - p'_\mu$ is the momentum transfer q^2.

One can always combine Eqs. (1.35)-(1.38) to obtain expressions that can be directly related to the matrix elements of the usual bilinear quark currents:

$$\langle K^*(p',\varepsilon^*)|\bar{s}\gamma_\mu P_{L,R}\, b|\bar{B}(p)\rangle = \varepsilon^{*\nu}\Bigg\{ -i\epsilon_{\nu\mu\rho\sigma}p'^\rho q^\sigma \frac{V(q^2)}{m_B+m_{K^*}} \mp \frac{1}{2}\Bigg[\frac{2m_{K^*}}{q^2}q_\nu q_\mu A_0(q^2) + (m_B+m_{K^*})\left(g_{\nu\mu}-\frac{q_\nu q_\mu}{q^2}\right)A_1(q^2) - \frac{q_\nu}{m_B+m_{K^*}}\left((2p'+q)_\mu - \frac{m_B^2-m_{K^*}^2}{q^2}q_\mu\right)A_2(q^2)\Bigg]\Bigg\} \tag{1.39}$$

$$\langle K^*(p',\varepsilon^*)|\bar{s}\, i\sigma_{\mu\nu}q^\nu P_{L,R}\, b|\bar{B}(p)\rangle = \varepsilon^{*\nu}\Bigg\{ i\epsilon_{\nu\mu\rho\sigma}p'^\rho q^\sigma T_1(q^2) \pm \frac{1}{2}\Bigg[\Big((m_B^2-m_{K^*}^2)g_{\nu\mu} - q_\nu(2p'+q)_\mu\Big)T_2(q^2) + q_\nu\left(q_\mu - \frac{q^2}{m_B^2-m_{K^*}^2}(2p'+q)_\mu\right)T_3(q^2)\Bigg]\Bigg\} \tag{1.40}$$

These hadronic quantities require a non-perturbative calculation. At present, there are two main methods to achieve such computation, namely:

- Light-Cone Sum Rules (LCSRs): at the Large Recoil Region, that is for small values of the invariant dilepton mass q^2, this method combines standard QCD sum rules techniques with the information on light-cone hadron distribution amplitudes (DAs). One can choose between relying on light-meson DAs [32, 33] or B meson DAs [23, 34] to describe the interpolating current of the transition. Our approach follows the latter prescription [23], as the error estimate is more conservative.

- Lattice calculations: at the Low Recoil Region, i.e. $q^2 \gtrsim 15\,\text{GeV}^2$, QCD lattice techniques can be safely applied, such as the computations in Ref. [35], which we include in our analysis. Moreover, in this region one has to use a model to estimate duality violations due to the resonances of partner channels such as $B^+ \to K^+\mu^+\mu^-$. To account for possible duality violations effects, we add a contribution of order $O(10\%)$ with an arbitrary phase to $\mathcal{C}_9^{\text{eff}}$ for each transversity amplitude, including NNLL corrections following Ref. [16].

Finally, let us introduce the so-called soft form factors (SFF), which are essential in order to define observables that have reduced sensitivity to the main source of theoretical uncertainty, that is hadronic contributions. Since the s quark is light with respect to the b quark, the interactions between the initial/final state quarks with the spectator quark inside the B meson occur mainly via soft-gluon exchanges. Therefore, one can apply the Heavy Quark Effective Theory (HQET) [36, 37] formalism to describe the b quark and the Large Energy Effective Theory (LEET) [38, 39] for the light energetic quark s. Then, in the Large Recoil Limit ($q^2 \ll m_B^2$), the seven form factors in Eqs. (1.35)-(1.38) reduce to only two soft form factors[5]:

[5]Here we focus on a $B \to K^*$ decay, but in the case of a $B \to P$ transition, the three form factors reduce to only one Isgur-Wise function in an analogous way [29, 39]. A discussion on this can be found later in Section 1.2.3

$$\langle K^*(p',\varepsilon^*)|\bar{s}\gamma^\mu b|\bar{B}(p)\rangle = 2iE\,\xi_\perp(E)\epsilon^{\mu\nu\rho\sigma}\varepsilon^*_\nu\, n_\rho v_\sigma \tag{1.41}$$

$$\langle K^*(p',\varepsilon^*)|\bar{s}\gamma^\mu\gamma_5 b|\bar{B}(p)\rangle = 2E\,[\xi_\perp(E)(\varepsilon^{*\mu} - \varepsilon^*\cdot v\, n^\mu) + \xi_\parallel(E)\varepsilon^*\cdot v\, n^\mu], \tag{1.42}$$

$$\langle K^*(p',\varepsilon^*)|\bar{s}\sigma^{\mu\nu}q_\nu b|\bar{B}(p)\rangle = 2Em_B\,\xi_\perp(E)\epsilon^{\mu\nu\rho\sigma}\varepsilon^*_\nu\, v_\rho\, n_\sigma \tag{1.43}$$

$$\begin{aligned}\langle K^*(p',\varepsilon^*)|\bar{s}\sigma^{\mu\nu}\gamma_5 q_\nu b|\bar{B}(p)\rangle = &-2iE\Big\{\xi_\perp(E)(\varepsilon^{*\mu} - \varepsilon^*\cdot v\, n^\mu) \\ &+ \xi_\parallel(E)\,\varepsilon^*\cdot v[(m_B - E)\,n^\mu - m_B v^\mu]\Big\}\end{aligned} \tag{1.44}$$

Therefore, neglecting corrections of order $O(\alpha_s)$ and $O(\Lambda_{\rm QCD}/m_b)$ and comparing Eqs. (1.35)-(1.38) with Eqs. (1.41)-(1.44) one finds the following symmetry relations between the $B \to K^*$ form factors at large recoil:

$$\frac{m_B}{m_B + m_{K^*}}V(q^2) = \frac{m_B + m_{K^*}}{2E}A_1(q^2) = T_1(q^2) = \frac{m_B}{2E}T_2(q^2) = \xi_\perp(E) \tag{1.45}$$

$$\frac{m_{K^*}}{E}A_0(q^2) = \frac{m_B + m_{K^*}}{2E}A_1(q^2) - \frac{m_B - m_{K^*}}{m_B}A_2(q^2) = \frac{m_B}{2E}T_2(q^2) - T_3(q^2) = \xi_\parallel(E) \tag{1.46}$$

1.2 Semileptonic, purely leptonic and radiative $b \to s$ observables

With all the elements needed at hand, we can proceed now to define observables that give us access to interesting information of the different channels available for $b \to s\ell^+\ell^-$ transitions and, specially, that can be effective probes of NP contributions. In this section we will describe the whole set of observables included in the global fits discussed in Section 1.3, that is, angular observables of the semileptonic vector decays $B \to K^*\ell^+\ell^-$ and $B_s \to \phi\ell^+\ell^-$, as well as the corresponding ones for the pseudoscalar channel $B \to K\ell^+\ell^-$. We will also review the branching ratio of the purely leptonic transition $B_s \to \mu^+\mu^-$ and discuss separately the crucial LFUV observables. Finally, we will introduce several observables providing information and constraints on different radiative $b \to s\gamma$ modes.

1.2.1 $B \to K^*\ell^+\ell^-$

We will first list down the observables related to the semileptonic B-meson decay to a light vector meson K^*. For that we will follow the work in Refs. [11, 28], where symmetries of the angular distribution were identified and used to establish the precise number of independent degrees of freedom of the distribution, which in turn lead to define the minimal number of observables needed to extract all the information encoded in the angular distribution. Subsequently, it was shown that this subset of observables constitutes a complete basis, that is, any angular observable can be written in terms of linear combinations of observables of the basis. Additionally, in Ref. [11] the seed of what would later become known as the *optimized observables*[6] was introduced. By choosing adequate ratios of angular coefficients, one could define *theoretically clean* observables, that is observables with cancellation of form factor dependence at LO in

[6] Indeed, the first observable proposed following this philosophy of building suitable ratios that minimize the sensitivity to hadronic uncertainties was already introduced in Ref. [40], where the first ratio $A_T^{(2)}$ was defined.

the HQET/LEET limit[7]. In Ref. [41], the final version of the basis was introduced, replacing $P_{4,5,6} \to P'_{4,5,6}$.

The complete set of optimized observables constitutes a central piece in our analysis of the flavour anomalies. We can define CP-averaged and CP-violating optimized observables in terms of the angular coefficients $J_i, \bar{J}_i$ [12] :

$$\langle P_1 \rangle_{\rm bin} = \frac{1}{2}\frac{\int_{\rm bin} dq^2[J_3 + \bar{J}_3]}{\int_{\rm bin} dq^2[J_{2s} + \bar{J}_{2s}]}, \qquad \langle P_1^{\rm CP} \rangle_{\rm bin} = \frac{1}{2}\frac{\int_{\rm bin} dq^2[J_3 - \bar{J}_3]}{\int_{\rm bin} dq^2[J_{2s} + \bar{J}_{2s}]}, \tag{1.47}$$

$$\langle P_2 \rangle_{\rm bin} = \frac{1}{8}\frac{\int_{\rm bin} dq^2[J_{6s} + \bar{J}_{6s}]}{\int_{\rm bin} dq^2[J_{2s} + \bar{J}_{2s}]}, \qquad \langle P_2^{\rm CP} \rangle_{\rm bin} = \frac{1}{8}\frac{\int_{\rm bin} dq^2[J_{6s} - \bar{J}_{6s}]}{\int_{\rm bin} dq^2[J_{2s} + \bar{J}_{2s}]}, \tag{1.48}$$

$$\langle P_3 \rangle_{\rm bin} = -\frac{1}{4}\frac{\int_{\rm bin} dq^2[J_9 + \bar{J}_9]}{\int_{\rm bin} dq^2[J_{2s} + \bar{J}_{2s}]}, \qquad \langle P_3^{\rm CP} \rangle_{\rm bin} = -\frac{1}{4}\frac{\int_{\rm bin} dq^2[J_9 - \bar{J}_9]}{\int_{\rm bin} dq^2[J_{2s} + \bar{J}_{2s}]}, \tag{1.49}$$

$$\langle P'_4 \rangle_{\rm bin} = \frac{1}{\mathcal{N}'_{\rm bin}}\int_{\rm bin} dq^2[J_4 + \bar{J}_4], \qquad \langle P'^{\rm CP}_4 \rangle_{\rm bin} = \frac{1}{\mathcal{N}'_{\rm bin}}\int_{\rm bin} dq^2[J_4 - \bar{J}_4], \tag{1.50}$$

$$\langle P'_5 \rangle_{\rm bin} = \frac{1}{2\mathcal{N}'_{\rm bin}}\int_{\rm bin} dq^2[J_5 + \bar{J}_5], \qquad \langle P'^{\rm CP}_5 \rangle_{\rm bin} = \frac{1}{2\mathcal{N}'_{\rm bin}}\int_{\rm bin} dq^2[J_5 - \bar{J}_5], \tag{1.51}$$

$$\langle P'_6 \rangle_{\rm bin} = \frac{-1}{2\mathcal{N}'_{\rm bin}}\int_{\rm bin} dq^2[J_7 + \bar{J}_7]\ , \qquad \langle P'^{\rm CP}_6 \rangle_{\rm bin} = \frac{-1}{2\mathcal{N}'_{\rm bin}}\int_{\rm bin} dq^2[J_7 - \bar{J}_7], \tag{1.52}$$

$$\langle P'_8 \rangle_{\rm bin} = \frac{-1}{\mathcal{N}'_{\rm bin}}\int_{\rm bin} dq^2[J_8 + \bar{J}_8]\ , \qquad \langle P'^{\rm CP}_8 \rangle_{\rm bin} = \frac{-1}{\mathcal{N}'_{\rm bin}}\int_{\rm bin} dq^2[J_8 - \bar{J}_8]\ , \tag{1.53}$$

where the $\langle P_i \rangle_{\rm bin}$ notation stands for the integration over the q^2 range of the given bin. Since experimental measurements are performed by fitting q^2-binned angular distributions, we need to integrate the theoretical predictions over the corresponding kinematic range determined by the experimental q^2 bins in order to compare theory/experiment. The normalization $\mathcal{N}'_{\rm bin}$ is defined as:

$$\mathcal{N}'_{\rm bin} = \sqrt{-\int_{\rm bin} dq^2[J_{2s} + \bar{J}_{2s}]\int_{\rm bin} dq^2[J_{2c} + \bar{J}_{2c}]}. \tag{1.54}$$

Besides the P_i observables above, there are other important observables included in our analysis:

$$\langle A_{FB} \rangle_{\rm bin} = -\frac{3}{4}\frac{\int dq^2[J_{6s} + \bar{J}_{6s}]}{4\langle d\Gamma/dq^2\rangle + \langle d\bar{\Gamma}/dq^2\rangle}\ , \qquad \langle A_{FB}^{\rm CP} \rangle_{\rm bin} = -\frac{3}{4}\frac{\int dq^2[J_{6s} - \bar{J}_{6s}]}{4\langle d\Gamma/dq^2\rangle + \langle d\bar{\Gamma}/dq^2\rangle} \tag{1.55}$$

$$\langle F_L \rangle_{\rm bin} = \frac{\int dq^2[J_{2c} + \bar{J}_{2c}]}{\langle d\Gamma/dq^2\rangle + \langle d\bar{\Gamma}/dq^2\rangle}\ , \qquad \langle F_L^{\rm CP} \rangle_{\rm bin} = \frac{\int dq^2[J_{2c} - \bar{J}_{2c}]}{\langle d\Gamma/dq^2\rangle + \langle d\bar{\Gamma}/dq^2\rangle} \tag{1.56}$$

[7] In other words, the optimized observables are built in such a way that there is an exact cancellation of the soft form factors, which is only valid at LO in α_s and $\Lambda_{\rm QCD}/m_b$, as we discussed previously in Section 1.1.3 (see Eqs. (1.41)-(1.46)).

$$\langle \frac{d\mathcal{B}}{dq^2} \rangle_{\text{bin}} = \tau_B \frac{\langle d\Gamma/dq^2 \rangle + \langle d\bar{\Gamma}/dq^2 \rangle}{2}\,, \qquad \langle A_{CP} \rangle_{\text{bin}} = \frac{\langle d\Gamma/dq^2 \rangle - \langle d\bar{\Gamma}/dq^2 \rangle}{\langle d\Gamma/dq^2 \rangle + \langle d\bar{\Gamma}/dq^2 \rangle} \tag{1.57}$$

where $A_{FB}^{(\text{CP})}$ corresponds to the CP-averaged(violating) Forward-Backward asymmetry, $F_L^{(\text{CP})}$ is the longitudinal polarisation fraction of the K^* meson, and $d\mathcal{B}/dq^2$ and A_{CP} are the differential branching ratio[8] and the CP-asymmetry of the given decay respectively, with τ_B denoting the lifetime of the B meson.

1.2.2 $B_s \to \phi\ell^+\ell^-$

The main difference between the two vector decays $B \to K^*\ell^+\ell^-$ and $B_s \to \phi\ell^+\ell^-$ is that the latter are not self-tagging processes, that is, the final state cannot discriminate between the parent meson B_s or its CP-conjugate $\bar{B}_s$. Therefore, the only measurements available for this decay are the following combinations of angular coefficients J_i (which are equivalent to the J_i from Eqs. (1.17)-(1.24)):

$$\langle J_i + \bar{J}_i \rangle \qquad i = 1s, 1c, 2s, 2c, 3, 4, 7 \tag{1.58}$$

$$\langle J_i - \bar{J}_i \rangle \qquad i = 5, 6s, 6c, 8, 9 \tag{1.59}$$

Since we do not consider CP-violating processes in our analysis, we will only include the CP-average quantities above in the form of the optimized observables P_1, P_4' and P_6', and also the longitudinal polarisation fraction F_L. However, the fact that the final state ϕ meson cannot distinguish between a B_s or a $\bar{B}_s$ decay introduces an interference from $B_s - \bar{B}_s$ mixing. This in turn induces a time-dependent contribution to the amplitude of the decay and in consequence to the angular distribution as well. Therefore, one has to make the following replacement [42, 43] to account for this time-dependence:

$$J_i(t) = J_i(A_X \to A_X(t))\,, \qquad \tilde{J}_i(t) = \tilde{J}_i(A_X \to \tilde{A}_X(t)) \tag{1.60}$$

where X includes all possible combinations of polarisations and chiralities and $\tilde{J}_i$ are related to the $\bar{J}_i$ coefficients by $\tilde{J}_i = \zeta_i \bar{J}_i$, with $\zeta_i = \pm 1$ for $i = 1s, 1c, 2s, 2c, 3, 4, 7(5, 6s, 6c, 8, 9)$. Then the combinations appearing in the time-dependent decay rates can be written as:

$$J_i(t) + \tilde{J}_i(t) = \mathrm{e}^{-\Gamma t}\left[(J_i + \tilde{J}_i)\cosh(y\Gamma t) - h_i \sinh(y\Gamma t)\right], \tag{1.61}$$

$$J_i(t) - \tilde{J}_i(t) = \mathrm{e}^{-\Gamma t}\left[(J_i - \tilde{J}_i)\cosh(x\Gamma t) - s_i \sinh(x\Gamma t)\right], \tag{1.62}$$

where $\Gamma \equiv (\Gamma_L + \Gamma_H)$, $x \equiv (m_H - m_L)\Gamma$ and $y \equiv \Delta\Gamma/(2\Gamma)$, being $\Gamma_L(\Gamma_H)$ the width of the lighter (heavier) mass eigenstate. The coefficients J_i and $\tilde{J}_i$ can be determined from flavour-specific decays, and s_i and h_i are defined as a new set of angular coefficients related to the time-dependent angular distribution (we refer the reader to Ref. [42] for their explicit definitions in terms of transversity amplitudes).

Following this formalism, we can therefore account for measurements of time-integrated observables by including $O(\Delta\Gamma/\Gamma)$ corrections to the analogous $B \to K^*\ell^+\ell^-$ expressions [42]

[8] We usually write $\langle d\mathcal{B}/dq^2 \rangle$ simply as $\mathcal{B}(B \to K^*\ell^+\ell^-)$ in order not to overload the notation.

$$\langle J_i(t) + \tilde{J}_i(t)\rangle_t = \frac{1}{\Gamma}\left[\frac{1}{1-y^2}(J_i + \tilde{J}_i) - \frac{y}{1-y^2}h_i\right], \tag{1.63}$$

$$\langle J_i(t) - \tilde{J}_i(t)\rangle_t = \frac{1}{\Gamma}\left[\frac{1}{1+x^2}(J_i - \tilde{J}_i) - \frac{x}{1+x^2}s_i\right], \tag{1.64}$$

where following a similar notation as in Eqs. (1.47)-(1.53) we define $\langle A\rangle_t$ as the integration over time of a given quantity A.

Finally, we can construct the same complete basis of optimized observables discussed for $B \to K^*\ell^+\ell^-$ for the $B_s \to \phi\ell^+\ell^-$ decay by making the following replacements in Eqs. (1.47)-(1.53):

$$J_i + \tilde{J}_i \longrightarrow \langle J_i(t) + \tilde{J}_i(t)\rangle_t, \tag{1.65}$$

$$J_i - \tilde{J}_i \longrightarrow \langle J_i(t) - \tilde{J}_i(t)\rangle_t. \tag{1.66}$$

1.2.3 $B \to K\ell^+\ell^-$

Another $b \to s$ process that presents good sensitivity to possible NP contributions is the pseudoscalar $B \to K\ell^+\ell^-$ decay channel. Since it is governed by the same quark transition reviewed in Section 1.1.1, observables related to this decay can be described by means of the same effective Hamiltonian. The only difference will appear at the level of the form factors needed, as in this case we are dealing with a pseudoscalar structure.

Therefore, the matrix element of a $B \to K\ell^+\ell^-$ transition reads [44]

$$\mathcal{M}(\bar{B} \to K\ell\bar{\ell}) = \frac{G_F\alpha}{\sqrt{2}\pi}V_{ts}^*V_{tb}\left[F_S(\bar{\ell}\ell) + F_P(\bar{\ell}\gamma_5\ell) + F_V p_\mu(\bar{\ell}\gamma^\mu\ell) + F_A p_\mu(\bar{\ell}\gamma^\mu\gamma_5\ell)\right] \tag{1.67}$$

where p_μ is the 4-momentum of the B meson. The terms $F_{S,P,V,A}$[9] are functions of Lorentz-invariant quantities that depend on the Wilson coefficients and also the form factors associated to this decay. They have the following expression [44]:

$$F_S = \frac{1}{2}(m_B^2 - m_K^2)f_0(q^2)\left(\frac{\mathcal{C}_S m_b + \mathcal{C}_{S'}m_s}{m_b - m_s}\right), \tag{1.68}$$

$$\begin{aligned} F_P =& -m_\ell(\mathcal{C}_{10} + \mathcal{C}_{10'})\left\{f_+(q^2) - \frac{m_B^2 - m_K^2}{q^2}\left(f_0(q^2) - f_+(q^2)\right)\right\} \\ &+ \frac{1}{2}(m_B^2 - m_K^2)f_0(q^2)\left(\frac{\mathcal{C}_P m_b + \mathcal{C}_{P'}m_s}{m_b - m_s}\right), \end{aligned} \tag{1.69}$$

$$F_A = (\mathcal{C}_{10} + \mathcal{C}_{10'})f_+(q^2), \tag{1.70}$$

$$F_V = (\mathcal{C}_9^{\text{eff}} + \mathcal{C}_{9'}^{\text{eff}})f_+(q^2) + 2(\mathcal{C}_7^{\text{eff}} + \mathcal{C}_{7'}^{\text{eff}})m_b\frac{f_T(q^2)}{m_B + m_K}, \tag{1.71}$$

where the three $B \to P$ form factors $f_{0,+,T}(q^2)$ are defined through the matrix elements

[9] In general, these transitions could also receive contributions from tensor operators, but since we do not explore this possibility in our analysis, we choose not include them here.

$$\langle K(k)|\bar{s}\gamma_\mu b|\bar{B}(p)\rangle = (2p-q)_\mu f_+(q^2) + \frac{m_B^2 - m_K^2}{q^2} q_\mu \left[f_0(q^2) - f_+(q^2)\right] , \tag{1.72}$$

$$\langle K(k)|\bar{s} i\sigma_{\mu\nu} q^\nu b|\bar{B}(p)\rangle = -\left[(2p-q)_\mu q^2 - (m_B^2 - m_K^2) q_\mu\right] \frac{f_T(q^2)}{m_B + m_K} \tag{1.73}$$

with $q^\mu = (p-k)^\mu$ being the transfer four-momentum. Moreover, by means of the equation of motion for the b and s quarks we can obtain from Eq. (1.72)

$$\langle K(k)|\bar{s}b|\bar{B}(p)\rangle = \frac{m_B^2 - m_K^2}{m_b - m_s} f_0(q^2) \tag{1.74}$$

Let us note in passing that the three $B \to P$ form factors reduce to one single Isgur-Wise function $\xi_P(q^2)$ due to the existing symmetry relations in the large energy limit of QCD (in an analogous way as the seven form factors for a $B \to K^*$ transition reduce to two soft form factors as discussed in Section 1.1.3) [29, 39].

By squaring the matrix element in Eq. (1.67) we can compute the decay distribution of a $B \to K\ell^+\ell^-$ process in terms of the dilepton invariant mass q^2 and the angle θ_ℓ between the B meson and the ℓ^- with respect to the dilepton rest frame [45]:

$$\frac{d^2\Gamma_\ell}{dq^2 d\cos\theta_\ell} = a_\ell(q^2) + b_\ell(q^2)\cos\theta_\ell + c_\ell(q^2)\cos^2\theta_\ell, \tag{1.75}$$

where $a_\ell(q^2)$, $b_\ell(q^2)$ and $c_\ell(q^2)$ are defined as [45]

$$\begin{aligned}\frac{a_\ell(q^2)}{\Gamma_0 \lambda^{1/2}\beta_\ell} &= q^2\left(\beta_\ell^2|F_S|^2 + |F_P|^2\right) + \frac{\lambda}{4}\left(|F_A|^2 + |F_V|^2\right) \\ &\quad + (m_B^2 - m_K^2 + q^2)\mathrm{Re}\left[F_P F_A^*\right] + 4m_\ell^2 m_B^2 |F_A|^2,\end{aligned} \tag{1.76}$$

$$\frac{b_\ell(q^2)}{\Gamma_0 \lambda^{1/2}\beta_\ell} = 2m_\ell \lambda^{1/2}\beta_\ell \mathrm{Re}\left[F_S F_V^*\right], \tag{1.77}$$

$$\frac{c_\ell(q^2)}{\Gamma_0 \lambda^{1/2}\beta_\ell} = -\frac{\lambda}{4}\beta_\ell^2\left(|F_A|^2 + |F_V|^2\right), \tag{1.78}$$

with β_ℓ and λ defined in Eq. (1.25) and Eq. (1.32) respectively, and

$$\Gamma_0 = \frac{G_F^2 \alpha_{em}^2 |V_{tb}V_{ts}^*|}{512\pi^5 m_B^3} \tag{1.79}$$

We are now ready to define the observables of interest that we consider in our analysis. Since they are experimentally measured in integrated q^2 bins, we already write their theoretical definitions as q^2 averaged expressions. By combining the q^2-integrated version of the coefficients $a_\ell(q^2)$, $b_\ell(q^2)$ and $c_\ell(q^2)$

$$\langle a_\ell\rangle_{\text{bin}} = \int_{\text{bin}} a_\ell(q^2)dq^2 , \quad \langle b_\ell\rangle_{\text{bin}} = \int_{\text{bin}} b_\ell(q^2)dq^2 , \quad \langle c_\ell\rangle_{\text{bin}} = \int_{\text{bin}} c_\ell(q^2)dq^2 , \tag{1.80}$$

we can define the decay rate Γ_ℓ and the forward-backward asymmetry A_{FB} [45]:

$$\left\langle \frac{d\Gamma_\ell}{dq^2} \right\rangle_{\text{bin}} = 2\left(\langle a_\ell \rangle_{\text{bin}} + \frac{1}{3}\langle c_\ell \rangle_{\text{bin}} \right), \tag{1.81}$$

$$\langle A_{FB}^\ell \rangle_{\text{bin}} = \frac{\langle b_\ell \rangle_{\text{bin}}}{\langle d\Gamma_\ell/dq^2 \rangle_{\text{bin}}} \tag{1.82}$$

Easily enough, we can transform Eq. (1.81) into the usual branching ratio by multiplying by the corresponding B-meson lifetime τ_B:

$$\mathcal{B}(B \to K\ell^+\ell^-) = \tau_B \left\langle \frac{d\Gamma_\ell}{dq^2} \right\rangle_{\text{bin}} \tag{1.83}$$

Finally, we can further define the observable [45]

$$\langle F_H^\ell \rangle_{\text{bin}} = \frac{2}{\langle d\Gamma_\ell/dq^2 \rangle_{\text{bin}}} \left(\langle a_\ell \rangle_{\text{bin}} + \langle c_\ell \rangle_{\text{bin}} \right) \tag{1.84}$$

Since the observable F_H^ℓ is normalized with respect to the total decay rate Γ_ℓ, it shows a reduced sensitivity to uncertainties due to cancellations between numerator and denominator. Notice that A_{FB}^ℓ is exactly zero in the SM[10]. Also, in the limit of massless leptons ($m_\ell \to 0$) F_H^ℓ vanishes in the SM due to a cancellation between a_ℓ and c_ℓ as can be seen in Eqs. (1.76) and (1.78).

1.2.4 $B_s \to \mu^+\mu^-$

We include in our analysis the branching ratio of the process $\mathcal{B}(B_s \to \mu\mu)$. This is an important observable to place constraints on axial, scalar and pseudoscalar structures of NP. The expression of such branching ratio at leading order is given by [46]:

$$\begin{aligned}\mathcal{B}(B_s \to \mu\mu) = &\frac{\lambda_t^2 G_F^2 m_{B_s}^3 \alpha_{em}^2 \tau_{B_s} f_{B_s}^2}{64\pi^3} \sqrt{1 - \frac{4m_\mu^2}{m_{B_s}^2}} \left\{ \frac{m_{B_s}^2}{m_b^2} (\mathcal{C}_S - \mathcal{C}_{S'})^2 \left(1 - 4\frac{m_\mu^2}{m_{B_s}^2} \right) \right. \\ &\left. + \left(\frac{m_{B_s}}{m_b} (\mathcal{C}_P - \mathcal{C}_{P'}) + 2\frac{m_\mu}{m_{B_s}} (\mathcal{C}_{10\mu} - \mathcal{C}_{10'\mu}) \right)^2 \right\}\end{aligned} \tag{1.85}$$

where τ_{B_s} is the B_s lifetime and $\mathcal{C}_{10\mu} = \mathcal{C}_{10\mu}^{\text{SM}} + \mathcal{C}_{10\mu}^{\text{NP}}$. Here $\mathcal{C}_{10'\mu}$ accounts for possible right-handed current NP contributions, and $\mathcal{C}_{S^{(\prime)}}, \mathcal{C}_{P^{(\prime)}}$ correspond to LH (RH) scalar and pseudoscalar contributions.

The most recent theoretical prediction for $\mathcal{B}(B_s \to \mu\mu)$ is presented in Ref. [47]. In this work, the authors compute a set of electromagnetic corrections from scales below m_b that are dynamically enhanced by a power of m_b/Λ_{QCD} and by large logarithms. The size of such corrections is found to be 1%, which is larger than previous estimates of next-to-leading order QED effects, assessed to be $\pm 0.3\%$. Despite that, these corrections are well within the estimated $\pm 1.5\%$ non-parametric uncertainty. To account for these new corrections in our prediction, we use as a reference the value in Ref. [48], where the effect of these QED corrections is introduced as a global factor $\eta_{\text{QED}} = 0.993$ to the previous theoretical prediction from Ref. [46]

$$\overline{\mathcal{B}}_{s\mu\mu} = \eta_{\text{QED}}(3.65 \pm 0.23) = (3.64 \pm 0.14) \tag{1.86}$$

[10] This can be seen from Eq. (1.77). Since $A_{FB}^\ell \propto b_\ell$, which is different from zero only in presence of scalar contributions, this observable automatically vanishes if there is no scalar NP.

In our analyses, we decided to rescale our theoretical prediction using our own set of input parameters in order to agree with the SM value in Eq. (1.86). This allows us to leave the NP terms in Eq. (1.85) untouched.

1.2.5 Lepton Flavour Universality Violating observables

Even though we have discussed observables for the pseudoscalar (vector) channel $B \to K^{(*)}\ell^+\ell^-$ in previous sections, there is a type of observable related to these transitions that deserves special attention due to the remarkable properties they show. The so-called Lepton Flavour Universality Violating observables, or LFUV observables, are a subset of observables built in such a way that they allow to directly test the amount of LFU breaking that data seems to point to.

Up to lepton masses effects, the SM predicts the same decay rate for LFUV observables, regardless of the lepton flavour in the final state. In other words, one expects the same amount of electrons and muons (and tau) in a $B \to K^{(*)}$ decay at the region $q^2 \gtrsim 1\,\text{GeV}^2$.

Therefore, by comparing observables that are equal except for the final lepton flavour, we can assess by how much the universality of the leptonic flavour in the SM is broken by possible contributions of NP. On top of that, since they are built from ratios or differences of the same observable, they show a very reduced sensitivity to hadronic uncertainties, making them very effective probes of the presence of LFUV NP.

First we consider the LFUV ratios $R_{K^{(*)}}$ [45], both for the neutral and charged $B^{0,+}$ meson decay:

$$R_{K^{(*)0,+}} = \frac{\mathcal{B}(B^{0,+} \to K^{(*)0,+}\mu^+\mu^-)}{\mathcal{B}(B^{0,+} \to K^{(*)0,+}e^+e^-)} \tag{1.87}$$

where $R_{K^{(*)0,+}}$ has to be understood as the q^2-integrated version of the observable, which we do not display here as it is customary to write the observable without the usual $\langle . \rangle$ brackets. Any R_X ratio constructed following Eq. (1.87), with X being any final state meson of a semileptonic B decay, will be 1 in the SM up to kinematic corrections of order $O(m_\ell/\sqrt{q^2})$.

Later on another type of LFUV observable, called Q_i, was introduced in Ref. [49]:

$$\langle Q_i \rangle_{\text{bin}} = \langle P_i^\mu \rangle_{\text{bin}} - \langle P_i^e \rangle_{\text{bin}} \tag{1.88}$$

with $i = 4, 5, 6, 8$. Since they are differences of optimized angular observables, which already have a limited sensitivity to hadronic uncertainties, they also constitute clean probes of the violation of LFU given that they cancel completely in the SM up to corrections of order $O(m_\ell/\sqrt{q^2})$ and exhibit a high sensitivity to the short-distance part of $\mathcal{C}_{9\mu}$. A measurement of Q_i deviating from zero would necessarily imply the existence of physics beyond the SM, with different implications that we will discuss in the following section. Currently, only experimental measurements of Q_4 and Q_5 are available [50], and therefore we only include those two in our analysis.

1.2.6 $B \to X_s\ell^+\ell^-$

In our analysis we include the inclusive decays $B \to X_s e^+e^-$ and $B \to X_s\mu^+\mu^-$, as they have a limited sensitivity to non-perturbative contributions while at the same time allow us to place important constraints on the electromagnetic and semileptonic coefficients $\mathcal{C}_{7^{(\prime)},9^{(\prime)},10^{(\prime)}}$[11]. Following the parametrisation in Ref. [25], their branching ratio have the following expression

[11] These observables can in principle also test other kinds of NP operators such as scalars or tensors. However, since we do not usually include those in our analysis we will not consider them here.

$b_{(0,0)} = 15.86 \quad \delta_b = 1.51$		
$b_{(0,7)} = -0.517$	$b_{(0,9)} = 2.663$	$b_{(0,10)} = -4.679$
$b_{(0,7')} = -0.680$	$b_{(0,9')} = -0.049$	$b_{(0,10')} = 0.061$
$b_{(7,7)} = b_{(7',7')} = 27.776$	$b_{(9,9)} = b_{(9',9')} = 0.534$	$b_{(10,10)} = b_{(10',10')} = 0.543$
$b_{(7,7')} = -0.399$	$b_{(9,9')} = -0.014$	$b_{(10,10')} = -0.014$
$b_{(7,9)} = b_{(7',9')} = 4.920$	$b_{(7,9')} = b_{(7',9)} = -0.113$	

Table 1.3: Coefficients of the parametrisation of $\mathcal{B}(B \to X_s \ell^+ \ell^-)$ in terms of the Wilson coefficients $\mathcal{C}_{7^{(\prime)},9^{(\prime)},10^{(\prime)}}$ [25].

$$\mathcal{B}(\bar{B} \to X_s \ell^+ \ell^-)_{[1,6]} = 10^{-7} \times \left[\sum_{i,j=0,7^{(\prime)},9^{(\prime)},10^{(\prime)}} b_{(i,j)}\, \delta\mathcal{C}_i \delta\mathcal{C}_j \pm \delta_b \right], \tag{1.89}$$

Here $\delta\mathcal{C}_i = \mathcal{C}_i - \mathcal{C}_i^{\mathrm{SM}}$, with $\delta\mathcal{C}_0 = 1$. The non-zero parameters $b_{(i,j)}$ can be found in Table 1.3. Notice that, since we are only considering the branching ratio in the bin $q^2 \in [1,6]\,\mathrm{GeV}^2$ (due to the fact that its theoretical prediction suffers from larger theoretical uncertainties in the high-q^2 region), lepton mass effects are small enough to be considered negligible, and therefore Eq. (1.89) applies to both muons and electrons, with only small differences in the SM prediction.

1.2.7 Radiative modes

Last, but not least, we list in this section several observables related to B decays with a photon in the final state. They are interesting quantities to constrain the space for NP contributions to the electromagnetic operators $\mathcal{O}_7$ and $\mathcal{O}_{7'}$, due to the fact that they are only sensitive to this kind of structure in the WEH.

- $\mathcal{B}(\bar{B} \to X_s\gamma)$: First, we consider the branching ratio of the inclusive decay $B \to X_s\gamma$, which we parametrise as [25]

$$\begin{aligned}\mathcal{B}(\bar{B} \to X_s\gamma)_{E_\gamma \geq 1.6\,\mathrm{GeV}} = \Big[& a_{(0,0)} \pm \delta_a + a_{(0,7)}\delta\mathcal{C}_7 + a_{(0,7')}\delta\mathcal{C}_{7'} \\ & + a_{(7,7)} \left(\delta\mathcal{C}_7^2 + \delta\mathcal{C}_{7'}^2\right) \Big] \times 10^{-4},\end{aligned} \tag{1.90}$$

  with the coefficients a_i in Table 1.4.

$a_{(0,0)} = 3.36 \quad \delta_a = 0.23$	$a_{(0,7)} = -14.81$	$a_{(7,7)} = 16.68$	$a_{(0,7')} = -0.23$

Table 1.4: Coefficients describing the dependence of $\mathcal{B}(B \to X_s\gamma)$ on $\mathcal{C}_{7^{(\prime)}}$ [22, 25]

- $A_I(B \to K^*\gamma)$: The isospin asymmetry $A_I(B \to K^*\gamma)$ vanishes within the SM in naive factorization [25], but receives non-negligible SM contributions once topologies with photon emission from the spectator quark line are calculated in the framework of QCD factorization. It is defined as

$$A_I \equiv \frac{\Gamma(\bar{B}^0 \to \bar{K}^{*0}\gamma) - \Gamma(B^- \to K^{*-}\gamma)}{\Gamma(\bar{B}^0 \to \bar{K}^{*0}\gamma) + \Gamma(B^- \to K^{*-}\gamma)} \tag{1.91}$$

Even though this observable is expected to be very sensitive to hadronic uncertainties, it gives direct access to the electromagnetic coefficients $\mathcal{C}_{7^{(\prime)}}$, and therefore we include it in our analysis, following the numerical expression [25]:

$$A_I(B \to K^*\gamma) = c \times \frac{\sum_k d_k\, \delta\mathcal{C}_7^k}{\sum_{k,l} e_{(k,l)}\, \delta\mathcal{C}_7^k \delta\mathcal{C}_{7'}^l} \pm \delta_c, \tag{1.92}$$

with the corresponding non-zero coefficients collected in Table 1.5.

$c = 4.11\%$	$\delta c = 2.52\%$
$d_0 = 1$	$d_1 = -2.51757$
$e_{(0,0)} = 1$	$e_{(1,0)} = -5.0165$
$e_{(0,1)} = -0.0919061$	$e_{(2,0)} = 6.30856$
$e_{(0,2)} = 7.49847$	

Table 1.5: Coefficients describing the dependence of $A_I(B \to K^*\gamma)$ on $\mathcal{C}_{7^{(\prime)}}$ [25].

- $S_{K^*\gamma}$: Finally, another radiative observable related to $b \to s$ processes is the time-dependent CP asymmetry in $B^0 \to K^{*0}\gamma$, which allows an indirect probe of the photon helicity:

$$\begin{aligned} A_{CP}(B^0 \to K^{*0}\gamma) &= \frac{\Gamma(\bar{B}^0(t) \to \bar{K}^{*0}\gamma) - \Gamma(B^0(t) \to K^{*0}\gamma)}{\Gamma(\bar{B}^0(t) \to \bar{K}^{*0}\gamma) + \Gamma(B^0(t) \to K^{*0}\gamma)} \\ &= S_{K^*\gamma} \sin(\Delta m_B t) - C_{K^*\gamma} \cos(\Delta m_B t) \end{aligned} \tag{1.93}$$

where K^{*0}, $\bar{K}^{*0}$ further decay into the CP eigenstate $K_S\pi^0$ and thus are observed, and we assume SM-like B^0 mixing. Due to the helicity suppression of right-handed photons, A_{CP} is dominated by B mixing in the SM, making it a good candidate for a null-test of the SM. Since we are interested in constraining contributions into $\mathcal{C}_{7^{(\prime)}}$, we only consider the $S_{K^*\gamma}$ term in Eq. (1.93), as it contains intereference effects of photons with different polarisations. We parametrise it as [25]:

$$S_{K^*\gamma} = f^{+\delta_f^u}_{-\delta_f^d} + \frac{\sum_{k,l} g_{(k,l)} \delta\mathcal{C}_7^k \delta\mathcal{C}_{7'}^l}{\sum_{k,l} h_{(k,l)} \delta\mathcal{C}_7^k \delta\mathcal{C}_{7'}^l}, \tag{1.94}$$

with f being the central value of its SM prediction and $\delta_f^{u,d}$ corresponds to the upper (lower) error bar. The non-vanishing g, h coefficients can be found in Table 1.6.

1.3 Global Fits after R_{K_S} and $R_{K^{*+}}$

In this section, based on Ref. [4], we present the results corresponding to our state-of-the-art global analysis of $b \to s\ell^+\ell^-$ data after the recent LHCb updates of quantities assessing the violation of lepton-flavour universality (LFU). On the one hand, we have the ratio R_K [51]:

$f = -0.0297336$	$\delta_f^u = 0.0089893$ $\delta_f^d = 0.0089767$
$g_{(0,1)} = +152.774$	$h_{(0,0)} = +39.9999$
$g_{(1,0)} = -3.17764$	$h_{(0,1)} = -4.51218$
$g_{(1,1)} = -415.441$	$h_{(1,0)} = -214.866$
$g_{(0,2)} = +8.63917$	$h_{(0,2)} = +290.553$
$g_{(2,0)} = +8.63917$	$h_{(2,0)} = +290.553$

Table 1.6: Coefficients describing the dependence of $S_{K^*\gamma}$ on $\mathcal{C}_{7^{(\prime)}}$ [25].

$$R_{K,\text{LHCb}}^{[1.1,6]} = 0.846^{+0.042\,+0.013}_{-0.039\,-0.012} \tag{1.95}$$

with an extended statistics corresponding to $9\,\text{fb}^{-1}$, reaching the level of statistical evidence (above 3 standard deviations). On the other hand, similar quantities have been recently measured for the experimentally challenging modes [52]

$$R_{K_S} = \frac{\mathcal{B}(B^0 \to K_S\mu^+\mu^-)}{\mathcal{B}(B^0 \to K_S e^+e^-)} \qquad R_{K^{*+}} = \frac{\mathcal{B}(B^+ \to K^{*+}\mu^+\mu^-)}{\mathcal{B}(B^+ \to K^{*+}e^+e^-)} \tag{1.96}$$

with the results

$$R_{K_S,\text{LHCb}}^{[1.1,6]} = 0.66^{+0.20\,+0.02}_{-0.14\,-0.04} \qquad R_{K^{*+},\text{LHCb}}^{[0.045,6]} = 0.70^{+0.18\,+0.03}_{-0.13\,-0.04} \tag{1.97}$$

in agreement each with the SM below the 2σ level but consistent with the downward trend compared to the predictions of the SM. Indeed, in the SM, these ratios are protected from hadronic contributions and are known to be 1 up to (tiny) electromagnetic corrections and (simple) kinematic mass effects.

As discussed in Section 1.1, the deviations observed in these modes can be efficiently and consistently analyzed in a model-independent EFT (WEH) framework (see, for instance, Refs. [22, 53–62]) [12].

This tool has proven particularly helpful in identifying NP scenarios (or patterns of NP) that could explain the data at the level of the EFT, providing guidelines for the construction of phenomenologically viable NP models.

This section represents the most updated version of the previous works in Refs. [53–55] to serve as an accurate guideline for model building, as well as an overview of observables relevant for the near future. We follow the same theoretical and statistical approach as in our previous works [53–55], updating and adding new experimental inputs and their corresponding SM predictions. It is important at this point to check if the inclusion of this new data alters some of our earlier conclusions, in particular concerning best-fit-points and confidence intervals that are required for model building as well as the hierarchy of the various NP scenarios that are

[12] It is interesting to point out that the results in Ref. [58] are very similar to the ones found in the analysis presented in this Thesis. Although they use a similar set of observables (with the addition of baryon decays), the analyses differ through the treatment of hadronic uncertainties (form factors, charm-loop contributions). This similarity illustrates the robustness of the results with respect to different assumptions on hadronic uncertainties.

favoured by the current global fits. It turns out that our conclusions remain unchanged and are thus very robust. We will therefore discuss the outcome of our updated global fits but we refer the interested reader to Ref. [56–58, 60] to see the different results obtained by groups following other approaches. A more detailed interpretation of our results can be found in Ref. [55].

1.3.1 Observables

We consider the same observables and theoretical inputs as in Ref. [55], taking into account the following updated measurements (replacing the previous ones):

- The experimental values of R_K, R_{K_S} and $R_{K^{*+}}$ from the LHCb collaboration already discussed [51, 52]. We also take into account their update of R_K [63] as well as the branching ratios for $B^{0,+} \to K^{0,+}\mu^+\mu^-$ updated by the Belle collaboration [64] (the Belle measurements of $R_{K^{(*)}}$ correspond to a combination of the charged and neutral channels $B^{0,+} \to K^{(*)0,+}\ell^+\ell^-$).

- The experimental value of the branching ratio $\mathcal{B}(B_s \to \mu^+\mu^-)$ from the LHCb collaboration [65], which is combined with the results from CMS [66] and ATLAS [67], leading to the average $\mathcal{B}(B_s \to \mu^+\mu^-) = 2.85^{+0.34}_{-0.31} \times 10^{-9}$ [68]. This is to be compared with the most updated theoretical computation [48].

- The angular distribution of $B^+ \to K^{*+}\mu^+\mu^-$ [69] using the optimized observables P_i [12] measured by LHCb, as well as the longitudinal polarisation and forward-backward asymmetry measured by the CMS collaboration [70]. Compared to the neutral case, our computation for the charged case takes into account the different spectator quark not only by modifying the mass and lifetime, but also the annihilation and hard-spectator interactions following Ref. [10].

- The angular distribution of $B^+ \to K^+\mu^+\mu^-$ from the CMS collaboration [71].

- The angular analysis of $B \to K^*e^+e^-$ at low q^2 from the LHCb collaboration [72]. The bins of this analysis are different from the previous ones [73], but the measurements are correlated since the latter analysis includes the data of the former, leading us to discard Ref. [73].

- The new angular analysis and branching ratio of $B_s \to \phi\mu^+\mu^-$ from the LHCb collaboration [74, 75] superseding the previous LHCb analysis [76]. We focus on CP-averaged quantities, as we will consider only CP-conserving NP.

We do not consider here the baryon mode $\Lambda_b \to \Lambda\mu^+\mu^-$ [77], as there is a known issue with the normalization provided by the Λ_b production fraction which may distort the results [3, 78]. We think that it is important that LHCb reanalyses this normalization without relying on combinations of LEP and Tevatron studies performed at different energies, so that corrected results of this mode could be included in future global analyses of $b \to s\ell^+\ell^-$ transitions in a completely safe way.

The full composition in terms of observables of the different kind of fits can be found in Appendix B, where we provide their theoretical prediction in the SM as well as the corresponding experimental measurement, which we include in our analysis.

1.3.2 Fit approach

Our evaluation of the various observables follows the same approach as in Ref. [22] with the updates of the theoretical inputs discussed in Refs. [53, 55]. As we already stated throughout

section 1.1, attention must naturally be paid to hadronic uncertainties [18, 20, 21, 30, 79–81], which stem from two different sources in exclusive $b \to s\ell^+\ell^-$ decays such as $B \to K^{(*)}\ell^+\ell^-$ and $B_s \to \phi\ell^+\ell^-$. First, form factors must be determined through different methods at large recoil of the final hadron (light-cone sum rules involving either light-meson [33, 82] or B-meson [23, 34, 83, 84] distribution amplitudes) or low recoil (lattice QCD [35, 85]). Second, the non-local contribution from $c\bar{c}$ loops can be tackled similarly either at low recoil, through quark-hadron duality arguments for observables averaged over a large dilepton invariant mass [86–89], or large recoil, using various approaches (order-of-magnitude estimates, light-cone sum rule computations [23, 83], interpolation from the unphysical region below the photon pole up to the lowest charmonium resonances [19, 84], ...). Obviously, the uncertainties of the theoretical predictions for these observables (within the SM or any NP scenario) are partly dependent on these assumptions. However, it is quite striking to notice that different analyses based on different underlying assumptions for these hadronic uncertainties may yield different numerical values for statistical quantities (significances, pulls, ...) but they have repeatedly led to very similar patterns of favoured scenarios, best-fit points and confidence regions for NP contributions to Wilson coefficients (see for instance Refs. [56–58, 68, 90]).

In practice, we perform fits to obtain information on the values of the parameters collectively denoted here as θ, which represent the unknown NP contributions from the different scenarios that we estimate (e.g. $\mathcal{C}_{9\mu}^{\rm NP}$, $\mathcal{C}_{9\mu}^{\rm NP} = -\mathcal{C}_{10\mu}^{\rm NP}$, etc). We work within a frequentist framework based on a gaussian approximation for the likelihood function $\mathcal{L}(\theta)$ where theoretical and experimental uncertainties are treated on the same footing:

$$\begin{aligned} -2\ln\mathcal{L}(\theta) &= \chi^2(\theta) \\ &= \sum_{i,j=1}^{N_{\rm obs}} \left(O^{th}(\theta) - O^{exp}\right)_i \left(V^{th}(\theta) + V^{exp}\right)_{ij} \left(O^{th}(\theta) - O^{exp}\right)_j , \end{aligned} \tag{1.98}$$

with $N_{\rm obs}$ the total number of observables in the fit, $O_i^{th}(\theta)$ the central value of the theory prediction for the i-th observable, O_i^{exp} the experimental measurement (i.e. the central value quoted by experiments) of the same observable and V_{ij}^{th} and V_{ij}^{exp} the theoretical and experimental covariance matrices respectively.

On the one hand, the experimental covariance matrix contains all the available information on the errors and correlations among the measurements of the relevant observables released by the different experiments. Whenever the correlations are not available, we take those measurements as uncorrelated. In the case of asymmetric uncertainties (such as R_K), in order to be consistent with the gaussian approximation of the likelihood function, we symmetrise the errors by taking the largest uncertainty, with no change in the central value. On the other hand, the theoretical covariance matrix is estimated by performing a multivariate gaussian scan over all the nuisance parameters entering the calculation of theory predictions which we do not fit through the minimisation procedure.

The central values of the unknown parameters in our analysis are estimated by means of the *method of maximum likelihood* (ML). By construction of the likelihood, the ML estimators $\hat{\theta}$ coincide with the best-fit points obtained by minimising the χ^2 function:

$$\left.\frac{\partial\chi^2}{\partial\theta_i}\right|_{\hat{\theta}} = 0 \qquad \text{such that} \qquad \chi_{\rm min} = \chi^2(\hat{\theta}), \tag{1.99}$$

for $i = 1, ..., n$, with n being the number of parameters. The minimisation is performed numerically using MIGRAD from the Python package `iMinuit` [91]. For computational reasons, the theoretical covariance is assumed to depend mildly on the NP parameters, hence we take $V^{th}(\theta)$ in Eq. (1.98) at the SM point. We checked that our results remain unchanged if we repeat the fits

with the $V^{th}(\theta)$ evaluated at different NP points, confirming the validity of our approximation. This is in agreement with the results of Refs. [22, 57, 92], where the impact of accounting for the correlated theoretical uncertainties at each point in the Wilson coefficient parameter space was analyzed in full detail.

In order to provide a complete description of the parameters, we also assess their errors and correlations. This information is encoded in the likelihood function and can be accessed through the Rao-Cramér-Fréchet formula for the inverse V^{-1} of the covariance matrix $V_{ij} = \text{cov}(\hat{\theta}_i, \hat{\theta}_j)$ of the estimators

$$\left(V^{-1}\right)_{ij} = -\left.\frac{\partial^2 \ln \mathcal{L}}{\partial\theta_i \partial\theta_j}\right|_{\hat{\theta}} = \frac{1}{2}\left.\frac{\partial^2 \chi^2}{\partial\theta_i \partial\theta_j}\right|_{\hat{\theta}}. \tag{1.100}$$

In practice, the likelihood's Hessian matrix is numerically computed by MIGRAD as one of the outputs of the minimisation routine. Instead, for the computation of confidence intervals we use `iMinuit`'s MINOS algorithm [91].

To quantify the level of agreement between a given hypothesis and the data, we compute the corresponding p-value of *goodness-of-fit*:

$$p = \int_{\chi^2_{\text{min}}}^{\infty} d\chi^2 \, f(\chi^2; n_{\text{dof}}), \tag{1.101}$$

where $n_{\text{dof}} = N_{\text{obs}} - n$. Finally, to compare the descriptions offered by two different nested hypotheses H_0 and H_1 (with n_{H_0}, n_{H_1} the respective number of degrees of freedom and $n_{\text{H}_0} < n_{\text{H}_1}$), we compute their relative Pull, measured in units of Gaussian standard deviations (σ):

$$\text{Pull}_{H_0 H_1} = \sqrt{2}\,\text{Erf}^{-1}\left[F(\Delta\chi^2_{H_0H_1}; n_{\text{H}_0\text{H}_1})\right], \tag{1.102}$$

with $\Delta\chi^2_{H_0H_1} = \chi^2_{H_0,\text{min}} - \chi^2_{H_1,\text{min}}$, $n_{\text{H}_0\text{H}_1} = n_{\text{H}_1} - n_{\text{H}_0}$, F the χ^2 cumulative distribution function and Erf^{-1} the inverse error function. Most of the time, we compare a given NP scenario with the SM case, denoting the result as Pull_{SM} unless there is a risk of ambiguity. Our statistical interpretation, based on Wilks' theorem [93], assumes that the large number of observables leads to a statistical question where the linear/Gaussian approximation holds and that all observables have a similar sensitivity to all Wilson coefficients, so that the number of degrees of freedom can be computed as described above. This issue has been recently discussed in Refs. [94, 95] (see also earlier discussions on this topic in Refs. [21, 96]). These studies suggest that the effective number of degrees of freedom to be actually considered could be lower than what a naive computation would indicate, due to a weak sensitivity of the χ^2 function to some of the Wilson coefficients. In that case, our interpretation would be conservative, since it yields higher p-values and lower pulls than with the smaller effective number of degree of freedom advocated in these references.

1.3.3 Fit Results

We start by considering the fits to NP scenarios which affect muon modes only. Tabs. 1.7-1.9 and Fig. 1.1 update the corresponding tables and figures of Ref. [55] based on fits to the full set of data ("All", 254 observables[13]) or restricted to quantities assessing LFUV ("LFUV", 24 observables). The results are similar to those in Ref. [55].

From the results in Tables 1.7-1.9, on can see that the combination of anomalies in some LFD ($b \to s\mu^+\mu^-$) angular observables and in LFUV ratios R_K and R_{K^*} mainly prefers hypotheses with a large NP contribution to the Wilson coefficient $\mathcal{C}_{9\mu}$ (of order 25% of the SM), or NP contributions to both $\mathcal{C}_{9\mu}$ and $\mathcal{C}_{10\mu}$.

[13] We detail the full list of the observables present in our fits in the appendix, where we also provide their theoretical predictions within the SM, as well as the individual tension with respect to the experimental value. In the LFUV fits we include the observables Q_4 and Q_5 (measured by Belle) instead of $P'_{4e,\mu}$, $P'_{5e,\mu}$.

	All				LFUV			
1D Hyp.	Best fit	$1\,\sigma/2\,\sigma$	Pull_{SM}	p-value	Best fit	$1\,\sigma/\,2\,\sigma$	Pull_{SM}	p-value
$\mathcal{C}_{9\mu}^{\text{NP}}$	-1.01	$[-1.15,-0.87]$ $[-1.29,-0.72]$	7.0	24.0 %	-0.87	$[-1.11,-0.65]$ $[-1.37,-0.45]$	4.4	40.7 %
$\mathcal{C}_{9\mu}^{\text{NP}}=-\mathcal{C}_{10\mu}^{\text{NP}}$	-0.45	$[-0.52,-0.37]$ $[-0.59,-0.30]$	6.5	16.9 %	-0.39	$[-0.48,-0.31]$ $[-0.56,-0.23]$	5.0	73.5 %
$\mathcal{C}_{9\mu}^{\text{NP}}=-\mathcal{C}_{9'\mu}$	-0.92	$[-1.07,-0.75]$ $[-1.22,-0.59]$	5.7	8.2 %	-1.60	$[-2.10,-0.98]$ $[-2.49,-0.46]$	3.2	8.4 %

Table 1.7: Most prominent 1D patterns of NP in $b\to s\mu^+\mu^-$. Pull_{SM} is quoted in units of standard deviation. The p-value of the SM hypothesis is 0.44% for the fit "All" and 0.91% for the fit LFUV.

	All			LFUV		
2D Hyp.	Best fit	Pull_{SM}	p-value	Best fit	Pull_{SM}	p-value
$(\mathcal{C}_{9\mu}^{\text{NP}},\mathcal{C}_{10\mu}^{\text{NP}})$	$(-0.92,+0.17)$	6.8	25.6 %	$(-0.16,+0.55)$	4.7	71.2 %
$(\mathcal{C}_{9\mu}^{\text{NP}},\mathcal{C}_{7'})$	$(-1.02,+0.01)$	6.7	22.8 %	$(-0.88,-0.04)$	4.1	37.5 %
$(\mathcal{C}_{9\mu}^{\text{NP}},\mathcal{C}_{9'\mu})$	$(-1.12,+0.36)$	6.9	27.4 %	$(-1.82,+1.09)$	4.5	60.2 %
$(\mathcal{C}_{9\mu}^{\text{NP}},\mathcal{C}_{10'\mu})$	$(-1.15,-0.26)$	7.1	31.8 %	$(-1.88,-0.59)$	5.0	88.1 %
$(\mathcal{C}_{9\mu}^{\text{NP}},\mathcal{C}_{9e}^{\text{NP}})$	$(-1.11,-0.26)$	6.7	23.8 %	$(-0.52,+0.34)$	4.0	35.3 %
Hyp. 1	$(-1.01,+0.31)$	6.7	24.0 %	$(-1.60,+0.32)$	4.5	62.5 %
Hyp. 2	$(-0.89,+0.06)$	5.4	8.0 %	$(-1.95,+0.25)$	3.6	20.4 %
Hyp. 3	$(-0.45,+0.04)$	6.2	15.9 %	$(-0.39,-0.14)$	4.7	70.2 %
Hyp. 4	$(-0.47,+0.07)$	6.3	16.8 %	$(-0.48,+0.15)$	4.8	79.6 %
Hyp. 5	$(-1.15,+0.17)$	7.1	31.1 %	$(-2.13,+0.50)$	5.0	89.4 %

Table 1.8: Most prominent 2D patterns of NP in $b\to s\mu^+\mu^-$. The last five rows correspond to Hypothesis 1: $(\mathcal{C}_{9\mu}^{\text{NP}}=-\mathcal{C}_{9'\mu},\mathcal{C}_{10\mu}^{\text{NP}}=\mathcal{C}_{10'\mu})$, 2: $(\mathcal{C}_{9\mu}^{\text{NP}}=-\mathcal{C}_{9'\mu},\mathcal{C}_{10\mu}^{\text{NP}}=-\mathcal{C}_{10'\mu})$, 3: $(\mathcal{C}_{9\mu}^{\text{NP}}=-\mathcal{C}_{10\mu}^{\text{NP}},\mathcal{C}_{9'\mu}=\mathcal{C}_{10'\mu})$, 4: $(\mathcal{C}_{9\mu}^{\text{NP}}=-\mathcal{C}_{10\mu}^{\text{NP}},\mathcal{C}_{9'\mu}=-\mathcal{C}_{10'\mu})$ and 5: $(\mathcal{C}_{9\mu}^{\text{NP}},\mathcal{C}_{9'\mu}=-\mathcal{C}_{10'\mu})$.

	$\mathcal{C}_7^{\text{NP}}$	$\mathcal{C}_{9\mu}^{\text{NP}}$	$\mathcal{C}_{10\mu}^{\text{NP}}$	$\mathcal{C}_{7'}$	$\mathcal{C}_{9'\mu}$	$\mathcal{C}_{10'\mu}$
Best fit	+0.00	-1.08	+0.15	+0.00	+0.16	-0.18
$1\,\sigma$	$[-0.02,+0.01]$	$[-1.25,-0.90]$	$[+0.02,+0.28]$	$[-0.01,+0.02]$	$[-0.20,+0.53]$	$[-0.36,+0.02]$
$2\,\sigma$	$[-0.04,+0.03]$	$[-1.41,-0.72]$	$[-0.10,+0.42]$	$[-0.03,+0.03]$	$[-0.56,+0.92]$	$[-0.54,+0.22]$

Table 1.9: 1 and 2 σ confidence intervals for the NP contributions to Wilson coefficients in the 6D hypothesis allowing for NP in $b\to s\mu^+\mu^-$ operators dominant in the SM and their chirally-flipped counterparts, for the fit "All". The Pull_{SM} is 6.3σ and the p-value is 27.8%.

Following this perspective we ought to be more precise on what goes under the "New Physics" landscape. For that reason, recalling Eq. (1.9), we consider that the short-distance Wilson coefficients $\mathcal{C}_{i\ell}$ can contain two types of NP contribution

$$\mathcal{C}_{i\ell}^{\text{NP}}=\mathcal{C}_{i\ell}^{\text{V}}+\mathcal{C}_i^{\text{U}} \tag{1.103}$$

with $\ell=e,\mu$ and $i=9^{(\prime)},10^{(\prime)}$ (the extension to τ is trivial, assuming true universality among e, μ and τ) where $\mathcal{C}_{i\ell}^{\text{V}}$ stands for Lepton Flavour Universality Violating NP and $\mathcal{C}_i^{\text{U}}$ for Lepton Flavour Universal-NP contributions. These short-distance contributions are all independent of the external hadronic states and their kinematics; they differ therefore from long-distance hadronic contributions which are LFU, but dependent on q^2 and on the nature and kinematics of the hadronic states. We will define the separation between the two types of contributions by imposing that LFUV contributions affect only muons

$$\mathcal{C}_{ie}^{\text{V}}=0 \tag{1.104}$$

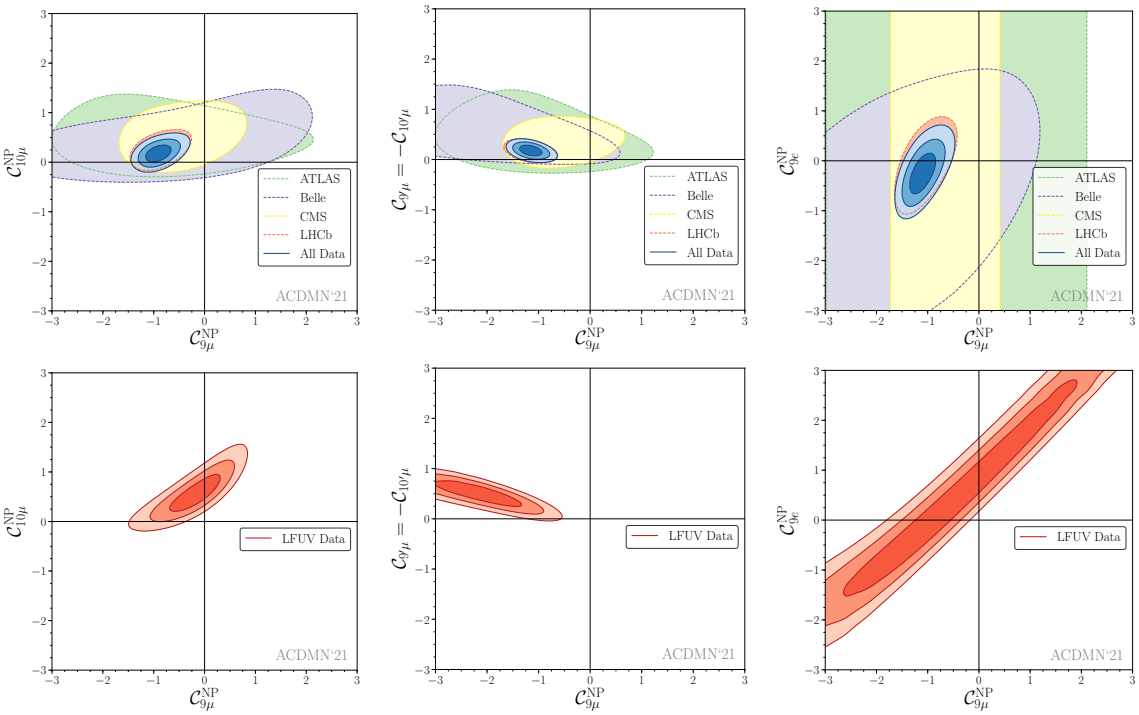

Figure 1.1: From left to right: Allowed regions in the $(\mathcal{C}_{9\mu}^{\rm NP}, \mathcal{C}_{10\mu}^{\rm NP})$, $(\mathcal{C}_{9\mu}^{\rm NP}, \mathcal{C}_{9'\mu} = -\mathcal{C}_{10'\mu})$ and $(\mathcal{C}_{9\mu}^{\rm NP}, \mathcal{C}_{9e}^{\rm NP})$ planes for the corresponding 2D hypotheses, using all available data (fit "All") upper row or LFUV fit lower row. Dashed lines represent the 3 σ regions while the solid lines represent 1, 2 and 3 σ regions.

There is no loss of generality here, since this term can always be absorbed in such a way that $\mathcal{C}_{i\mu}^{\rm V}$ can be interpreted as the difference of NP contributions to muons and electrons. Following the parametrisation described in Eqs. (1.103),(1.104), we turn now to scenarios that allow for the presence of lepton flavour universal NP [54, 97] in addition to LFUV contributions to muons only,

We update the scenarios considered in Ref. [55] in Tab. 1.10 and Fig. 1.2. Interestingly, when we perform the 10-dimensional fit allowing for NP in both muon and electron coefficients (i.e. $\mathcal{C}_7, \mathcal{C}_{9\ell}, \mathcal{C}_{10\ell}$ and $\mathcal{C}_{7'}, \mathcal{C}_{9'\ell}, \mathcal{C}_{10'\ell}$ for both $\ell = e$ and μ), we obtain almost the same results as in Tab. 1.9 for the muon coefficients, whereas the electron coefficients are only very loosely constrained, indicating the need for more data on electronic modes. We obtain a $\text{Pull}_{\rm SM}$ of 6.0σ (p-value of 28.3%) for this 10-dimensional fit.

1.3.4 Favoured scenarios and connection with other observables

Several scenarios exhibit a significant improvement in the description of the data compared to the SM. Fig. 1.3 shows the predictions for the observables Q_5, R_K and R_{K^*} in several of these scenarios. The large uncertainties for R_{K^*} in most NP scenarios come from the presence of three different helicity amplitudes involving different combinations of form factors: if the $SU(2)_L$ symmetry of the SM is respected, one amplitude dominates leading to reduced uncertainties for the prediction of R_{K^*}, but in other cases, the presence of several helicity amplitudes leads to larger uncertainties. One can also notice that Q_5 is able to separate three cases of interest: the SM, scenario 8 ($\mathcal{C}_{9\mu}^{\rm V} = -\mathcal{C}_{10\mu}^{\rm V}, \mathcal{C}_9^{\rm U}$), and the scenarios with right-handed couplings and a large negative contribution to $\mathcal{C}_{9\mu}$ (Fig. 1.4a illustrates the importance of R_K and P_5' in highlighting these scenarios compared to others considered in the previous section).

Scenario		Best-fit point	1 σ	2 σ	Pull_{SM}	p-value
Scenario 5	$\mathcal{C}^{\text{V}}_{9\mu}$	-0.55	$[-1.02, -0.11]$	$[-1.56, +0.32]$	6.6	25.2 %
	$\mathcal{C}^{\text{V}}_{10\mu}$	$+0.49$	$[+0.08, +0.84]$	$[-0.44, +1.15]$		
	$\mathcal{C}^{\text{U}}_{9} = \mathcal{C}^{\text{U}}_{10}$	-0.35	$[-0.73, +0.07]$	$[-1.06, +0.60]$		
Scenario 6	$\mathcal{C}^{\text{V}}_{9\mu} = -\mathcal{C}^{\text{V}}_{10\mu}$	-0.52	$[-0.59, -0.44]$	$[-0.67, -0.37]$	6.9	26.6 %
	$\mathcal{C}^{\text{U}}_{9} = \mathcal{C}^{\text{U}}_{10}$	-0.38	$[-0.50, -0.26]$	$[-0.60, -0.13]$		
Scenario 7	$\mathcal{C}^{\text{V}}_{9\mu}$	-0.85	$[-1.07, -0.63]$	$[-1.30, -0.42]$	6.7	23.8 %
	$\mathcal{C}^{\text{U}}_{9}$	-0.26	$[-0.52, +0.01]$	$[-0.79, +0.30]$		
Scenario 8	$\mathcal{C}^{\text{V}}_{9\mu} = -\mathcal{C}^{\text{V}}_{10\mu}$	-0.34	$[-0.41, -0.27]$	$[-0.49, -0.20]$	7.2	34.5 %
	$\mathcal{C}^{\text{U}}_{9}$	-0.82	$[-0.99, -0.63]$	$[-1.16, -0.42]$		
Scenario 9	$\mathcal{C}^{\text{V}}_{9\mu} = -\mathcal{C}^{\text{V}}_{10\mu}$	-0.53	$[-0.63, -0.43]$	$[-0.74, -0.33]$	6.3	17.5 %
	$\mathcal{C}^{\text{U}}_{10}$	-0.24	$[-0.44, -0.05]$	$[-0.63, +0.15]$		
Scenario 10	$\mathcal{C}^{\text{V}}_{9\mu}$	-0.98	$[-1.13, -0.84]$	$[-1.27, -0.69]$	6.9	27.9 %
	$\mathcal{C}^{\text{U}}_{10}$	$+0.27$	$[+0.13, +0.42]$	$[-0.01, +0.56]$		
Scenario 11	$\mathcal{C}^{\text{V}}_{9\mu}$	-1.06	$[-1.20, -0.91]$	$[-1.34, -0.76]$	6.9	27.4 %
	$\mathcal{C}^{\text{U}}_{10'}$	-0.23	$[-0.35, -0.10]$	$[-0.47, +0.02]$		
Scenario 12	$\mathcal{C}^{\text{V}}_{9'\mu}$	$+0.49$	$[+0.34, +0.65]$	$[+0.19, +0.81]$	3.2	1.4 %
	$\mathcal{C}^{\text{U}}_{10}$	-0.25	$[-0.38, -0.13]$	$[-0.50, -0.00]$		
Scenario 13	$\mathcal{C}^{\text{V}}_{9\mu}$	-1.11	$[-1.27, -0.96]$	$[-1.41, -0.79]$	6.7	29.6 %
	$\mathcal{C}^{\text{V}}_{9'\mu}$	$+0.37$	$[+0.13, +0.60]$	$[-0.11, +0.84]$		
	$\mathcal{C}^{\text{U}}_{10}$	$+0.28$	$[+0.10, +0.47]$	$[-0.08, +0.66]$		
	$\mathcal{C}^{\text{U}}_{10'}$	$+0.03$	$[-0.15, +0.21]$	$[-0.33, +0.40]$		

Table 1.10: Most prominent patterns for LFU and LFUV NP contributions from Fit "All". Scenarios 5 to 8 were introduced in Ref. [54]. Scenarios 9 (motivated by 2HDMs [98]) and 10 to 13 (motivated by Z' models with vector-like quarks [99]) were introduced in Ref. [55].

As discussed in Ref. [55], scenario 8 allows for a model-independent connection between the anomalies in $b \to s\ell^+\ell^-$ decays and those in $b \to c\tau\nu$ transitions [100]. This connection arises in the SMEFT scenario where $\mathcal{C}^{(1)} = \mathcal{C}^{(3)}$ expressed in terms of the following $SU(2)_L$-invariant dimension-6 operators [101, 102]:

$$\mathcal{O}^{(1)}_{ijkl} = [\bar{Q}_i \gamma_\mu Q_j][\bar{L}_k \gamma^\mu L_l], \tag{1.105}$$

$$\mathcal{O}^{(3)}_{ijkl} = [\bar{Q}_i \gamma_\mu \sigma^I Q_j][\bar{L}_k \gamma^\mu \sigma^I L_l], \tag{1.106}$$

where the Pauli matrices σ^I act on the weak-isospin component of the quark (lepton) doubles $Q(L)$.

The operator involving third-generation leptons explains $R_{D^{(*)}}$ and the one involving the second generation gives a LFUV effect in $b \to s\mu^+\mu^-$ processes. The constraint from $b \to c\tau\nu$ and $SU(2)_L$ invariance leads to large contributions enhancing $b \to s\tau^+\tau^-$ processes [102], whereas the mixing into $\mathcal{O}_9$ generates $\mathcal{C}^{\text{U}}_9$ at $\mu = m_b$ [103]. Therefore, the SMEFT scenario described above reproduces scenario 8 with an additional correlation between $\mathcal{C}^{\text{U}}_9$ and $R_{D^{(*)}}$ [102, 103]:

$$\mathcal{C}^{\text{U}}_9 \approx 7.5 \left(1 - \sqrt{\frac{R_{D^{(*)}}}{R_{D^{(*)}\text{SM}}}}\right)\left(1 + \frac{\log(\Lambda^2/(1\text{TeV}^2))}{10.5}\right), \tag{1.107}$$

where Λ is the typical scale of NP involved. We show the global fit of scenario 8 without and with the additional input on $R_{D^{(*)}}$ from Ref. [100] in Fig. 1.4b, taking the scale $\Lambda = 2$ TeV. The best-fit point for $(\mathcal{C}^{\text{V}}_{9\mu} = -\mathcal{C}^{\text{V}}_{10\mu}, \mathcal{C}^{\text{U}}_9)$ is $(-0.36, -0.68)$, with 1 σ intervals $[-0.43, -0.29]$ and $[-0.80, -0.55]$ respectively. The agreement among all data is very good, shown by the fact that scenario 8 supplemented with $R_{D^{(*)}}$ exhibits a pull with respect to the SM of 8.0 σ and a p-value

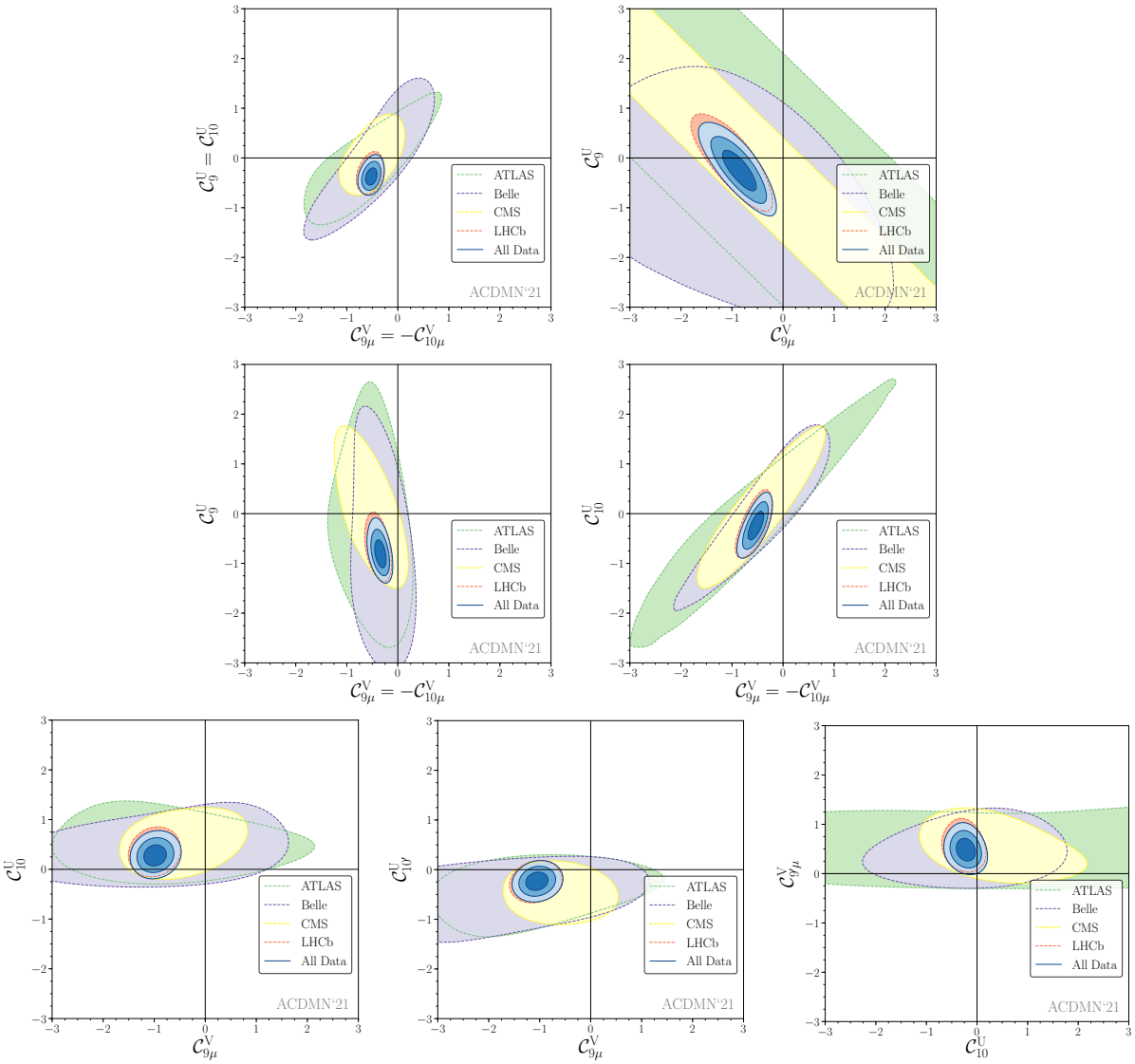

Figure 1.2: From left to right: Allowed regions for the 2D scenarios presented in Tab. 1.10. Scenarios 6 and 7 on the upper row, 8 and 9 in the middle row and 10 to 12 in the bottom row using all available data (fit "All"). Dashed lines represent the 3 σ regions while the solid lines represent 1, 2 and 3 σ regions.

of 33.1%. Interestingly, the agreement between scenario 8 and the allowed region for $R_{D^{(*)}}$ has increased with the addition of R_{K_S}, $R_{K^{*+}}$ and $B_s \to \phi\mu^+\mu^-$ into the global analysis, with a fit favouring less negative values for $\mathcal{C}_9^{\rm U}$. An even better agreement could be reached if $R_{D^{(*)}}$ is slightly further away from the SM expectations, or if the scale of NP is increased.

1.4 Summary and Conclusions

We have presented in this chapter our most complete and updated results of the global fit to $b \to s\ell^+\ell^-$ data including 254 observables. We see that the recent measurements of LFUV observables R_K, R_{K_S}, $R_{K^{*+}}$ by the LHCb collaboration together with the $B_s \to \phi\mu^+\mu^-$ update confirm the main conclusions of the previous update of R_K and $B_s \to \mu^+\mu^-$ with only marginal changes. Indeed, the slight reduction of significances in most scenarios is mostly driven by the inclusion of more SM-like observables coming from the update of $B_s \to \phi\mu^+\mu^-$ (new bins) with

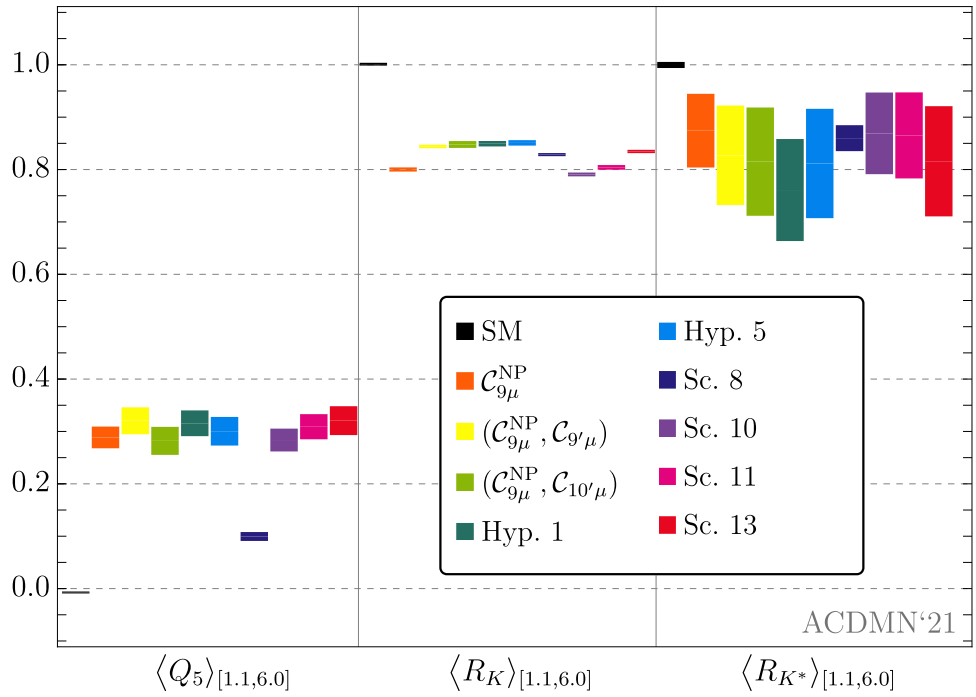

Figure 1.3: Values of $\langle Q_5 \rangle_{[1.1,6]}$, $\langle R_K \rangle_{[1.1,6]}$, $\langle R_{K^*} \rangle_{[1.1,6]}$ in the SM and nine different scenarios: SM (black), $\mathcal{C}_{9\mu}^{\rm NP}$ (orange), $(\mathcal{C}_{9\mu}^{\rm NP}, \mathcal{C}_{9'\mu})$ (yellow), $(\mathcal{C}_{9\mu}^{\rm NP}, \mathcal{C}_{10'\mu})$ (light green), $(\mathcal{C}_{9\mu}^{\rm NP} = -\mathcal{C}_{9'\mu}, \mathcal{C}_{10\mu}^{\rm NP} = \mathcal{C}_{10'\mu})$ (dark green), $(\mathcal{C}_{9\mu}^{\rm NP}, \mathcal{C}_{9'\mu} = -\mathcal{C}_{10'\mu})$ (light blue), $(\mathcal{C}_{9\mu}^{\rm V} = -\mathcal{C}_{10\mu}^{\rm V}, \mathcal{C}_{9}^{\rm U})$ (dark blue), $(\mathcal{C}_{9\mu}^{\rm V}, \mathcal{C}_{10}^{\rm U})$ (purple), $(\mathcal{C}_{9\mu}^{\rm V}, \mathcal{C}_{10'}^{\rm U})$ (pink), $(\mathcal{C}_{9\mu}^{\rm V}, \mathcal{C}_{9'\mu}^{\rm V}, \mathcal{C}_{10}^{\rm U}, \mathcal{C}_{10'}^{\rm U})$ (red). The boxes correspond to the predictions of the 1 σ regions at the b.f.p. value of the Wilson coefficients in each of the scenarios for the fit to the "All" data set.

little sensitivity to $\mathcal{C}_{9\mu}$ and higher experimental precision. On the other side, even if the scenario $\mathcal{C}_{9\mu} = -\mathcal{C}_{9'\mu}$ can explain neither R_K nor R_{K_S}, it yields an acceptable solution for R_{K^*} and $R_{K^{*+}}$ leading to a marginal increase of its significance in the LFUV fit.

The overall hierarchy of preferences for specific scenarios remains unchanged. In our previous update [55] we observed an increase in the consistency among the data analyzed in the framework of the favoured scenarios. More specifically, we saw that the most favoured 1D scenario remains the case of a vector coupling to muons encoded in $\mathcal{C}_{9\mu}$. The LHCb update of the $B_s \to \mu^+\mu^-$ branching ratio, in better agreement with the SM expectation, reduced marginally the room available for NP in $\mathcal{C}_{10\mu}$ for the scenarios considered here, which do not feature NP contributions from (pseudo)scalar operators.

Finally, the two classes of favoured scenarios of Ref. [55] find their status strengthened, namely

- The purely muonic hypotheses with right handed currents $(\mathcal{C}_{9\mu}^{\rm NP}, \mathcal{C}_{10'\mu})$ and $(\mathcal{C}_{9\mu}^{\rm NP}, \mathcal{C}_{9'\mu} = -\mathcal{C}_{10'\mu})$. The latter scenario (called Hypothesis 5 in Table 1.8) features a right-handed contribution which becomes compatible with zero once the 2σ confidence region is considered. Such right-handed currents tend to counterbalance the impact on R_K of a large negative $\mathcal{C}_{9\mu}$ which is preferred by many observables considered in the global fit.

- Scenario 8 $(\mathcal{C}_{9\mu}^{\rm V} = -\mathcal{C}_{10\mu}^{\rm V}, \mathcal{C}_{9}^{\rm U})$ with a universal component $\mathcal{C}_{9}^{\rm U}$ together with a muonic component obeying $SU(2)_L$ invariance. As illustrated in Fig. 1.4b, this scenario reaches 8.0 σ once combined with R_D and R_{D^*} in an EFT framework explaining $b \to c\ell\nu$ and $b \to s\ell^+\ell^-$ through correlated singlet and triplet dimension-6 operators combining quark and lepton bilinears.

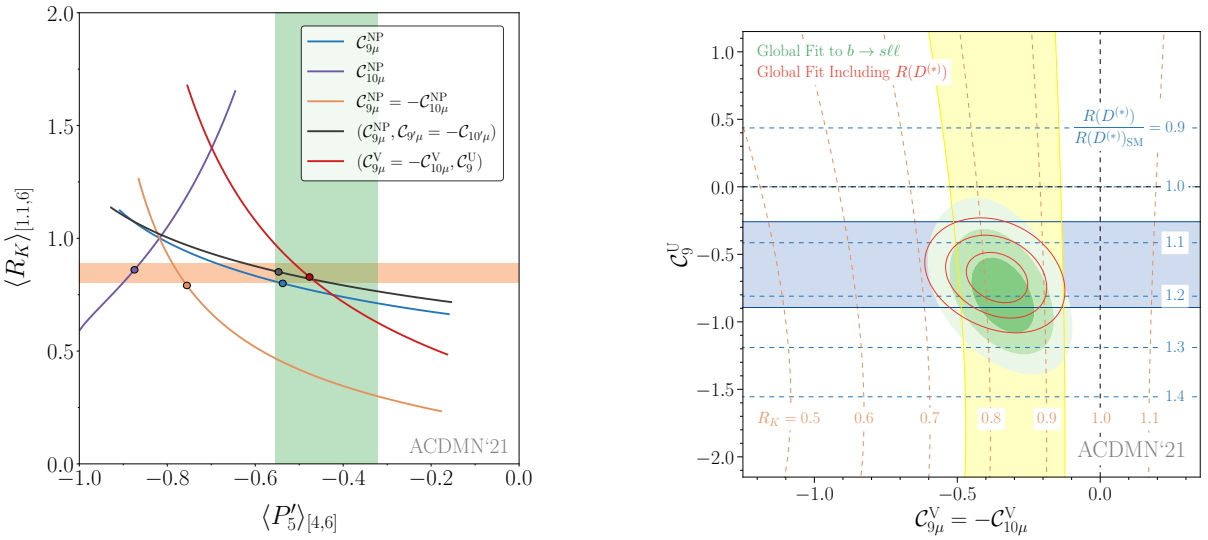

(a) (b)

Figure 1.4: Left: $\langle R_K \rangle_{[1.1,6]}$ versus $\langle P_5' \rangle_{[4,6]}$ in five different scenarios: $\mathcal{C}_{9\mu}^{\rm NP}$ (blue), $\mathcal{C}_{9\mu}^{\rm NP} = -\mathcal{C}_{10\mu}^{\rm NP}$ (orange), and $(\mathcal{C}_{9\mu}^{\rm V} = -\mathcal{C}_{10\mu}^{\rm V}, \mathcal{C}_9^{\rm U})$ (red), $(\mathcal{C}_{9\mu}^{\rm NP}, \mathcal{C}_{9'\mu} = -\mathcal{C}_{10'\mu})$ (black), and $\mathcal{C}_{10\mu}^{\rm NP}$ (purple). The curves correspond only to the predictions for central values. In the 2D scenarios (red and black) the Wilson coefficient not shown is set to its b.f.p. value. The current experimental values from the LHCb collaboration are also indicated (orange horizontal and green vertical bands respectively). The dots correspond to the b.f.p. values of the corresponding scenario for the fit to the "All" data set. Right: Preferred regions at the 1, 2 and $3\,\sigma$ level (green) in the $(\mathcal{C}_{9\mu}^{\rm V} = -\mathcal{C}_{10\mu}^{\rm V}, \mathcal{C}_9^{\rm U})$ plane from $b \to s\ell^+\ell^-$ data. The red contour lines show the corresponding regions once $R_{D^{(*)}}$ is included in the fit (for $\Lambda = 2$ TeV). The horizontal blue (vertical yellow) band is consistent with $R_{D^{(*)}}$ (R_K) at the $2\,\sigma$ level and the contour lines show the predicted values for these ratios.

As an outlook for the future, besides the importance of updating the LFU ratios $R_{K^{(*)}}$ and the angular distributions of $B \to K^*\ell^+\ell^-$ and $B_s \to \phi\ell^+\ell^-$ modes, two experimental inputs can help guiding future analyses. First, the observation of enhanced $b \to s\tau^+\tau^-$ transitions would favour naturally a scenario with a LFU contribution in $\mathcal{C}_9^{\rm U}$. Second, the measurement of a large Q_5 would favour a scenario with a large negative vector coupling $\mathcal{C}_{9\mu}$, possibly with additional right-handed currents. Indeed, as illustrated by Fig. 1.3, the observable Q_5 [49] can distinguish between the purely muonic hypotheses with right handed currents (e.g. Hypothesis 5) and scenario 8 with a universal component in $\mathcal{C}_9^{\rm U}$, with a higher value in the former case and a slightly lower value in the latter [97].

Further progress may also be achieved through a better understanding of the theoretical uncertainties involved [34, 84, 104], more data on other modes and with other experimental setups (in particular Belle II [105]), but also the determination of additional observables [106–108]. This supplementary information should help us to corner the actual NP pattern hinted at by the $b \to s\ell^+\ell^-$ anomalies currently observed and confirmed as an evidence in R_K by the LHCb collaboration.

Such identification at the EFT level is the first and mandatory step to build viable phenomenological models for NP, to be probed and confirmed through decays involving other families of quarks and leptons, as well as direct production experiments.

Chapter 2

P- and S-wave contributions to the $B^0 \to K^{*0}(\to K^+\pi^-)\ell^+\ell^-$ decay

As reviewed in Chapter 1, different observables constructed upon the $B^0 \to K^{*0}(\to K^+\pi^-)\ell^+\ell^-$ decay with the $K^+\pi^-$ system in a P-wave configuration give rise to some of the anomalies observed in semileptonic B-decays, therefore an improved understanding of these transitions is essential to distinguish between the SM and possible NP scenarios. In their experimental analyses, the LHCb collaboration has observed the presence of a large $K^+\pi^-$ S-wave component in $B^0 \to K^{*0}(\to K^+\pi^-)\ell^+\ell^-$ decay [109, 110]. Unfortunately, the lack of reliable $B^0 \to K^+\pi^-$ S-wave form factors implies that the physics potential of this component remains untapped.

In this chapter, based off of Ref. [108], we present the potential of $B^0 \to K^{*0}(\to K^+\pi^-)\ell^+\ell^-$ transitions to search for physics beyond the SM, considering both P- and S-wave contributions to the $K^+\pi^-$ system. Other works studying the impact of the S-wave contribution are Refs. [111–118]. A key aspect of our analysis is the identification of the symmetries of the five dimensional decay rate that underpins the complete set of $B^0 \to K^{*0}(\to K^+\pi^-)\ell^+\ell^-$ observables and the relations between them. In particular, we identify new observables related to the interference between the S- and P-wave amplitudes of the $B^0 \to K^+\pi^-$ system, and use the symmetry relations to investigate the potential of S-wave observables as precision probes of NP. We work under the hypothesis of no scalar or tensor NP contributions in our study of the symmetries. In addition, we present a new and robust way to extract information on both NP scenarios and non-perturbative hadronic contributions by studying the common position in dilepton mass squared at which a subset of P- and S-wave observables cross zero.

This chapter is organised as follows. In Section 2.1, we discuss the structure of the differential angular distribution including P- and S-wave contributions. In the case of P-wave observables with massive leptons, we study the sensitivity of previously identified observables to new scalar and pseudoscalar contributions. In the case of the S wave, we define new observables. In Section 2.2 we first perform an analysis of the degrees of freedom required to fully describe the angular distribution, identify the symmetries of the angular distributions and derive a set of relations between P- and S-wave observables that are a consequence of the transformation symmetries of the angular distribution. These relations offer control tests for both experimental and theoretical analyses. Significantly, given the lack of knowledge of S-wave form factors, these relations also enable predictions for some combinations of S-wave observables in terms of P-wave observables. In Section 2.3, the relations are used to obtain the first bounds on the complete set of S-wave observables and the potential to observe NP with some of these observables is discussed. In Section 2.4, a set of P- and S-wave observables that share a zero at the same position in dilepton invariant mass q^2 is highlighted and the resulting information on both NP scenarios and on hadronic effects is discussed. A brief discussion on the precision expected to be achieved experimentally for some of the P- and S-wave observables in the future is presented in Section 2.5. Finally, a summary and conclusions are presented in Section 2.6. Appendix C provides the necessary steps to derive one particularly lengthy relation in the massive case.

2.1 Structure of the differential decay rate: P and S waves

The differential decay rate of the four-body transition $B^0 \to K^+\pi^-\ell^+\ell^-$ receives contributions from the amplitude of the P-wave decay $B^0 \to K^{*0}(\to K^+\pi^-)\ell^+\ell^-$, as well as from the amplitude of the S-wave decay $B^0 \to K_0^*(\to K^+\pi^-)\ell^+\ell^-$, with K_0^* being a broad scalar resonance. The rate can then be decomposed into:

$$\frac{d^5\Gamma}{dq^2\, dm^2_{K\pi}\, d\Omega} = \frac{d^5\Gamma_P}{dq^2\, dm^2_{K\pi}\, d\Omega} + \frac{d^5\Gamma_S}{dq^2\, dm^2_{K\pi}\, d\Omega} \tag{2.1}$$

where $d\Omega = d\cos\theta_\ell d\cos\theta_K d\phi$ and Γ_P contains the pure P-wave contribution and Γ_S contains the contributions from pure S-wave exchange, as well as from S-P interference. Here, q^2 denotes the square of the invariant mass of the lepton pair and $m_{K\pi}$ the invariant mass of the $K\pi$ system. The angles θ_ℓ, θ_K describe the relative directions of flight of the final-state particles, while ϕ is the angle between the dilepton and the dimeson plane (see Ref. [28] for definitions). The differential rate for a $\bar{B}^0$ decay to a final state in the P-wave configuration is

$$\begin{aligned}\frac{d^5\Gamma_P}{dq^2\, dm^2_{K\pi}\, d\Omega} = \frac{9}{32\pi}\big[&J_{1s}\sin^2\theta_K + J_{1c}\cos^2\theta_K + J_{2s}\sin^2\theta_K\cos 2\theta_\ell \\ &+J_{2c}\cos^2\theta_K\cos 2\theta_\ell + J_3\sin^2\theta_K\sin^2\theta_\ell\cos 2\phi \\ &+J_4\sin 2\theta_K\sin 2\theta_\ell\cos\phi + J_5\sin 2\theta_K\sin\theta_\ell\cos\phi \\ &+J_{6s}\sin^2\theta_K\cos\theta_\ell + J_{6c}\cos^2\theta_K\cos\theta_\ell \\ &+J_7\sin 2\theta_K\sin\theta_\ell\sin\phi + J_8\sin 2\theta_K\sin 2\theta_\ell\sin\phi \\ &+J_9\sin^2\theta_K\sin^2\theta_\ell\sin 2\phi\big] \times |BW_P(m_{K\pi})|^2,\end{aligned} \tag{2.2}$$

with a similar form for the B^0 rate. The $m_{K\pi}$ dependence, denoted by $BW_P(m_{K\pi})$, can be modelled by a relativistic Breit-Wigner amplitude describing the K^{*0} resonance, including the apposite angular momentum and phase-space factors. The Breit-Wigner amplitude is normalized such that the integral of the modulus squared of the amplitude over the $m_{K\pi}$ region of the analysis is one. For the exact form of the Breit-Wigner functions $BW_i(m_{K\pi})$ for $i = P, S$ we refer the reader to Ref. [111]. Notice that Eq. (2.2) differs from the angular distribution in Eq. (1.14) by this factor $BW_P(m_{K\pi})$, which was not present in the discussion in Chapter 1 since there we considered the narrow-width approximation approach for the $K\pi$ system.

The differential rate of the S-wave final state configuration is

$$\begin{aligned}\frac{d^5\Gamma_S}{dq^2\, dm^2_{K\pi}\, d\Omega} = +\frac{1}{4\pi}\Big[&(\tilde{J}^c_{1a} + \tilde{J}^c_{2a}\cos 2\theta_\ell)|BW_S(m_{K\pi})|^2 \\ &+\tilde{J}^c_{1b}\cos\theta_K + \tilde{J}^c_{2b}\cos 2\theta_\ell\cos\theta_K \\ &+\tilde{J}_4\sin 2\theta_l\sin\theta_K\cos\phi + \tilde{J}_5\sin\theta_l\sin\theta_K\cos\phi \\ &+\tilde{J}_7\sin\theta_l\sin\theta_K\sin\phi + \tilde{J}_8\sin 2\theta_l\sin\theta_K\sin\phi\Big]\,.\end{aligned} \tag{2.3}$$

The coefficients J_i, $\tilde{J}^c_{1a}$ and $\tilde{J}^c_{2a}$ are functions of q^2. Those for the S-P interference, $\tilde{J}^c_{1b}$, $\tilde{J}^c_{2b}$ and $\tilde{J}_{4-8}$ depend on both q^2 and $m_{K\pi}$. The $m_{K\pi}$ amplitude for the S wave, $BW_S(m_{K\pi})$ may be described with the LASS parameterisation [119, 120]. Similarly to the P wave, the S-wave $m_{K\pi}$-amplitude is normalized such that the integral of the modulus squared of the amplitude over the analyzed $m_{K\pi}$ range is one.

If not explicitly stated otherwise, we will not consider the presence of scalar or tensor contributions in the following (this implies, in particular, that J_{6c} in Eq. (2.2) is taken to be zero). The decays $B^0 \to K^{*0}\ell^+\ell^-$ and $B^0 \to K_0^*\ell^+\ell^-$ are described by seven complex amplitudes $A^{L,R}_{\parallel,\perp,0}$, A_t

and three complex amplitudes $A_0^{\prime L,R}$, $A_t^\prime$, respectively, where the upper index L, R refers to the chirality of the outgoing lepton current, while in the case of the P-wave the lower index $\parallel, \perp, 0$ indicates the transversity amplitude of the K^*-meson.

Since the distribution is summed over the spins of the leptons, the observables J_i and $\tilde{J}_i$ are described in terms of spin-summed squared amplitudes of the form $A_i^{L*}A_j^L \pm A_i^{R*}A_j^R$. This structure suggests that the amplitudes can be arranged in a set of two-component complex vectors:

$$n_\parallel = \begin{pmatrix} A_\parallel^L \\ A_\parallel^{R*} \end{pmatrix}, \quad n_\perp = \begin{pmatrix} A_\perp^L \\ -A_\perp^{R*} \end{pmatrix}, \quad n_0 = \begin{pmatrix} A_0^L \\ A_0^{R*} \end{pmatrix}, \quad n_S = \begin{pmatrix} A_0^{\prime L} \\ A_0^{\prime R*} \end{pmatrix}, \quad n_S^\prime = \begin{pmatrix} A_0^{\prime L} \\ -A_0^{\prime R*} \end{pmatrix}. \tag{2.4}$$

Two vectors are needed to parametrize the L and R components of the $A_0^\prime$ amplitude, and the A_t and $A_t^\prime$ amplitudes are not expressed in terms of two-complex vectors. Except for the lepton mass terms that mix the L and R components and include the A_t (or $A_t^\prime$) amplitudes, one can express the coefficients of the distribution in terms of these vectors. The expression for the coefficients in the P-wave terms can be found in Eqs. (1.17)-(1.24). For the S-wave terms we find

$$\tilde{J}_{1a}^c = \frac{3}{8}\left[|A_0^{\prime L}|^2 + |A_0^{\prime R}|^2 + (1-\beta^2)\left(|A_t^\prime|^2 + 2\mathrm{Re}\left[A_0^{\prime L}A_0^{\prime R*}\right]\right)\right] \tag{2.5}$$

$$\tilde{J}_{2a}^c = -\frac{3}{8}\beta^2\left(|A_0^{\prime L}|^2 + |A_0^{\prime R}|^2\right) = -\frac{3}{8}\beta^2|n_S|^2. \tag{2.6}$$

Similarly for the P-S (real) interference terms

$$\begin{aligned}\tilde{J}_{1b}^c &= \frac{3}{4}\sqrt{3}\mathrm{Re}\left[\left(A_0^{\prime L}A_0^{L*} + A_0^{\prime R}A_0^{R*} + (1-\beta^2)\left(A_0^{\prime L}A_0^{R*} + A_0^L A_0^{\prime R*} + A_t^\prime A_t^*\right)\right)BW_S BW_P^*\right] \\ &= \tilde{J}_{1b}^{c,r}\mathrm{Re}(BW_S BW_P^*) - \tilde{J}_{1b}^{c,i}\mathrm{Im}(BW_S BW_P^*)\end{aligned} \tag{2.7}$$

$$\begin{aligned}\tilde{J}_{2b}^c &= -\frac{3}{4}\sqrt{3}\beta^2\mathrm{Re}\left[\left(A_0^{\prime L}A_0^{L*} + A_0^{\prime R}A_0^{R*}\right)BW_S BW_P^*\right] \\ &= \tilde{J}_{2b}^{c,r}\mathrm{Re}(BW_S BW_P^*) - \tilde{J}_{2b}^{c,i}\mathrm{Im}(BW_S BW_P^*)\end{aligned} \tag{2.8}$$

$$\begin{aligned}\tilde{J}_4 &= \frac{3}{4}\sqrt{\frac{3}{2}}\beta^2\mathrm{Re}\left[(A_0^{\prime L}A_\parallel^{L*} + A_0^{\prime R}A_\parallel^{R*})BW_S BW_P^*\right] \\ &= \tilde{J}_4^r\mathrm{Re}(BW_S BW_P^*) - \tilde{J}_4^i\mathrm{Im}(BW_S BW_P^*)\end{aligned} \tag{2.9}$$

$$\begin{aligned}\tilde{J}_5 &= \frac{3}{2}\sqrt{\frac{3}{2}}\beta\mathrm{Re}\left[(A_0^{\prime L}A_\perp^{L*} - A_0^{\prime R}A_\perp^{R*})BW_S BW_P^*\right] \\ &= \tilde{J}_5^r\mathrm{Re}(BW_S BW_P^*) - \tilde{J}_5^i\mathrm{Im}(BW_S BW_P^*)\end{aligned} \tag{2.10}$$

and finally for the P-S (imaginary) interference terms

$$\begin{aligned}\tilde{J}_7 &= \frac{3}{2}\sqrt{\frac{3}{2}}\beta\mathrm{Im}\left[(A_0^{\prime L}A_\parallel^{L*} - A_0^{\prime R}A_\parallel^{R*})BW_S BW_P^*\right] \\ &= \tilde{J}_7^r\mathrm{Im}(BW_S BW_P^*) + \tilde{J}_7^i\mathrm{Re}(BW_S BW_P^*)\end{aligned} \tag{2.11}$$

$$\begin{aligned}\tilde{J}_8 &= \frac{3}{4}\sqrt{\frac{3}{2}}\beta^2\mathrm{Im}\left[(A_0^{\prime L}A_\perp^{L*} + A_0^{\prime R}A_\perp^{R*})BW_S BW_P^*\right] \\ &= \tilde{J}_8^r\mathrm{Im}(BW_S BW_P^*) + \tilde{J}_8^i\mathrm{Re}(BW_S BW_P^*),\end{aligned} \tag{2.12}$$

where $\beta = \sqrt{1 - 4m_\ell^2/q^2}$ and the superscript indices r and i (here and for the rest of the chapter) refer to the real and imaginary parts of the bilinears, respectively.

The form of the differential decay rate given through Eqs. (2.2), (2.3), (2.9), (2.11) assumes that the q^2 and $m_{K\pi}$ dependence of the $B^0 \to K^+\pi^-$ form factor can be factorized [111, 112, 121]. The breaking of this factorization, as presented for instance in the analysis of generalized S-wave $B^0 \to K^+\pi^-$ form factors in Ref. [116], may be tested through the validity of the symmetry relations between the observables derived in Section 2.2.

The study of the S-wave observables presented here is the first to consider the complete set of observables that arise when the decay rate is written differentially with respect to $m_{K\pi}$. As a consequence, the interference between the S-P-wave $m_{K\pi}$ lineshapes projects out additional bilinear combinations of S- and P-wave amplitudes, giving rise to the 12 new observables $\tilde{J}_i^{r,i}$ in Eqs. (2.9) and (2.11). Previous studies, such as those of Ref. [122], only considered the differential decay rate integrated over $m_{K\pi}$. In this case one obtains the six well-known S-P interference observables $\tilde{J}_i$ that can be described by a single two-dimensional S-wave amplitude vector n_S, without the need for n'_S. Concerning possible contributions from D- and higher partial waves, in Ref. [113] the authors considered the role of such terms and concluded that S+P+D contributions correct S+P at the few permille level, beyond the expected precision at any near-future facility.

2.1.1 P-wave massive observables

The so-called optimized observables are designed to reduce form factor uncertainties. The set of such observables that describes the P-wave $K\pi$ system has been discussed at length in a series of papers [11, 12, 22] and quoted in Eq. (1.47). However, due to improvements in experimental precision, there is increasingly sensitivity to observables that are suppressed by factors of the lepton mass. For the optimized observables, P_i, the impact that lepton masses have in the very low q^2 region via the kinematical prefactor β is well known.

Our interest here is to explore two further optimized observables M_1 and M_2, introduced in Ref. [11], that can be neglected in the massless limit. These observables are defined in terms of the coefficients of the distribution as follows[1]:

$$M_1 = \frac{J_{1s}}{3J_{2s}} \qquad M_2 = -\frac{J_{1c}}{J_{2c}}. \tag{2.13}$$

For this specific type of observable it makes sense to explore the impact from NP scalar and pseudoscalar contributions. Therefore, we will relax in this section the hypothesis of no scalar or pseudoscalar contributions.

Even considering a large set of NP scenarios, the observable M_1 is found to be practically insensitive to NP and is not analyzed further. By contrast, M_2 can potentially provide information on scalar and/or pseudoscalar NP scenarios. In order to explore reasonable values of (pseudo)scalar contributions, we constrain the range for the coefficients $\mathcal{C}_{P,S}$ by considering only those values allowed by the experimental measurement of $\mathcal{B}(B_s \to \mu\mu)$. Thus, we write the following ratio [123], which is used to define the 1σ region from $\mathcal{B}^{\rm exp}(B_s \to \mu\mu)$:

$$R_{B_s\to\mu\mu} = \frac{\mathcal{B}^{\rm exp}(B_s \to \mu\mu)}{\mathcal{B}^{\rm SM}(B_s \to \mu\mu)} = |S|^2 + |P|^2\,, \tag{2.14}$$

[1] In order to make the comparison with experimental prospects easier, in this work we have slightly changed the definition of $M_{1,2}$ by removing the constant terms appearing in Ref. [11].

where the quantities S, P[2] contain the different NP contributions and are given by:

$$S = \sqrt{1 - 4\frac{m_\mu^2}{m_{B_s}^2}}\,\frac{m_{B_s}^2}{2m_b m_\mu}\left(\frac{\mathcal{C}_S - \mathcal{C}_{S'}}{\mathcal{C}_{10\mu}^{\rm SM}}\right), \tag{2.15}$$

$$P = \frac{\mathcal{C}_{10\mu}^{\rm SM} + \mathcal{C}_{10\mu}^{\rm NP} - \mathcal{C}_{10'\mu}}{\mathcal{C}_{10\mu}^{\rm SM}} + \frac{m_{B_s}^2}{2m_b m_\mu}\left(\frac{\mathcal{C}_P - \mathcal{C}_{P'}}{\mathcal{C}_{10\mu}^{\rm SM}}\right). \tag{2.16}$$

Fig. 2.1 shows the allowed region for S and P once the latest experimental value for $\mathcal{B}(B_s \to \mu\mu) = (2.85 \pm 0.34)$ [68] is included, corresponding to $R_{B_s\to\mu\mu} = (0.78 \pm 0.10)$. In this analysis we have not allowed for the presence of right-handed currents.

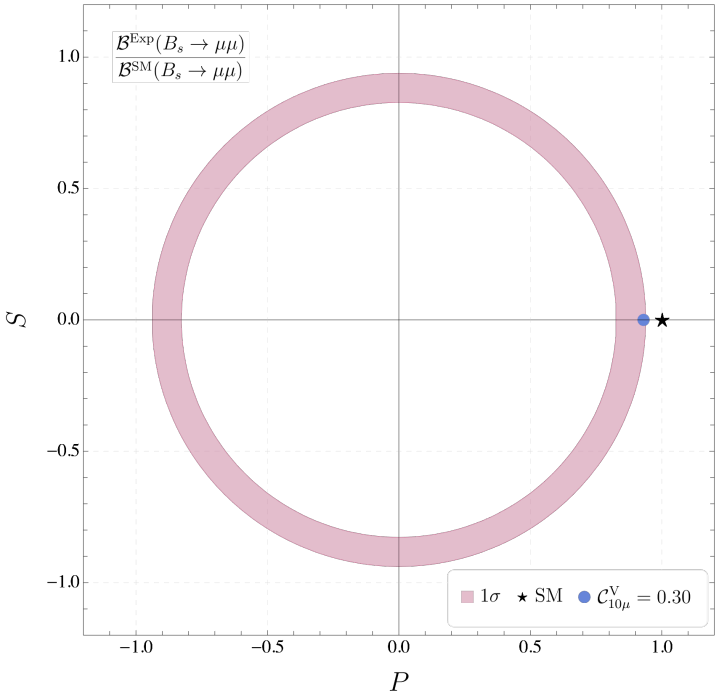

Figure 2.1: Region of allowed values for S, P that fulfill the condition $|R_{B_s\to\mu\mu}^{\rm SM} - R_{B_s\to\mu\mu}^{\rm NP}| \leq 0.10$. In order to illustrate the sensitivity of this observable to NP contributions, we display its value in the SM (black star) and in one of the favoured scenario from Ref. [4] (blue dot): $\{\mathcal{C}_{9\mu}^{\rm V} = -\mathcal{C}_{10\mu}^{\rm V} = -0.34, \mathcal{C}_9^{\rm U} = -0.82\}$. Only the dependence on $\mathcal{C}_{10\mu}$ is displayed in the plot. The tiny difference of this scenario with the SM illustrates that M_2 is an observable with low sensitivity to the preferred scenarios of present global fits. For this reason we explore its sensitivity under other types of NP, namely scalars and pseudoscalars.

We perform an analysis of the behaviour of the observable M_2 under different hypotheses for (pseudo)scalar NP contributions that are compatible with Fig. 2.1. The case $S = 0, P = 1$ corresponds to the SM, as can be seen from Eqs. (2.15) and (2.16). We consider three other possible scenarios, corresponding to maximal values of S, P:

i) $S = \pm 0.94, P = 0$,

ii) $S = P = 0.66$,

iii) $S = 0, P = -0.94$.

[2]Not to be confused with the P- and S-wave components of the decay, this S, P refer to Scalar and Pseudoscalar NP contributions entering $R_{B_s\to\mu\mu}$. The latter includes the SM axial-vector contribution.

These three benchmark cases are: i) only a scalar contribution (with two possible signs) and no pseudoscalar NP, ii) both S and P contributions present and equal in magnitude and iii) the opposite sign of the SM case with a negative pseudoscalar contribution. Fig. 2.2 shows the theoretical prediction of the large- and low-recoil bins of M_2 in the four scenarios mentioned above.

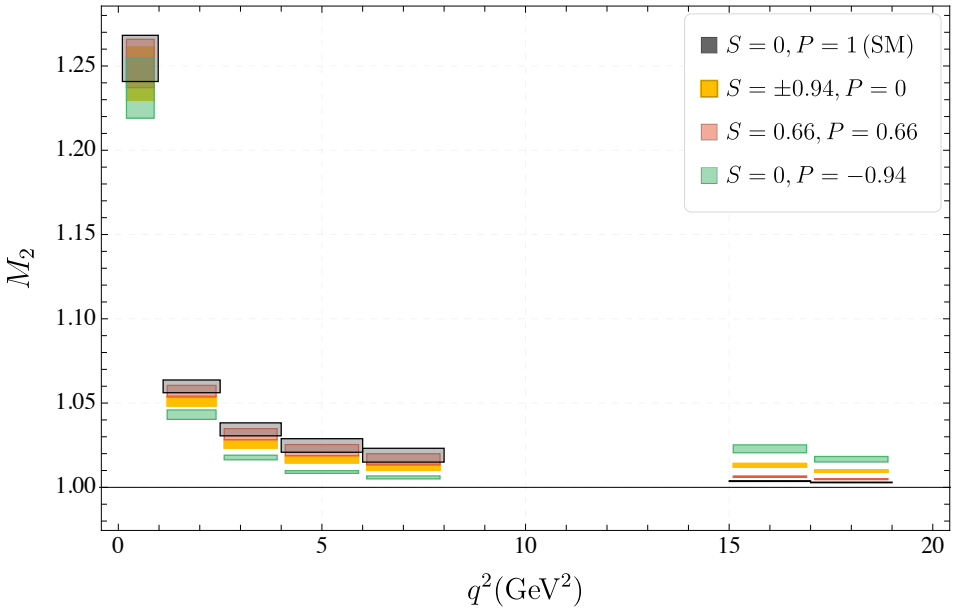

Figure 2.2: Binned theoretical predictions for M_2 in the SM and in selected NP scenarios including pseudoscalar and scalar contributions.

It is evident from Fig. 2.2 that the rather small sensitivity of M_2 to (pseudo)scalar contributions makes it difficult to get a significant distinction between the different scenarios. This is especially the case in the very low q^2 region, where the uncertainties associated with the theoretical prediction of this observable are larger. Only for the $S = 0, P = -0.94$ scenario in the large-recoil region is a clean separation between hypotheses possible, given suitably high precision measurements. The situation is somewhat better in the low-recoil q^2 region, where the theoretical errors are smaller but an even higher experimental resolution will be required. The experimental prospects for such a separation of NP hypotheses is outlined in Section 2.5.

2.1.2 Definition of S-wave observables: massless and massive case

In this section we define the list of S-wave observables that can be constructed using the coefficients of the distribution. They follow from the previous section including P and S waves in the massless case but also taking into account lepton mass terms. The S-wave observables that were mostly treated as nuisance parameters thus far will become an interesting target for future experimental analyses.

Our goal here will be to define the S-wave observables but it is beyond the scope of this thesis to provide SM predictions and enter into a discussion of the form factors or other hadronic uncertainties. Our first interest is to determine how many of the observables are genuinely independent. The question of the number of degrees of freedom is critical for the stability of experimental fits and is discussed further in Section 2.2.

As discussed in Section 2.1, the new S-P interference observables defined in Eqs. (2.9) and (2.11), can be defined in terms of the vectors in Eq. (2.4) as follows:

$$\begin{aligned}
S^r_{S1} &= -\frac{3}{4}\sqrt{3}\frac{1}{\Gamma'}\beta^2\mathrm{Re}(n_0^\dagger\, n_S) + CP, & S^i_{S1} &= -\frac{3}{4}\sqrt{3}\frac{1}{\Gamma'}\beta^2\mathrm{Im}(n_0^\dagger\, n'_S) + CP,\\
S^r_{S2} &= \frac{3}{4}\sqrt{\frac{3}{2}}\frac{1}{\Gamma'}\beta^2\mathrm{Re}(n_\parallel^\dagger\, n_S) + CP, & S^i_{S2} &= \frac{3}{4}\sqrt{\frac{3}{2}}\frac{1}{\Gamma'}\beta^2\mathrm{Im}(n_\parallel^\dagger n'_S) + CP,\\
S^r_{S3} &= \frac{3}{2}\sqrt{\frac{3}{2}}\frac{1}{\Gamma'}\beta\mathrm{Re}(n_\perp^\dagger\, n_S) + CP, & S^i_{S3} &= \frac{3}{2}\sqrt{\frac{3}{2}}\frac{1}{\Gamma'}\beta\mathrm{Im}(n_\perp^\dagger n'_S) + CP,\\
S^r_{S4} &= \frac{3}{2}\sqrt{\frac{3}{2}}\frac{1}{\Gamma'}\beta\mathrm{Re}(n_\parallel^\dagger n'_S) + CP, & S^i_{S4} &= \frac{3}{2}\sqrt{\frac{3}{2}}\frac{1}{\Gamma'}\beta\mathrm{Im}(n_\parallel^\dagger n_S) + CP,\\
S^r_{S5} &= \frac{3}{4}\sqrt{\frac{3}{2}}\frac{1}{\Gamma'}\beta^2\mathrm{Re}(n_\perp^\dagger n'_S) + CP, & S^i_{S5} &= \frac{3}{4}\sqrt{\frac{3}{2}}\frac{1}{\Gamma'}\beta^2\mathrm{Im}(n_\perp^\dagger\, n_S) + CP,
\end{aligned} \tag{2.17}$$

where

$$\begin{aligned}
\Gamma' &= \Gamma'_P + \Gamma'_S + CP\\
\Gamma'_P &= \frac{3}{4}(2J_{1s} + J_{1c}) - \frac{1}{4}(2J_{2s} + J_{2c}) + CP\\
\Gamma'_S &= 2\tilde{J}^c_{1a} - \frac{2}{3}\tilde{J}^c_{2a} + CP.
\end{aligned} \tag{2.18}$$

Here the prime stands for the differential distribution. Note that once we include lepton mass terms, F_S should be extracted from $\tilde{J}^c_{2a}$ and not from the combination with $\tilde{J}^c_{1a}$ such that:

$$F_S = \frac{|n_S^\dagger n_S|}{\Gamma'} = -\frac{8}{3\beta^2}\frac{\tilde{J}^c_{2a}}{\Gamma'}. \tag{2.19}$$

In order not to overload excessively the notation it should be understood that in Eqs.(2.19-2.28) each explicit J or $\tilde{J}$ is accompanied by its CP-conjugate partner. In the case that B^0 and $\bar{B}^0$ decays were experimentally separated, a set of CP-asymmetries corresponding to each J and $\tilde{J}$ observable would also become accessible.

In terms of these observables, the angular distribution in the massless limit (taking $\beta \to 1$ in Eq. (2.17)) is given by:

$$\begin{aligned}
\frac{1}{\mathrm{d}(\Gamma+\bar{\Gamma})/\mathrm{d}q^2}\left.\frac{\mathrm{d}^4(\Gamma+\bar{\Gamma})}{\mathrm{d}q^2\,\mathrm{d}\vec{\Omega}}\right|_{\mathrm{S+P}} &= (1-F_\mathrm{S})|BW_P|^2\,\frac{1}{\mathrm{d}(\Gamma+\bar{\Gamma})/\mathrm{d}q^2}\left.\frac{\mathrm{d}^4(\Gamma+\bar{\Gamma})}{\mathrm{d}q^2\,\mathrm{d}\vec{\Omega}}\right|_{\mathrm{P}} +\\
&+\frac{1}{4\pi}\left[\frac{3}{4}F_\mathrm{S}|BW_S|^2\sin^2\theta_\ell\right.\\
&-2[S^r_{S1}\mathrm{Re}(BW_S BW_P^*) - S^i_{S1}\mathrm{Im}(BW_S BW_P^*)]\sin^2\theta_\ell\cos\theta_K\\
&+[S^r_{S2}\mathrm{Re}(BW_S BW_P^*) - S^i_{S2}\mathrm{Im}(BW_S BW_P^*)]\sin 2\theta_\ell\sin\theta_K\cos\phi\\
&+[S^r_{S3}\mathrm{Re}(BW_S BW_P^*) - S^i_{S3}\mathrm{Im}(BW_S BW_P^*)]\sin\theta_\ell\sin\theta_K\cos\phi\\
&+[S^r_{S4}\mathrm{Im}(BW_S BW_P^*) + S^i_{S4}\mathrm{Re}(BW_S BW_P^*)]\sin\theta_\ell\sin\theta_K\sin\phi\\
&\left.+[S^r_{S5}\mathrm{Im}(BW_S BW_P^*) + S^i_{S5}\mathrm{Re}(BW_S BW_P^*)]\sin 2\theta_\ell\sin\theta_K\sin\phi\right].
\end{aligned} \tag{2.20}$$

The corresponding angular distribution in the massive case can be obtained from Eq. (2.3) using optimized S-wave observables and mass terms defined by:

$$M_3' = \frac{-\beta^2 \tilde{J}^c_{1a} - \tilde{J}^c_{2a}}{\tilde{J}^c_{2a}}, \tag{2.21}$$

together with the extra S-P interference massive optimized terms:

$$\begin{aligned} M_4' &= \frac{-\beta^2 \tilde{J}^{c,r}_{1b} - \tilde{J}^{c,r}_{2b}}{\sqrt{J_{2c}\tilde{J}^c_{2a}}}, \\ M_5' &= \frac{-\beta^2 \tilde{J}^{c,i}_{1b} - \tilde{J}^{c,i}_{2b}}{\sqrt{J_{2c}\tilde{J}^c_{2a}}}. \end{aligned} \tag{2.22}$$

Then the massive distribution becomes:

$$\begin{aligned} \frac{1}{\mathrm{d}(\Gamma+\bar{\Gamma})/\mathrm{d}q^2} \frac{\mathrm{d}^4(\Gamma+\bar{\Gamma})}{\mathrm{d}q^2\,\mathrm{d}\vec{\Omega}}\bigg|_{\mathrm{S+P}} &= (1-F_S')|BW_P|^2 \frac{1}{\mathrm{d}(\Gamma+\bar{\Gamma})/\mathrm{d}q^2} \frac{\mathrm{d}^4(\Gamma+\bar{\Gamma})}{\mathrm{d}q^2\,\mathrm{d}\vec{\Omega}}\bigg|_{\mathrm{P}} + \\ &+ \frac{1}{4\pi}\left[\left(\frac{3}{8}F_S(1+M_3') - \frac{3}{8}\beta^2 F_S\cos 2\theta_l\right)|BW_S|^2\right. \\ &+ \left(-\frac{1}{\beta^2}(S^r_{S1}+M_4'N_L)\mathrm{Re}(BW_S BW_P^*)\right. \\ &\left.\left. + \frac{1}{\beta^2}(S^i_{S1}+M_5'N_L)\mathrm{Im}(BW_S BW_P^*)\right)\cos\theta_K\right. \\ &+ [S^r_{S1}\mathrm{Re}(BW_S BW_P^*) - S^i_{S1}\mathrm{Im}(BW_S BW_P^*)]\cos 2\theta_l\cos\theta_K \\ &+ [S^r_{S2}\mathrm{Re}(BW_S BW_P^*) - S^i_{S2}\mathrm{Im}(BW_S BW_P^*)]\sin 2\theta_l\sin\theta_K\cos\phi \\ &+ [S^r_{S3}\mathrm{Re}(BW_S BW_P^*) - S^i_{S3}\mathrm{Im}(BW_S BW_P^*)]\sin\theta_l\sin\theta_K\cos\phi \\ &+ [S^r_{S4}\mathrm{Im}(BW_S BW_P^*) + S^i_{S4}\mathrm{Re}(BW_S BW_P^*)]\sin\theta_l\sin\theta_K\sin\phi \\ &\left.+ [S^r_{S5}\mathrm{Im}(BW_S BW_P^*) + S^i_{S5}\mathrm{Re}(BW_S BW_P^*)]\sin 2\theta_l\sin\theta_K\sin\phi\right]. \end{aligned} \tag{2.23}$$

We define

$$\begin{aligned} N_L &= \sqrt{J_{2c}\tilde{J}^c_{2a}} = \frac{1}{2}\sqrt{\frac{3}{2}}\beta^2\Gamma'\sqrt{(1-F_S')F_S F_L} \\ N_T &= \sqrt{-J_{2s}\tilde{J}^c_{2a}} = \frac{1}{4}\sqrt{\frac{3}{2}}\beta^2\Gamma'\sqrt{(1-F_S')F_S F_T} \end{aligned} \tag{2.24}$$

and

$$F_S' = \frac{\Gamma_S'}{\Gamma'} = F_S - \epsilon_S \qquad \epsilon_S = \frac{1}{4}F_S(1-\beta^2-3M_3'). \tag{2.25}$$

Notice that in the massless limit ($M_i^{(\prime)} \to 0$, $\beta \to 1$) Eq. (2.23) reduces to Eq. (2.20).

Finally, in order to write the whole distribution with massive terms and optimized observables, the substitution:

$$S^{r/i}_{S1} \to PS^{r/i}_1 \frac{N_L}{\Gamma'} \quad S^{r/i}_{S2-S5} \to PS^{r/i}_{2-5} \frac{N_T}{\Gamma'} \tag{2.26}$$

is needed, where the optimized observables for the interference terms in all q^2 bins are

$$PS^{r/i}_1 = \frac{\tilde{J}^{c,r/i}_{2b}}{\sqrt{J_{2c}\tilde{J}^c_{2a}}}, \quad PS^{r/i}_{2-5} = \frac{\tilde{J}^{r/i}_{4-8}}{\sqrt{-J_{2s}\tilde{J}^c_{2a}}}\,. \tag{2.27}$$

Using the expressions[3]

$$\begin{aligned} J_{2s} &= \frac{1}{4}N_1, \quad J_{2c} = -N_2, \quad J_3 = \frac{1}{2}P_1 N_1, \quad J_4 = \frac{1}{2}P'_4 N_3, \quad J_5 = P'_5 N_3, \\ J_{6s} &= 2P_2 N_1, \quad J_7 = -P'_6 N_3, \quad J_8 = -\frac{1}{2}P'_8 N_3, \quad J_9 = -P_3 N_1, \end{aligned} \tag{2.28}$$

where $N_{1,2} = \beta^2 F_{T,L}\Gamma'_P$, $N_3 = \beta^2\sqrt{F_T F_L}\Gamma'_P$ (and the addition of the CP conjugate in Γ'_P is implicit) and including the definitions of $M_{1,2}$, one finds:

$$\begin{aligned} \frac{1}{\mathrm{d}(\Gamma+\bar{\Gamma})/\mathrm{d}q^2}\frac{\mathrm{d}^4(\Gamma+\bar{\Gamma})}{\mathrm{d}q^2\,\mathrm{d}\vec{\Omega}}\bigg|_{\mathrm{P}} = \frac{9}{32\pi}\Bigg[&\frac{3}{4}\hat{F}_T M_1 \sin^2\theta_K + \hat{F}_L M_2 \cos^2\theta_K + \left(\frac{1}{4}\hat{F}_T \sin^2\theta_K - \hat{F}_L\cos^2\theta_K\right)\cos 2\theta_l \\ &+ \frac{1}{2}P_1\hat{F}_T \sin^2\theta_K \sin^2\theta_l \cos 2\phi + \sqrt{\hat{F}_T\hat{F}_L}\Bigg(\frac{1}{2}P'_4 \sin 2\theta_K \sin 2\theta_l \cos\phi \\ &+ P'_5 \sin 2\theta_K \sin\theta_l \cos\phi\Bigg) + 2P_2\hat{F}_T \sin^2\theta_K \cos\theta_l \\ &- \sqrt{\hat{F}_T\hat{F}_L}\left(P'_6 \sin 2\theta_K \sin\theta_l \sin\phi + \frac{1}{2}P'_8 \sin 2\theta_K \sin 2\theta_l \sin\phi\right) \\ &- P_3\hat{F}_T \sin^2\theta_K \sin^2\theta_l \sin 2\phi\Bigg]\,. \end{aligned} \tag{2.29}$$

where a global pre-factor β^2 has been absorbed inside the re-definition $\hat{F}_{T,L} = \beta^2 F_{T,L}$.

2.2 Symmetries of the distribution

In this section we present the explicit form of the symmetry transformations of the amplitudes that leave the full distribution (including P and S wave) invariant, and obtain explicitly the relations among the observables. The massless and the massive cases are discussed separately.

The number of symmetries of the distribution is determined by performing an infinitesimal transformation $\vec{A}' = \vec{A} + \vec{\delta}$, where $\vec{A}$ is a vector collecting the real and imaginary parts of all the amplitudes entering the distribution (the vector $\vec{A}$ depends on whether the massless or massive hypothesis is taken), and the condition to be a symmetry is that the vector $\vec{\delta}$ is perpendicular to the hyperplane spanned by the set of gradient vectors:

$$\forall i \in J_i, \tilde{J}_i : \vec{\nabla}_i \perp \vec{\delta}\,. \tag{2.30}$$

The gradients are defined then by the derivatives of the coefficients with respect to the real and imaginary parts of all the amplitudes. The difference between the dimension of the hyperplane that the gradient vectors span if they are all independent (equal to the number of coefficients of the distribution) and

[3] One may add to this list another observable, related to the presence of scalars, associated with the coefficient J_{6c}. Given that in the present paper we only allow for scalars when analyzing the observable M_2, we direct the reader to Ref. [11], where this case is discussed.

the dimension of the hyperplane that they effectively span tells us the number of relations among the coefficients that exist. By relations we will refer only to non-trivial relations. We will discuss these relations in the following subsections. For completeness, we first find explicitly the form of the continuous symmetries.

In Ref. [11], the massless and massive symmetries were discussed for the P wave. There it was found that, in the massless case, four symmetries (two phase transformations for the left and right components and two "angle rotations") leave the P-wave part of the distribution invariant. Alternatively, using the vectors n_i we can implement the four symmetry transformations by means of a 2×2 unitary matrix, i.e, $n'_i = U n_i$ with $i = \perp, \parallel, 0$. However, the inclusion of the S wave that requires two different vectors n_S and n'_S breaks two of the symmetries[4] and only the two independent phase transformations survive, i.e.,

$$A_i^L \to e^{i\phi_L} A_i^L, \qquad A_0'^L \to e^{i\phi_L} A_0'^L, \qquad A_i^R \to e^{i\phi_R} A_i^R, \qquad A_0'^R \to e^{i\phi_R} A_0'^R \tag{2.31}$$

with $i = 0, \perp, \parallel$.

The massive case is relatively similar and again only two phase transformations survive. However, the existence of interference terms between left and right components fixes $\phi_L = \phi_R = \phi$, but this is compensated by the independent transformation of the extra amplitudes $A_t^{(\prime)}$:

$$\begin{aligned} A_i^L &\to e^{i\phi} A_i^L, & A_i^R &\to e^{i\phi} A_i^R, \\ A_0'^L &\to e^{i\phi} A_0'^L, & A_0'^R &\to e^{i\phi} A_0'^R \\ A_t &\to e^{i\varphi} A_t, & A_t' &\to e^{i\varphi} A_t' \end{aligned} \tag{2.32}$$

with $i = 0, \perp, \parallel$[5] .

2.2.1 Counting degrees of freedom: massive and massless cases

One important question is how many degrees of freedom there are or, in other words, how many observables in the set discussed in Section 2.1.2 are independent. The number of independent observables to fully describe the distribution depends on whether massless or massive leptons are considered. We again work under the hypothesis that there are no scalar contributions but pseudoscalar ones are allowed in the massive case.

The number of observables that can be constructed out of the complex amplitudes is given by:

$$n_{obs} = 2n_A - n_{sym}\,. \tag{2.33}$$

Each symmetry transformation of the amplitudes that leaves the distribution invariant reduces the number of independent observables.

In the following, we determine the number of relations for the massless and massive case and consequently the number of independent observables required to have a full description of the corresponding distribution.

Massless case:

Assuming the absence of scalars, we have 11 coefficients for the P-wave and 14 coefficients for the S-wave distribution. Under the approximation of negligible lepton masses, there are two trivial relations for the P-wave coefficients:

$$J_{1s} = 3J_{2s} \qquad J_{1c} = -J_{2c} \tag{2.34}$$

and three trivial relations for the S-wave coefficients:

$$\tilde{J}^c_{1a} = -\tilde{J}^c_{2a} \qquad \tilde{J}^{cr}_{1b} = -\tilde{J}^{cr}_{2b} \qquad \tilde{J}^{ci}_{1b} = -\tilde{J}^{ci}_{2b}\,, \tag{2.35}$$

reducing the number of coefficients to $n_c = 20$. The vector $\vec{A}$ in the massless case is given by:

[4] This is easily shown by simply transforming the sum $n_S + n'_S$

[5] Another example of the convenience of using symmetries but in the semileptonic charged-current $b \to c\ell\nu$ transition can be found in Chapter 3, based on Ref. [124].

$$\begin{aligned}\vec{A} \;=\; \Big(&\mathrm{Re}(A_\perp^L),\mathrm{Im}(A_\perp^L),\mathrm{Re}(A_\parallel^L),\mathrm{Im}(A_\parallel^L),\mathrm{Re}(A_0^L),\mathrm{Im}(A_0^L),\mathrm{Re}(A_0^{L\prime}),\mathrm{Im}(A_0^{L\prime}),\\ &\mathrm{Re}(A_\perp^R),\mathrm{Im}(A_\perp^R),\mathrm{Re}(A_\parallel^R),\mathrm{Im}(A_\parallel^R),\mathrm{Re}(A_0^R),\mathrm{Im}(A_0^R),\mathrm{Re}(A_0^{R\prime}),\mathrm{Im}(A_0^{R\prime})\Big)\end{aligned} \tag{2.36}$$

Using Eq. (2.30), we find that the dimension of the space spanned by the gradient vectors (given by the rank of the matrix $M_{ij} = \nabla_i X_j$ with $X = J, \tilde{J}$ and i being the elements of $\vec{A}$ in Eq. (2.36)) is $n_{rank} = 14$. This rank gives the number of independent observables n_{obs}. According to the discussion above, the number of relations fulfills:

$$n_{rel} = n_c - n_{rank}\,. \tag{2.37}$$

Therefore for the massless case $n_{rel} = 6$. There is one well-known relation among the coefficients for the P wave (see Ref. [28, 125]) and five, previously unknown, relations for the S wave. An independent cross check of the rank of the matrix is provided by the fact that the number of degrees of freedom counting amplitudes minus symmetries, or coefficients minus relations should agree. This implies the equation:

$$2n_A - n_{sym} = n_{rank} = n_c - n_{rel}\,. \tag{2.38}$$

The number of complex amplitudes $n_A = 8$ and the number of symmetries of the full distribution (P and S wave) is $n_{sym} = 2$ (see Eq. (2.31)).

The set of 14 independent observables consists of 8 (9 coefficients minus one relation) independent observables for the P wave and 6 (11 coefficients minus 5 relations) independent observables for the S wave. This implies that in the massless case the basis of 20 observables,

$$\begin{aligned}\mathcal{O}_{m_\ell=0} \;=\; \{&\Gamma', F_L, P_1, P_2, P_3, P_4', P_5', P_6', P_8',\\ &F_S, S_{S1}^r, S_{S2}^r, S_{S3}^r, S_{S4}^r, S_{S5}^r, S_{S1}^i, S_{S2}^i, S_{S3}^i, S_{S4}^i, S_{S5}^i\},\end{aligned} \tag{2.39}$$

has some redundancy. Among these 20 observables there are 6 relations leading to only 14 independent observables. The set of 6 massless relations can be obtained from the 6 massive expressions given below, after taking the massless limit. Notice that the seventh relation, given in Appendix C, is exactly zero in the massless limit.

Massive case:

The counting in this case, following the same steps as in the massless case, goes as follows. Our starting point is the same number of coefficients 11 (14) for the P wave (S wave), but now there are no trivial relations, i.e., $n_c = 25$. Here the vector $\vec{A}$ is:

$$\begin{aligned}\vec{A} \;=\; \Big(&\mathrm{Re}(A_\perp^L),\mathrm{Im}(A_\perp^L),\mathrm{Re}(A_\parallel^L),\mathrm{Im}(A_\parallel^L),\mathrm{Re}(A_0^L),\mathrm{Im}(A_0^L),\mathrm{Re}(A_0^{L\prime}),\mathrm{Im}(A_0^{L\prime}),\mathrm{Re}A_t,\mathrm{Im}A_t,\\ &\mathrm{Re}(A_\perp^R),\mathrm{Im}(A_\perp^R),\mathrm{Re}(A_\parallel^R),\mathrm{Im}(A_\parallel^R),\mathrm{Re}(A_0^R),\mathrm{Im}(A_0^R),\mathrm{Re}(A_0^{R\prime}),\mathrm{Im}(A_0^{R\prime}),\mathrm{Re}A_t',\mathrm{Im}A_t'\Big)\,.\end{aligned}$$

Notice that pseudoscalar contributions are included in the amplitude A_t. Evaluating the rank of the corresponding matrix M_{ij}, one finds $n_{rank} = 18$, indicating that in the massive case the number of independent observables is $n_{obs} = 18$. Following Eq. (2.37), one immediately finds that the number of relations should be 7. These relations are discussed and presented in the next subsection.

As in the previous case, we can repeat the counting using the amplitudes that build the observables. The number of complex amplitudes is $n_A = 10$ with the same number of symmetries $n_{sym} = 2$ (see Eq. (2.32)) as in the massless case, such that we confirm that there are 18 independent observables.

The set of 18 independent observables in the massive case consists of 10 (11 coefficients minus one relation) independent observables for the P wave and 8 (14 coefficients minus 6 relations) independent observables for the S wave. The corresponding basis of 25 observables is:

$$\begin{aligned}\mathcal{O}_{m_\ell\neq 0} \;=\; \{&\Gamma', F_L, M_1, M_2, P_1, P_2, P_3, P_4', P_5', P_6', P_8',\\ &F_S, M_3', M_4', M_5', S_{S1}^r, S_{S2}^r, S_{S3}^r, S_{S4}^r, S_{S5}^r, S_{S1}^i, S_{S2}^i, S_{S3}^i, S_{S4}^i, S_{S5}^i\}\,. \end{aligned} \tag{2.40}$$

Therefore, among this set of 25 observables there are 7 relations and only 18 observables are independent.

2.2.2 P-wave and S-wave symmetry relations among observables

In this subsection we present for the first time the full set of symmetry relations of the P and S wave in the massive case. These complete the previous partial results given in Refs. [11, 28, 122, 125]. It is helpful to express the observables J_i and $\tilde{J}_i$ in terms of scalar products $n_i^\dagger n_j$, as shown in Eq. (2.17). All the relations found in this section are functions of J_i and $\tilde{J}_i$ and an equivalent set of relations in terms of the CP-conjugate partners $\bar{J}_i$ and $\bar{\tilde{J}}_i$ can be written. However, the observables are functions of the coefficients and their CP partners. This means that when writing one of these relations in terms of observables the substitution $J_j \to aP_i$ is strictly speaking $J_j \to a(P_i + P_i^{CP})/2$ (with a being some normalization factor). The observable P_i^{CP} is the CP asymmetry associated with the observable P_i, defined in Ref. [12, 125], and similarly for $\tilde{J}_i$. For the following analysis and for simplicity, we will neglect the CP asymmetries for both the P and S wave. This is a very good approximation, given that such asymmetries are tiny both in the SM and in presence of NP models that do not have large NP phases.

Following the strategy in Ref. [122], we exploit the fact that a couple of n_i vectors (with $i = \perp, \parallel, 0, S$ or $i = \perp, \parallel, 0, S'$) span the space of complex 2-component vectors. We therefore express the other vectors as linear combinations of these vectors. For instance,

$$n_i = a_i n_\parallel + b_i n_\perp, \quad i = 0, S. \tag{2.41}$$

Contracting with the vectors $n_\parallel$ and $n_\perp$, we obtain a system of linear equations [122]

$$\begin{aligned} n_\parallel^\dagger n_i &= a_i |n_\parallel|^2 + b_i (n_\parallel^\dagger n_\perp),\\ n_\perp^\dagger n_i &= a_i (n_\perp^\dagger n_\parallel) + b_i |n_\perp|^2, \end{aligned} \tag{2.42}$$

which can be solved for a_i, b_i:

$$a_i = \frac{|n_\perp|^2 (n_\parallel^\dagger n_i) - (n_\parallel^\dagger n_\perp)(n_\perp^\dagger n_i)}{|n_\parallel|^2 |n_\perp|^2 - |n_\perp^\dagger n_\parallel|^2}, \qquad b_i = \frac{|n_\parallel|^2 (n_\perp^\dagger n_i) - (n_\perp^\dagger n_\parallel)(n_\parallel^\dagger n_i)}{|n_\parallel|^2 |n_\perp|^2 - |n_\perp^\dagger n_\parallel|^2}. \tag{2.43}$$

Using the decomposition of n_0, n_S in terms of $n_\parallel, n_\perp$ (Eq. (2.41)) to calculate the scalar products $|n_0|^2, |n_S|^2, n_0^\dagger n_S$, the first three relations are obtained. We leave the expressions explicitly in terms of J_i to let the reader choose between different bases or conventions to write the P-wave observables.

I. From $i = 0$ in Eq. (2.41) one finds $|n_0|^2 = a_0 (n_0^\dagger n_\parallel) + b_0 (n_0^\dagger n_\perp)$ yielding the first relation:

$$\begin{aligned} 0 = \;&+\; J_{2c}(16 J_{2s}^2 - 4J_3^2 - \beta^2 J_{6s}^2 - 4J_9^2) + 2(J_3(4J_4^2 + \beta^2(-J_5^2 + J_7^2) - 4J_8^2)\\ &+\; 2J_{2s}(4J_4^2 + \beta^2(J_5^2 + J_7^2) + 4J_8^2) - 2(\beta^2(J_4 J_5 J_{6s} + J_{6s} J_7 J_8 + J_5 J_7 J_9) - 4J_4 J_8 J_9))\,. \end{aligned} \tag{2.44}$$

This first relation was found in the massless case in Ref. [28] and in the massive case in Ref. [12] and its consequences discussed in Ref. [125] once re-expressed in terms of optimized observables:

$$P_2 = \frac{(P_4' P_5' + \delta_1)}{2k_1} + \frac{1}{2k_1 \beta}\sqrt{(-1 + P_1 + P_4'^2)(-1 - P_1 + \beta^2 P_5'^2) + \delta_2 + \delta_3 P_1 + \delta_4 {P_1}^2} \tag{2.45}$$

where the parameters k_1 and δ_i (with $i = 1, ...4$) are defined in Ref. [125].

II. Similarly for $i = S$ in Eq. (2.41) one finds $|n_S|^2 = a_S(n_S^\dagger n_\parallel) + b_S(n_S^\dagger n_\perp)$ and this translates to:

$$\begin{aligned} 0 = \quad & -\frac{27}{16}\beta^4 F_S J_{6s}^2 + \Gamma'[-8(2J_{2s}+J_3)S_{S2}^{r\,2} - 16J_9 S_{S2}^r S_{S5}^i + 8(-2J_{2s}+J_3)S_{S5}^{i\,2}] \\ & +2\beta^2(\frac{27}{8}F_S(4J_{2s}^2 - J_3^2 - J_9^2) + \Gamma'[(-2J_{2s}+J_3)S_{S3}^{r\,2} + 2J_9 S_{S3}^r S_{S4}^i \\ & -(2J_{2s}+J_3)S_{S4}^{i\,2} + 2J_{6s}(S_{S2}^r S_{S3}^r + S_{S4}^i S_{S5}^i)]), \end{aligned} \tag{2.46}$$

once expressed in terms of S-wave observables.

III. Finally, the scalar product $n_0^\dagger n_S$ leads to the third relation:

$$\begin{aligned} 0 = \quad & 2\,[-16J_{2s}^2 + 4J_3^2 + \beta^2 J_{6s}^2 + 4J_9^2]S_{S1}^r + 4[\beta^2 J_5 J_{6s} - 4J_8 J_9 - 8J_{2s}J_4 - 4J_3 J_4]S_{S2}^r \\ & +4\beta^2[J_4 J_{6s} + J_7 J_9 - 2J_{2s}J_5 + J_3 J_5]S_{S3}^r + 4\beta^2[J_{6s}J_8 + J_5 J_9 \\ & -2J_{2s}J_7 - J_3 J_7]S_{S4}^i + 4[\beta^2 J_{6s}J_7 - 4J_4 J_9 - 8J_{2s}J_8 + 4J_3 J_8]S_{S5}^i. \end{aligned} \tag{2.47}$$

Eq. (2.46) and Eq. (2.47) are the generalizations of the massless limit ($\beta \to 1$) expressions found in Ref. [122].

Following the same methodology but using instead the vector n'_S yields three new relations. Expressing n'_S in terms of $n_\perp$ and $n_\parallel$:

$$n'_S = a'_S n_\parallel + b'_S n_\perp, \tag{2.48}$$

and contracting with $n_\parallel$ and $n_\perp$ we get a system of linear equations

$$\begin{aligned} n_\perp^\dagger n'_S &= a'_S(n_\perp^\dagger n_\parallel) + b'_S|n_\perp|^2, \\ n_\parallel^\dagger n'_S &= a'_S|n_\parallel|^2 + b'_S(n_\parallel^\dagger n_\perp). \end{aligned} \tag{2.49}$$

We can determine a'_S and b'_S:

$$a'_S = \frac{(n_\parallel^\dagger n'_S)|n_\perp|^2 - (n_\perp^\dagger n'_S)(n_\parallel^\dagger n_\perp)}{|n_\parallel|^2|n_\perp|^2 - |n_\perp^\dagger n_\parallel|^2}, \qquad b'_S = \frac{(n_\parallel^\dagger n'_S)(n_\perp^\dagger n_\parallel) - (n_\perp^\dagger n'_S)|n_\parallel|^2}{|n_\perp^\dagger n_\parallel|^2 - |n_\parallel|^2|n_\perp|^2}. \tag{2.50}$$

Using the properties of the vector n'_S we then obtain the following three relations:

IV. From the equality of the modulus of both vectors n_S and n'_S one obtains

$$|n'_S|^2 = |n_S|^2 = a'_S(n'^\dagger_S n_\parallel) + b'_S(n'^\dagger_S n_\perp)\,, \tag{2.51}$$

which implies the following relation:

$$\begin{aligned} 0 = \quad & +\frac{27}{16}\beta^2 F_S(16J_{2s}^2 - 4J_3^2 - \beta^2 J_{6s}^2 - 4J_9^2) - 2\Gamma'[-2(\beta^2 J_{6s}S_{S2}^i S_{S3}^i - \beta^2 J_9 S_{S3}^i S_{S4}^r \\ & +4J_9 S_{S2}^i S_{S5}^r + \beta^2 J_{6s}S_{S4}^r S_{S5}^r) + 4S_{S2}^{i\,2}(J_3 + 2J_{2s}) + \beta^2 S_{S3}^{i\,2}(2J_{2s} - J_3) \\ & +\beta^2 S_{S4}^{r\,2}(J_3 + 2J_{2s}) + 4S_{S5}^{r\,2}(2J_{2s} - J_3)]. \end{aligned} \tag{2.52}$$

V. Above we focus on relations constructed from the real part of the product of vectors. The imaginary parts provide additional new relations:

$$\mathrm{Im}[n_0^\dagger n'_S] = \mathrm{Im}[a'_S(n_0^\dagger n_\parallel) + b'_S(n_0^\dagger n_\perp)]\,, \tag{2.53}$$

which leads to:

$$\begin{aligned} 0 = \quad & 2\,[-16J_{2s}^2 + 4J_3^2 + \beta^2 J_{6s}^2 + 4J_9^2]S_{S1}^i + [4\beta^2 J_5 J_{6s} - 16J_8 J_9 - 16J_3 J_4 - 32J_{2s}J_4]S_{S2}^i \\ & +4\beta^2[J_4 J_{6s} + J_7 J_9 + J_3 J_5 - 2J_{2s}J_5]S_{S3}^i + 4\beta^2[-J_{6s}J_8 - J_5 J_9 + J_3 J_7 + 2J_{2s}J_7]S_{S4}^r \\ & +[-4\beta^2 J_{6s}J_7 + 16J_4 J_9 - 16J_3 J_8 + 32J_{2s}J_8]S_{S5}^r. \end{aligned} \tag{2.54}$$

VI. Finally, combining the vectors n_S and n'_S one finds:

$$\mathrm{Im}[n_S^\dagger n_S'] = 0 = a_S'(n_S^\dagger n_\parallel) + b_S'(n_S^\dagger n_\perp)\,, \tag{2.55}$$

which corresponds to

$$\begin{aligned} 0 = \quad & \beta^2 J_{6s}[-S^r_{S2}S^i_{S3} - S^i_{S2}S^r_{S3} + S^r_{S4}S^i_{S5} + S^i_{S4}S^r_{S5}] + J_9[-\beta^2 S^i_{S3}S^i_{S4} + \beta^2 S^r_{S3}S^r_{S4} + 4S^i_{S2}S^i_{S5} \\ & -4S^r_{S2}S^r_{S5}] + 2J_{2s}[4S^i_{S2}S^r_{S2} + \beta^2(S^i_{S3}S^r_{S3} - S^i_{S4}S^r_{S4}) - 4S^i_{S5}S^r_{S5}] + J_3[4S^i_{S2}S^r_{S2} \\ & -\beta^2(S^i_{S3}S^r_{S3} + S^i_{S4}S^r_{S4}) + 4S^i_{S5}S^r_{S5}]. \end{aligned} \tag{2.56}$$

These six relations are common to the massive and massless cases, and they reduce to the massless case when taking the limit $\beta \to 1$. There is a cumbersome seventh relation that applies only to the massive case, i.e. it is zero in the limit of massless leptons. For this reason and given that it is difficult to extract information from such a long relation, we refrain from writing it explicitly and, instead, provide only the main steps to obtain this relation in Appendix C.

2.3 Bounds on S-wave observables and $W_{1,2}$ observables

Following the strategy of Ref. [122], the relations found in the previous section enable bounds to be placed on the S^r_{Si} observables and the newly defined S^i_{Si} observables. For instance, solving for S^r_{S2} and imposing a real solution in relation II gives:

$$\begin{aligned} 0 \le \Delta(S^r_{S2}) = \quad & - \quad \beta^2 x (S^r_{S3})^2 - 4x(S^i_{S5})^2 - \beta^2(2P_3S^r_{S3} + (1+P_1)S^i_{S4} - 4P_2S^i_{S5})^2 \\ & + \quad \frac{27}{16}\beta^4 x F_S(1-F_S')F_T(1+P_1)\,, \end{aligned} \tag{2.57}$$

where

$$x = 1 - P_1^2 - 4\beta^2 P_2^2 - 4P_3^2 \ge 0 \tag{2.58}$$

(see Ref. [122]) and Δ stands for the discriminant of S^r_{S2} when solved from relation II (Eq. (2.46)). The first three terms are negative definite and each of them separately has to be smaller than the last positive definite term. In a similar way but solving for S^r_{S3} and imposing a real solution one finds:

$$\begin{aligned} 0 \le \Delta(S^r_{S3}) = \quad & - \quad \beta^2 x (S^i_{S4})^2 - 4x(S^r_{S2})^2 - 4(2P_3S^r_{S2} - (1-P_1)S^i_{S5} + \beta^2 P_2 S^i_{S4})^2 \\ & + \quad \frac{27}{16}\beta^4 x F_S(1-F_S')F_T(1-P_1)\,. \end{aligned} \tag{2.59}$$

This implies the following constraints for $S^r_{S2,3}$:

$$|S^r_{S2}| \le \beta^2 \frac{3}{4}\sqrt{\frac{3}{4}F_S(1-F_S')F_T(1-P_1)} \quad |S^r_{S3}| \le \beta\frac{3}{4}\sqrt{3F_S(1-F_S')F_T(1+P_1)}, \tag{2.60}$$

and for $S^i_{S4,5}$:

$$|S^i_{S4}| \le \beta\frac{3}{4}\sqrt{3F_S(1-F_S')F_T(1-P_1)} \quad |S^i_{S5}| \le \beta^2\frac{3}{4}\sqrt{\frac{3}{4}F_S(1-F_S')F_T(1+P_1)}\,. \tag{2.61}$$

Similarly using relation IV, one finds

$$\begin{aligned} 0 \le \Delta(S^r_{S4}) = \quad & - \quad \beta^2 x (S^i_{S3})^2 - 4x(S^r_{S5})^2 - 4(2P_3S^r_{S5} + (1+P_1)S^i_{S2} - \beta^2 P_2 S^i_{S3})^2 \\ & + \quad \frac{27}{16}\beta^4 x F_S(1-F_S')F_T(1+P_1)\,, \end{aligned} \tag{2.62}$$

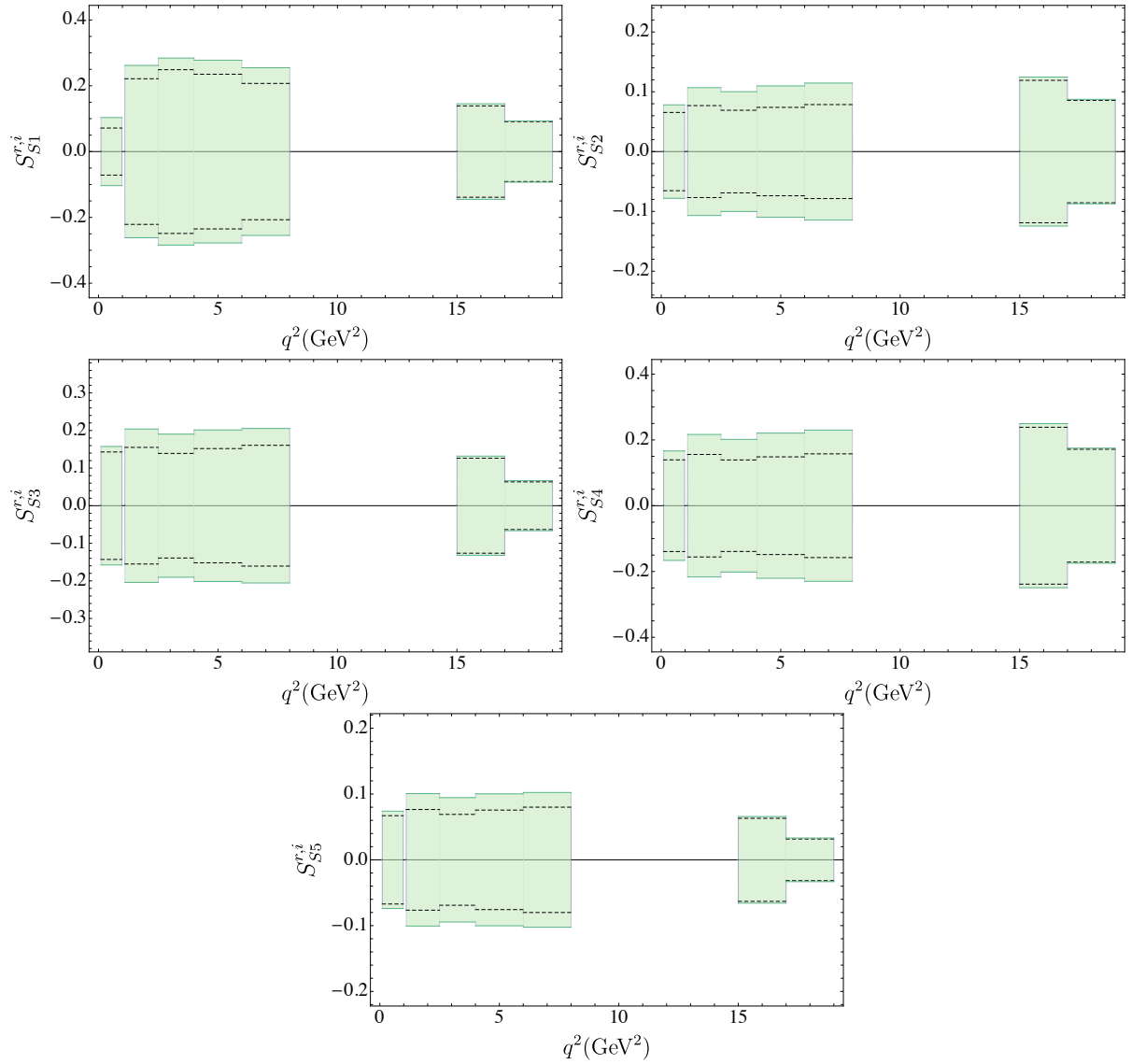

Figure 2.3: Bounds for $S^{r,i}_{Si}$ binned observables with $i = 1, 2, 3, 4, 5$. The dashed line corresponds to the central value of the bound in the SM, while the green regions include the uncertainty of the observables that define the bound in the SM.

and

$$\begin{aligned} 0 \leq \Delta(S^r_{S5}) = & - \beta^2 x (S^r_{S4})^2 - 4x(S^i_{S2})^2 - \beta^2(4P_2 S^i_{S2} - (1-P_1)S^i_{S3} + 2P_3 S^r_{S4})^2 \\ & + \frac{27}{16}\beta^4 x F_S(1-F'_S)F_T(1-P_1)\,, \end{aligned} \tag{2.63}$$

which leads to the following bounds:

$$|S^r_{S4}| \leq \beta\frac{3}{4}\sqrt{3F_S(1-F'_S)F_T(1-P_1)}\,, \quad |S^r_{S5}| \leq \beta^2\frac{3}{4}\sqrt{\frac{3}{4}F_S(1-F'_S)F_T(1+P_1)}\,, \tag{2.64}$$

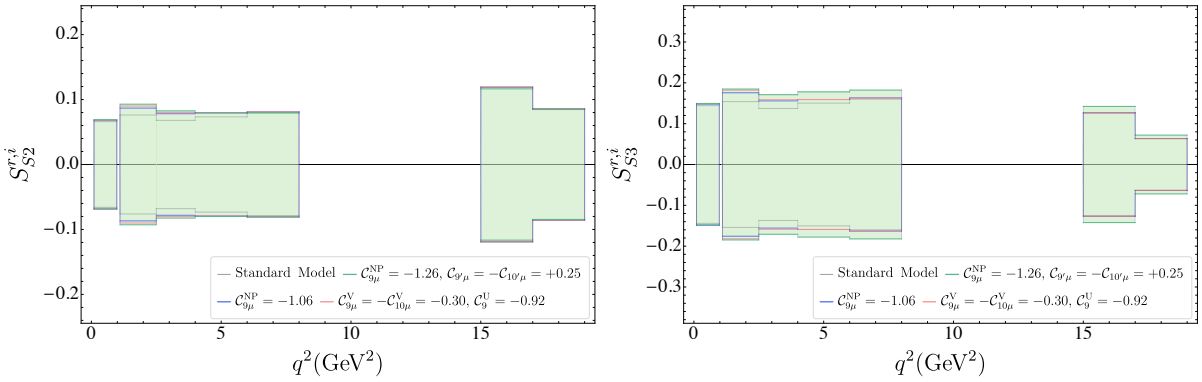

Figure 2.4: Illustration of the sensitivity of the central value of the bound to the preferred NP scenarios for two observables $S^{r,i}_{S2}$ and $S^{r,i}_{S3}$. We have checked explicitly that the variation of the bound in the most significant NP scenarios amounts to at most a 20-25% enhancement.

and

$$|S^i_{S2}| \leq \beta^2 \frac{3}{4}\sqrt{\frac{3}{4}F_S(1-F'_S)F_T(1-P_1)}\,, \quad |S^i_{S3}| \leq \beta\frac{3}{4}\sqrt{3F_S(1-F'_S)F_T(1+P_1)}\,. \tag{2.65}$$

In summary,

$$|S^{r,i}_{S2}| \leq \beta^2\frac{k_1}{2}, \quad |S^{r,i}_{S3}| \leq \beta k_2, \quad |S^{r,i}_{S4}| \leq \beta k_1, \quad |S^{r,i}_{S5}| \leq \beta^2\frac{k_2}{2}, \tag{2.66}$$

with $k_1 = \frac{3}{4}\sqrt{3F_S(1-F'_S)F_T(1-P_1)}$ and $k_2 = \frac{3}{4}\sqrt{3F_S(1-F'_S)F_T(1+P_1)}$. All the bounds above can alternatively be obtained using the Cauchy-Schwarz inequalities. For the observables $S^{r,i}_{S1}$ this is the only way to obtain the bounds. For instance, from $|n_0^\dagger n_S|^2 \leq |n_0|^2|n_S|^2$ and a corresponding inequality with n'_S using the properties of the vectors Eq. (2.4) one arrives at

$$|S^{r,i}_{S1}| \leq \beta^2\frac{3}{4}\sqrt{3}\sqrt{F_S(1-F'_S)F_L}\,. \tag{2.67}$$

All the bounds on the other observables can be re-derived using the four inequalities:

$$|n_\parallel^\dagger n_S^{(\prime)}|^2 \leq |n_\parallel|^2|n_S|^2\,, \qquad |n_\perp^\dagger n_S^{(\prime)}|^2 \leq |n_\perp|^2|n_S|^2\,. \tag{2.68}$$

We have computed explicitly the bounds of the $S^{r,i}_{Si}$ observables in the SM in Fig. 2.3. The relatively low sensitivity of the central value of the bound for $S^{r,i}_{S2,3}$ on the dominant NP scenarios is illustrated in Fig. 2.4. We work under the approximation of substituting q^2 dependent observables by their binned equivalents, where we denote the latter using angular brackets. This introduces some uncertainty but, as shown in Ref. [125], this uncertainty is negligible, especially for slowly varying observables like those involved in the bounds. To compute the binned form of the bounds from Eq. (2.66) we consider the theoretical prediction for the observables $\langle F_{L,T}\rangle$, $\langle P_1\rangle$, taking into account the 1σ ranges of such observables. Therefore Fig. 2.3 shows the maximum value allowed for such constraints. For $\langle F_S\rangle$ we extract the value from a reduced $m_{K\pi}$ resonance window, $0.795 < m_{K\pi} < 0.995\,\mathrm{GeV}$. In Fig. 2.4 we evaluate $\langle F_{L,T}\rangle$ and $\langle P_1\rangle$ in the corresponding NP scenarios, while taking the SM prediction for $\langle F_S\rangle$. The computation of $\langle F_S\rangle$ is the only place where we use S-wave form factors. If $\langle F_S\rangle$ is taken as an experimental input, then no S-wave form factors are required. Finally, notice that the bounds include a term $(1-F'_S)$. However, in evaluating these bounds we have neglected a small lepton mass dependent term (see Eq. (2.25)) taking F_S instead of F'_S.

The third term in Eqs. (2.57),(2.59),(2.62),(2.63) should tend to zero when $x(q_1^2) \to 0$, in order not to violate the condition of a real solution. Indeed, if we repeat the same procedure using relation II but impose a real solution for $\Delta(S^i_{S4})$ and $\Delta(S^i_{S5})$ and for relation IV impose a real solution for $\Delta(S^i_{S2})$ and

$\Delta(S^i_{S3})$, we find respectively:

$$\begin{aligned}
\left((1+P_1)S^r_{S2} - \beta^2 P_2 S^r_{S3} - 2P_3 S^i_{S5}\right)_{q_1^2} &= 0,\\
\left(4P_2 S^r_{S2} - (1-P_1)S^r_{S3} - 2P_3 S^i_{S4}\right)_{q_1^2} &= 0,\\
\left(4P_2 S^r_{S5} - (1+P_1)S^r_{S4} + 2P_3 S^i_{S3}\right)_{q_1^2} &= 0,\\
\left((1-P_1)S^r_{S5} - \beta^2 P_2 S^r_{S4} + 2P_3 S^i_{S2}\right)_{q_1^2} &= 0.
\end{aligned} \tag{2.69}$$

Neglecting quadratically suppressed terms, $P_3 S^i_{Sj} \ll P_2 S^r_{Sj}$ with $j = 2...5$, the previous equations can be combined to obtain:

$$\begin{aligned}
S^r_{S2}|_{q_1^2} &= \left[\frac{\beta}{2}\sqrt{\frac{1-P_1}{1+P_1}}S^r_{S3}\right]_{q_1^2},\\
S^r_{S5}|_{q_1^2} &= \left[\frac{\beta}{2}\sqrt{\frac{1+P_1}{1-P_1}}S^r_{S4}\right]_{q_1^2},
\end{aligned} \tag{2.70}$$

and from $x(q_1^2) = 0$, neglecting P_3^2, one finds at q_1^2 that $P_2 = \sqrt{1-P_1^2}/(2\beta)$.

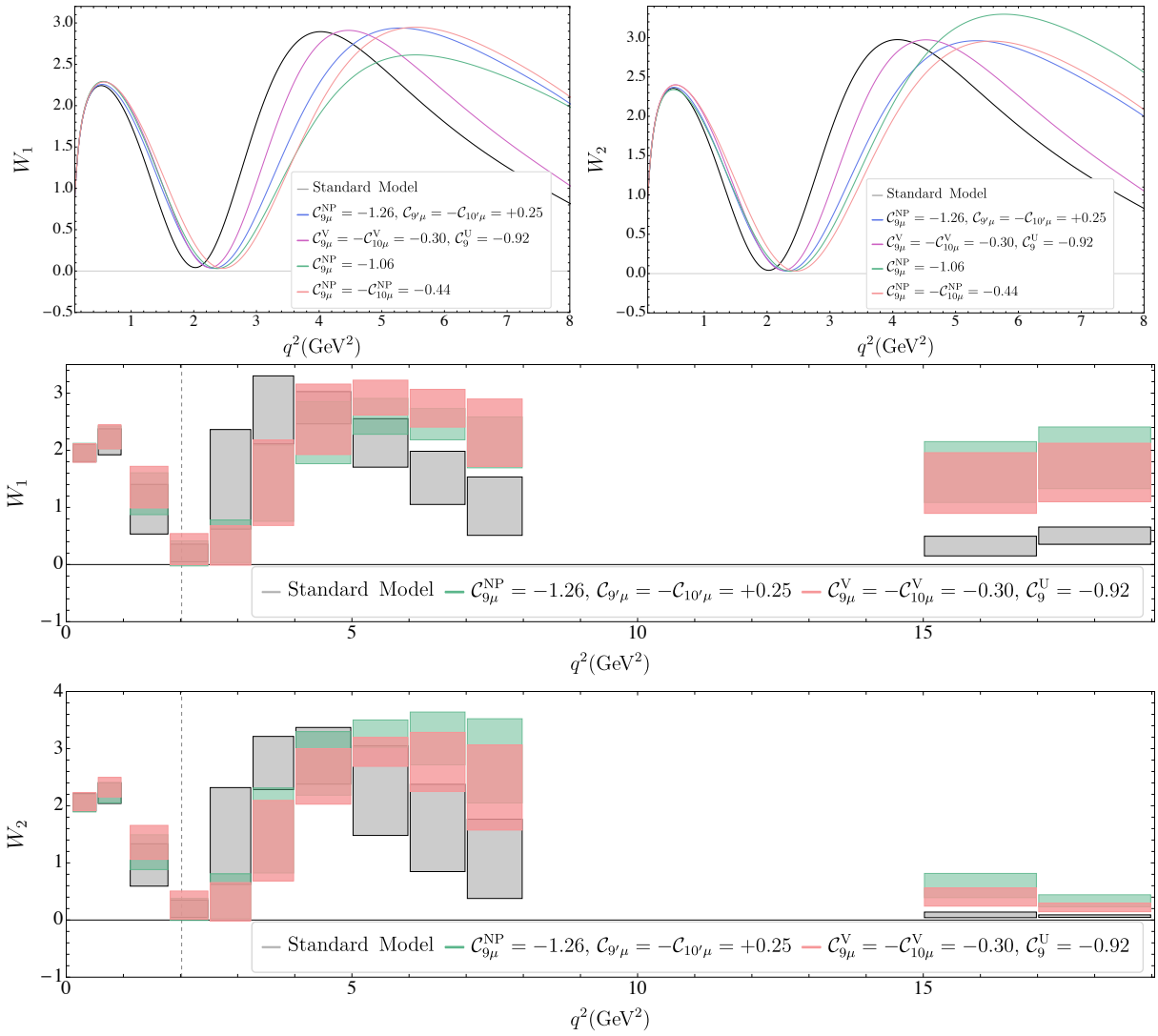

Figure 2.5: SM and NP predictions for the observables W_1 and W_2 as continuous functions of q^2 and binned in q^2.

Another example of the information that can be extracted from the relations, neglecting quadratic terms of the type $\mathcal{O}(P_3 S^i_{Sj}, P_3^2)$, are the following expressions. These are valid for all q^2 and derive from relations II and IV, respectively. They can be tested as a cross-check of the experimental analyses:

$$W_1 = (2\hat{S}^r_{S2})^2 + p(\beta\hat{S}^r_{S3})^2 + q\hat{S}^r_{S2}\hat{S}^r_{S3} = 3\beta^4\frac{1}{1+P_1}x\,, \tag{2.71}$$

where

$$\hat{S}^r_{Si} = \frac{4}{3}\frac{S^r_{Si}}{\sqrt{(1-F'_S)F_S F_T}} = \frac{\beta^2}{\sqrt{6}}PS^r_i\,, \tag{2.72}$$

with $i = 2...5$, $p = (1-P_1)/(1+P_1)$ and $q = -8\beta^2 P_2/(1+P_1)$. Similarly,

$$W_2 = (2\hat{S}^r_{S5})^2 + p'(\beta\hat{S}^r_{S4})^2 + q'\hat{S}^r_{S4}\hat{S}^r_{S5} = 3\beta^4\frac{1}{1-P_1}x, \tag{2.73}$$

where $p' = (1+P_1)/(1-P_1)$ and $q' = -8\beta^2 P_2/(1-P_1)$, and x is defined in Eq. (2.58).

Eq. (2.71) is particularly interesting because at the zero of $\hat{S}^r_{S3}$ (or equivalently PS^r_3) one can predict the absolute value of $\hat{S}^r_{S2}$ (or PS^r_2) as a function of P-wave observables with no need to rely on any S-wave form factors. In the case of Eq. (2.73), at the zero of $\hat{S}^r_{S4}$ one can predict the absolute value of $\hat{S}^r_{S5}$ at this particular value of q^2. These are valuable tests to compare with future predictions using calculations of the form factors.

Given that Eq. (2.71) and Eq. (2.73) are functions of P- and S-wave optimized observables (PS^r_i and $P_{1,2}$), $W_{1,2}$ are also optimized observables. We can compute SM and NP predictions for these two observables using the right hand side of Eq. (2.71) and Eq. (2.73), respectively. These relations then give access to the $n_{\perp,\parallel,0}$ components inside the new S-wave observables, cancelling the dependence on n_S and n'_S and hence their predictions do not require the S-wave form factors. The $W_{1,2}$ observables bring new information that can help to disentangle the SM from different NP scenarios, as illustrated in Fig. 2.5. From W_1 in the region above 4 GeV^2, the SM and $\mathcal{C}^{\rm NP}_{9\mu} = -\mathcal{C}^{\rm NP}_{10\mu}$ are not distinguishable but all the other scenarios shown can in principle be distinguished from the SM. The expected experimental precision for such measurements is detailed in Section 2.5.

Finally we can use relation III, again neglecting all terms including quadratic products of observables sensitive to imaginary parts of bilinears (P_3, $P_{6',8'}$ and $S^i_{S3,5}$), to find:

$$S^r_{S1} = -\frac{1}{x}\frac{F_L}{\sqrt{F_L F_T}}\left(2(P'_4(1+P_1) - 2\beta^2 P_2 P'_5)S^r_{S2} + \beta^2(P'_5(1-P_1) - 2P_2 P'_4)S^r_{S3}\right)\,, \tag{2.74}$$

however, this does not give any additional experimental insight.

2.4 Common zeroes of P- and S-wave observables

The optimized observable P_2 can be rewritten in terms of the q^2-dependent complex-vectors $n_\perp$ and $n_\parallel$ in the following way:

$$P_2 = \frac{1}{2\beta}\left(1 - \frac{(n_\perp - n_\parallel)^\dagger(n_\perp - n_\parallel) + CP}{|n_\perp|^2 + |n_\parallel|^2 + CP}\right). \tag{2.75}$$

In the absence of right-handed currents, the maximum of P_2, denoted P_2^{max}, occurs at a certain value of q^2, which we denote q_1^2. At the maximum, $P_2^{max}(q_1^2) \simeq 1/(2\beta)$. To a very good approximation, this maximum occurs when

$$n_\perp(q_0^2) \simeq n_\parallel(q_0^2)\,, \tag{2.76}$$

where in principle a different q^2 is involved. This is because this expression is in fact four equations (two for the real and two for the imaginary part) and, moreover, they have to be combined with their CP conjugated equivalents. Strictly speaking this would require that real and imaginary parts and left and right handed parts have the zero at the same point in q^2, which is not the case. If we restrict ourselves to only $\mathrm{Re}(A^L_\perp(q_0^2)) = \mathrm{Re}(A^L_\parallel(q_0^2))$ the obtained position of the zero q_0^2 is in very good agreement with the position of the maximum given by q_1^2, as illustrated in Table 2.1.

Hypotheses	q_0^2	q_1^2	q_2^2
SM	2.03	2.02	2.02
$\mathcal{C}_{9\mu}^{\rm NP}$	2.31	2.30	2.30
Hypothesis V: $(\mathcal{C}_{9\mu}^{\rm NP}, \mathcal{C}_{9'\mu} = -\mathcal{C}_{10'\mu})$	2.37	2.37	2.36
LFU Scenario 8: $(\mathcal{C}_{9\mu}^{\rm V} = -\mathcal{C}_{10\mu}^{\rm V}, \mathcal{C}_9^{\rm U})$	2.43	2.46	2.45
Hypothesis I: $(\mathcal{C}_{9\mu}^{\rm NP} = -\mathcal{C}_{9'\mu}, \mathcal{C}_{10\mu}^{\rm NP} = \mathcal{C}_{10'\mu})$	2.45	2.34	2.18

Table 2.1: Position of the zero evaluated from: a) $\mathrm{Re}(A_\perp(q_0^2)) = \mathrm{Re}(A_\parallel(q_0^2))$, b) position of $P_2^{\max}(q_1^2)$ and c) the exact position given by $X_2(q_2^2)$. This shows that only in the presence of right handed currents that do not fulfill condition$_R$, as in Hypothesis I [4], do the zero points differ significantly from one another.

In the presence of right-handed currents the condition $n_\perp(q_0^2) \simeq n_\parallel(q_0^2)$ can only be fulfilled if a very concrete combination of Wilson coefficients is realized in Nature:

$$\mathcal{C}_{7'} \simeq -\frac{\mathcal{C}_7^{\rm eff}}{\mathcal{C}_{10\mu} - \mathcal{C}_{9\mu}^{\rm eff}}(\mathcal{C}_{10'\mu} + \mathcal{C}_{9'\mu}). \tag{2.77}$$

One of the NP scenarios that presently has the highest pull with respect to the SM, $(\mathcal{C}_{7'} = 0,\ \mathcal{C}_{9\mu}^{\rm NP}, \mathcal{C}_{9'\mu} = -\mathcal{C}_{10'\mu})$ indeed fulfills this condition. From now on we will refer to this combination (Eq. (2.77)) as condition$_R$.

In the SM, in the absence of right-handed currents, or in the presence of right-handed currents that fulfill condition$_R$, Table 2.1 illustrates that q_0^2 and q_1^2 are within 1% of each other. This can be understood due to the small phases entering, but also because the equation:

$$\mathrm{Re}(A_\perp^R(q_0^2)) = -\mathrm{Re}(A_\parallel^R(q_0^2)), \tag{2.78}$$

is exactly fulfilled in the large recoil limit in the absence of right handed currents, or if such currents are present but obey condition$_R$. Under these conditions, deviations from this relation then owe to departures from the large recoil limit. We can parametrise these tiny deviations and the effect of imaginary terms in the following form[6]:

$$\frac{1}{N}\left(n_\perp - n_\parallel\right) = \frac{1}{N}\begin{pmatrix} A_\perp^L(q_0^2) - A_\parallel^L(q_0^2) \\ -A_\perp^{R*}(q_0^2) - A_\parallel^{R*}(q_0^2) \end{pmatrix} = \begin{pmatrix} i\epsilon_L \\ \delta + i\epsilon_R \end{pmatrix}, \tag{2.81}$$

where N is the normalization factor for the helicity amplitudes defined in Eq. (1.31).

For NP scenarios with right handed currents that satisfy condition$_R$ or in the absence of right handed currents, a number of other observables are zero at the same point in q^2 at which P_2 is maximal. The relevant observables are formed from pairs of P- and S-wave angular observables:

$$X_1 = P_2^{\max}(q_1^2), \quad X_2 = \beta P_5' - P_4', \quad X_3 = \beta S_{S4}^r - 2S_{S5}^r, \quad X_4 = \beta S_{S3}^r - 2S_{S2}^r. \tag{2.82}$$

In Fig. 2.6 the dependence of the position of the zero for several P-wave observables is shown for different NP scenarios. The observables P_3 and $P_{6,8}'$ would also in principle give a further zero. However, given that they are numerically small over the entire low-q^2 region, they are difficult to determine experimentally.

[6] Besides the fact that we can compute δ, ϵ_L and ϵ_R, these quantities can be bounded experimentally using Eq. (2.75) and Eq. (2.81) and rewriting P_2 at the point of its maximum (again, for NP scenarios with right-handed currents that satisfy condition$_R$, or in the absence of right handed currents) as:

$$P_2(q_0^2) = \frac{1}{2\beta}\left(1 - N^2\frac{|\delta|^2 + |\epsilon_L|^2 + |\epsilon_R|^2 + CP}{|n_\perp|^2 + |n_\parallel|^2 + CP}\right). \tag{2.79}$$

This implies that the tiny difference between $1/(2\beta)$ and the maximum imposes a bound on each term $|\delta|$, $|\epsilon_L|$ and $|\epsilon_R|$ separately:

$$|\delta|^2, |\epsilon_L|^2, |\epsilon_R|^2 \leq (1/(2\beta) - P_2^{\rm measured}(q_0^2))F_T(d\Gamma/dq^2)/N^2. \tag{2.80}$$

However, measuring the difference $1/(2\beta) - P_2^{\rm measured}(q_0^2)$ would require an experimental precision that is presently unattainable.

Moreover, the small contribution coming from the $\lambda_u = V_{ub}V_{us}^*$ piece of the Hamiltonian distorts the position of the zero for such observables, which motivates their omission from the list above. For the same reason, the S_{Si}^i observables and P_1 in the absence of right handed currents are also not included.

The $X_{2,3,4}$ observables then offer the possibility of looking at the compatibility of multiple zeros, rather than just the zero of single variables such as $A_{\rm FB}$. In the presence of sizeable right handed currents that do not fulfill condition$_R$, P_2 does not reach the maximal value $1/(2\beta)$, and a small difference between the X_i observables should be observed. Misalignment between the zeroes of the X_i observables could then help confirm a right handed current scenario, although another possible reason for a tiny misalignment is the presence of scalar or pseudoscalar contributions. The observable X_1 is not included in the list above because it is difficult to identify precisely the position of the maximum experimentally.

The point where P_5' and P_4' cross gives the zero of X_2, as shown in Fig. 2.6. Unfortunately, when including theory uncertainties using the KMPW computation [23] of the form factors $V, A_{0,1,2}, T_{1,2,3}$ and long-distance charm, the overlap between the zeroes of different NP scenarios is as shown in Fig. 2.7. This implies that further efforts are required to improve on the theoretical uncertainty of the observables.

We use the complete longitudinal and transverse (perpendicular and parallel) amplitudes defined in Eqs. (1.28)-(1.27) to determine the corresponding theoretical position of the zero, which is the solution of the following implicit equation:

$$\frac{q_0^2}{2m_b} = \frac{\mathcal{C}_7^{\rm eff}\left[T_1(1+\frac{m_s}{m_b})\lambda^{\frac{1}{2}} + T_2(1-\frac{m_s}{m_b})(m_B^2 - m_{K^*}^2)\right] + \mathcal{T}_\perp\left[\lambda^{\frac{1}{2}} + (m_B^2 - m_{K^*}^2)\frac{m_B^2-q_0^2}{m_B^2}\right]}{(\mathcal{C}_{10} - \mathcal{C}_9^{\rm eff}(q_0^2))(\frac{\lambda^{\frac{1}{2}}}{m_B+m_{K^*}}V + (m_B+m_{K^*})A_1)}, \tag{2.83}$$

where $\mathcal{C}_9^{\rm eff}(q^2)$ collects all pieces and, in order to simplify the expression, we take all non-factorizable power corrections at their central values but keep long distance charm (see Eq. (1.34)) explicit inside $\mathcal{C}_9^{\rm eff}$ (taking $c_\perp^{\rm long} = c_\parallel^{\rm long} = c^{\rm long}$):

$$\mathcal{C}_{9\perp,\parallel}^{\rm eff}(q^2) = \mathcal{C}_9 + Y_t + \frac{\lambda_u}{\lambda_t}Y_u + c_{\perp,\parallel}^{\rm long}(s)s_{\perp,\parallel}. \tag{2.84}$$

The form factors $T_{1,2}$ include soft form factors, α_s and power corrections and $\mathcal{T}_\perp$ also includes the non-factorizable QCDf contribution. Eq. (2.83) offers an interesting combined test of form factors, Wilson coefficients and long-distance charm at a specific point in q^2.

2.4.1 A closer look at the observable X_2: from New Physics to hadronic contributions

In this section the properties of the observable $X_2 = \beta P_5' - P_4'$ are analyzed in detail, focusing on the q^2 bin where the zeroes fall both in the SM and in the NP scenarios considered [4, 55]. While all the relevant observable information is already included inside global fits, analyzing particular observables like X_2 can provide guidance on how to disentangle NP effects in the longer term. This observable has a simple structure in terms of Wilson coefficients when evaluated in the q^2 bin [1.8,2.5]:

$$\langle X_2\rangle_{[1.8,2.5]} \sim -0.14 + 0.22\,(\mathcal{C}_{10\mu}^{\rm NP} - \mathcal{C}_{9\mu}^{\rm NP}) + \epsilon\,, \tag{2.85}$$

where ϵ in this equation refers to a tiny contribution that is non-zero only in the presence of right handed currents, in particular contributing to $\mathcal{C}_{9'\mu}$, that can be cast as $-0.02\,\mathcal{C}_{9'\mu}(1+2(\mathcal{C}_{9'\mu} - \mathcal{C}_{9\mu}^{\rm NP}))$. As can be seen immediately from this equation, $\langle X_2\rangle_{[1.8,2.5]}^{\rm SM} \sim -0.14$. Independent of the details of the physics model, almost all NP scenarios with $\mathcal{C}_{9\mu}^{\rm NP} \neq 0$ yield $0.88 < \mathcal{C}_{10\mu}^{\rm NP} - \mathcal{C}_{9\mu}^{\rm NP} < 1.26$, implying $0.05 \leq \langle X_2\rangle_{[1.8,2.5]} \leq 0.14$. One relevant exception is Scenario 8, corresponding to $\langle X_2\rangle_{[1.8,2.5]} = 0.19$. This scenario contains a LFU contribution in $\mathcal{C}_9$, which would imply a contribution to the electronic mode too, $\langle X_{2e}\rangle_{[1.8,2.5]} = \langle \beta P_{5,e}' - P_{4,e}'\rangle_{[1.8,2.5]} \simeq 0.07$.

In summary, given that $\langle X_2\rangle_{[1.8,2.5]}$ is predicted to be approximately -0.1 in the SM and up to $+0.2$ in some relevant NP scenarios, an experimental precision of ± 0.1 would allow some of the NP scenarios to be disentangled from the SM. However, as shown above, with the present theoretical accuracy the theory predictions in q^2 bins yield a large overlap, preventing any clear discrimination. This is not surprising,

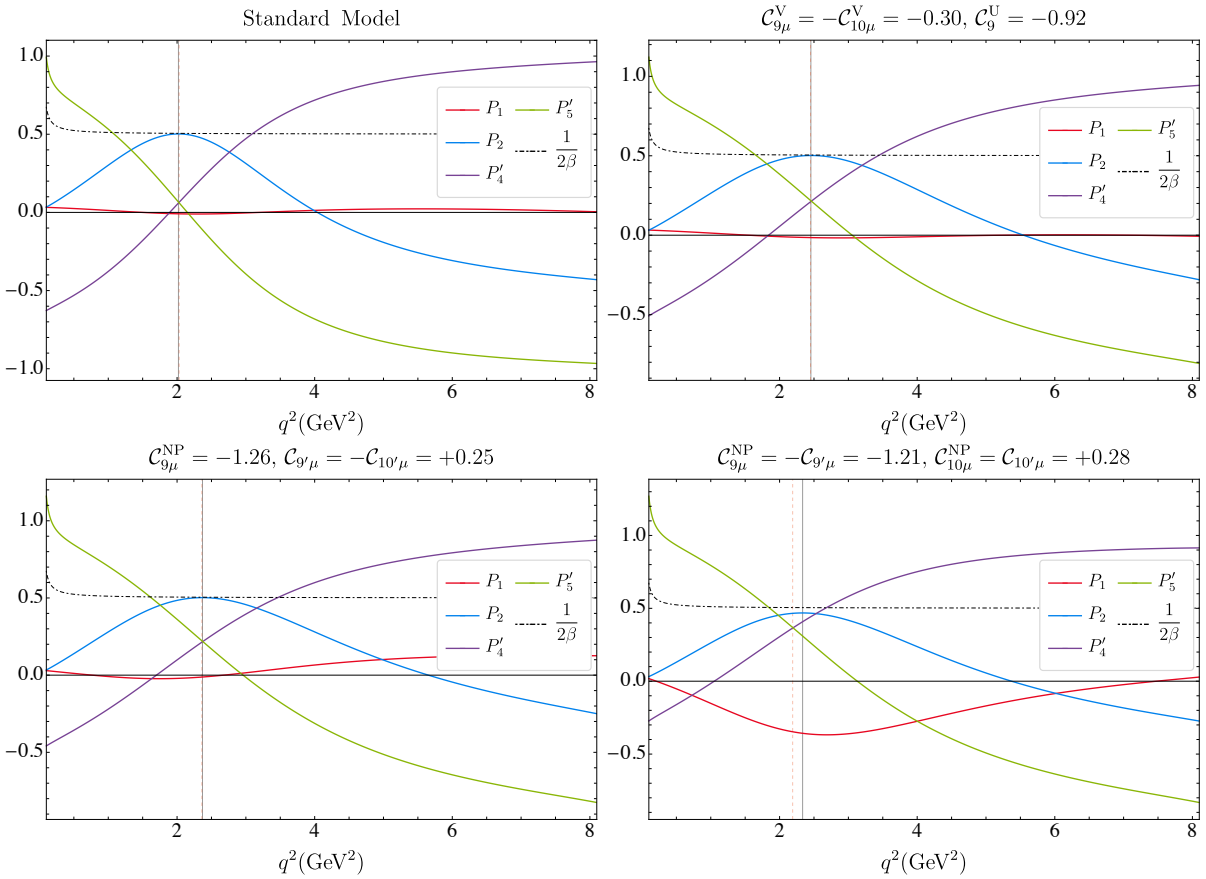

Figure 2.6: Predictions for different P_i observables in (top left) the SM, (top right) Scenario 8, (bottom left) Hypothesis V and (bottom right) Hypothesis I.

because the deviation of P_5' in the $[1.8, 2.5]$ bin is not so large compared to the anomalies in the bins [4,6] or [6,8]. Moreover, given that P_4' is quite SM-like (see discussion below), it is expected that the largest deviation for this observable will occur in the [4,6] and [6,8] bins. This is confirmed in Fig. 2.8.

Due to the stability of X_2 under most NP scenarios, it is essential to improve on its theoretical uncertainties. In parallel we can explore the sensitivity that P_5' and P_4' may offer individually in the $[1.8, 2.5]$ bin. For completeness, we provide the relevant expressions here:

$$\begin{aligned} \langle P_4' \rangle_{[1.8,2.5]} &\simeq 0.13 - 0.22(\mathcal{C}_{10\mu}^{\rm NP} - \mathcal{C}_{10'\mu}) + 0.03(\mathcal{C}_{9\mu}^{\rm NP} - \mathcal{C}_{9'\mu})^2 \,, \\ \langle P_5' \rangle_{[1.8,2.5]} &\simeq -0.01 + 0.22\mathcal{C}_{10'\mu} - 0.26\mathcal{C}_{9\mu}^{\rm NP} + 0.06\mathcal{C}_{10\mu}^{\rm NP}\mathcal{C}_{10'\mu} \,. \end{aligned} \tag{2.86}$$

For the most prominent NP scenarios, we find the ranges $0.04 < \langle P_4' \rangle_{[1.8,2.5]} < 0.33$ and $0.10 < \langle P_5' \rangle_{[1.8,2.5]} < 0.38$, with theory uncertainties of ± 0.20 and ± 0.13 for $\langle P_4' \rangle_{[1.8,2.5]}$ and $\langle P_5' \rangle_{[1.8,2.5]}$, respectively. These show that $\langle P_4' \rangle_{[1.8,2.5]}$ exhibits a SM-like behaviour (in the absence of right handed currents) and gets a wider range only if right handed currents are rather large, as in Hypothesis I (see Table 2.1 and Refs. [4, 55]). This is different in the case of $\langle P_5' \rangle_{[1.8,2.5]}$, which exhibits an enhanced sensitivity to $\mathcal{C}_{9\mu}^{\rm NP}$ that drives the wider range. Moreover, the current size of the theory uncertainty of $\langle P_4' \rangle_{[1.8,2.5]}$ erases any possibility of discrimination between the SM and NP scenarios, but in the case of $\langle P_5' \rangle_{[1.8,2.5]}$ the smaller size of the error leaves some discrimination power.

In order to discern hadronic contributions, the following strategy can be employed. The best fit point from a global fit that excludes P_5' and P_4' can be used to predict the NP contributions entering $\langle X_2 \rangle_{[1.8,2.5]}$, as well as P_5' and P_4' individually. These predictions can be contrasted with the experimental results in order to assess the SM contributions to P_5' and P_4'. As noted above, the SM predicts $\langle X_2 \rangle_{[1.8,2.5]} = -0.14$, but $\langle P_5' \rangle_{[1.8,2.5]} = -0.01$ and $\langle P_4' \rangle_{[1.8,2.5]} = 0.13$. Such values arise from a complex interplay between several SM sources, among them the hadronic form factors, non-factorizable power corrections inside

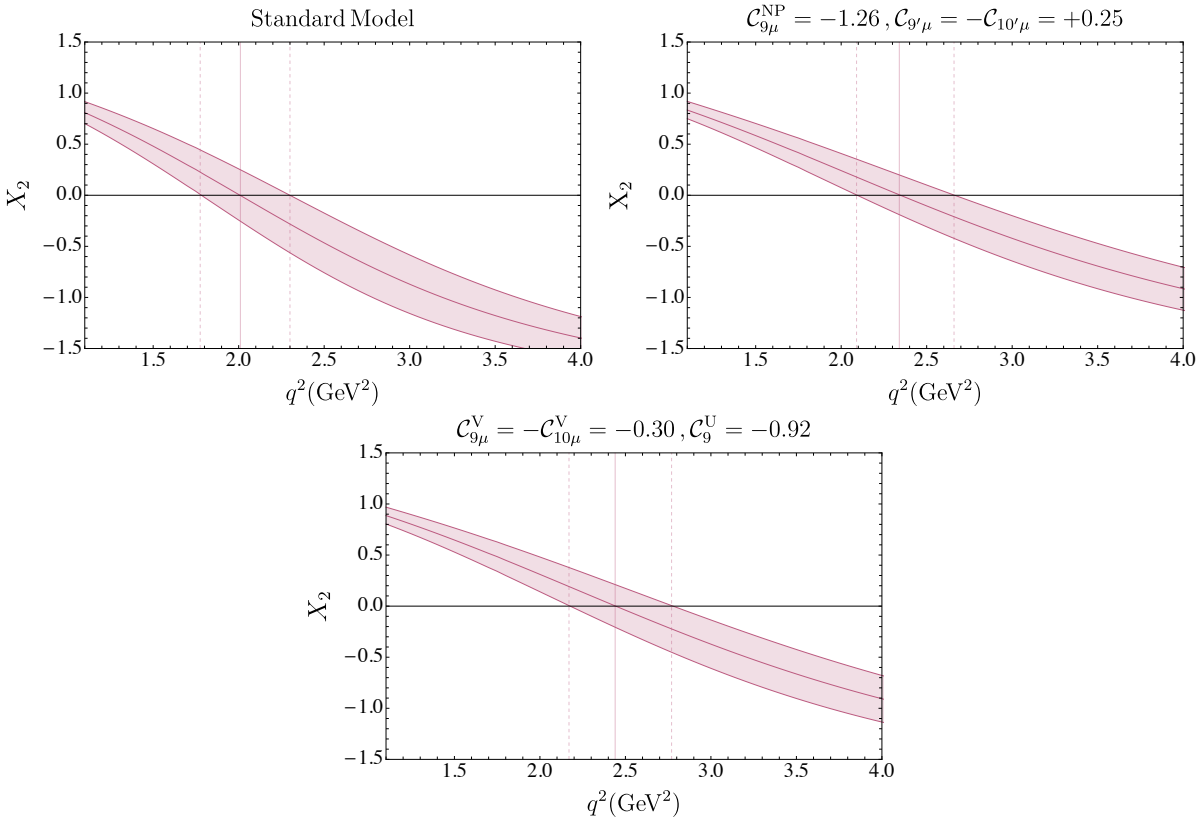

Figure 2.7: X_2 predictions for the SM, Hypothesis V and Scenario 8, including theory uncertainties.

$\mathcal{T}_\perp, \mathcal{T}_\parallel$ (see Ref. [14, 29] for their explicit definitions), the value of the Wilson coefficients in the SM but also perturbative charm-loop contributions. Here we parametrise the remaining charm loop long-distance contributions in a manner that matches the non-perturbative computation from Ref. [23]. In practice, when quoting long-distance charm loops we refer to Eq. (1.34) for the transverse and perpendicular components and for the longitudinal one.

Using Eqs. (1.28-1.27) we can write the observables as follows[7]:

$$\begin{aligned}
\langle P_4' \rangle^{\rm SM}_{[1.8,2.5]} &= 0.35 + 10.63\,{\rm Re}\mathcal{T}_\perp + 1.43\,{\rm Re}\mathcal{T}_\parallel + 49.30\,({\rm Re}\mathcal{T}_\perp)^2 + 0.01 s_\perp - 0.05 s_0\,, \\
\langle P_5' \rangle^{\rm SM}_{[1.8,2.5]} &= -0.34 - 11.71\,{\rm Re}\mathcal{T}_\perp + 1.57\,{\rm Re}\mathcal{T}_\parallel - 55.32\,{\rm Re}(\mathcal{T}_\perp)^2 - 0.01 s_\parallel - 0.05 s_0\,, \\
\langle X_2 \rangle^{\rm SM}_{[1.8,2.5]} &= -0.68 - 22.33\,{\rm Re}\mathcal{T}_\perp + 0.13{\rm Re}\mathcal{T}_\parallel - 104.62\,({\rm Re}\mathcal{T}_\perp)^2 - 0.01 s_\parallel - 0.01 s_\perp\,,
\end{aligned} \tag{2.87}$$

where in the SM in this particular bin one expects: ${\rm Re}\mathcal{T}_\perp \sim -0.028$, ${\rm Re}\mathcal{T}_\parallel \sim +0.025$, and in Refs. [4, 53, 55] $s_{\perp,\parallel,0}$ is taken as a nuisance parameter allowed to vary in the range $s_i \in [-1, 1]$. The constant coefficients in these equations are intricate combinations of Wilson coefficients and form factors in the SM.

The first point to notice is that both $\langle P_4' \rangle_{[1.8,2.5]}$ and $\langle P_5' \rangle_{[1.8,2.5]}$ are dominated by ${\rm Re}\mathcal{T}_\perp$ and the dominant long distance comes from s_0, in both cases with a very similar magnitude. Subleading contributions arise from $\mathcal{T}_\parallel$ and $s_{\perp,\parallel}$. Secondly, $\langle X_2 \rangle_{[1.8,2.5]}$ has a negligible sensitivity to $\mathcal{T}_\parallel$ and s_0, and the first long-distance piece enters via subleading contributions from $s_{\perp,\parallel}$. Thus this observable is basically dominated by ${\rm Re}\mathcal{T}_\perp$ and proves to be quite robust against long-distance charm loop contributions in this bin.

[7] We neglect tiny contributions from ${\rm Im}\mathcal{T}_\perp$

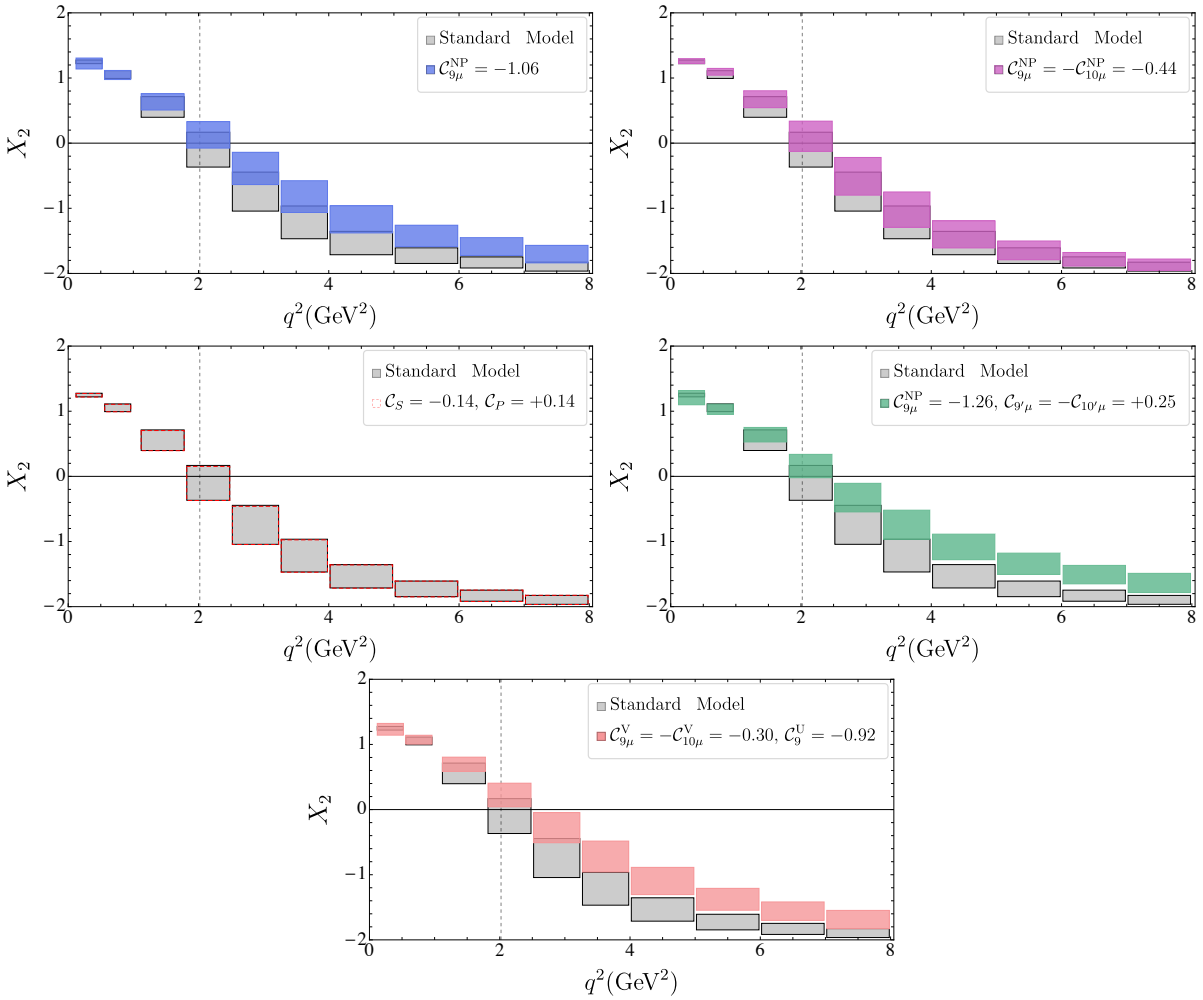

Figure 2.8: SM and NP predictions for X_2 binned in q^2.

Finally, recalling the stability of $\langle X_2\rangle_{[1.8,2.5]}$ under different NP scenarios, we can parametrise this observable to a very good approximation as:

$$\langle X_2\rangle_{[1.8,2.5]} = -0.68 - 22.33\text{Re}\mathcal{T}_\perp - 104.62\,(\text{Re}\mathcal{T}_\perp)^2 + 0.22(\mathcal{C}_{10\mu}^{\rm NP} - \mathcal{C}_{9\mu}^{\rm NP})\,, \tag{2.88}$$

where the interplay between NP and the non-factorizable QCDf hadronic contributions is clearly encoded. This implies that a measurement of $\langle X_2\rangle_{[1.8,2.5]}$ could provide an experimental constraint on $\text{Re}\mathcal{T}_\perp$ in $[1.8, 2.5]$, correlated with the NP scenario used, to be confronted with the SM prediction. The determination of $\text{Re}\mathcal{T}_\perp$ can be seen as a non-trivial test of QCDf. Notice also that, as discussed at the beginning of this section, $\text{Re}\mathcal{T}_\perp$ has a significant impact on the position of the zero of X_2. As soon as $\mathcal{T}_\perp$ is experimentally determined, the correlated measurement of the individual observables $\langle P_4'\rangle_{[1.8,2.5]}$ and $\langle P_5'\rangle_{[1.8,2.5]}$ will provide a handle on s_0, the dominant long-distance charm loop in this bin (see Eqs. (2.87)). The size of such effects should be clearly seen with the precision that should be attained during Run 4 of the LHC.

2.5 Experimental prospects and precision

Finally, in this section we provide a brief comparison of the theoretical predictions of the observables described in the previous sections with the corresponding projected experimental measurements in future runs at the LHC. For the experimental study, data sets are generated with the expected sample sizes collected by the LCHb collaboration at various points in time. The data the experiment currently has

in hand, referred to as the Run 2 data set, is the combination of the Run 1 and Run 2 data with integrated luminosity of $9\,\text{fb}^{-1}$. Projections are made for future LHCb runs: Run 3 with $23\,\text{fb}^{-1}$, Run 4 with $50\,\text{fb}^{-1}$ [126], and Run 5 representing the total data collected by the proposed Upgrade II with $300\,\text{fb}^{-1}$ [127].

The SM values of the angular observables are used in the generation of the pseudo-data. For the P-wave observables (and only for the experimental sensitivity study), the $B^0 \to K^{*0}$ form factors are taken from Ref. [128] and rely on a combination of Light Cone Sum Rules and Lattice QCD calculations. For the S-wave observables, the $B^0 \to K_0^*$ form factors are taken from Ref. [116]. For all observables the non-local charm contribution is taken from Ref. [17], with the longitudinal and S-wave phase difference for all $J^{PC} = 1^{--}$ dimuon resonances relative to the rare mode set to zero. The exact choice of these parameters has no impact on the conclusions of this study. The stability of the fit and the experimental precision on the P-wave observables is largely independent of the details of the model.

2.5.1 Experimental test of symmetry relations

The six symmetry relations may be applied to the results of the binned fits as an independent check of the robustness of the experimental methodology. As the fitted observables are averaged over a q^2 bin the relations are not exact in this experimental context. This is particularly apparent in the lowest q^2 bin, where the changes in the variables with q^2 are most notable. Furthermore, as only the bins for $q^2 < 1\,\text{GeV}^2$ are treated as having massive leptons[8] there is some small imprecision in the symmetry relations for the bins immediately above $1\,\text{GeV}^2$ albeit rather marginal effects of the massless lepton treatment. Example distributions of the relations are shown in Fig. 2.9.

These distributions of the symmetry relations may be used for a ready check by an experimenter of their fit to real data. If the relation calculated from the data lies outside these distributions the fit can be discounted and the experimenter invited to check their method. Care must be taken however as the experimental relations are calculated with q^2 averaged observables. This introduces some model dependence in the distributions of the pseudo-experiments.

2.5.2 S wave in the global fits

Equations (2.71) and (2.73) allow us to include S-wave interference observables in Wilson coefficient fits for NP without having to calculate the S-wave form-factors. The expected precision for W_1 and W_2 with only the P-wave observables, with the interference observables, and the combination of the two has been assessed. Pseudo-experiments are run with the SM hypothesis and using the new optimized interference observables, $PS_i^{r/i}$ introduced in Section 2.1.2. For each of the 1000 pseudo experiments used, W_1 and W_2 are calculated along with their uncertainties, accounting for the correlations between the fitted parameters. The correlation between the expressions involving only P-wave observables and that including the interference observables is assessed for each of W_1 and W_2. Subsequently the average and statistical uncertainty when combining the P wave only part with the interference part is found for each observable.

For the Run 2 data set the narrow bins cannot reliably be used to extract the optimized observables. Therefore here the wider q^2 bins are used. The expected precision of W_1 and W_2 is shown in Fig. 2.10. It can be seen that the combination of P-wave only with the P- and S-wave observables is only marginally more precise than for the P-wave only alone. This is to be expected due to the small contribution of the S wave that is simulated and the presence of P-wave parameters in the combination with the interference observables such that the contribution of the S wave is not statistically independent.

In the future the size of the data sets will become sufficient for the narrower bins to be readily used. An example is shown in Fig. 2.11 of the putative LHCb Run 4 data set with $50\,\text{fb}^{-1}$.

[8] Results corresponding to binned quantities in the region $q^2 > 1.1\,\text{GeV}^2$ are assumed to be massless, since lepton mass effects are small enough so that they can be safely neglected in this range.

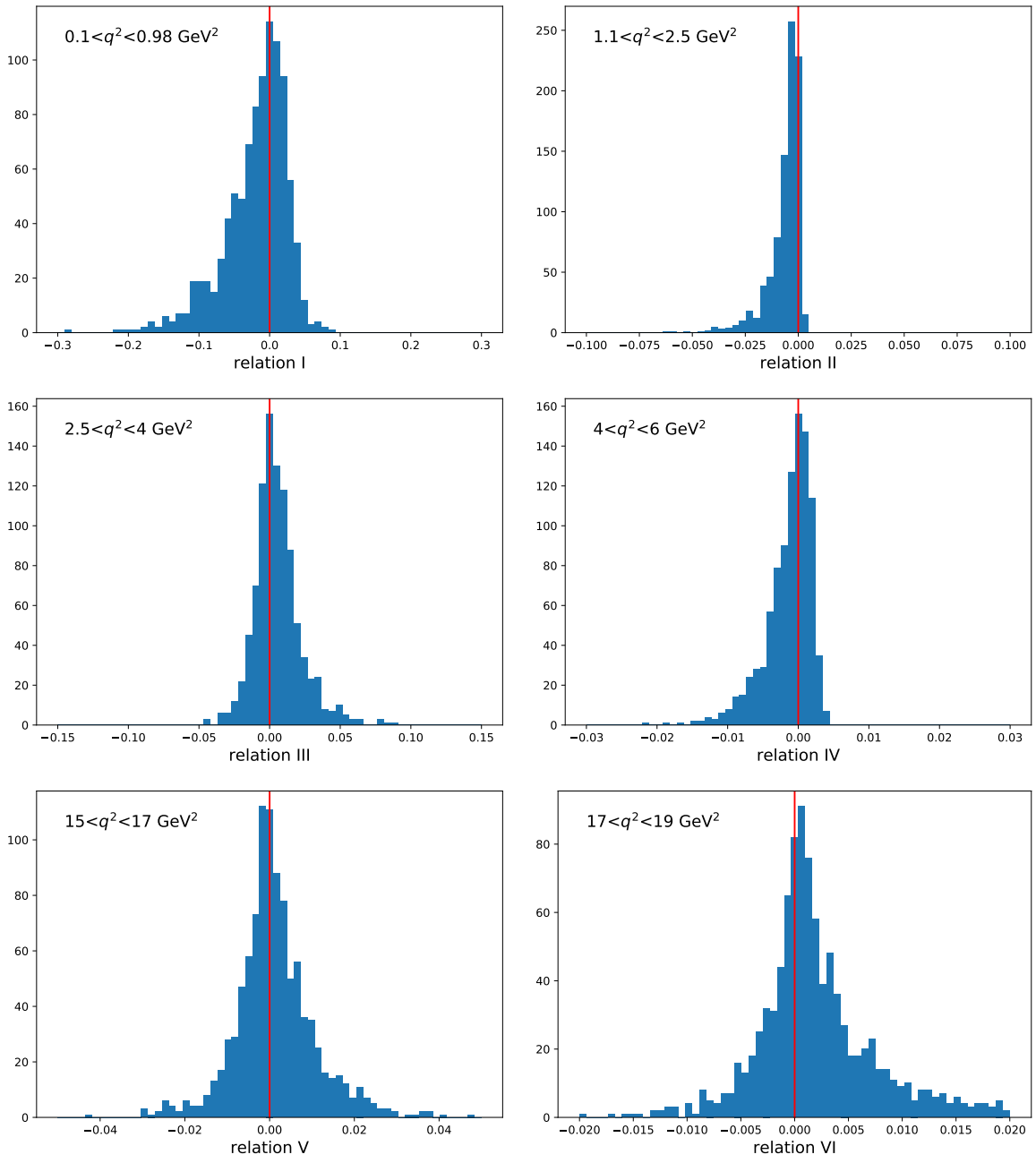

Figure 2.9: Example distributions of the six symmetry relations for the various q^2 bins. The red line is a reference at 0 for the case when the relations are exact. The spread of the distributions is a reflection of the statistical precision of the fit.

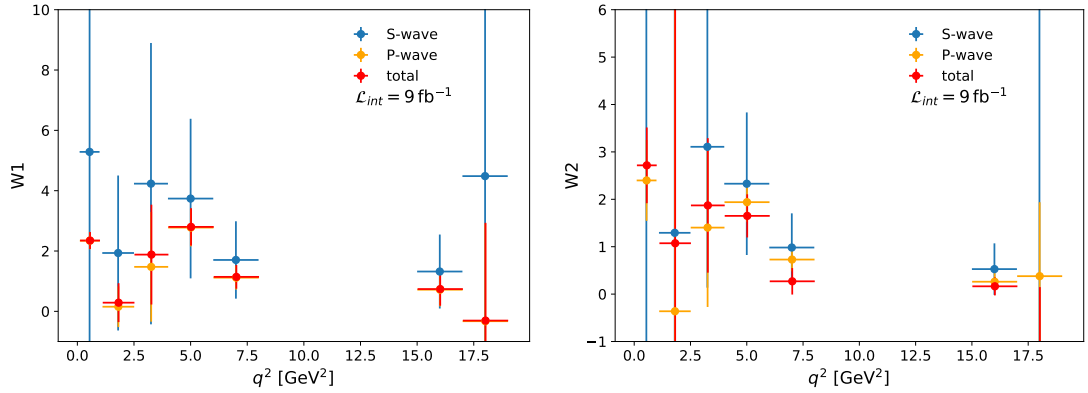

Figure 2.10: Pseudo-experiment results for (left) W_1 and (right) W_2 with the LHCb Run 2 data set.

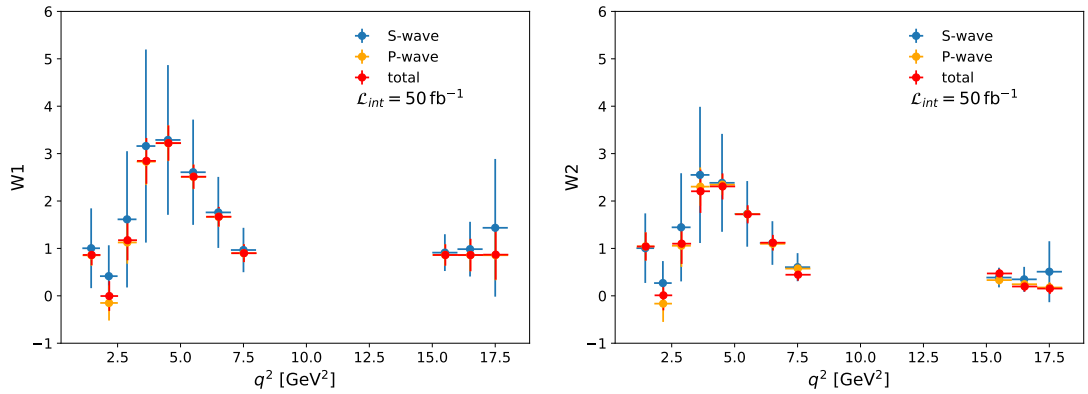

Figure 2.11: Pseudo-expriment results for (left) W_1 and (right) W_2 with the expected LHCb Run 4 data set of $50\,\text{fb}^{-1}$.

2.6 Summary and Conclusions

This chapter presents a study of the $B^0 \to K^{*0}(\to K^+\pi^-)\ell^+\ell^-$ decay once the fully differential decay rate, including contributions of the $K^+\pi^-$ system in a P- or S-wave configuration, is considered. This can be used to analyze such decays in current and future experiments, paving the way for the next step in the analysis of this decay, going beyond previous analyses by identifying and exploring the experimental prospects of massive and S-wave observables that were previously neglected or treated as nuisance parameters. Our analysis relies on a complete description of the symmetries that apply to the full distribution. This enables us to define the complete set of observables that describe the decay and the relations between them, excluding only the presence of scalar or tensor NP contributions.

Our study shows, in particular, that the symmetries of the $B^0 \to K^+\pi^-\ell^+\ell^-$ decay rate give rise to relations that allow a combination of S-wave observables, $W_{1,2}$, to be expressed in terms of P-wave only observables. These combined observables then have no dependence on the poorly known S-wave form factors and therefore offer genuine probes of physics beyond the SM. This opens a new seam in the phenomenology and, for the first time, will allow S-wave events in the data to contribute to global fits for the underlying physics coefficients.

We also present strong bounds on the set of new S-wave observables using two different methods, the relations themselves and Cauchy-Schwartz inequalities relying only on the structure of the observables in terms of 2D complex vectors. They serve as important experimental cross-checks.

Finally, concerning the comparison between the theoretical and the experimental status, we have shown that the exploitation of the symmetry relations for the observables will allow an immediate test of the robustness of the experimental fits to data without resorting to theoretical predictions.

Chapter 3

Symmetries in $B \to D^* \ell \nu$ angular observables

Following the hints of a growing tension with respect to SM expectations concerning b-quark decays, we have reviewed in previous chapters the state-of-the-art analysis of the anomalies in the neutral-current $b \to s\ell^+\ell^-$ transition. However, those are not the only type of semileptonic B decays that currently exhibit discrepancies with respect to the SM. While observables related to the neutral channel $b \to s\ell^+\ell^-$ show tensions in global significances at the level of $\sim 7\sigma$, charged-current $b \to c\ell\nu$ transitions also exhibit deviations from the SM predictions, mainly in LFUV observables comparing $\ell = \tau$ and lighter leptons. First measured as deviating significantly from the SM in 2012 [129, 130], the relevant ratios R_D and R_{D^*} have been updated regularly, leading to a recent decrease of the tension with respect to the SM down to 3.1σ [131–135]. Additional observables have been considered for $B \to D^*\tau\nu$ concerning the polarisation of both the D^* meson [136] and the τ lepton [137, 138]. If the latter agrees with the SM within large uncertainties, the precise Belle measurement of the integrated $F_L^{D^*}$ yields a relatively high value compared to the SM prediction, which appears difficult to accommodate with NP scenarios, as can be seen in Refs. [139–144] that considered a wide set of NP benchmark points.

While neutral-current anomalies observed in a large set of channels and observables can be caused by NP contributions competing with the SM ones generated at the loop level, charged-current anomalies seen in two LFUV ratios require a much larger NP contribution able to compete with tree-level SM processes. In this sense, the latter were much more unexpected and should be scrutinised in more detail, in order to confirm their existence.

In this chapter, based upon Ref. [124], we pay close attention to the decay $B \to D^*\ell\nu$ governed by the quark level transition $b \to c\ell\bar{\nu}$ with $\ell = \tau$ and $\ell = e, \mu$, and more specifically to its angular distribution. Depending on the NP hypotheses chosen, we will identify a set of symmetries for the massless (electron and muon) and massive (tau) distributions that will lead us to find a set of dependencies or relations among the angular coefficients of the distribution. A similar exercise was done in Refs. [28, 122, 125] for the case of the decay mode $B \to K^*\mu^+\mu^-$. Here we will follow closely the detailed work in Ref. [28] (in a very similar way to the one described in Chapter 2) to use the symmetries of the distribution in order to show that depending on the assumptions of the type of NP at work and the mass of the leptons, not all angular coefficients are independent. These relations can be used in the case of the $B \to D^*\ell\nu$ decay as a way of cross-checking the consistency of the measurements of angular observables[1], but also to provide hints on which kind of NP can be responsible for deviations with respect to the SM observed in these observables.

These relations among the observables, based on the symmetries of the angular distribution, lead to a new way of measuring $F_L^{D^*}$ for $B \to D^*\tau\nu$, relying on different coefficients of the distribution compared to the direct measurement performed by the Belle experiment. This can provide a different handle for experimentalists to cross-check the polarisation fraction and confirm or not its unexpectedly high value. Such an alternative extraction of the longitudinal D^* polarisation can also be useful if instabilities occur when extracting the p.d.f. of angular observables due to values of $F_L^{D^*}$ beyond physical boundaries for

[1] An alternative approach is illustrated in Ref. [145] in the case of $B \to \rho(a_1)\ell\nu$ semileptonic decays where the study of specific NP operators extending the SM effective hamiltonian and the large-energy limit of form factors allows one to disentangle the role of the possible new structures in the differential 4-body distribution.

instance[2]. We will provide general expressions for the relations among observables but we will focus mainly on a baseline case without tensor contributions[3] (for the benchmark points analyzed in Ref. [141], the presence of tensor operators decreases the value of $F_L^{D^*}$ for $B \to D^* \tau \nu$ substantially, increasing the discrepancy with the measured value). On the other hand, we will consider the contribution of the pseudoscalar operator that can help to increase $F_L^{D^*}$ and bring it closer to the Belle measurement, as found in Ref. [141]. We will also discuss the simplified case where there are no large NP phases in the Wilson coefficients, i.e. we assume the coefficients are real or the NP phases are small.

This chapter is structured as follows. First, in Section 3.1 we recall the structure of the angular distribution and define the most relevant observables following Ref. [141]. In Section 3.2 we describe the formalism and explain how to count the number of symmetries and dependencies for each particular case and we work out the dependencies in the massless and massive cases, paying special attention to the presence of pseudoscalar operators. In Section 3.3 these dependencies are used to determine $F_L^{D^*}$ (or equivalently $F_T^{D^*}$) in terms of the other observables in various ways and we discuss the impact of binning when using these relations. In Section 3.4 we discuss a possible signature of the presence of light right-handed neutrinos in the absence of tensors and imaginary contributions using the different determinations of $F_L^{D^*}$, and in Section 3.5 the expected experimental sensitivity of forthcoming experiments is discussed. We summarize our conclusions in Section 3.6. In Appendix D.1 some details on the derivation of the exact massive dependencies are provided. Finally, illustrations of the binning effects for the relations discussed in this chapter are given in Appendix D.2.

3.1 $\bar{B} \to D^* \ell \bar{\nu}$ angular distribution

3.1.1 Effective Hamiltonian and angular observables

The angular distribution for $B \to D^* \ell \nu$ has been extensively studied in the literature [148–154]. We will base our studies on the approach described in Ref. [141]. Assuming that there are no light right-handed neutrinos, the distribution can be computed using the effective Hamiltonian:

$$\begin{aligned}\mathcal{H}_{\text{eff}} = \sqrt{2} G_F V_{cb} \big[&(1+g_V)(\bar{c}\gamma_\mu b)(\bar{\ell}_L \gamma^\mu \nu_L) + (-1+g_A)(\bar{c}\gamma_\mu\gamma_5 b)(\bar{\ell}_L \gamma^\mu \nu_L) \\ &+ g_S (\bar{c} b)(\bar{\ell}_R \nu_L) + g_P (\bar{c}\gamma_5 b)(\bar{\ell}_R \nu_L) \\ &+ g_T (\bar{c}\sigma_{\mu\nu} b)(\bar{\ell}_R \sigma^{\mu\nu} \nu_L) + g_{T5} (\bar{c}\sigma_{\mu\nu}\gamma_5 b)(\bar{\ell}_R \sigma^{\mu\nu} \nu_L) \big] + h.c.\end{aligned} \tag{3.1}$$

As it can be seen, we do not include right-handed neutrinos at this stage, which will be discussed later on. One may also use the equivalent notation of Refs. [139, 140] (for instance)

$$\begin{aligned}\mathcal{H}_{\text{eff}} = 4 \frac{G_F}{\sqrt{2}} V_{cb} \big[&(1+g_{V_L})(\bar{c}_L \gamma_\mu b_L)(\bar{\ell}_L \gamma^\mu \nu_L) + g_{V_R} (\bar{c}_R \gamma_\mu b_R)(\bar{\ell}_L \gamma^\mu \nu_L) \\ &+ g_{S_L} (\bar{c}_R b_L)(\bar{\ell}_R \nu_L) + g_{S_R} (\bar{c}_L b_R)(\bar{\ell}_R \nu_L) + g_{T_L} (\bar{c}_R \sigma_{\mu\nu} b_L)(\bar{\ell}_R \sigma^{\mu\nu} \nu_L) \big] + h.c.\end{aligned} \tag{3.2}$$

with the corresponding effective coefficients

$$g_{V,\,A} = g_{V_R} \pm g_{V_L} \,, \qquad g_{S,\,P} = g_{S_R} \pm g_{S_L} \,, \qquad g_T = -g_{T5} = g_{T_L} \,. \tag{3.3}$$

The resulting angular distribution is

[2] This kind of problem was already found in the analysis of the angular distribution of $B \to K^* \mu^+ \mu^-$ by CMS: the fit to data [146] used to extract P_1, P_5' and F_L altogether from the data exhibited instabilities that forced the authors of Ref. [146] to include additional information on F_L rather than leave it free in the fit.

[3] See Ref. [147] for the impact of tensor operators on R_{D^*} and other observables.

$$\frac{d^4\Gamma}{dq^2 d\cos\theta_D d\cos\theta_\ell d\chi} = \frac{9}{32\pi}\Big\{ I_{1c}\cos^2\theta_D + I_{1s}\sin^2\theta_D + \big[I_{2c}\cos^2\theta_D + I_{2s}\sin^2\theta_D\big]\cos 2\theta_\ell + \big[I_{6c}\cos^2\theta_D + I_{6s}\sin^2\theta_D\big]\cos\theta_\ell + \big[I_3\cos 2\chi + I_9\sin 2\chi\big]\sin^2\theta_\ell\sin^2\theta_D + \big[I_4\cos\chi + I_8\sin\chi\big]\sin 2\theta_\ell\sin 2\theta_D + \big[I_5\cos\chi + I_7\sin\chi\big]\sin\theta_\ell\sin 2\theta_D \Big\}, \tag{3.4}$$

where the angular coefficients $I_i \equiv I_i(q^2)$ are given in Ref. [141]:

$$I_{1c} = 2N\left[|\tilde{H}_0^-|^2 + \frac{m_\ell^2}{q^2}|\tilde{H}_0^+|^2 + 2\frac{m_\ell^2}{q^2}|\tilde{H}_t|^2\right], \tag{3.5}$$

$$I_{1s} = \frac{N}{2}\left[3\big(|\tilde{H}_+^-|^2 + |\tilde{H}_-^-|^2\big) + \frac{m_\ell^2}{q^2}\big(|\tilde{H}_+^+|^2 + |\tilde{H}_-^+|^2\big)\right], \tag{3.6}$$

$$I_{2c} = 2N\left[-|\tilde{H}_0^-|^2 + \frac{m_\ell^2}{q^2}|\tilde{H}_0^+|^2\right], \tag{3.7}$$

$$I_{2s} = \frac{N}{2}\left[|\tilde{H}_+^-|^2 + |\tilde{H}_-^-|^2 - \frac{m_\ell^2}{q^2}\big(|\tilde{H}_+^+|^2 + |\tilde{H}_-^+|^2\big)\right], \tag{3.8}$$

$$I_3 = -2N\,\mathrm{Re}\left[\tilde{H}_+^-\tilde{H}_-^{-*} - \frac{m_\ell^2}{q^2}\tilde{H}_+^+\tilde{H}_-^{+*}\right] \tag{3.9}$$

$$I_4 = N\,\mathrm{Re}\left[(\tilde{H}_+^- + \tilde{H}_-^-)\tilde{H}_0^{-*} - \frac{m_\ell^2}{q^2}(\tilde{H}_+^+ + \tilde{H}_-^+)\tilde{H}_0^{+*}\right] \tag{3.10}$$

$$I_5 = 2N\,\mathrm{Re}\left[(\tilde{H}_+^- - \tilde{H}_-^-)\tilde{H}_0^{-*} - \frac{m_\ell^2}{q^2}(\tilde{H}_+^+ + \tilde{H}_-^+)\tilde{H}_t^*\right], \tag{3.11}$$

$$I_{6c} = 8N\frac{m_\ell^2}{q^2}\,\mathrm{Re}\big[\tilde{H}_0^+\tilde{H}_t^*\big], \tag{3.12}$$

$$I_{6s} = 2N\big(|\tilde{H}_+^-|^2 - |\tilde{H}_-^-|^2\big), \tag{3.13}$$

$$I_7 = 2N\,\mathrm{Im}\left[(\tilde{H}_+^- + \tilde{H}_-^-)\tilde{H}_0^{-*} - \frac{m_\ell^2}{q^2}(\tilde{H}_+^+ - \tilde{H}_-^+)\tilde{H}_t^*\right], \tag{3.14}$$

$$I_8 = N\,\mathrm{Im}\left[(\tilde{H}_+^- - \tilde{H}_-^-)\tilde{H}_0^{-*} - \frac{m_\ell^2}{q^2}(\tilde{H}_+^+ - \tilde{H}_-^+)\tilde{H}_0^{+*}\right] \tag{3.15}$$

$$I_9 = -2N\,\mathrm{Im}\left[\tilde{H}_+^-\tilde{H}_-^{-*} - \frac{m_\ell^2}{q^2}\tilde{H}_+^+\tilde{H}_-^{+*}\right], \tag{3.16}$$

where N is a normalization

$$N = \mathcal{B}_{D^*\to D\pi}\frac{G_F^2|V_{cb}|^2}{48(2\pi)^3 m_B^3}q^2\lambda_{BD^*}^{1/2}(q^2)\left(1 - \frac{m_\ell^2}{q^2}\right)^2, \tag{3.17}$$

with $\lambda_{BD^*}(q^2) = m_B^4 + m_{D^*}^4 + q^4 - 2(m_B^2 m_{D^*}^2 + m_B^2 q^2 + m_{D^*}^2 q^2)$ and the amplitudes $\tilde{H}$ correspond to linear combinations of transversity amplitudes for various currents. We can write them in the following way to make the dependence on m_ℓ explicit:

$$\tilde{H}_i^+ = H_i - 2\frac{\sqrt{q^2}}{m_\ell}H_{T,i} \qquad \tilde{H}_i^- = H_i - 2\frac{m_\ell}{\sqrt{q^2}}H_{T,i} \qquad \tilde{H}_t = \frac{\sqrt{q^2}}{m_\ell}\tilde{H}_P \tag{3.18}$$

where $i = 0, +, -$ and H_i correspond to vector and axial currents whereas $H_{T,i}$ correspond to tensor currents, and $\tilde{H}_P$ combines two amplitudes H_t and H_P:

$$\tilde{H}_P = \frac{m_\ell}{\sqrt{q^2}}H_t + H_P \tag{3.19}$$

The H_i amplitudes depend on form factors and on q^2, but not on the lepton mass. In particular,

the presence of $1/m_\ell$ in $\tilde{H}_i^+$ means that the discussion of the limit $m_\ell \to 0$ should be considered after expressing all the angular coefficients in terms of H_i.

3.1.2 Observables

Contrary to $B \to K^* \ell^+ \ell^-$ [11, 12], in the $B \to D^*$ transition any ratio of angular observables is appropriate to reduce uncertainties from form factors. We thus take almost the same list as Ref. [141] for the 12 observables that form a basis[4]:

$$O_i = \left\{ A_0, A_3, A_4, A_5, A_{6s}, A_7, A_8, A_9, A_{\rm FB}, R_{A,B}, F_L^{D^*}, d\Gamma/dq^2 \right\} \tag{3.20}$$

Compared to Ref. [141], we do not include the observable A_{λ_ℓ} in this list because it is related to the τ polarisation and requires one coefficient not included in the angular distribution. Instead we must introduce an additional observable (not included in Ref. [141]) so that the numbers of angular coefficients and observables match. We may choose for instance:

$$A_0 = \frac{1}{d\Gamma/dq^2}(I_{1c} + I_{1s}) \tag{3.21}$$

We recall here the definition of the observables defined in Ref. [141] that will play an important role in this chapter:

- The differential decay rate
$$\frac{d\Gamma}{dq^2} = \frac{1}{4}(3I_{1c} + 6I_{1s} - I_{2c} - 2I_{2s}) \tag{3.22}$$
- The longitudinal and transverse D^* polarisation decay rates:
$$F_L^{D^*} = \frac{d\Gamma_L/dq^2}{d\Gamma/dq^2} = \frac{1}{d\Gamma/dq^2}\frac{1}{4}(3I_{1c} - I_{2c}) \tag{3.23}$$
$$F_T^{D^*} = 1 - F_L^{D^*} = \frac{d\Gamma_T/dq^2}{d\Gamma/dq^2} = \frac{1}{d\Gamma/dq^2}\frac{1}{2}(3I_{1s} - I_{2s}) \tag{3.24}$$
In order to make a more explicit contact with the integrated longitudinal polarisation we also introduce $\tilde{F}_L^{D^*} = (d\Gamma_L/dq^2)/\Gamma$ and $\tilde{F}_T^{D^*} = (d\Gamma_T/dq^2)/\Gamma$, where $\Gamma = \Gamma(B \to D^* \ell\nu)$ with $\ell = \tau, \mu, e$.
- The ratio $R_{A,B}$ describing the relative weight of the various angular coefficients in the partial differential decay rate with respect to θ_ℓ, in analogy with the longitudinal polarisation fraction
$$R_{A,B}(q^2) = \frac{d\Gamma_A/dq^2}{d\Gamma_B/dq^2} = \frac{1}{2}\frac{(I_{1c} + 2I_{1s} - 3I_{2c} - 6I_{2s})}{(I_{1c} + 2I_{1s} + I_{2c} + 2I_{2s})} \tag{3.25}$$

Eqs. (3.22), (3.23) and (3.24) are the "standard definitions" of $d\Gamma/dq^2$, $F_L^{D^*}$ and $F_T^{D^*}$ respectively, and they are used to determine these observables with this particular functional dependence of the angular coefficients I.

Similarly to the discussion in Ref. [157], the definition of observables integrated over a bin (or over the whole phase space) requires some care. Experimentally, the measurement yields the integrated angular coefficients $\langle I_k \rangle_\ell$ with the definition[5]

$$\langle X \rangle_\ell = \int_{m_\ell^2}^{(m_B - m_{D^*})^2} dq^2\, X \tag{3.26}$$

where the subscripts ℓ and 0 indicate the massive case (with m_ℓ) and the massless case respectively. We can then define the "standard" integrated longitudinal and transverse polarisations

[4] Further discussions of this differential decay rate can be found in Ref. [155] including CP-violating observables and in Ref. [156] when D^* subsequently decays either to $D\pi$ or to $D\gamma$.

[5] Notice that the definition of $\langle I_i \rangle$ in Ref. [141] is normalized with $\Gamma(B \to D^* \ell\nu)$, while we prefer to keep the dependence on $\Gamma(B \to D^* \ell\nu)$ explicit.

$$\langle \tilde{F}_L^{D^*} \rangle_\ell = \frac{1}{4\Gamma} \left(3\langle I_{1c} \rangle_\ell - \langle I_{2c} \rangle_\ell\right) \tag{3.27}$$

$$\langle \tilde{F}_T^{D^*} \rangle_\ell = \frac{1}{2\Gamma} (3\langle I_{1s} \rangle_\ell - \langle I_{2s} \rangle_\ell) \tag{3.28}$$

The Belle measurement is actually $\langle \tilde{F}_L^{D^*} \rangle_\tau^{\text{Belle}} = 0.60 \pm 0.09$.

3.1.3 Global fits

At this stage, a brief overview of our current understanding of the possible NP contributions is useful. Global fits to $b \to c\tau\nu$ favour overwhelmingly a NP contribution through a real g_{V_L} for $b \to c\tau\nu$, as it allows one to modify the tauonic branching ratios involved in R_D and R_{D^*} by the same amount without altering the angular observables, in agreement with the current data (apart from $F_L^{D^*}$ already discussed) [139–141]. For real contributions, scenarios based purely on scalar and pseudoscalar contributions exhibit some tension with the B_c lifetime, depending on the relative size of the contribution allowed for $B_c \to \tau\nu$ in the total lifetime, which requires the pseudoscalar contribution to be somewhat small [158–160]. Similarly, real tensor contributions are disfavoured, as they tend to decrease the longitudinal polarisation of the D^* meson compared to the SM [141], when the first measurement from the Belle experiment indicated a value higher than SM expectations [136]. If g_{V_L} is allowed as well as contributions of other operators, the former is dominant and the other operators (scalar, pseudoscalar, tensors) are subleading. Other constraints on $b \to c\tau\nu$ come from direct searches at LHC involving mono-τ jets [161]. The corresponding bounds are again much tighter on tensor operators than on vector or scalar operators.

Some of these scenarios allow large imaginary parts [139–141], with a similar hierarchy of scenarios as in the real case. However, one must take into account that such large imaginary parts are allowed due to the limited number of observables. Additional observables could bring a dramatic modification of the landscape of the allowed scenarios, restricting the possible size of imaginary parts and the applicability of scenarios currently viable severely. Indeed some of the NP scenarios favour large imaginary parts so that there are no interferences between the SM and NP contributions, which add up in quadrature only (see for instance the scenario of a purely imaginary g_{S_L} discussed in Ref. [162]). Restricting the size of these imaginary parts would enhance the interferences between SM and NP parts and would restrict the viability of the NP models where these interferences are negative.

This trend is confirmed by model-dependent analyses. Most of the models with a single-particle exchange aiming at reproducing the data in $b \to c\ell\nu$ do not generate tensor contributions, apart from the scalar $SU(2)_L$-doublet leptoquark R_2 (as illustrated, for instance, in Ref. [163]) which however generates much larger contributions to g_{S_L} (i.e. g_S and g_P) than to g_{T_L} (i.e. g_T and g_{T5}). This effect is enhanced by the running from the NP scale (1 TeV) down to the m_b scale (reducing the tensor contribution by $\sim 20\%$ and increasing the scalar contribution by $\sim 80\%$), so that scalar contributions are likely to be larger than the tensor contributions if the latter are present [139]. In Ref. [139, 140], a model with a single R_2 leptoquark with complex couplings was shown to have a lower SM-pull than other NP scenarios once the constraint from the B_c lifetime was taken into account. In Ref. [162], a viable model with the R_2 leptoquark was proposed in combination with the S_1 leptoquark, leading to (large real) vector couplings as well as (large imaginary) scalar and (smaller imaginary) tensor couplings.

We will thus consider as a baseline scenario that tensor contributions are subleading compared to other operators. We will also consider that the imaginary parts of the amplitudes can be neglected. In the SM as well as in the case of real NP, the only phase comes from the CKM matrix element, and it is actually the same for all the amplitudes. Under our baseline scenario, for instance, the angular coefficients corresponding to imaginary parts ($I_{7,8,9}$) are either small or vanishing, as well as any imaginary contribution. For completeness we will provide full expressions for the relations among the coefficients including these terms (see Appendix D.1 for the general expressions in the massive case).

m_ℓ	Tensor ops.	Pseudoscalar op.	Coefficients	Dependencies	Amplitudes	Symmetries
0	No	No	11	6	3	1
0	No	Yes	11	5	4	2
0	Yes	No	11	0	6	1
0	Yes	Yes	12	0	7	2
$\neq 0$	No	No	12	5	4	1
$\neq 0$	No	Yes	12	5	4	1
$\neq 0$	Yes	No	12	0	7	2
$\neq 0$	Yes	Yes	12	0	7	2

Table 3.1: Symmetries and dependencies among the $B \to D^* \ell \nu$ angular observables depending on the mass of the lepton and the contribution of tensor and pseudoscalar operators.

3.2 Relations among angular coefficients

3.2.1 Symmetries and dependencies

The decay $B \to D^* \ell \nu$ has a rich angular structure, and it is interesting to investigate whether all the angular observables defined in the previous section are independent, following the same steps as in Refs. [11, 28, 122, 125] for $B \to K^* \ell^+ \ell^-$[6]. We can consider the angular coefficients as being bilinears in

$$\begin{aligned} \vec{A} \;=\; \Big(&\mathrm{Re}(H_0), \mathrm{Im}(H_0), \mathrm{Re}(H_+), \mathrm{Im}(H_+), \mathrm{Re}(H_-), \mathrm{Im}(H_-), \\ &\mathrm{Re}(H_{T,0}), \mathrm{Im}(H_{T,0}), \mathrm{Re}(H_{T,+}), \mathrm{Im}(H_{T,+}), \mathrm{Re}(H_{T,-}), \mathrm{Im}(H_{T,-}), \mathrm{Re}(\tilde{H}_P), \mathrm{Im}(\tilde{H}_P)\Big) \end{aligned} \tag{3.29}$$

Recalling the discussion in Section 2.2, an infinitesimal transformation will be given by

$$\vec{A}' = \vec{A} + \vec{\delta} \tag{3.30}$$

For the infinitesimal transformation to leave the coefficients I unchanged, the vector $\vec{\delta}$ has to be perpendicular to the hyperplane spanned by the set of gradient vectors $\vec{\nabla} I_i$ (with the derivatives taken with respect to the various elements of $\vec{A}$). If the I_i are all independent, the gradient vectors should span the whole space available for the coefficients, i.e. the dimension of the space for the gradient vectors should be identical to the number of angular coefficients.

One can define:

- The number of coefficients n_c, given directly by the angular distribution
- The number of dependencies n_d, given by the difference between the number of angular coefficients I_i and the dimension of the space given by the gradient vectors (provided by the rank of the matrix $M_{ij} = \nabla_i I_j$)
- The number of helicity/transversity amplitudes n_A, leading to $2n_A$ real degrees of freedom
- The number of continuous symmetries n_s explaining the degeneracies among angular coefficients

One has the following relation

$$n_c - n_d = 2n_A - n_s \tag{3.31}$$

which we can investigate in various cases for $B \to D^* \ell \nu$ summarised in Table 3.1.

As discussed above, the assumption of no tensor contributions seems favoured by the current global fits and we will stick to this assumption. In this case it is expected according to Table 3.1 the existence of 5 or 6 relations. The presence or absence of the pseudoscalar operator does not modify the outcome of the analysis and the number of dependencies in the massive case due to Eq. (3.19). However, we

[6] See also Section 2.2 in Chapter 2 of this thesis for a review on the strategy to determine the number of independent coefficients and existing symmetries in the case of $B \to K^* \ell^+ \ell^-$.

find interesting to discuss its effect separately as it was found in Ref. [141] that such a pseudoscalar contribution can help to alleviate the tension in $F_L^{D^*}$ for $B \to D^* \tau \nu$.

We can now explore the dependence relations between angular coefficients, depending on the lepton mass, the presence of pseudoscalar and tensor operators. These relations can be used as a consistency test among the observables if all of these observables are measured in order to check the very general assumptions made to derive them. If these relations are not fulfilled, it means that there is an issue with one or more of the measurements or some of the underlying assumptions (negligible NP in tensor operator, negligible imaginary parts) are not correct. Such tests are completely independent on the details of the NP model or the hadronic inputs.

3.2.2 Massless case with no pseudoscalar operator and no tensor operators

The expressions for the angular observables become in terms of the amplitudes themselves

$$
\begin{aligned}
I_{1c} &= 2N \times |H_0|^2 && (3.32)\\
I_{1s} &= \frac{N}{2} \times 3\left[|H_+|^2 + |H_-|^2\right] && (3.33)\\
I_{2c} &= 2N \times (-1)|H_0|^2 && (3.34)\\
I_{2s} &= \frac{N}{2}\left[|H_+|^2 + |H_-|^2\right] && (3.35)\\
I_3 &= -2N \times \mathrm{Re}[H_+ H_-^*] && (3.36)\\
I_4 &= N\left[\mathrm{Re}[H_0 H_+^* + \mathrm{Re}[H_0 H_-^*]\right] && (3.37)\\
I_5 &= 2N\left[\mathrm{Re}[H_0 H_+^* - \mathrm{Re}[H_0 H_-^*]\right] && (3.38)\\
I_{6c} &= 0 && (3.39)\\
I_{6s} &= 2N\left[|H_+|^2 - |H_-|^2\right] && (3.40)\\
I_7 &= 2N\left[-\mathrm{Im}[H_0 H_+^*] - \mathrm{Im}[H_0 H_-^*]\right] && (3.41)\\
I_8 &= N\left[-\mathrm{Im}[H_0 H_+^*] + \mathrm{Im}[H_0 H_-^*]\right] && (3.42)\\
I_9 &= -2N \times \mathrm{Im}[H_+ H_-^*] && (3.43)
\end{aligned}
$$

In this case, the only continuous symmetry that can be found is simply

$$
H_0 \to e^{i\alpha} H_0\,, \qquad H_- \to e^{i\alpha} H_-\,, \qquad H_+ \to e^{i\alpha} H_+ \tag{3.44}
$$

and only 5 of the 11 observables[7] are independent and 6 dependencies are found. Consequently, one can invert the system to determine the value of the real and imaginary parts of the amplitudes in terms of some of the angular coefficients, and re-express the other ones in terms of the same angular coefficients leading to the following relations:

$$
\begin{aligned}
I_{1c} &= -I_{2c} && (3.45)\\
I_{1s} &= 3I_{2s} && (3.46)\\
-4I_3 I_{2c} &= -4I_4^2 + I_5^2 - I_7^2 + 4I_8^2 && (3.47)\\
-2I_9 I_{2c} &= I_5 I_7 - 4I_4 I_8 && (3.48)\\
-4I_{2c}\left(\frac{1}{2}I_{6s} + \frac{2}{3}I_{1s}\right) &= (2I_4 + I_5)^2 + (I_7 + 2I_8)^2 && (3.49)\\
-4I_{2c}\left(-\frac{1}{2}I_{6s} + \frac{2}{3}I_{1s}\right) &= (-2I_4 + I_5)^2 + (I_7 - 2I_8)^2 && (3.50)
\end{aligned}
$$

These relations can be used as a consistency test among the observables if all of these observables are measured, under the hypothesis that we have outlined (negligible lepton mass, negligible pseudoscalar and tensor operators).

Another way of exploiting these equations consists in combining the non-trivial relations Eqs. (3.47)-(3.50) under the assumption that $I_{7,8,9} = 0$ (taking all imaginary parts to be zero). For future use under

[7] Notice that there are 11 coefficients in this case: $I_{6c} = 0$ and consequently there are 11 observables since A_{FB} and A_{6s} are proportional.

this assumption we reorganise these equations, allowing us to make contact with the massive ones later on:

$$I_3^2 = \frac{4}{9} I_{1s}^2 - \frac{1}{4} I_{6s}^2 \tag{3.51}$$

$$I_4^2 = -\frac{1}{3} I_{1s} I_{2c} + \frac{1}{2} I_{2c} I_3 \tag{3.52}$$

$$I_5^2 = -\frac{2}{3} I_{2c} (2 I_{1s} + 3 I_3) \tag{3.53}$$

One of the dependencies disappears once $I_{7,8,9} = 0$ is taken.

3.2.3 Massless case with pseudoscalar operator but no tensor operators

The same relations between angular observables and amplitudes hold as in the previous case, apart from

$$I_{1c} = 2N \left[|H_0|^2 + 2|H_P|^2 \right] \tag{3.54}$$

One can see that the two symmetries are

$$H_0 \to e^{i\alpha} H_0 \,, \qquad H_- \to e^{i\alpha} H_- \,, \qquad H_+ \to e^{i\alpha} H_+ \,, \qquad H_P \to e^{i\beta} H_P \,, \tag{3.55}$$

Again, by inverting the system one can obtain the same relations as in the massless case without pseudoscalar contributions, see Eqs. (3.46)-(3.50), except for Eq. (3.45) which is not fulfilled.

Like in the previous case, these relations can be used as a consistency test among the observables if all of these observables are measured, under the hypothesis that we have outlined (negligible lepton mass, negligible tensor operators).

3.2.4 Massive case with pseudoscalar operator but no tensor operators

The symmetries in the massive case with pseudoscalar operator but no tensors are in principle a simple extension of the analogous massless case. However, obtaining the expression of the dependencies in the massive case is a rather non-trivial task. The absence of tensors implies that there is no distinction between "+" and "-" components of $\tilde{H}_i^+$ and $\tilde{H}_i^-$ (see Eq. (3.18)) and the only surviving symmetry in this case is

$$H_0 \to e^{i\alpha} H_0 \,, \quad H_- \to e^{i\alpha} H_- \,, \quad H_+ \to e^{i\alpha} H_+ \,, \quad H_t \to e^{i\alpha} H_t \,, \quad H_P \to e^{i\alpha} H_P \tag{3.56}$$

One finds five dependencies in this case, which are identified by solving the system of non-linear equations. The first one is trivial:

$$0 = I_{1s} \left(1 - \frac{m_\ell^2}{q^2} \right) - I_{2s} \left(3 + \frac{m_\ell^2}{q^2} \right) \tag{3.57}$$

and the other exact four non-trivial dependencies are detailed in Appendix D.1.

We will consider the simplifying case where all Wilson coefficients are real so that $I_{7,8,9}$ and all imaginary contributions can be neglected (see Appendix D.1 for the general case without these assumptions). The remaining four dependencies are then simplified substantially

$$I_3^2 = \left(1 - \frac{m_\ell^2}{q^2} \right)^2 \left[\left(\frac{2 I_{1s}}{3 + m_\ell^2/q^2} \right)^2 - \frac{I_{6s}^2}{4} \right] \tag{3.58}$$

$$I_4^2 = \frac{I_{2c} (2 I_{1s} (m_\ell^2 - q^2) + I_3 (m_\ell^2 + 3 q^2))}{2 (m_\ell^2 + 3 q^2)} \tag{3.59}$$

$$\begin{aligned} I_5^2 = {} & \left[-4 I_{2c} I_{6c} I_{6s} (m_\ell^2 - q^2)^2 (m_\ell^2 + 3 q^2) + I_{6c}^2 (m_\ell^2 - q^2)^2 \left[2 I_{1s} (m_\ell^2 - q^2) + I_3 (m_\ell^2 + 3 q^2) \right] \right. \\ & \left. -16 I_{2c}^2 q^4 \left[2 I_{1s} (-m_\ell^2 + q^2) + I_3 (m_\ell^2 + 3 q^2) \right] \right] / \left[8 I_{2c} (m_\ell^2 - q^2)^2 (m_\ell^2 + 3 q^2) \right] \end{aligned} \tag{3.60}$$

$$I_{6c}^2 = -8 m_\ell^2 \left[I_{1c} I_{2c} (-m_\ell^2 + q^2) + I_{2c}^2 (m_\ell^2 + q^2) \right] / \left[(m_\ell^2 - q^2)^2 \right] \tag{3.61}$$

The first three equations above are the generalisation of Eqs. (3.51)-(3.53) in the massive case while the last equation is new: it would vanish in the massless limit with no tensors. These relations can be used as a consistency test among the observables if all of these observables are measured, under the hypothesis that we have outlined (no tensor operators, imaginary contributions negligible).

The last two equations can be combined to get rid of the I_{6c}^2 term and obtain the massive counterpart of Eq. (3.53):

$$\begin{aligned} I_5^2 \;=\; & \left[4(m_\ell^2-q^2)^2 I_{1s}(m_\ell^2(I_{1c}-I_{2c})-2q^2 I_{2c})+2(m_\ell^2+3q^2)(m_\ell^4(I_{1c}-I_{2c})-2q^4 I_{2c}\right. \\ & \left. -m_\ell^2 q^2(I_{1c}+I_{2c}))I_3-(m_\ell^2-q^2)^2(m_\ell^2+3q^2)I_{6c}I_{6s}\right] / \left[2(m_\ell^2-q^2)^2\,(m_\ell^2+3q^2)\right] \end{aligned} \tag{3.62}$$

Eq. (3.61) has obviously no counterpart in the massless case, as it vanishes then[8].

3.2.5 Cases with tensor operators

In the massive case with tensors the degeneracy between the $\tilde{H}_i^+$ and $\tilde{H}_i^-$ is broken and two symmetries are identified. The symmetries are better described in terms of the tilde-fields:

$$\tilde{H}_i^- \to e^{i\alpha}\tilde{H}_i^-\,, \qquad \tilde{H}_i^+ \to e^{i\beta}\tilde{H}_i^+\,, \qquad \tilde{H}_t \to e^{i\beta}\tilde{H}_t\,. \tag{3.63}$$

Unfortunately there are no dependencies in this case. The same is true in the massless case.

3.3 Expressions of the D^* polarisation

In the previous section, we have obtained several relationships between the angular coefficients under various hypotheses, assuming that tensor contributions are negligible. We can use these relations in order to obtain alternative determinations of the longitudinal polarisation $F_L^{D^*}$. From Section 3.3.2 to Section 3.3.4, we will provide these exact relationships in their binned form, but the corresponding unbinned versions have exactly the same form.

3.3.1 Massless case without pseudoscalar operator

For completeness we discuss the case with zero mass and no pseudoscalar operator, but still including all imaginary terms. Eqs. (3.45)-(3.46) are trivial. Eqs. (3.47)-(3.50) can be rewritten in terms of observables providing different determinations of $F_L^{D^*}$:

$$\pi A_3 F_L^{D^*} = \frac{2}{9}(A_5^2-A_7^2)-\frac{1}{8}\pi^2(A_4^2-A_8^2) \tag{3.64}$$

$$\pi A_9 F_L^{D^*} = \frac{4}{9}A_5A_7+\frac{1}{4}\pi^2 A_4A_8 \tag{3.65}$$

$$(F_L^{D^*})^2 = \left[\frac{8}{9}(A_5^2+A_7^2)+\frac{1}{2}\pi^2\left(A_4^2+A_8^2\right)\right]R_{A,B} \tag{3.66}$$

$$A_{FB}F_L^{D^*} = \pi\left(A_4A_5-A_7A_8\right) \tag{3.67}$$

We recall that A_i are defined from the angular observables up to a numerical normalization given in Ref. [141]. A similar set of expressions can be written for $\tilde{F}_L^{D^*}$, $\tilde{A}_i$ and $\tilde{A}_{FB}$ rather than $F_L^{D^*}$, A_i and A_{FB}, respectively, by substituting the normalization in terms of $d\Gamma/dq^2$ by the integrated decay rate Γ. These expressions can then be binned trivially, however they are rather cumbersome to use. In the following two subsections we will restrict to the case of removing any imaginary contribution corresponding to our baseline scenario that will be relevant to the extraction of $F_L^{D^*}$.

[8] In the massive case, this relation provides access to a sum of two related observables A_{6s} and A_{FB}:

$$2\langle A_{6s}\rangle_\ell + 9\langle A_{\rm FB}\rangle_\ell = \frac{27}{2\sqrt{2}}\frac{1}{\Gamma}\,m_\ell\left\langle\frac{1}{q^2-m_\ell^2}\sqrt{I_{1c}I_{2c}(m_\ell^2-q^2)-I_{2c}^2(m_\ell^2+q^2)}\right\rangle_\ell$$

3.3.2 Massless case without imaginary contributions

Using Eqs. (3.46) and (3.51) we obtain one of the most relevant results of this chapter:

$$\langle \tilde{F}_T^{D^*} \rangle_0 = \frac{1}{\Gamma} \Big\langle 2\sqrt{I_3^2 + \frac{1}{4} I_{6s}^2} \Big\rangle_0 \qquad \text{where} \qquad \langle \tilde{F}_T^{D^*} \rangle_0 = 1 - \langle \tilde{F}_L^{D^*} \rangle_0 \tag{3.68}$$

This expression can be used as an alternative way to determine the integrated $F_L^{D^*}$ in the massless case (without imaginary contributions but allowing for the presence of pseudoscalars) from experiment instead of the traditional determination in terms of I_{1s} and I_{2s} in Eq. (3.27) and Eq. (3.28).

This expression can be generalised to the case of smaller bins spanning only part of the whole kinematic range, leading to

$$\langle \tilde{F}_T^{D^*} \rangle_0^i = \frac{1}{\Gamma} \Big\langle 2\sqrt{I_3^2 + \frac{1}{4} I_{6s}^2} \Big\rangle_0^i \tag{3.69}$$

where i means that the integral in Eq. (3.26) is taken over the bin i with a narrower $[q^2_{i,\text{min}}, q^2_{i,\text{max}}]$ range[9].

If we restrict further to the case without pseudoscalars (in this case $I_{1c} = -I_{2c}$ is fulfilled), we obtain further expressions using Eqs. (3.52) and (3.53):

$$\langle \tilde{F}_L^{D^*} \rangle_0 = \frac{1}{\Gamma} \Big\langle \frac{I_5^2 - 4 I_4^2}{4 I_3} \Big\rangle_0 \tag{3.70}$$

$$= \frac{1}{\Gamma} \Big\langle R_{A,B} \left(I_3 + \sqrt{4 \frac{I_4^2}{R_{A,B}} + I_3^2} \right) \Big\rangle_0 = \frac{1}{\Gamma} \Big\langle R_{A,B} \left(-I_3 + \sqrt{\frac{I_5^2}{R_{A,B}} + I_3^2} \right) \Big\rangle_0 \tag{3.71}$$

where $R_{A,B}$ is positive and non-vanishing by construction.

3.3.3 Massive case with pseudoscalar operator but without imaginary contributions

In this case, we focus on Eqs. (3.57), (3.58) and (3.59) to derive new descriptions of $F_L^{D^*}$ since Eq. (3.60) is too involved to provide a useful alternative approach to $F_L^{D^*}$. Eqs. (3.57) and (3.58) yield:

$$\langle \tilde{F}_T^{D^*} \rangle_\ell = \frac{1}{\Gamma} \Big\langle \sqrt{(A\, I_3)^2 + \frac{1}{4} (B\, I_{6s})^2} \Big\rangle_\ell \qquad \text{where} \qquad \langle \tilde{F}_T^{D^*} \rangle_\ell = 1 - \langle \tilde{F}_L^{D^*} \rangle_\ell \tag{3.72}$$

where we define the auxiliary kinematic quantities (whose value in the massless case is two)

$$A = \frac{m_\ell^2 + 2q^2}{q^2 - m_\ell^2} \qquad B = 2 + \frac{m_\ell^2}{q^2} \tag{3.73}$$

One can write an equivalent equation to Eq. (3.72) for narrower q^2 bins similary to the previous section. In the case of Eq. (3.59) we do not substitute I_{2c}, leading to:

$$\langle \tilde{F}_T^{D^*} \rangle_\ell = 1 - \langle \tilde{F}_L^{D^*} \rangle_\ell = \frac{1}{\Gamma} \Big\langle A \left(I_3 - 2 \frac{{I_4}^2}{I_{2c}} \right) \Big\rangle_\ell \tag{3.74}$$

Relating this equation with the massless case is not straightforward given that in the massless case I_{2c} was substituted (before integrating) in terms of $F_L^{D^*}$ and $R_{A,B}$.

[9] Notice that $\langle \tilde{F}_L^{D^*} \rangle_0 + \langle \tilde{F}_T^{D^*} \rangle_0 = 1$ holds because the integration is performed over the whole kinematic range. For the observables $\langle \tilde{F}_L^{D^*} \rangle_0^i$ and $\langle \tilde{F}_T^{D^*} \rangle_0^i$ shown in Figs. 3.1-3.3 and also in Figs. D.1-D.6, this is no longer the case due to the normalization of $\tilde{F}_L^{D^*}$ and $\tilde{F}_T^{D^*}$: $\langle \tilde{F}_L^{D^*} \rangle_0^i + \langle \tilde{F}_T^{D^*} \rangle_0^i = \langle d\Gamma/dq^2 \rangle_0^i / \Gamma < 1$. It is trivial to check that a different normalization for $\tilde{F}_L^{D^*}$ and $\tilde{F}_T^{D^*}$ would only affect the normalization $1/\Gamma$ appearing in the binned expressions.

3.3.4 Cases with pseudoscalar operator and imaginary contributions

This corresponds to the most complete expression allowing for the presence of pseudoscalars and also imaginary parts, but no tensors. This can be achieved, as in the previous section, by using I_{1s} and I_{2s} instead of I_{1c} and I_{2c} as a starting point. The corresponding expression in the massless case is:

$$\langle \tilde{F}_T^{D^*} \rangle_0 \quad = \quad \frac{1}{\Gamma} \Big\langle 2\sqrt{I_3^2 + I_9^2 + \frac{1}{4} I_{6s}^2} \Big\rangle_0 \qquad \text{where} \qquad \langle \tilde{F}_T^{D^*} \rangle_0 = 1 - \langle \tilde{F}_L^{D^*} \rangle_0 \tag{3.75}$$

and in the massive case

$$\langle \tilde{F}_T^{D^*} \rangle_\ell = \frac{1}{\Gamma} \Big\langle \sqrt{(A\, I_3)^2 + (A\, I_9)^2 + \frac{1}{4} (B\, I_{6s})^2} \Big\rangle_\ell \qquad \text{where} \qquad \langle \tilde{F}_T^{D^*} \rangle_\ell = 1 - \langle \tilde{F}_L^{D^*} \rangle_\ell \tag{3.76}$$

Similar expressions can be written for $\langle \tilde{F}_T^{D^*} \rangle_\ell^i$ defined for narrower q^2 bins. These expressions represent the most general alternative ways to determine the massless and massive polarisation fractions. Compared to the previous case, one can see that the presence of imaginary contributions comes simply from the additional I_9 term in Eqs. (3.75) and (3.76), see also Eq. (D.10) in Appendix D.1.

Within this more general framework, Eqs. (3.57) and (D.10) yield the following simple relation among the observables defined in Section 3.1.2:

$$\langle x_1 (\tilde{F}_T^{D^*})^2 \rangle_\ell = \langle x_2 \left(\tilde{A}_3^2 + \tilde{A}_9^2 \right) + x_3 \left(\tilde{A}_{6s} \right)^2 \rangle_\ell \tag{3.77}$$

where $\tilde{A}_i$ stands for the observables A_i normalized to Γ rather than $d\Gamma/dq^2$, $x_1 = (m_\ell^2 - q^2)^2$, $x_2 = 4\pi^2 (m_\ell^2 + 2q^2)^2$ and $x_3 = 4 x_1 x_2 / (729 \pi^2 q^4)$ (A_9 vanishes in the absence of large imaginary contributions). This relation implies that the large (small) value of $F_L^{D^*}$ ($F_T^{D^*}$) requires a corresponding suppression in $A_3^2 + A_9^2$, in A_{6s} or both. For this reason it would be particularly interesting to have available predictions in specific models for this couple of observables in case that the unexpectedly large value of this polarisation fraction remains.

3.3.5 Binning

We have obtained these alternative expressions for $\langle \tilde{F}_L^{D^*} \rangle_\ell$ (or $\langle \tilde{F}_T^{D^*} \rangle_\ell$) assuming that there are no tensors and (in some cases) no large imaginary contributions at short distances. From now on we introduce the notation $\langle \tilde{F}_T^{D^* \,\mathrm{alt}} \rangle_\ell$ (or $\langle \tilde{F}_L^{D^* \,\mathrm{alt}} \rangle_\ell$) to refer to Eq. (3.76) as the alternative way to extract $F_T^{D^*}$ (or $F_L^{D^*}$). In the absence of imaginary contributions we will use the notation $\langle \tilde{F}_T^{D^* \,\mathrm{alt}} \rangle_\ell^{I_9=0}$ corresponding to Eq. (3.72). In the massless case we denote $\langle \tilde{F}_T^{D^* \,\mathrm{alt}} \rangle_0$ for Eq. (3.75) and $\langle \tilde{F}_T^{D^* \,\mathrm{alt}} \rangle_0^{I_9=0}$ for Eq. (3.68).

Experimentally we have to consider binned versions of these expressions, which are nonlinear functions of the angular coefficients. Since the binned angular coefficients are the only quantities measured, we should be careful that $f(\langle I_k \rangle_\ell) \neq \langle f(I_k) \rangle_\ell$ when f is non-linear. From an experimental perspective there are two ways to proceed: *i)* measure the coefficients I_3 and I_{6s} of the massless or massive distribution in very small bins in order to reconstruct a q^2 dependence of these functions, so that we can perform the integration in Eq. (3.68) for the massless case or in Eq. (3.72) in the massive case (or their counterparts including imaginary parts Eq. (3.75) and Eq. (3.76)); *ii)* use an unbinned measurement method (as was done for $B \to K^* \mu^+ \mu^-$ [164]) to determine the q^2 dependence of the coefficients and introduce the obtained expressions inside Eq. (3.68) or Eq. (3.72) as explained above.

Both approaches are however difficult to implement when statistics are low, and one has to choose between the extraction of the whole angular distribution and the study of the q^2 dependence of simpler observables like the decay rate. Currently, the measurements are integrated over the whole kinematic range, which constitutes a single bin for the analysis.

By comparing with our exact results, we will thus investigate the accuracy of the approximation $f(\langle I_k \rangle_\ell) = \langle f(I_k) \rangle_\ell$, which requires the following transformation on the unbinned expressions:

$$d\Gamma_X/dq^2 \to \langle d\Gamma_X/dq^2 \rangle \qquad I_i \to \langle I_i \rangle \qquad w I_i \to \langle w I_i \rangle \qquad w I_i^2 \to \langle \sqrt{|w|} I_i \rangle^2 \tag{3.78}$$

where w stands for any positive weight depending on m and q^2. This leads to the following "approximate formulae" in the massless case, starting from Eq. (3.75):

$$\langle \tilde{F}_T^{D^*\,\mathrm{alt}} \rangle_0 \simeq \frac{1}{\Gamma} 2 \sqrt{\langle I_3 \rangle_0^2 + \langle I_9 \rangle_0^2 + \frac{1}{4} \langle I_{6s} \rangle_0^2} \tag{3.79}$$

and in the massive case, starting from Eq. (3.76):

$$\langle \tilde{F}_T^{D^*\,\mathrm{alt}} \rangle_\ell \simeq \frac{1}{\Gamma} \sqrt{\langle A\, I_3 \rangle_\ell^2 + \langle A\, I_9 \rangle_\ell^2 + \frac{1}{4} \langle B\, I_{6s} \rangle_\ell^2} \tag{3.80}$$

In the massive case, one should measure the I_i and multiply each event by a numerical factor A for I_3, I_9 and B for I_{6s}.

Similarly, in the absence of imaginary parts, we obtain the approximate binned expression, starting from Eq. (3.72):

$$\langle \tilde{F}_T^{D^*\,\mathrm{alt}} \rangle_\ell^{I_9=0} \simeq \frac{1}{\Gamma} \sqrt{\langle A\, I_3 \rangle_\ell^2 + \frac{1}{4} \langle B\, I_{6s} \rangle_\ell^2} \tag{3.81}$$

and the approximate expression for $\langle \tilde{F}_T^{D^*} \rangle_\ell$ starting from Eq. (3.74)

$$\frac{1}{\Gamma} \left\langle A \left(I_3 - 2 \frac{{I_4}^2}{I_{2c}} \right) \right\rangle_\ell \simeq \frac{1}{\Gamma} \left[\langle A I_3 \rangle_\ell - 2 \frac{\langle A I_4 \rangle_\ell^2}{\langle A I_{2c} \rangle_\ell} \right] \tag{3.82}$$

All these expressions have a corresponding expression for $\langle \tilde{F}_T^{D^*} \rangle_\ell^i$ for narrower bins where $\langle \rangle_\ell$ is transformed into $\langle \rangle_\ell^i$ corresponding to the integration over the narrow bin i.

In order to get an idea of the accuracy of these approximate relations, we perform the following numerical exercise. We consider a set of benchmark points corresponding to the best-fit-points of the 1D and 2D NP hypotheses in Ref. [139, 140]. Among the 1D hypotheses, the most favoured one is assuming NP in g_{V_L}, followed by NP in g_{S_R}. Specifically we will take for this numerical analysis as benchmark points the best-fit-points of the following four different NP hypotheses (in each case, the remaining couplings are set to zero):

$$(R1) \quad : \quad g_{V_L} = 0.07 \tag{3.83}$$
$$(R2) \quad : \quad g_{S_R} = 0.09 \tag{3.84}$$
$$(R3) \quad : \quad g_{S_L} = 0.07 \tag{3.85}$$
$$(R4) \quad : \quad g_{S_L} = 4 g_T = -0.03 \tag{3.86}$$

where the values are given at the scale $\mu = 1\,\mathrm{TeV}$, and we run them down to the scale $\mu = m_b$ [139, 140, 165]. For 2D hypotheses, there is a wider range of relevant possibilities, and we select the following ones[10]:

$$(R5) \quad : \quad (g_{V_L}, g_{S_L} = -4 g_T) = (0.10, -0.04) \tag{3.87}$$
$$(R6) - (R7) \quad : \quad (g_{S_R}, g_{S_L}) = (0.21, -0.15) \text{ or } (-0.26, -0.61) \tag{3.88}$$
$$(R8) \quad : \quad (g_{V_L}, g_{S_R}) = (0.08, -0.01) \tag{3.89}$$
$$(C0) - (C0)^* \quad : \quad g_{S_L} = 4 g_T = -0.06 \pm i\, 0.31 \tag{3.90}$$

where once again we run these coefficients down to $\mu = m_b$.

In Ref. [141], a set of benchmark points is determined by considering the best-fit points of different scenarios with one free complex parameter. The resulting 2D benchmark points (in each case, the remaining couplings are set to zero) at the scale $\mu = m_b$ are:

[10] Even though $(C0)$ and $(C0)^*$ are formally different scenarios corresponding to opposite imaginary parts, they yield the same results for our observables which are not sensitive to the sign of the imaginary part.

$$(C1) \quad : \quad g_{V_L} = 0.07 - i0.16 \tag{3.91}$$
$$(C2) \quad : \quad g_{V_R} = -0.01 - i0.39 \tag{3.92}$$
$$(C3) \quad : \quad g_{S_L} = 0.29 - i0.67 \tag{3.93}$$
$$(C4) \quad : \quad g_{S_R} = 0.19 + i0.08 \tag{3.94}$$
$$(C5) \quad : \quad g_T = 0.11 - i0.18 \tag{3.95}$$

Using a different operator basis, alternative benchmark points are found to be[11]:

$$(C6) \quad : \quad g_V = 0.20 + i0.19 \tag{3.96}$$
$$(C7) \quad : \quad g_A = 0.69 + i1.04 \tag{3.97}$$
$$(C8) \quad : \quad g_S = 0.17 - i0.16 \tag{3.98}$$
$$(C9) \quad : \quad g_P = 0.58 + i0.21 \tag{3.99}$$

In the following we will check the relations given in the previous sections against these benchmark scenarios. We have used the binned approximation of the relations using 6 bins of equal length as shown in Fig. 3.1. On the one hand, this allows us to test the quality of the binned approximation. On the other hand, we can check the impact of the assumptions used in order to derive the various relations: for instance, checking the expressions obtained for real NP contributions in Section 3.3.3 in the case of the scenarios $(C0) - (C9)$ with complex parameters provides an estimate of the impact of realistic NP imaginary contributions on these expressions.

We need to choose a set of form factors to evaluate the hadronic contributions and to be able to test how accurate the relations remain within the binned approximation discussed above, taking into account possible unexpected NP contributions (imaginary parts, tensor contributions). Since our goal is only to check the accuracy of this approximation for the various NP benchmark points it is enough to work using a simplified setting. For this reason, we refrain from using form factors obtained by elaborate combinations of heavy-quark effective theory [166–169] sum rules and lattice simulations [34, 139, 141, 170–177] and we stick to the simpler quark model in Ref. [178] without attempting to assign uncertainties to these computations.

A sample of the results is shown in Figs. 3.1, 3.2 and 3.3 to illustrate the accuracy of the determinations from Eqs. (3.80) (taking into account the contribution from imaginary parts) and (3.81) or (3.82) (neglecting this contribution). Additional scenarios are considered in Appendix D.2. In order to be more precise, the relative errors of the approximate binned expression for $\tilde{F}_T^{D^*\,\mathrm{alt}}$ with respect to $\tilde{F}_T^{D^*}$ are given in Tabs. D.1 and D.2. Let us add that the I_i are integrated with the kinematical weight A or B defined in Eq. (3.73) for the evaluation of the massive expressions whenever needed. We obtain the following results for the benchmark points considered:

- The binned approximation works very well in all cases when testing the relations in the case of scenarios where they are expected to hold. Conversely, when one considers a NP scenario with significant tensor contributions (like $(C0)$ or $(C5)$), the expressions are off by $\sim 70\%$ in the worst cases. Only when the NP contribution to the tensor coefficients is very small ($|g_T| \ll 1$), the expressions work quite well, for example $\sim 5\%$ for $(R4)$.
- When we consider NP scenarios for the τ lepton with complex values for the Wilson Coefficients but without tensor contributions, i.e. $(C1)-(C4)$ and $(C6)-(C9)$, the expressions hold with errors at the percent level. This occurs even when we consider the expressions meant for real coefficients (Section 3.3.3). We stress again that this does not apply to scenarios with tensor contributions such as $(C0)$ and $(C5)$.
- We also tested the massless expressions in the case of NP scenarios affecting light leptons at the same level as the τ lepton. Such scenarios are ruled out by the current data, but they provide a further check of the robustness of our expressions. In these cases, the expressions that do not contain the angular coefficients containing imaginary parts of the amplitudes ($I_{7,8,9}$) (Section 3.3.2)

[11] For completeness, we quote $(C8)$ although this NP scenario has no impact on $B \to D^* \ell\nu$ and is thus equivalent to the SM for our purposes.

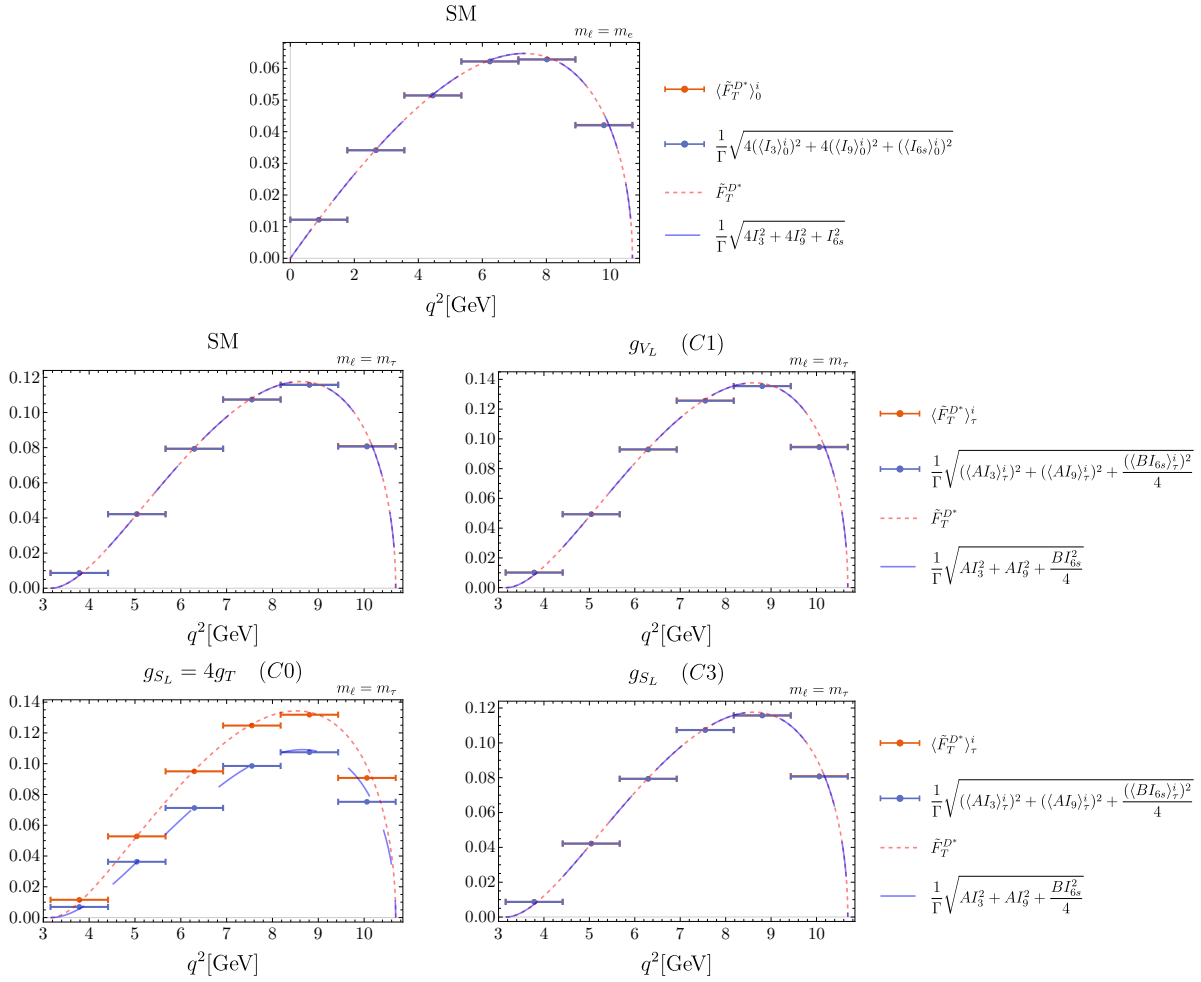

Figure 3.1: Illustration of the errors induced by binning on the relation in Eq. (3.80). The orange dashed curve corresponds to the standard definition of $\tilde{F}_T^{D^*}$, whereas the blue one corresponds to $\tilde{F}_T^{D^* \text{ alt}}$. The orange bins in this plot are obtained using the binning form of the "standard" expression for $\tilde{F}_T^{D^*}$ while the blue ones are obtained using the approximate binned expression of $\tilde{F}_T^{D^* \text{ alt}}$ in Eq. (3.80). The plots labelled SM correspond to the case $m_\ell = m_e$ and $m_\ell = m_\tau$ in the SM and the other plots correspond to $\tilde{F}_T^{D^*}$ in $B \to D^* \tau \nu$ in different NP scenarios described in the text. The differences come from the presence of tensor currents for $(C0)$ or from binning effects for the SM case.

are off by $\sim 20\%$ at worst. The agreement can be restored once we generalise the corresponding expressions so that they include these angular coefficients (Section 3.3.4), where we find a perfect agreement.

- In the first bin of most of the massless expressions, the relations are not completely fulfilled, with a difference up to 10% due to binning effects enhanced at the endpoint of the massless distribution.

This study shows that the expressions derived above under the assumption of no imaginary NP contributions and no tensor contributions in Sections 3.3.2 and 3.3.3 work very well even in the binned approximation. They are very accurate even in the presence of imaginary NP contributions. Their simple generalization including imaginary parts in Section 3.3.4 are as expected to be even more accurate also in the binned approximation. Finally, all relations fail in the presence of large tensor contributions.

3.3.6 Decision Tree

We have proposed different ways of determining $F_L^{D^*}$ (or $F_T^{D^*}$) which can be compared to the usual definition, based on the existing symmetries if additional assumptions are made about the nature of

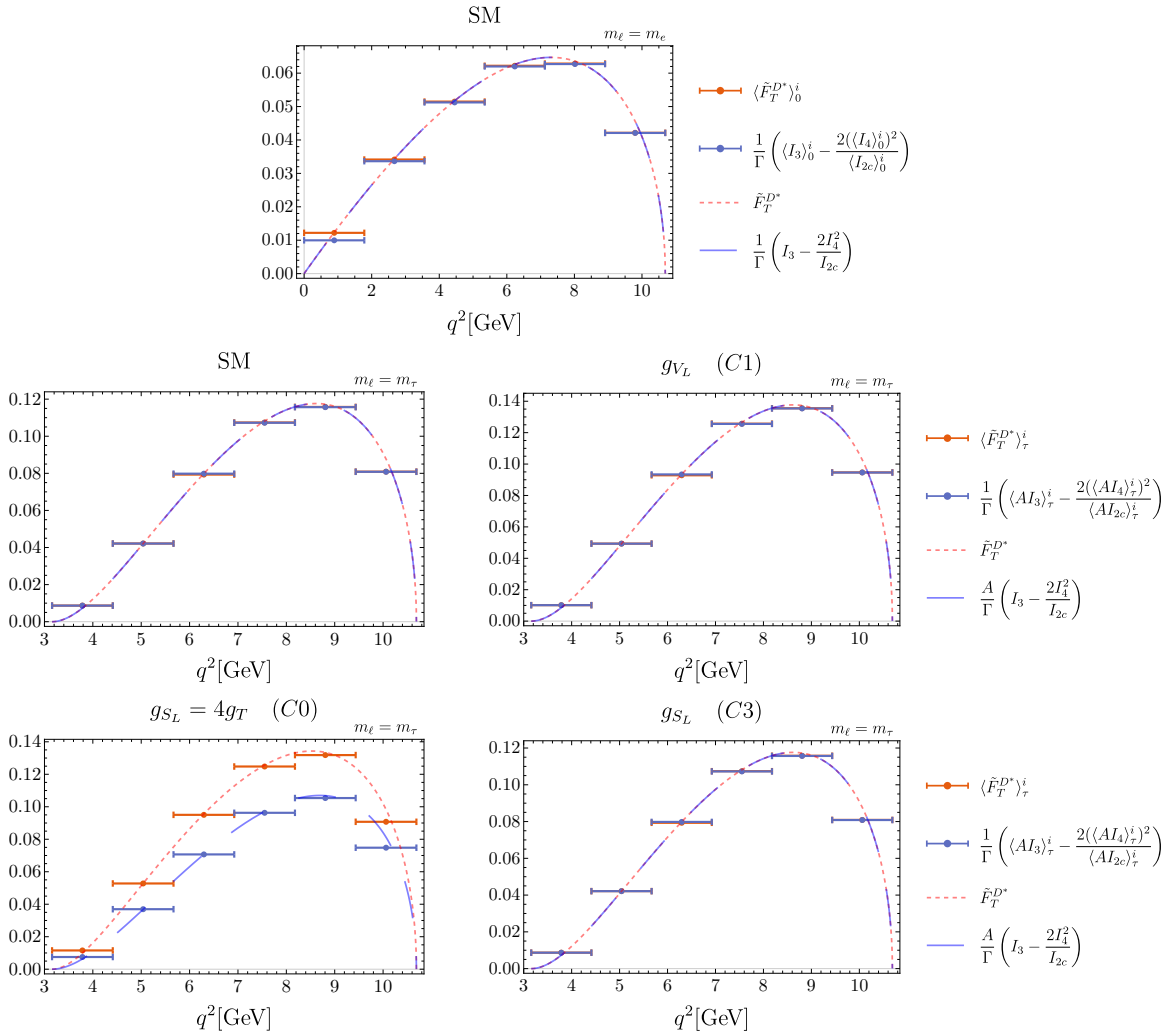

Figure 3.2: Same as Fig. 3.1 for Eq. (3.82).

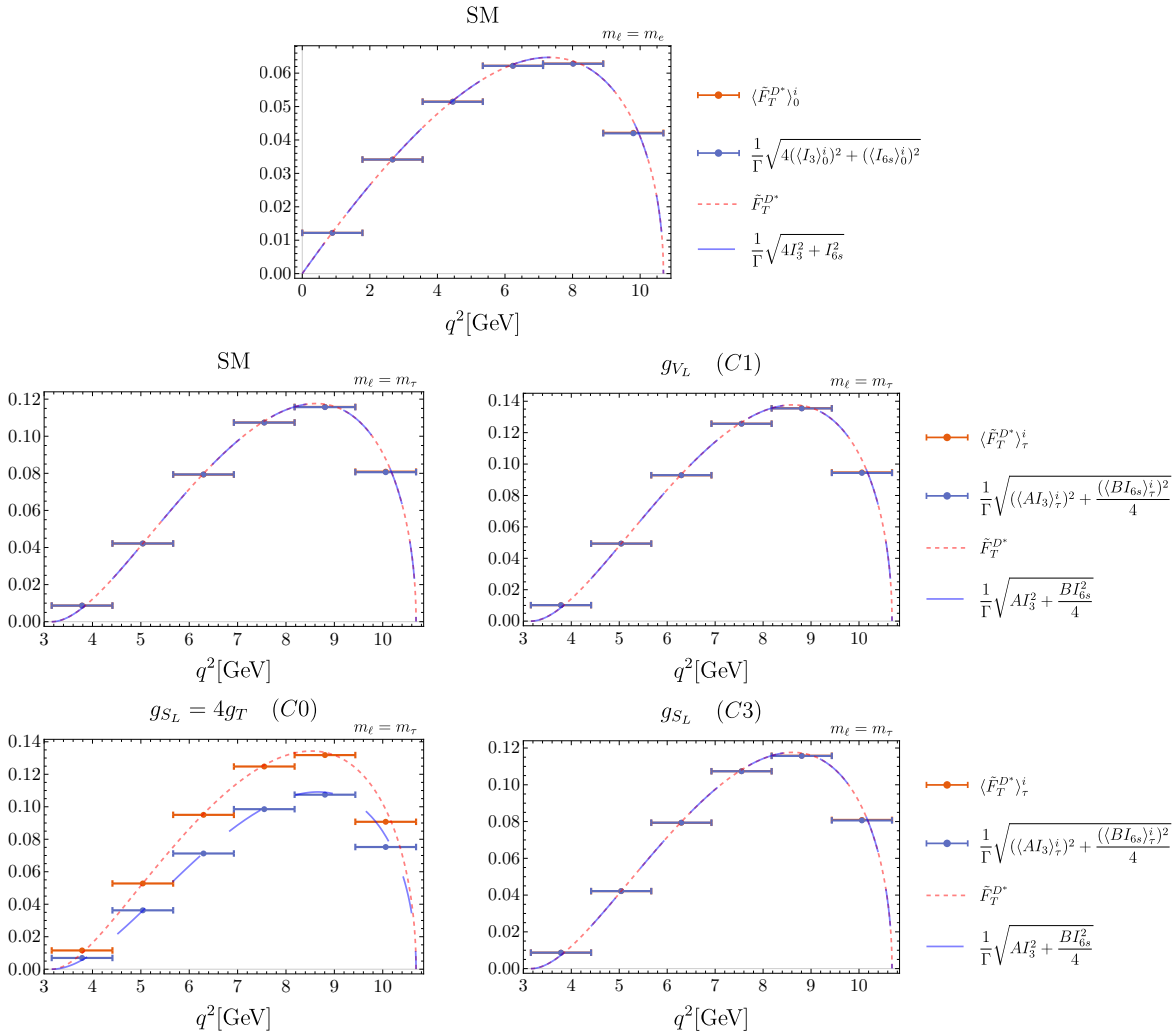

Figure 3.3: Same as Fig. 3.1 for Eq. (3.81).

NP (no tensors, real contributions). One may then wonder how to interpret the situation when the determination of $F_T^{D^*}$ in a narrow bin in the case of the tau lepton yields different results from Eq. (3.72) and from the traditional determination. While we have provided different possible determinations we will focus on Eq. (3.72) because it includes pseudoscalar contributions and it is easily generalised in the presence of phases, see Eq. (3.76). There are three possible conclusions:

1) Our first hypothesis is the absence (or negligible size) of tensors. In the presence of tensors, there are no dependencies among the angular observables, and we cannot use Eq. (3.72) to determine $F_T^{D^*}$. This first possibility seems to be in disagreement with the study in [141] that shows that tensors tend to substantially worsen the situation reducing even further the value of $F_L^{D^*}$ (or increasing $F_T^{D^*}$). If needed, this question can be tested by probing the relationships shown in Section 3.2 among the angular coefficients.

2) The second hypothesis is the absence of large imaginary parts. In this case one can generalise the expression Eq. (3.72) to the presence of imaginary parts to get Eq. (3.76), simply substituting:

$$(A\, I_3)^2 \to (A\, I_3)^2 + (A\, I_9)^2 \tag{3.100}$$

and similarly for the massless case. This simple substitution covers the presence of large phases but of course at the cost of measuring also I_9. Alternatively one can also measure $I_{7,8,9}$ which are sensitive to large imaginary parts and determine if they differ from zero in a significant way.

3) The third option is the presence of an experimental issue in the determination of $F_L^{D^*}$ in the traditional way for $B \to D^* \tau \nu$. The alternative determination proposed here could help to determine the problem to be fixed and whether this second determination is also in disagreement not only with the SM but also with NP models.

3.4 Impact of the presence of light right-handed neutrinos

We turn now to the analysis of a case beyond the framework considered up to now, namely, the presence of light right-handed neutrinos (RHN) entering the decay $b \to c\tau\bar{\nu}$. The inclusion of light RHN was discussed in Refs. [152, 179–188] as a way to obey all phenomenological constraints as well as cosmological and astrophysical limits. Here we will follow closely the recent discussion in Ref. [188] and we will use the results presented there to generalise our expressions.

If one neglects neutrino masses, the $b \to c\tau\bar{\nu}$ decay probability is given by an incoherent sum of the contributions from left- and right-handed neutrinos. This introduces a substantial change in the structure of the angular distribution, requiring a separate discussion.

The inclusion of RHN leads to a more general dimension-six effective Hamiltonian (see Ref. [188] for the definitions of the operators):

$$\mathcal{H}_{\text{eff}} = \frac{4G_F V_{cb}}{\sqrt{2}} \left(\mathcal{O}_{LL}^V + \sum_{X=S,V,T}^{A,B=L,R} C_{AB}^X \mathcal{O}_{AB}^X \right) \tag{3.101}$$

The Wilson coefficients are defined in such a way that $\mathcal{C}_{AB}^X = 0$ in the SM. Eq. (17) of Ref. [188] provides a translation table between our helicity basis and the transversity basis used in that reference.

The inclusion of RHN requires us to consider left and right chiralities of the leptonic current, while the hadronic current is not modified. Consequently the coefficients of the angular distribution get modified (see Ref. [188]):

$$I_j \to I_j(L) \pm I_j(R) \tag{3.102}$$

where the relative sign depends on the angular observable considered, and $I_j(L)$ and $I_j(R)$ involve different helicity amplitudes including $\mathcal{C}^L$ and $\mathcal{C}^R$ Wilson coefficients respectively. The total number of amplitudes entering the distribution gets thus enlarged from 7 to 14 (two of the helicity amplitudes always come in the same combination).

We can now discuss the impact of RHN on our previous discussion. Let us assume that there are neither tensor nor imaginary contributions, but that RHN are indeed present. We can compare the

two determinations of $\tilde{F}_T^{D^*}$: the standard definition in Eq. (3.28) and the alternative determination in Eq. (3.72). The following relation holds:

$$\frac{\langle (\tilde{F}_T^{D^*})^2 - (\tilde{F}_T^{D^*\,\text{alt},\,\text{I}_9=0})^2 \rangle_\tau}{\langle (B\tilde{A}_{6s})^2 \rangle_\tau} = \Delta^F \equiv \frac{64}{729} \frac{(C_{LR}^V(1+C_{LL}^V) - C_{RL}^V C_{RR}^V)^2}{((1+C_{LL}^V)^2 - {C_{LR}^V}^2 - {C_{RL}^V}^2 + {C_{RR}^V}^2)^2} \tag{3.103}$$

where $\tilde{A}_{6s}$ refers to the observable including left and right components defined by

$$\langle \tilde{A}_{6s} \rangle_\tau = -\frac{27}{8} \frac{1}{\Gamma} \langle I_{6s} \rangle_\tau \tag{3.104}$$

In order that the previous expression becomes useful we have checked that Eq. (3.103) still holds in the following binned form[12]:

$$\frac{(\langle \tilde{F}_T^{D^*} \rangle_\tau)^2 - (\langle \tilde{F}_T^{D^*\,\text{alt}} \rangle_\tau^{\text{I}_9=0})^2}{\langle B\tilde{A}_{6s} \rangle_\tau^2} \simeq \Delta^F \tag{3.105}$$

Notice that given that Δ^F is always positive, Eq. (3.105) implies that an experimental determination using $\langle \tilde{F}_T^{D^*\,\text{alt}} \rangle_\tau^{\text{I}_9=0}$ should always be found equal or smaller than the "standard" $\langle \tilde{F}_T^{D^*} \rangle_\tau$ in absence of tensors and imaginary contributions.

We derived this expression assuming the hypotheses above and using the fact that Eq. (3.57) is valid in presence of RHN while Eq. (3.58) holds if the constraint

$$C_{LR}^V(1+C_{LL}^V) - C_{RL}^V C_{RR}^V = 0 \tag{3.106}$$

is imposed. In other words, only if this constraint is fulfilled, $\langle \tilde{F}_T^{D^*\,\text{alt}} \rangle_\tau$ can be interpreted as the physical transverse polarization fraction.

In Ref. [188] several interesting scenarios are identified which are able to fulfill the constraints from $\mathcal{B}_{B_c \to \tau\bar{\nu}}$, $\mathcal{R}_{D,D^*}$, $F_L^{D^*}$ and $\mathcal{P}_\tau^{D^*}$:

1) The scenario with the highest pull_{SM} corresponds to scenario 3 (V_μ) with NP only in C_{RR}^V. Since $C_{LL}^V = C_{LR}^V = C_{RL}^V = 0$ in this scenario, Eq. (3.106) is fulfilled and $\Delta^F = 0$. However, in this scenario the NP contributions to $F_L^{D^*}$ cancel exactly and the tension with the experimental value is not relaxed.

2) A second interesting scenario is called 4b (Φ_b) in Ref. [188]. This scenario can be generated by a two Higgs doublet model and it yields non-zero values for C_X^S with $X = LL, LR, RL, RR$. Assuming $\mathcal{B}_{B_c \to \tau\bar{\nu}} < 30\%$, this scenario is able to relax the tensions of all observables including $F_L^{D^*}$. Since this scenario yields NP contributions only in C_i^S it fulfills automatically the constraint, leading to $\Delta^F = 0$.

3) In scenario 1 of Ref. [188], there are two solutions with non-vanishing values for $C_{LL,LR,RR}^V$ as well as $C_{LR,RR}^S$ and C_{RR}^T. One of the two solutions has a tensor contribution compatible with zero at 1σ. If we take this solution to remain under our initial hypothesis of the absence of tensor contributions we obtain $\Delta^F \sim 10^{-3}$ (central value of b.f.p) if $C_{RL}^V = 0$, which, obviously, cannot be detected. In Ref. [188] the coefficient C_{RL}^V is neglected because it is lepton-flavour universal within SMEFT and it cannot help to accommodate any of the deviations observed with LFUV observables. However, assuming the best-fit point of this scenario does not change when non-vanishing values of C_{RL}^V are allowed, we find that Δ^F can be much larger when C_{RL}^V approaches $\pm\sqrt{(1+C_{LL}^V)^2 - {C_{LR}^V}^2 + {C_{RR}^V}^2}$, leading to a rather visible effect.

In summary, a difference between the two measurements of $F_T^{D^*}$ (or $F_L^{D^*}$) in absence of tensors and imaginary contributions could be attributed, barring experimental issues, to contributions coming from RHN. For some RHN scenarios, this would generate a non-zero value for Δ^F.

[12] We have scanned over a range of values of the RHN coefficients $C_{LL,LR,RL,RR}^V$ to compare Eq. (3.103) and Eq. (3.105). The result of this test clearly indicates that for combinations of RHN resulting in reasonably small values of $\Delta_F < 1$, the two expressions agree up to $\mathcal{O}(10^{-3})$ corrections in all bins.

3.5 Experimental sensitivity

Our analysis is based on the possibility of performing a full angular analysis of the $B \to D^* \ell \nu$ with a reasonable accuracy to check the relationships derived among angular observables. There is a major experimental challenge associated to the difficulty of measuring angular distributions of semitauonic decays due to the loss of the two neutrinos, one from the B decay and the other from the subsequent τ decay, making it difficult to reconstruct the τ direction. This problem arises both when the τ decays into a pion or a lepton [151, 152]. A novel approach [153] has been proposed using the three-prong $\tau^+ \to \pi^+\pi^+\pi^-\bar{\nu}_\tau$ decay instead of the muonic τ decay and a multidimensional template fit able to measure the coefficients of the angular distribution. We can use the numerical results from Ref. [153] to compare the expected experimental sensitivity of $F_L^{D^*}$ using the standard definition in Eq. (3.28) with the one using the alternative determination in Eq. (3.72)[13].

Taking the results of the template fit for the $50\,\text{fb}^{-1}$ collider scenario given in Tab. 11 and Fig. 10 of Ref. [153] and applying the transformation described in Eq. (3.78) we can obtain a rough estimate of the sensitivity of $\langle \tilde{F}_L^{D*\,\text{alt}} \rangle_\tau^{\text{I}_9=0}$. Obtaining this estimate is not straightforward since $\langle \tilde{F}_L^{D*\,\text{alt}} \rangle_\tau^{\text{I}_9=0}$ includes not only the angular observables I_3 and I_{6s} but also the kinematic factors A and B. As mentioned in Section 3.3.5, experimentalists can measure directly $A\,I_3$, and $B\,I_{6s}$ following the same binning as the angular observables arising in the differential branching ratio. In order to get a rough idea of these quantities in the absence of a dedicated experimental study including estimates of AI_3 and BI_{6s}, we study the ratios $\langle A\,I_3\rangle/\langle I_3\rangle$ and $\langle B\,I_{6s}\rangle/\langle I_{6s}\rangle$ and how they change in the presence of NP. Scanning the parameter space, we find these ratios to be rather independent of the NP considered. We find that $\langle A\,I_3\rangle/\langle I_3\rangle \approx 4.1$ and $\langle BI_{6s}\rangle/\langle I_{6s}\rangle \approx 2.4$, leading to our approximate determination of the binned observables

$$\langle A\,I_3\rangle_{\text{exp}} \approx 4.1 \langle I_3\rangle_{\text{exp}} \qquad \langle B\,I_{6s}\rangle_{\text{exp}} \approx 2.4\,\langle I_{6s}\rangle_{\text{exp}} \tag{3.107}$$

It is important to emphasise that this approximation would not be needed for future experimental measurements as long as $A\,I_3$, $A\,I_9$ and $B\,I_{6s}$ are measured directly.

Under these approximations and considering the uncertainties and correlations given for the $50\,\text{fb}^{-1}$ collider scenario in Ref. [153], we obtain the following rough estimate for the alternative determination for the SM case considered in this reference

$$\langle \tilde{F}_L^{D*\,\text{alt}} \rangle_{50\ \text{fb}^{-1}}^{\text{I}_9=0} = 0.47 \pm 0.12 \tag{3.108}$$

to be compared with the standard determination

$$\langle \tilde{F}_L^{D*} \rangle_{50\ \text{fb}^{-1}} = 0.45 \pm 0.01 \tag{3.109}$$

The alternative determination suffers from the larger errors of the angular observables involved in its definition, in comparison with the standard determination which is dominated by I_{1s} with a smaller uncertainty than the other angular observables, as shown in Fig. 10 of Ref. [153].

These uncertainties would be enough to identify discrepancies coming from tensor contributions, such as our scenario C5. The smaller differences between the two determinations coming from other types of scenarios (such as Wilson coefficients with imaginary parts) could not be distinguished and the two determinations should yield similar results. Conversely, it means that our relations will provide a non-trivial experimental cross-check of the angular analyses projected in Ref. [153], unless large tensor contributions are present.

3.6 Summary and Conclusions

The charged-current $B \to D^* \ell \nu$ transition has been under scrutiny recently, as it exhibited a deviation from the SM in the LFUV ratio R_{D^*} comparing the branching ratios $\ell = \tau$ and lighter leptons. Moreover, the polarisation of both the D^* meson and the τ lepton have been measured for $B \to D^* \tau \nu$. If the latter agrees with the SM within large uncertainties, the Belle measurement of $F_L^{D^*}$ yields a rather high value compared to the SM prediction, which appears difficult to accommodate with NP scenarios.

[13] We refrain from using the more complete alternative definition in Eq (3.76) because the ratio $\langle A\,I_9\rangle/\langle I_9\rangle$ necessary to get the rough estimate described in the text is not properly defined in the SM.

We could understand better this situation by considering in more detail the angular observables that can be extracted from the differential decay rate, as described in Ref. [141]. We applied the formalism of amplitude symmetries of the angular distribution of the decays $B \to D^* \ell\nu$ for $\ell = e, \mu, \tau$. We showed that the set of angular observables used to describe the distribution of this class of decays are not independent in absence of NP contributing to tensor operators. We derived sets of relations among the angular coefficients of the decay distribution for the massless and massive lepton cases. These relations can be used to probe in a very general way the consistency among the angular observables and the underlying NP at work, and in particular whether it involves tensor operators or not.

We used these relations to access the integrated longitudinal polarisation fraction of the D^* using different angular coefficients from the ones used by Belle experiment. This in the near future can provide an alternative strategy to measure $F_L^{D^*}$ for $B \to D^* \tau\nu$ and to understand the relatively high value measured by Belle. We presented expressions in Eqs. (3.75) and (3.76) for the massless and massive case that cover the most general NP scenario including also pseudoscalars and imaginary contributions, with the only exception of tensor contributions.

We then studied the accuracy of these expressions if only binned observables are available, or if they are used in the case of scenarios beyond the assumptions made in their derivation (imaginary contributions, tensor contributions). We used several benchmark points corresponding to best-fit points from global fits to $b \to c\tau\nu$ observables, relying on a simple quark model for the hadronic form factors for this exploratory study. The expressions derived under the assumption of no imaginary NP contributions and no tensor contributions work very well even in the binned approximation. They are very accurate even in the presence of imaginary NP contributions. As expected, their generalisations, derived assuming the presence of imaginary contributions, are very well behaved also in the binned approximation. All relations fail in the presence of large tensor contributions, where no dependencies can be found among the angular observables.

Besides presenting the most general expressions for $F_L^{D^*}$ in the massless and massive case, we also derived a relation among observables ($\tilde{A}_{3,9,6s}$ and $F_L^{D^*}$) that are potentially interesting from the NP point of view if the deviation in $F_L^{D^*}$ is confirmed. Having specific model building predictions for these observables would be highly interesting. We also discussed the impact of the presence of light right-handed neutrinos. We showed that we could test their presence in some specific cases under the hypothesis that there are no tensor nor imaginary contributions, by comparing our two determinations of $F_L^{D^*}$. Moreover, under this hypothesis, the sign of the difference between the two determinations is fixed.

In addition, these alternative determinations of $F_L^{D^*}$ provide an important cross check for the experimental measurements: if our relations are not fulfilled by the experimental measurements, this would imply either a problem on the experimental side or the presence of large tensor contributions. Using recent projections on the experimental prospects for the measurements of angular observables, we find that these relations could be checked with an accuracy of 0.1 in the scenario of a 50 fb^{-1} hadron collider, which would be enough to spot a scenario with tensor contributions and would provide an interesting cross-check of the determination of the angular observables.

These additional measurements needed for this extraction make obviously this determination more challenging experimentally, but they can help to corner the kind of NP responsible for this high value or to understand if there exists an experimental problem responsible for this unexpected value of the D^* polarisation. We hope that our results will be of particular interest once the LHCb and Belle II experiments are able to analyze the $B \to D^* \ell\nu$ decays in more detail and thus to provide us with a more detailed picture of the intriguing deviations currently observed in $b \to c\ell\nu$ transitions.

Part II

Nonleptonic B decays

Chapter 4

A new B-flavour anomaly in $B_{d,s} \to K^{*0}\bar{K}^{*0}$: anatomy and interpretation

If NP is indeed at the origin of the anomalies in semileptonic B decays, it is natural to expect signals in other observables involving $b \to s$ transitions, possibly with different realisations though sharing some common features. A natural place to explore the possible existence of these signals are nonleptonic B decays. This type of decays suffer from larger uncertainties compared to semileptonic B decays and are therefore more difficult to compute with a high accuracy. In particular, branching ratios and polarisation fractions receive contributions from transverse amplitudes that suffer from large uncertainties due to power-suppressed but infrared-divergent weak annihilation and hard-spectator scattering [189, 190]. In this sense a deviation with respect to the SM prediction in nonleptonic B decays requires to be much more conservative regarding these uncertainties than in the case of semileptonic B decays.

In this chapter, based on Ref. [191], we will follow a similar strategy to the one we used in Refs. [11, 12] for semileptonic rare B decays and we will establish a parallelism constructing observables in nonleptonic B decays with a limited sensitivity to hadronic uncertainties. As described in Chapter 1, in $b \to s\ell\ell$ decays one can build two different kinds of observables with a reduced sensitivity to hadronic uncertainties: on the one hand, angular observables from decays involving muons in the final state [12, 157] constructed exploiting heavy quark symmetry. On the other hand, ratios of branching ratios with muons versus electrons in the final state that test LFUV and where the dependence on the form factors cancels almost exactly in the SM [192]. We observe tensions with respect to the SM predictions in observables involving leptons of the second family (for the former) and between the second and the first family of leptons (for the latter).

For that reason, we explore the parallel approach of using nonleptonic B decays rather than semileptonic ones, comparing quark transitions involving quarks of the second and first families instead of muons and electrons, through the use of the R_{sd} observable defined in [193]. More specifically, we compare transitions involving s-quarks and d-quarks to benefit from the approximate U-spin symmetry of the SM in analogy with Lepton-Flavour Universality used to build the LFUV ratios in $b \to s\ell^+\ell^+$ decays. The analogy has evident limitations: since both symmetries are broken by fermion mass effects, the size of the corrections is easier to compute or estimate for LFU (involving mainly QED) than for U-spin (involving QCD). However, even in the nonleptonic case it is well known that ratios of this type offer many advantages in reducing hadronic uncertainties, explaining the popularity of the ratio ξ to describe neutral-meson mixing in lattice QCD and phenomenological studies. We may reach an even better control of hadronic uncertainties by combining several approaches. In Refs. [193–195] it was shown that the specific structure of penguin-mediated nonleptonic B-decays could lead to a better theoretical control on combinations of hadronic matrix elements within factorization approaches. In the case of vector final states, it is also known that the decays into longitudinally polarised light mesons can be described more precisely than the transverse ones within these factorization approaches, providing a further guide to build optimized observables (in analogy with the angular observables in semileptonic decays). Finally, if the B_d-meson decays have been studied at B-factories extensively, LHCb is now able to provide accurate measurements for many B_s-meson decays with the possibility to assess the correlation between B_d and B_s mesons decaying into the same final state.

We will thus focus on a type of observables for penguin-mediated nonleptonic decays of B mesons into two vector particles, that we will refer as *L-observables*. These correspond essentially to the R_{sd}

observable from Ref. [193] in the case of $B_{d,s} \to K^{*0}\bar{K}^{*0}$ (up to a phase space). We present here a detailed and complete anatomy of this observable in the SM, updating the SM prediction and observing an increase in the tension with the experimental measurement compared to Ref. [193]. We then discuss NP explanations for the tension observed. We also point out possible improvements of the theoretical prediction of this observable.

In Section 4.1 we develop the theoretical framework that will be used to compute the L observable. We put particular emphasis on the sources of hadronic uncertainties coming from infrared divergences that affect mostly branching ratios and polarisations. In Section 4.2 we construct this observable and we compute it. Then, using the data of the previous section, we determine its experimental value and the pull. In Section 4.3 we explore possible solutions in terms of NP shifts to Wilson coefficients in a model-independent EFT approach, before considering particular models illustrating the difficulty to explain this nonleptonic anomaly together with the $b \to s\ell\ell$ anomalies in Section 4.4. We finally conclude in Section 4.5. In Appendix E.1 we discuss the framework used, providing the expressions of the set of operators of the Weak Effective Hamiltonian as well as the parametrisation based on QCD factorization. Appendix E.2 consists of the semi-analyical expressions of the relevant hadronic matrix elements, and in Appendix E.3 we show complementary details of the sensitivity of L to different sources of NP.

4.1 Theoretical framework

4.1.1 Helicity amplitudes

We start by considering the theoretical description of a generic transition $B_Q \to VV$ with $Q = d, s$. Since the initial state has spin 0, the two vector mesons must have the same helicity, leading to a description of the decay in terms of three helicity amplitudes A^0, A^+ and A^-. A naive factorization analysis [190] indicates a hierarchy of the type: $\bar{A}^0 > \bar{A}^- > \bar{A}^+$ for a $\bar{B} \to VV$ decay and $A^0 > A^+ > A^-$ for a $B \to VV$ decay. This hierarchy with a dominance of longitudinal amplitudes is easy to understand by means of the V-A structure of the SM [196] together with the fact that high energy QCD interactions conserve helicity [39]. Each amplitude is suppressed with respect to the previous one by $\mathcal{O}(\Lambda/m_b)$ due to helicity suppression [189]. The longitudinal amplitude in a $b \to s$ transition is dominant as compared to the positive helicity: the s quark is produced with an helicity $-1/2$ by weak interactions (in the limit $m_s \to 0$), which is not affected by the strong interactions, then the strange quark combines with the light spectator quark to form a V with a helicity which can reach 0 or -1 but not $+1$. In $\bar{A}^-$, a light-quark helicity flip is required to obtain both vector mesons with a negative helicity, whereas in $\bar{A}^+$, two helicity flips are required to reach a positive helicity for both vector mesons. Each of these helicity flips yields a suppression by a factor $\mathcal{O}(\Lambda/m_b)$, as expected in naive factorization.

4.1.2 Hadronic matrix elements

For a $\bar{B}_Q$ meson decaying through a $b \to q$ penguin-mediated process into a V_1V_2 state with a definite polarisation, the decomposition

$$\bar{A}_f \equiv A(\bar{B}_Q \to V_1V_2) = \lambda_u^{(q)} T_q + \lambda_c^{(q)} P_q \,, \tag{4.1}$$

is always possible, with the CKM factors $\lambda_U^{(q)} = V_{Ub}V_{Uq}^*$. We denote by T_q and P_q the matrix elements accompanying the $\lambda_u^{(q)}$ and $\lambda_c^{(q)}$ CKM factors respectively. In the SM, P_q is usually associated to penguin topologies, whereas T_q receives contributions from tree topologies (but it can also contain only penguin topologies in some decays). As discussed above, if we consider the longitudinal polarisation, T_q and P_q can be computed using factorization approaches based on a $1/m_b$ expansion (see Appendix E.1). In QCD factorization [197], T_q and P_q are affected by possibly large long-distance $1/m_b$-suppressed effects that will be discussed in the next section. In the case of penguin mediated decays like $B_{(d,s)} \to K^{*0}\bar{K}^{*0}$ the same type of (long-distance) infrared divergences affect both P_q and T_q, so one can construct [194, 195]

$$\Delta_q = T_q - P_q \,, \tag{4.2}$$

free from these next-to-leading-order infrared divergences.

Using the unitarity relation $\lambda_u^{(q)} + \lambda_c^{(q)} + \lambda_t^{(q)} = 0$, we can write Eq. (4.1) in terms of $\lambda_u^{(q)}$ and $\lambda_t^{(q)}$

$$\bar{A}_f = \lambda_u^{(q)}\,\Delta_q - \lambda_t^{(q)} P_q\,. \tag{4.3}$$

The weak phase in $\lambda_t^{(q)}$ is the angle β_q, defined as

$$\beta_q \equiv \arg\left(-\frac{V_{tb}V_{tq}^*}{V_{cb}V_{cq}^*}\right) = \arg\left(-\frac{\lambda_t^{(q)}}{\lambda_c^{(q)}}\right)\,, \tag{4.4}$$

whereas $\lambda_c^{(q)}$ is real to a very good approximation for both $q = d, s$, and $\lambda_u^{(q)} = -\lambda_c^{(q)} - \lambda_t^{(q)}$. The CP-conjugate amplitude is given by

$$A_{\bar{f}} = (\lambda_u^{(q)})^* T_q + (\lambda_c^{(q)})^* P_q = (\lambda_u^{(q)})^* \Delta_q - (\lambda_t^{(q)})^* P_q\,. \tag{4.5}$$

If $f = V_1V_2$ is a CP-eigenstate, note that $A_{\bar{f}}$ is different from $A = A(B \to V_1V_2)$, even though the two types of amplitudes are related:

$$\bar{A} = \bar{A}_f \qquad A = \eta_f A_{\bar{f}}\,, \tag{4.6}$$

where η_f is the CP-parity of the final state, given for $j = 0, ||, \perp$ respectively as $\eta, \eta, -\eta$ where $\eta = 1$ if V_1 is the charge conjugate of V_2 (this is the case for $K^{*0}\bar{K}^{*0}$).

4.2 The L-observable for $B_Q \to K^{*0}\bar{K}^{*0}$

4.2.1 Definition and experimental determination

The 2019 LHCb analysis with $3fb^{-1}$ data measured the ratio of the untagged and time integrated decay rates [198]

$$\begin{aligned}\frac{\mathcal{B}_{B_d\to K^{*0}\bar{K}^{*0}}}{\mathcal{B}_{B_s\to K^{*0}\bar{K}^{*0}}} = 0.0758 \quad &\pm \quad 0.0057(\text{stat}) \pm 0.0025(\text{syst}) \\ &\pm \quad 0.0016\left(\frac{f_s}{f_d}\right),\end{aligned} \tag{4.7}$$

The longitudinal polarisation of both modes has been measured as well. The average of $B_d \to K^{*0}\bar{K}^{*0}$ from LHCb [198] and Babar [199]:

$$f_L^{\text{LHCb}}(B_d \to K^{*0}\bar{K}^{*0}) = 0.724 \pm 0.051 \pm 0.016, \tag{4.8}$$
$$f_L^{\text{Babar}}(B_d \to K^{*0}\bar{K}^{*0}) = 0.80^{+0.10}_{-0.12} \pm 0.06, \tag{4.9}$$

yields

$$f_L(B_d \to K^{*0}\bar{K}^{*0}) = 0.73 \pm 0.05, \tag{4.10}$$

whereas the polarisation for the $B_s \to K^{*0}\bar{K}^{*0}$ mode is [198]:

$$f_L(B_s \to K^{*0}\bar{K}^{*0}) = 0.240 \pm 0.031(\text{stat}) \pm 0.025(\text{syst})\,.$$

Most of the experimental determinations are made assuming no direct CP-violation; however, the ones searching for CP violation found no hint in these decays [200].

One can notice already that the longitudinal polarisations are very different for these two modes, although they are related by U-spin symmetry in its most obvious form, i.e. the $d \leftrightarrow s$ exchange. In the SM, U-spin is broken only by the quark masses, and it is thus expected to be fairly well obeyed (up to a 20-30% correction). We propose to define an observable that will be sensitive to this effect but with a cleaner theoretical prediction:

$$L_{V_1V_2} = \frac{\mathcal{B}_{b\to s}}{\mathcal{B}_{b\to d}} \frac{g_{b\to d} f_L^{b\to s}}{g_{b\to s} f_L^{b\to d}} = \frac{|A_0^s|^2 + |\bar{A}_0^s|^2}{|A_0^d|^2 + |\bar{A}_0^d|^2}\,, \tag{4.11}$$

where $\mathcal{B}_{b\to q}$ ($f_L^{b\to q}$) refers to the branching ratio (longitudinal polarisation) of the $\bar{B}_Q \to V_1V_2$ decay governed by a $b \to q$ transition. A_0^q and $\bar{A}_0^q$ are the amplitudes for the B_Q and $\bar{B}_Q$ decays governed by $b \to q$ with final vector mesons being polarised longitudinally and

$$g_{b\to q} = \omega \sqrt{\left[M_{B_Q}^2 - \Sigma_{V_1V_2}\right]\left[M_{B_Q}^2 - \Delta_{V_1V_2}\right]}\,, \tag{4.12}$$

stands for the phase space factor involved in the corresponding branching ratio, with

$$\omega = \frac{\tau_{B_Q}}{16\pi M_{B_Q}^3}\,, \quad \Sigma_{ab} = (m_a + m_b)^2\,, \quad \Delta_{ab} = (m_a - m_b)^2 \tag{4.13}$$

and all quantities are CP-averaged.

This observable is defined such that the dependence on the troublesome transverse (parallel and perpendicular) amplitudes entering the branching ratio and longitudinal polarisation fraction cancel and it is close to the observable R_{sd} for the case of $B_{d,s} \to K^{*0}\bar{K}^{*0}$ up to a phase space factor [193].

Being purely sensitive to the longitudinal amplitudes, L is less affected by the hadronic uncertainties which impact the transverse polarisation amplitudes significantly and which are difficult to estimate within QCD factorization (QCDF) or other approaches based on a $1/m_b$ expansion. The choice of this observable thus avoids the difficulties encountered in the interpretation of low longitudinal polarisation fractions observed in some nonleptonic modes [189]. In this article we will focus on:

$$L_{K^*\bar{K}^*} = \frac{\mathcal{B}_{B_s\to K^{*0}\bar{K}^{*0}}}{\mathcal{B}_{B_d\to K^{*0}\bar{K}^{*0}}} \frac{g_{b\to d} f_L^{B_s}}{g_{b\to s} f_L^{B_d}} = \frac{|A_0^s|^2 + |\bar{A}_0^s|^2}{|A_0^d|^2 + |\bar{A}_0^d|^2}\,, \tag{4.14}$$

where the spectator quark Q of the initial b-flavoured meson and the quark q from the $b \to q$ transition coincide.

In the definition of $L_{K^*\bar{K}^*}$ and its connection with the longitudinal amplitudes $|A_0^q|^2$ in Eq. (4.14), we have not included the effect of B_s-meson mixing that arises in branching ratios when measured at hadronic machines. This effect of time integration at hadronic machines generates a correction of $\mathcal{O}(\Delta\Gamma/(2\Gamma))$, as discussed in Refs. [193, 201], which would multiply the last term in Eq. (4.14) by:

$$\frac{1 + A_{\Delta\Gamma}^s y_s}{1 + A_{\Delta\Gamma}^d y_d} \frac{1 - y_d^2}{1 - y_s^2}, \tag{4.15}$$

where $y_q = \Delta\Gamma_{B_q}/(2\Gamma_{B_q})$ is well measured (y_d is negligible and $y_s \simeq 0.065$) and the asymmetries $-1 \leq A_{\Delta\Gamma}^q \leq 1$ combining CP violation in mixing and decay are difficult to estimate theoretically, leading to a correction of at most 7%.

Since we use the LHCb measurement Eq. (4.7) and since there are other sources of (theoretical and experimental) uncertainties, we treat Eq. (4.15) as a systematic uncertainty of 7% combined in quadrature with the other uncertainties, leading to the experimental value:

$$\text{Exp}: \quad L_{K^*\bar{K}^*} = 4.43 \pm 0.92. \tag{4.16}$$

4.2.2 Theoretical prediction in the SM and comparison with data

On the theory side, we have

$$A_0^q = (\lambda_c^{(q)*} + \lambda_u^{(q)*})\,[P_q + (\alpha^q)^*\Delta_q]\,, \tag{4.17}$$

$$\bar{A}_0^q = (\lambda_c^{(q)} + \lambda_u^{(q)})\,[P_q + \alpha^q\Delta_q]\,, \tag{4.18}$$

where $\alpha^q = \lambda_u^q/(\lambda_c^q + \lambda_u^q)$. We thus get

$$L_{K^*\bar{K}^*} = \kappa \left|\frac{P_s}{P_d}\right|^2 \left[\frac{1+|\alpha^s|^2\left|\frac{\Delta_s}{P_s}\right|^2 + 2\mathrm{Re}\left(\frac{\Delta_s}{P_s}\right)\mathrm{Re}(\alpha^s)}{1+|\alpha^d|^2\left|\frac{\Delta_d}{P_d}\right|^2 + 2\mathrm{Re}\left(\frac{\Delta_d}{P_d}\right)\mathrm{Re}(\alpha^d)}\right], \tag{4.19}$$

with the combinations of CKM factors (estimated using the summer 2019 CKMfitter update [202–204] (see Table E.1):

$$\begin{aligned}
\alpha^d &= (-0.0136^{+0.0095}_{-0.0096}) + i(0.4181^{+0.0085}_{-0.0064}), && (4.20)\\
\alpha^s &= (0.00863^{+0.00040}_{-0.00036}) + i(-0.01829^{+0.00037}_{-0.00042}), && (4.21)\\
\kappa &= \left|\frac{\lambda_c^s+\lambda_u^s}{\lambda_c^d+\lambda_u^d}\right|^2 = 22.92^{+0.52}_{-0.30}. && (4.22)
\end{aligned}$$

From QCD factorization and the discussion in Section 4.1, we have

$$\begin{aligned}
\frac{\Delta_d}{P_d} &= (-0.16 \pm 0.15) + (0.23 \pm 0.20)i,\\
\frac{\Delta_s}{P_s} &= (-0.15 \pm 0.22) + (0.23 \pm 0.25)i, && (4.23)
\end{aligned}$$

so that the brackets in Eq. (4.19) are very close to 1, with the main uncertainty of 1% from the term proportional to $|\alpha^d|^2$ (which will be included in the theoretical uncertainties below). The leading uncertainty in the theoretical evaluation of $L_{K^*\bar{K}^*}$ comes thus from the ratio $|P_s/P_d|$, which we can attempt to estimate in different ways. A naive $SU(3)$ approach would consist in assuming

$$\text{naive } SU(3): \left|\frac{P_s}{P_d}\right| = 1 \pm 0.3\,, \tag{4.24}$$

while a naive factorization approach would rather yield

$$\text{fact } SU(3): \left|\frac{P_s}{P_d}\right| = f = 0.91^{+0.20}_{-0.17}\,, \tag{4.25}$$

where the $SU(3)$-breaking ratio related to the form factors of interest is given by

$$f = \frac{A^s_{K^*\bar{K}^*}}{A^d_{K^*\bar{K}^*}} = \frac{m^2_{B_s} A_0^{B_s\to K^*}(0)}{m^2_{B_d} A_0^{B_d\to K^*}(0)}\,, \tag{4.26}$$

and we used the values of Ref. [128] for the form factors to estimate f. A last possibility amounts to using QCD factorization. Using the same inputs as before, we obtain

$$\text{QCD fact}: \left|\frac{P_s}{P_d}\right| = 0.92^{+0.20}_{-0.18}\,. \tag{4.27}$$

The QCD factorization-based prediction follows the theoretical computations of the different contributions to the amplitudes from Refs. [190, 205]. The numerical values of the input parameters used are updated with respect to the ones in Ref. [205] and can be found in Table E.1 of Appendix E.1.

Observable	1σ	2σ
$L_{K^*\bar{K}^*}$	$[12.7, 28.8]$	$[7.5, 43]$

Table 4.1: 1σ and 2σ confidence intervals for the SM prediction of $L_{K^*\bar{K}^*}$ within QCD factorization.

Hard-gluon exchanges with the spectator quark and weak annihilation feature $1/m_b$ suppressed contributions exhibiting infrared divergences related to the endpoint of the meson light-cone distribution amplitudes. These divergences are parametrised in the same manner as in Ref. [205], involving two

contributions X_H and X_A treated as universal for all channels:

$$X_{H,A} = (1 + \rho_{H,A} e^{i\varphi_{H,A}}) \ln\left(\frac{m_B}{\Lambda_h}\right). \tag{4.28}$$

We take $\rho_{H,A} \in [0,1]$ and $\varphi_{H,A} \in [0, 2\pi]$ with flat distributions. This translates into assigning a 100% uncertainty to the magnitude of such corrections.

We propagate the uncertainties by varying each input (given in Tab. E.1) entering the penguin ratios in Eqs. (4.24), (4.25) and (4.27) and the CKM contribution κ following Eq. (4.22), using Gaussian distributions. We determine then the distribution of L in each case, leading to the 1σ ranges:

$$\text{naive } SU(3) : L_{K^*\bar{K}^*} = \quad 23^{+16}_{-12} \qquad 1.9\sigma\,, \tag{4.29}$$

$$\text{fact } SU(3) : L_{K^*\bar{K}^*} = \quad 19.2^{+9.3}_{-6.5} \qquad 3.0\sigma\,, \tag{4.30}$$

$$\text{QCD fact} : L_{K^*\bar{K}^*} = \quad 19.5^{+9.3}_{-6.8} \qquad 2.6\sigma\,, \tag{4.31}$$

where we put the level of discrepancy with experiment, in units of σ. We stress that these discrepancies are obtained using the whole distribution for L and not just the 1σ confidence intervals in the Gaussian approximation (see Tab. 4.1 for the 1 and 2σ confidence intervals). In Tab. 4.2 we present the error budget for $L_{K^*\bar{K}^*}$ in the SM. The comparison with the error budget of $|P_{d,s}|^2$ shows that the impact of X_A (X_H) is reduced from 18% (2%) in $|P_{d,s}|^2$ to 4% (0.2%) in $L_{K^*\bar{K}^*}$. A similar reduction is observed for other inputs such as f_{K^*}, showing the benefit of defining the ratio $L_{K^*\bar{K}^*}$. It also indicates that the accuracy of the theoretical prediction of $L_{K^*\bar{K}^*}$ could be improved significantly by determining the correlations among the relevant $B \to K^*$ form factors in order to compute the associated $SU(3)$ breaking. Moreover, the impact of the weak annihilation and hard-scattering divergences on the uncertainty is subdominant and would not be affected strongly by using a different approach for these power-suppressed infrared divergences.

From the comparison of the SM predictions in Eqs. (4.29)-(4.31) with the experimental result in Eq. (4.16), we see that all our theoretical estimates point towards a deficit in the $b \to s$ transition compared to the $b \to d$ one for these penguin-mediated modes, in analogy with the deficit observed in semileptonic decays to muons versus the decay to electrons in $b \to s\ell^+\ell^+$ decays.

	Relative Error		
Input	$L_{K^*\bar{K}^*}$	$\lvert P_s\rvert^2$	$\lvert P_d\rvert^2$
f_{K^*}	$(-0.1\%, +0.1\%)$	$(-6.8\%, +7.1\%)$	$(-6.8\%, +7\%)$
$A_0^{B_d}$	$(-22\%, +32\%)$	–	$(-24\%, +28\%)$
$A_0^{B_s}$	$(-28\%, +33\%)$	$(-28\%, +33\%)$	–
λ_{B_d}	$(-0.6\%, +0.2\%)$	$(-4.6\%, +2.1\%)$	$(-4.1\%, +1.9\%)$
$\alpha_2^{K^*}$	$(-0.1\%, +0.1\%)$	$(-3.6\%, +3.7\%)$	$(-3.6\%, +3.6\%)$
X_H	$(-0.2\%, +0.2\%)$	$(-1.8\%, +1.8\%)$	$(-1.6\%, +1.6\%)$
X_A	$(-4.3\%, +4.4\%)$	$(-17\%, +19\%)$	$(-13\%, +14\%)$
κ	$(-1.4\%, +2.2\%)$	–	–
Others	$(-1.3\%, +1.1\%)$	$(-2.7\%, +2.5\%)$	$(-1.6\%, +1.6\%)$

Table 4.2: Error budget of $L_{K^*\bar{K}^*}$ and $|P_{d,s}|^2$. The relative error of each theoretical input is obtained by varying them individually. The main sources of uncertainty are the form factors, followed by weak annihilation at a significantly smaller level.

4.3 Model-independent NP analysis

Even though the deviation in $L_{K^*\bar{K}^*}$ is not yet at the level of a troublesome discrepancy with the SM, its potential connection with other B-flavour anomalies makes it interesting to investigate it further in terms of possible $SU(3)$-breaking NP contributions. We may explore in a model-independent way how to explain this anomaly via contributions only to the Wilson coefficients of the $b \to s$ transition, while keeping the corresponding $b \to d$ SM-like (or with opposite NP contributions).

This can be performed by using the weak effective theory, whose basis within the SM we recall in Eq. (E.1) of Appendix E.1. Note that in the presence of generic NP, the basis of operators must be extended since we expect this NP contribution to couple with different strength to different flavours (and in particular to d and s quarks), there is no a priori reason for it to yield "strong" and "electroweak" penguin operators with sums over all quark flavours following the same pattern as in the SM [206].

However, for simplicity, and in parallel with the results of the global fits for NP in $b \to s\ell^+\ell^-$ decays favouring SM operators or chirally-flipped versions of it, we consider here NP only entering the Wilson coefficients associated with the SM operators Q_i or the chirally-flipped ones $\tilde{Q}_i$ as defined in Ref. [196] by exchanging $V-A$ and $V+A$ in all quark bilinears constituting the operators. These right-handed currents would modify the longitudinal amplitude by adding contributions that are functions of $\mathcal{C}_i^{\rm NP} - \tilde{\mathcal{C}}_i$ (where $\tilde{\mathcal{C}}_i$ is the coefficient of the chirally-flipped operator) leading to the structure $A_0[\mathcal{C}_i^{\rm SM}] + A_0[\mathcal{C}_i^{\rm NP} - \tilde{\mathcal{C}}_i]$. In practice this means that the NP contribution to each coefficient entering the longitudinal amplitude should be interpreted as stemming not only from the standard operators but also from the chirally flipped ones (with opposite sign).

We consider the sensitivity of $L_{K^*\bar{K}^*}$ on each Wilson coefficient. We want to determine if there is a dominant operator that can naturally explain the low experimental value of $L_{K^*\bar{K}^*}$, as it happens for $b \to s\ell\ell$ with $\mathcal{O}_9$. We assume that NP enters as described above with the further requirement that there are no additional NP phases, leading to real-valued Wilson coefficients. We can then compute the hadronic matrix elements within QCD factorization exactly like in the SM. In Appendix E.2 we provide semi-analytical expressions for P_d and P_s, needed to compute $L_{K^*\bar{K}^*}$ in terms of Wilson coefficients. We provide the explicit dependence on the infrared divergences X_A and X_H although their numerical impact on the uncertainty is limited. Let us note in passing that the quantity Δ_q is still protected from infrared divergences in this NP extension: the structure of the longitudinal hadronic amplitudes T and P is unchanged, and only the numerical values of Wilson coefficients are modified compared to the SM (the protection of Δ from infrared divergences would not necessarily hold in more general NP extensions).

Considering the sensitivity of $L_{K^*\bar{K}^*}$ on each Wilson coefficient of the weak effective theory individually, we can determine the coefficients where a limited NP contribution would be sufficient to explain the discrepancy observed. We thus identify three dominant coefficients: $\mathcal{C}_{1q}^c$, $\mathcal{C}_{4q}$ and $\mathcal{C}_{8gq}^{\rm eff}$ (see Fig. 4.1 and Fig. E.2 in Appendix E.3). The strong dependence on these coefficients with respect to the others can be seen already in the explicit form of $P_{d,s}$:

$$\begin{aligned} P_s &= (1.98 - 5.04i) + (2.37 - 1.65i)\mathcal{C}_{1s}^{c,\rm NP} + (9.98 + 148.76i)\mathcal{C}_{4s}^{\rm NP} - 7.98i\mathcal{C}_{8gs}^{\rm eff,NP} + \dots \\ P_d &= (2.17 - 5.49i) + (2.60 - 1.80i)\mathcal{C}_{1d}^{c,\rm NP} + (10.95 + 161.74i)\mathcal{C}_{4d}^{\rm NP} - 8.76i\mathcal{C}_{8gd}^{\rm eff,NP} + \dots \end{aligned}$$

which translates into a dominant contribution for $L_{K^*\bar{K}^*}$ as well.

The reason behind this strong dependence on these coefficients can be understood in the following way. Let us consider a penguin-mediated decay, so that the SM tree-level operator $\mathcal{C}_{1s}^c$ contributes through a closed $c\bar{c}$ loop to the decay, putting its contribution at the same level as the "strong" penguin operators $i = 3 \dots 6$ in the SM. A very similar contribution at the level of the underlying SM diagrams comes thus from both $\mathcal{C}_{1s}^c$ and $\mathcal{C}_{4s}$, as can be seen from the $V-A$ structure of the operators (this is also the case for $\mathcal{C}_{8gs}^{\rm eff}$ with the emission of a gluon coupling to a $q\bar{q}$ pair). The effect of the diagrams is similar in the SM, but the separation between long and short distances in the weak effective theory yields $\mathcal{C}_{4s}$ and $\mathcal{C}_{8gs}^{\rm eff}$ much smaller than $\mathcal{C}_{1s}^c$, which must be compensated by larger weights in Eqs. (4.32) and (4.32). The other penguin operators are suppressed either because of color suppression ($\mathcal{C}_3$, thus associated with $1/N_c$ factors in the QCD factorization formula) or helicity suppression ($\mathcal{C}_5$ and $\mathcal{C}_6$, which yield a vanishing contribution in the naive factorization approach as they must be Fierzed into (pseudo)scalar operators with vanishing matrix elements). In the SM, the "electroweak" penguins $i = 7 \dots 10$ are suppressed. Their contributions might be very significantly enhanced by NP which would not require such an electromagnetic suppression, although it would be difficult to obtain then "electroweak" operators at the m_b-scale since they involve

explicitly the quark electric charges. If we nevertheless allowed for such very large contributions for the electroweak part (which we will discard in the following), the same argument would apply as in the case of the "strong" penguins, so that the leading contribution from the "electroweak" penguins would be $\mathcal{C}_{10q}$.

As can be seen in Fig. E.2, the coefficient $\mathcal{C}_{1s}^{c}$ requires a very large NP contribution w.r.t. the SM of order 60% to reduce this discrepancy at 1σ. We will not pursue the possibility of a contribution to $\mathcal{C}_{1q}^{c}$, as the size of the effect being so large at an absolute scale is in conflict with recent analyses of the global constraints on this coefficient [207] that suggest that the room for NP contributions is of $\mathcal{O}(10\%)$ of the SM. Dijet angular distributions [208], together with flavour bounds following from $SU(2)_L$ gauge invariance, suggest bounds which are even tighter.

The penguin coefficient $\mathcal{C}_{4s}$ requires a NP contribution of order 25% (which is incidentally similar to the NP contribution needed in $\mathcal{C}_9$ for $b \to s\mu\mu$) in order to reduce the discrepancy in $L_{K^*\bar{K}^*}$ at 1σ. The NP contribution needed is thus quite large but not significantly constrained from other nonleptonic decays where many other coefficients enter [197].

Finally, $\mathcal{C}_{8gs}^{\text{eff}}$ would require a NP contribution of order 100% of the SM in order to obtain a similar reduction of the discrepancy. Although it might seem a large contribution, it is actually very difficult to obtain a precise bound on this effective coefficient which combines $\mathcal{C}_{8gs}$ with some Wilson coefficients of four-quark operators (see Appendix E.1). Due to QCD loop effects, the constraint from $b \to s\gamma$ is actually on a linear combination of the Wilson coefficients $\mathcal{C}_{7\gamma s}^{\text{eff}}$ and $\mathcal{C}_{8gs}^{\text{eff}}$ at the scale μ_b [209]. Therefore, an effect in $\mathcal{C}_{8gs}^{\text{eff}}$ can always be cancelled by an effect in $\mathcal{C}_{7\gamma s}^{\text{eff}}$ so that the experimental bound from $b \to s\gamma$ is obeyed (the same is also true for $b \to d\gamma$ [210]). Even without such a cancellation from $\mathcal{C}_{7\gamma s}^{\text{eff}}$, the current measurements can accommodate a NP contribution to $\mathcal{C}_{8gs}^{\text{eff}}$ of the order of the SM. Another more direct bound on $\mathcal{C}_{8gs}^{\text{eff}}$ is provided by the $b \to sg$ contribution to inclusive nonleptonic charmless decays. The current bound on the $b \to sg$ branching ratio in Ref. [211] is at the level of 6.8%, whereas the SM contribution [212] is estimated at the level of 0.5%, leaving room for a NP contribution to $\mathcal{C}_{8gs}^{\text{eff}}$ up to three times as large as the SM one.

Naturally, in each case, if we allow for NP in both $\mathcal{C}_{is}$ and $\mathcal{C}_{id}$, we may get the same reduction of the discrepancy by assigning half of the NP contribution (with opposite signs) to both coefficients, as illustrated for $\mathcal{C}_4$ in Fig. 4.2. Thus, allowing NP in $b \to d$ transitions in addition to $b \to s$ transitions requires smaller NP contributions in each type of transition, and allows one to evade some of the bounds discussed above as they applied only to $b \to s$ transitions (e.g. $\mathcal{C}_{8gs}$). $\mathcal{C}_{8gd}$ is constrained from $b \to d\gamma$.

4.4 Simplified NP models

Our model-independent analysis showed that $L_{K^*\bar{K}^*}$ is mostly sensitive to color-octet operators and to a lesser extent to the chromomagnetic operator. In the following, we will consider NP models able to generate such contributions, and for concreteness, present the formula for the case of $b \to s$ transitions.

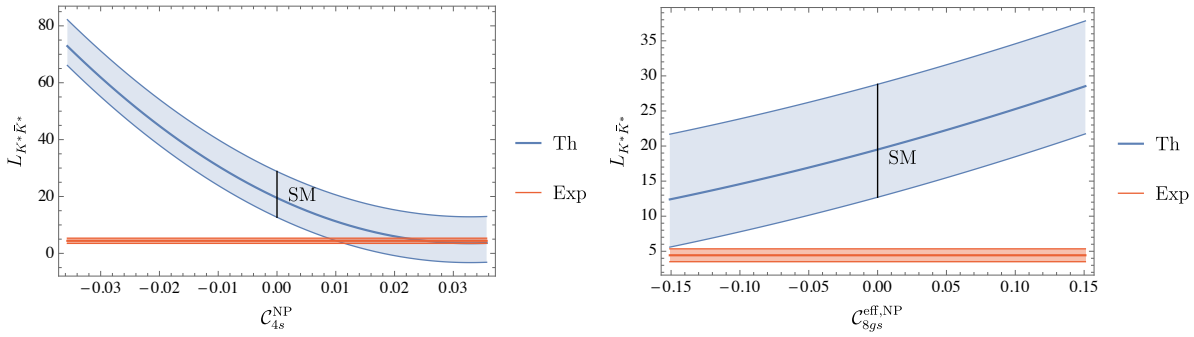

Figure 4.1: The tension between the theoretical prediction (blue) and the experimental value (orange) is reduced below 1σ for $\mathcal{C}_{4s}^{\text{NP}} \simeq 0.25\mathcal{C}_{4s}^{\text{SM}}$ (upper plot) or $\mathcal{C}_{8gs}^{\text{eff,NP}} \simeq -\mathcal{C}_{8gs}^{\text{eff,SM}}$ (lower plot). The predictions are given for $\mathcal{C}_{4s}^{\text{NP}}$ and $\mathcal{C}_{8gs}^{\text{eff,NP}}$ for a range corresponding to 100% of their respective SM values. The plots for the remaining Wilson coefficients can be found in Appendix E.3.

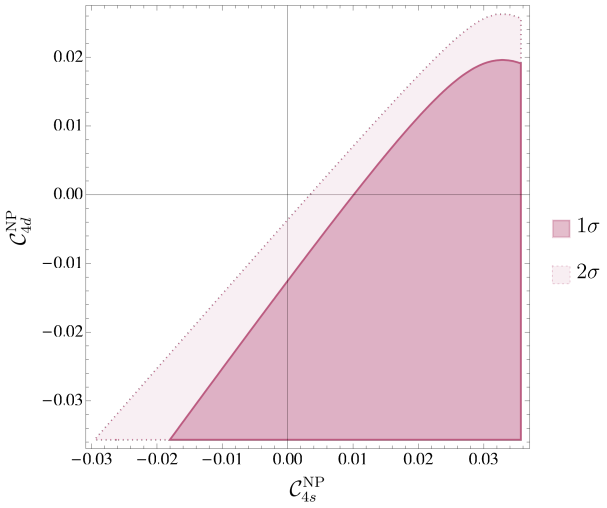

Figure 4.2: 1σ and 2σ CL regions from $L_{K^*\bar{K}^*}$ allowing NP contributions to both $\mathcal{C}_{4s}$ and $\mathcal{C}_{4d}$.

Concerning $\mathcal{C}_{4s}$, it is natural to search for a tree-level explanation in terms of NP and a massive $SU(3)_c$ octet vector particle, i.e. a Kaluza-Klein (KK) gluon, also called axi-gluon, comes naturally to mind. We parametrise its couplings to down quarks of different flavours as

$$\mathcal{L} = \Delta_{sb}^{L}\bar{s}\gamma^{\mu}P_L T^a b G_{\mu}^a + \Delta_{sb}^{R}\bar{s}\gamma^{\mu}P_R T^a b G_{\mu}^a \,. \tag{4.32}$$

with $\Delta_{sb}^{L,R}$ assumed real. We also define from Eq. (4.32) analogous flavour diagonal couplings which we will denote as $\Delta_{qq}^{L,R}$.

We may consider the constraints from neutral-meson mixing through the effective Hamiltonian of Ref. [213]

$$\begin{aligned}
H_{eff}^{\Delta F=2} &= \sum_{j=1}^{5} \mathcal{C}_j^{B_s\bar{B}_s}\mathcal{O}_j^{B_s\bar{B}_s} + \sum_{j=1}^{3}\tilde{\mathcal{C}}_j^{B_s\bar{B}_s}\tilde{\mathcal{O}}_j^{B_s\bar{B}_s}\,, \\
\mathcal{O}_1^{B_s\bar{B}_s} &= [\bar{s}_\alpha\gamma^{\mu}P_L b_\alpha]\,[\bar{s}_\beta\gamma_{\mu}P_L b_\beta]\,, && (4.33)\\
\mathcal{O}_4^{B_s\bar{B}_s} &= [\bar{s}_\alpha P_L b_\alpha]\,[\bar{s}_\beta P_R b_\beta]\,, && (4.34)\\
\mathcal{O}_5^{B_s\bar{B}_s} &= [\bar{s}_\alpha P_L b_\beta]\,[\bar{s}_\beta P_R b_\alpha]\,, && (4.35)
\end{aligned}$$

where only the operators relevant for the discussion are displayed and where the operators with a tilde are obtained by exchanging the chirality projectors P_L and P_R. We get the matching contributions

$$\begin{aligned}
\mathcal{C}_1^{B_s\bar{B}_s} &= \frac{1}{2m_{KK}^2}\left(\Delta_{sb}^{L}\right)^2\frac{1}{2}\left(1-\frac{1}{N_C}\right)\,, && (4.36)\\
\tilde{\mathcal{C}}_1^{B_s\bar{B}_s} &= \frac{1}{2m_{KK}^2}\left(\Delta_{sb}^{R}\right)^2\frac{1}{2}\left(1-\frac{1}{N_C}\right)\,, && (4.37)\\
\mathcal{C}_4^{B_s\bar{B}_s} &= -\frac{1}{m_{KK}^2}\Delta_{sb}^{L}\Delta_{sb}^{R}\,, && (4.38)\\
\mathcal{C}_5^{B_s\bar{B}_s} &= \frac{1}{N_C m_{KK}^2}\Delta_{sb}^{L}\Delta_{sb}^{R}\,, && (4.39)
\end{aligned}$$

where m_{KK} is the mass of the KK gluon. Using the two-loop Renormalization Group Equations of Refs. [214, 215] and the bag factors of Ref. [216] this translates to

$$\frac{\Delta M_{B_s}^{\rm NP}}{\Delta M_{B_s}^{\rm SM}} \times 10^{-10} = \left(1.1(\mathcal{C}_1^{B_s\bar{B}_s} + \tilde{\mathcal{C}}_1^{B_s\bar{B}_s}) + 8.4\mathcal{C}_4^{B_s\bar{B}_s} + 3.1\mathcal{C}_5^{B_s\bar{B}_s}\right) \text{GeV}^2\,, \tag{4.40}$$

for a NP scale around 5 TeV. This has to be compared with the outcome of global fits allowing for NP in mixing [217, 218], favouring a value slightly above 1 for the ratio $\Delta M_{B_s}^{\rm exp}/\Delta M_{B_s}^{\rm SM}$. Encompassing the results obtained from these recent fits in a conservative manner, we consider here

$$\frac{\Delta M_{B_s}^{\rm exp}}{\Delta M_{B_s}^{\rm SM}} = 1.11 \pm 0.09\,. \tag{4.41}$$

We obtain the allowed region shown in blue in Fig. 4.3 for real values of the Wilson coefficients and neglecting the bag factor uncertainties related to $\mathcal{C}_{4,5}^{B_s\bar{B}_s}$.

Assuming that the KK gluon has universal flavour-diagonal coupling to the first two generations of quarks, which is also needed to avoid unacceptably large effects in $K-\bar{K}$ and/or $D^0-\bar{D}^0$ mixings [219], our model generates [1] a NP contribution to $\mathcal{C}_{4s}$ given at the matching scale by

$$\mathcal{C}_{4s} = -\frac{1}{4}\frac{\Delta_{sb}^L\Delta_{qq}^L}{\sqrt{2}G_F V_{tb}V_{ts}^* m_{KK}^2}\,, \tag{4.42}$$

(and similarly for $\tilde{\mathcal{C}}_{4s}$ with L replaced by R). The couplings $\Delta_{sb}^{L,R}$ are defined in Eq. (4.32) while $\Delta_{qq}^{L,R}$ stand for the corresponding flavour-diagonal couplings to up and down quarks of the first two generations.

However, couplings of first generation quarks to KK gluons are strongly constrained by di-jet searches [220]: $(\Delta_{qq}^L/m_{KK})^2 < (2.2/(10\,\text{TeV}))^2$. Allowing for NP also in $b \to d$ transitions could increase the effect in $L_{K^*\bar{K}^*}$, but since here the effect is bounded by $B_d-\bar{B}_d$ mixing, whose constraints are of the same order as $B_s-\bar{B}_s$ mixing, one can only gain a factor ≈ 2. Using this maximal coupling for the Δ_{qq}^L couplings and setting the Δ_{qq}^R couplings to zero, we can see from Fig. 4.3 that a significant amount of fine-tuning is needed to account for $L_{K^*\bar{K}^*}$.

Alternatively, one could try to explain $L_{K^*\bar{K}^*}$ with a NP contribution in the chirally-flipped coefficient $\tilde{\mathcal{C}}_{4s}$, given by Eq. (4.42) with the Δ_{sb}^L and Δ_{qq}^L couplings replaced by Δ_{sb}^R and Δ_{qq}^R, respectively. In principle, one could exploit the fact that the couplings do not have to respect a $U(2)$ flavour symmetry (since up- and down-type quark couplings are not related via $SU(2)_L$), so that couplings to first-generation quarks could be avoided, which would relax LHC bounds and reduce the fine-tuning needed in $B_s-\bar{B}_s$ mixing. However, as in the previous case, flavour universality for diagonal couplings to quarks is needed to be able to make use of our expressions for $L_{K^*\bar{K}^*}$. Moreover, according to QCD factorization, the dominant LO effect in $L_{K^*\bar{K}^*}$ originates from the term in Q_{4s} with down quarks in the bilinear summed over flavours. Therefore, (dominant) right-handed couplings cannot be used to evade LHC bounds and still fine-tuning in $B_s-\bar{B}_s$ mixing, like in the case of left-handed couplings, is needed.

As indicated earlier, one could also try to explain $L_{K^*\bar{K}^*}$ with the Wilson coefficient of the chromo-magnetic operator O_{8gs}. Here an effect of the order of the SM contribution is required. $\mathcal{C}_{8gs}$ can only be generated at the loop level and involves necessarily colored particles for which strong LHC limits exist. Therefore, a value of the order of the SM contribution can only be obtained thanks to chiral enhancement.

A simplified model fulfilling these requirements features two vector-like quarks, one $SU(2)_L$ doublet and one $SU(2)_L$ singlet (with a large coupling λ to the SM Higgs doublet) and an additional neutral scalar particle [221]. In this setup, $\mathcal{C}_{8gs}$ receives a contribution which scales like $\lambda/(m_b/v)\times v^2/M^2$ w.r.t. the SM, where M is the NP scale. Inevitably an effect in $\mathcal{C}_{7\gamma s}$ is generated at the matching scale M which however has free sign and magnitude as it depends on the (not necessarily quantized) electric charges of the new fermions and scalar inside the loop. Therefore, the electric charges of the new particles can be chosen in such a way that in $\mathcal{C}_{7\gamma s}$ (at the m_b scale) the NP contributions to $\mathcal{C}_{7\gamma s}$ and $\mathcal{C}_{8gs}$ (taken at the matching scale) cancel. As we need a NP contribution to $\mathcal{C}_{8gs}$ of the order of the SM one, and $\mathcal{C}_{7\gamma s}$ at the low scale is known at the 5% level, a tuning of the order of 1/20 is necessary here.

[1] Note that our model is only flavour universal with respect to four but not five flavours and does not fulfill the requirements of Section 4.3. However, the effect of bottom quarks within the Q_{4s} operator in $L_{K^*\bar{K}^*}$ is $O(\alpha_s)$-suppressed within QCD factorization and thus the impact of our model on $L_{K^*\bar{K}^*}$ can be mimicked by a shift in $\mathcal{C}_{4s}$ to a good approximation.

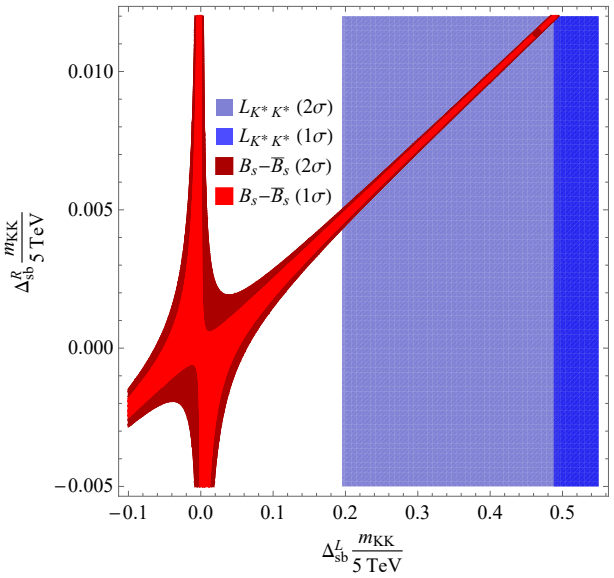

Figure 4.3: Preferred regions from $B_s - \bar{B}_s$ mixing (red) and $L_{K^*\bar{K}^*}$ (blue) for $\Delta^R_{qq} = 0$ and the maximal value of Δ^L_{qq} compatible with LHC searches assuming real couplings. Note that explaining $L_{K^*\bar{K}^*}$ requires some fine-tuning in Δ^L_{sb} vs Δ^R_{sb}.

Both simplified models allow for the possibility of a connection with the $b \to s\ell^+\ell^-$ anomalies. On the one hand, the KK gluon may be part of the particle spectrum of a composite/extra-dimensional model and is then accompanied by a Z' boson. This could explain $b \to s\ell^+\ell^-$ without violating LHC di-lepton bounds [222] due to the large sb coupling of the Z' needed to explain $L_{K^*\bar{K}^*}$, leading to NP contributions with the correct sign in both types of anomalies. On the other hand, the model generating a large effect in $\mathcal{C}_{8g}$ could easily be extended by a vector-like lepton in order to account for $b \to s\ell^+\ell^-$ [221].

4.5 Summary and Conclusions

In this chapter we have analyzed the nonleptonic penguin decays $B_d \to K^{*0}\bar{K}^{*0}$ and $B_s \to K^{*0}\bar{K}^{*0}$, where recent LHCb results indicate striking differences in the longitudinal polarisation of these two modes. This is unexpected since they are related by U-spin and should thus have a similar QCD and EW dynamics (up to tiny corrections due to the down and strange quark masses).

We introduced the L-observable as a combination of polarisation fractions and branching ratios in order to compare the longitudinal amplitudes in both modes, as they can be computed with better theoretical control in a $1/m_b$ expansion such as QCD factorization. We exploited the fact that these penguin-mediated decays exhibit very similar hadronic matrix elements for the "tree" and "penguin" contributions in the usual decomposition based on CKM factors, so that these contributions are very strongly correlated. This means that the L-observable is a measure of U-spin breaking between the penguin contributions to B_d and B_s decays, with a deviation from the SM expectation between 2σ and 3σ depending on the specific theoretical framework considered. This observation reinforces and puts on a firmer ground the hint for NP already suspected by considering the difference between the longitudinal polarisation fractions in these two modes. We performed a detailed error budget analysis for $L_{K^*\bar{K}^*}$ and we found a relatively small impact of infrared divergences coming from weak annihilation and hard-spectator scattering, compared to observables like branching ratios or polarisation fractions involving troublesome transverse amplitudes.

We then interpreted this deviation in a model-independent approach using the weak effective theory. For simplicity, we allowed NP only in SM Wilson coefficients or their chirally-flipped counterparts. We identified three operators which could accommodate the deviation with NP contributions at most as large as the SM. While $\mathcal{C}_{1q}$ is already very significantly constrained by other nonleptonic modes and LHCb bounds (up to the point of excluding this solution), the situation is less constrained for the strong penguin coefficient $\mathcal{C}_{4q}$ and the chromomagnetic one $\mathcal{C}^{\text{eff}}_{8gq}$ where NP contributions of a similar size to the SM one are allowed and could explain the deviation in $L_{K^*\bar{K}^*}$. We discussed examples of simplified NP

models that could provide large contributions, at the price of accepting fine tuning to accommodate the bounds on $B_s - \bar{B}_s$ mixing and $b \to s\gamma$. Interestingly, within a general composite or extra-dimensional model [223], the Kaluza-Klein gluon contribution to the $b \to s$ amplitude in $B_s \to K^{*0}\bar{K}^{*0}$ has the same sign as the Z' contribution to $b \to s\ell^+\ell^-$ w.r.t the SM. Therefore, if one accepts the fine-tuning in $B_s - \bar{B}_s$ mixing, such models can provide a common explanation of $L_{K^*\bar{K}^*}$ and $b \to s\ell^+\ell^-$ data.

This hint of NP in $L_{K^*\bar{K}^*}$ could be sharpened with a precise estimate of U-spin breaking in the form factors involved, as they drive the theoretical uncertainty of the SM prediction and their correlation is not known precisely. A comparison of the theoretical and experimental information on the polarisations in $B_s \to K^*\phi$ and $B_d \to K^*\phi$ could also be valuable to check whether a similar tension arises. Complementary information could be obtained also from PV and PP penguin-mediated modes ($K^0\bar{K}^{*0}$ and $K^0\bar{K}^0$). Moreover, if the same source of NP is responsible for the suppression of $b \to sq\bar{q}$ versus $b \to dq\bar{q}$ and $b \to s\mu^+\mu^-$ versus $b \to se^+e^-$, it would be certainly interesting to perform a thorough study of $b \to d\ell^+\ell^-$ modes compared to $b \to s\ell^+\ell^-$ ones, which should be accessible with more data from the LHCb and Belle II experiments. This interplay between nonleptonic and semileptonic rare decays could prove highly beneficial in the coming years to identify new B-flavour anomalies and understand their actual origin in terms of physics beyond the SM.

Part III

Connecting Different Sectors of Flavour Physics

Chapter 5

Importance of $Z - Z'$ Mixing in $b \to s\ell^+\ell^-$ and the W mass

We have seen in previous chapters that simple patterns where NP couples solely to muons can in fact explain the discrepancies between the SM and experiment very well. However, it turns out that structures with additional Lepton Flavour Universal (LFU) contributions can describe data even better [54]. This means that allowing simultaneously for presence of Lepton Flavour Universality Violating (LFUV) and LFU NP effects, one can further improve the goodness of the global fits. Indeed, some of these hypotheses exhibit the highest significance among all studied scenarios [4, 53, 55, 57], showing preferences of more than 7σ compared to the SM hypothesis[1]. However, in such a model-independent approach it is difficult to be certain that the most optimal and/or minimal NP hypothesis have been found due to the large number of possibilities. One way to make progress is to use UV complete (or simplified) models where the number of generated scenarios is usually smaller. In this context several models giving rise simultaneously to LFUV and LFU effects have been proposed in the literature, including 2HDMs [98], leptoquarks [103, 226], $SU(2)_L$ triplets vector bosons [227] and models with vector-like quarks [99, 228].

In this chapter, based off of Ref. [229], we will focus on SM extensions by new heavy neutral gauge bosons (Z') which are very popular NP solutions of the $b \to s\ell^+\ell^-$ anomalies [228, 230–281]. While the Z' at tree-level preferably gives LFUV effects in $b \to s\ell^+\ell^-$, LFU effects can be generated via $Z - Z'$ mixing. In fact, because both bosons have the same quantum numbers, this mixing cannot be avoided by any symmetry. Furthermore, in the case that electroweak (EW) symmetry breaking and the breaking of the symmetry giving rise to the Z' mass are connected, one even expects a mixing of the order of $m_Z^2/m_{Z'}^2$. Importantly, $Z - Z'$ mixing has also an impact on the global EW fit, in particular on $Z\ell^+\ell^-$ and $Z\nu\nu$ couplings and if the Z' is an $SU(2)_L$ singlet (i.e. not the neutral component of an $SU(2)_L$ multiplet), also the prediction of the W mass is altered compared to the SM. The latter is very important since the current global EW fit displays a tension of 1.8σ [282] (before adding the new CDF measurement [283]) and, as we will see, the effect of $Z - Z'$ mixing has the right sign to account for this.

Therefore, in Z' models an interesting interplay between $b \to s\ell^+\ell^-$ processes and the global EW fit arises if the $Z - Z'$ mixing angle is non-zero. While this mixing has usually been assumed to be negligibly small[2] in the literature, this is not at all given for granted. Therefore, the goal of this chapter is to assess the possibility and size of $Z - Z'$ mixing via a combined analysis of flavour and EW data. For this purpose, the chapter is structured as follows: in the next section we will define our setup, then consider the relevant observables in Section 5.2 and discuss the impact of $Z - Z'$ mixing on the EW fit and $b \to s\ell^+\ell^-$ data in Section 5.3. We reassess our results in light of the new measurement of the mass of the W boson in Section 5.4 and eventually we conclude in Section 5.5. Relevant details on the observables are provided in Appendix F.

[1] Very close results and pulls were found in the analysis of Ref. [68] using also a complete set of observables but a different treatment of hadronic uncertainties and form factors. See also results in Ref. [57] for an analysis using a smaller subset of the available data as well as Ref. [56, 78, 224, 225] (see Ref. [3] for a detailed comparison).

[2] Note that the effect of $Z - Z'$ mixing in the W mass in the context of $b \to s\ell^+\ell^-$ was already pointed out in Ref. [278].

5.1 Setup

We extend the SM by adding a heavy neutral $SU(2)_L$ singlet gauge boson[3]. Following the notation of Ref. [284, 285] the kinetic term and the mass term of this new boson, before EW symmetry breaking, are

$$\mathcal{L}_{Z_0'} = -\frac{1}{4} Z'_{0,\mu\nu} Z_0'^{\mu\nu} + \frac{\mu_Z'^2}{2} Z'_{0\mu} Z_0'^{\mu} + g_{Z'} Z'_{0\mu} Z_0'^{\mu} \phi^\dagger \phi - i g_{Z'}^{\phi} Z_0'^{\mu} \phi^\dagger \overleftrightarrow{D}_\mu \phi \,, \tag{5.1}$$

where $Z'_{0,\mu\nu} \equiv \partial_\mu Z'_{0\nu} - \partial_\nu Z'_{0\mu}$ is the field strength tensor, $\overleftrightarrow{D}_\mu = \overrightarrow{D}_\mu - (\overleftarrow{D}_\mu)^\dagger$, ϕ is the SM Higgs $SU(2)_L$ doublet and we use

$$D_\mu = \partial_\mu + i g_2 W_\mu^a T^a + i g_1 Y B_\mu \,, \tag{5.2}$$

as the definition of the SM part of the covariant derivative and $g_{Z'}^{\phi}$ is real by hermicity. The physical Z and Z' masses are obtained from diagonalizing the mass matrix

$$\mathcal{M}^2 = \begin{pmatrix} m_{Z_0}^2 & -\frac{y}{c_W} \\ -\frac{y}{c_W} & m_{Z_0'}^2 \end{pmatrix} , \qquad y \equiv \frac{v^2}{2} g_2 \, g_{Z'}^{\phi} \,, \tag{5.3}$$

in the Z_0, Z_0' basis, where Z_0 coincides with the SM Z for $g_{Z'}^{\phi} = 0$ with $m_{Z_0}^2 = \frac{v^2}{4}\left(g_1^2 + g_2^2\right)$, $\frac{v}{\sqrt{2}} \approx 174\,\text{GeV}$ and c_W is the cosine of the Weinberg angle. At leading order in $v/m_{Z_0'}$ we have

$$m_Z^2 \simeq m_{Z_0}^2 - \frac{y^2}{c_W^2 m_{Z_0'}^2} \equiv m_{Z_0}^2 \left(1 + \delta m_Z^2\right) . \tag{5.4}$$

Note that the corrections to the mass of the Z with respect to the SM value m_{Z_0} can only be negative. The mass eigenstates $Z^{(\prime)}$ can then be expressed as

$$\begin{pmatrix} Z \\ Z' \end{pmatrix} = \begin{pmatrix} Z_0' \sin\xi + Z_0 \cos\xi \\ Z_0' \cos\xi \; - Z_0 \sin\xi \end{pmatrix} , \tag{5.5}$$

where

$$\sin\xi \simeq \frac{y}{c_W m_{Z_0'}^2} \,, \tag{5.6}$$

describes the $Z - Z'$ mixing.

The interactions with the SM fields are given by

$$\begin{aligned} \mathcal{L}_{Z_0'}^{\text{fermions}} =& \bar{u}_j \gamma_\mu (g_{ji}^{uL} P_L + g_{ji}^{uR} P_R) u_i \, Z_0'^{\mu} + \bar{d}_j \gamma_\mu (g_{ji}^{dL} P_L + g_{ji}^{dR} P_R) d_i \, Z_0'^{\mu} \\ &+ g_{ji}^{\ell L} (\bar{\nu}_j \gamma_\mu P_L \nu_i) \, Z_0'^{\mu} + \bar{\ell}_j \gamma_\mu (g_{ji}^{\ell L} P_L + g_{ji}^{\ell R} P_R) \ell_i \, Z_0'^{\mu} \,, \end{aligned} \tag{5.7}$$

where, in the down basis, $g_{ji}^{uL} = V_{jk} g_{kk'}^{dL} V_{ik'}^*$. Note that the couplings to left-handed charged leptons and neutrinos (up and down quarks) are the same (up to a CKM rotation), due to $SU(2)_L$ invariance and that only the relative phase between $\sin\xi$ and $g_{ij}^{L,R}$ is physical, such that one can assume $\sin\xi$ to be positive without loss of generality. In the following, we will assume flavour diagonal coupling to leptons and in the quark sector disregard all couplings except left-handed $b - s$ couplings.

[3] We do not consider the case in which the Z' is the neutral component of a triplet because then no effect in the W mass would be generated and the necessarily purely left-handed lepton couplings could not explain the P_5' anomaly.

5.2 Observables

5.2.1 $b \to s\ell^+\ell^-$

In Z' models without $Z - Z'$ mixing, the simple one dimensional scenario with the best fit to data is obtained from a left-handed $b - s$ coupling and a vectorial muon coupling, i.e. the $\mathcal{C}^{\rm V}_{9\mu}$ scenario [4]. Allowing in addition for $Z - Z'$ mixing we have

$$\begin{aligned} \mathcal{C}^{\rm V}_{9\mu} &= -\frac{\pi^2}{e^2}\frac{4\sqrt{2}g^{dL}_{23}g^{\ell V}_{22}}{G_F m^2_{Z'}V_{tb}V^*_{ts}}\,, \\ \mathcal{C}^{\rm U}_{10} &= -k\mathcal{C}^{\rm U}_9 = \frac{\sqrt{2}\pi^2}{e^2}\frac{g_2\, g^{dL}_{23}\sin\xi}{c_W G_F m^2_Z V_{tb}V^*_{ts}}\,, \end{aligned} \tag{5.8}$$

where $g^{\ell V}_{22} = (g^{\ell L}_{22} + g^{\ell R}_{22})/2$. This corresponds to the scenario

$$\{\mathcal{C}^{\rm V}_{9\mu}\,,\, \mathcal{C}^{\rm U}_{10} = -k\mathcal{C}^{\rm U}_9\}\,, \tag{5.9}$$

with $k = 1/(1 - 4s^2_w)$ (see Eq. (1.5) and Eq. (1.6) for the definitions of the operators associated to the Wilson coefficients in Eq. (5.9)). The superscript V (U) in the Wilson coefficient stands for a LFUV (LFU) contribution.

We perform the most recent fit [4] to the scenario in Eq. (5.9), including 254 observables as described in Section 1.3 (see Appendix B for SM predictions of the whole set of observables included in the fit). We obtain the best fit point and confidence level regions in Table 5.1 and the corresponding confidence level regions in Fig. 5.1. Note that this scenario is preferred over the SM hypothesis by 6.9σ.

	Best-fit point	1 σ CI	2 σ CI
$\mathcal{C}^{\rm V}_{9\mu}$	-0.96	$[-1.11, -0.80]$	$[-1.25, -0.64]$
$\mathcal{C}^{\rm U}_{10} = -k\mathcal{C}^{\rm U}_9$	$+0.30$	$[+0.15, +0.45]$	$[+0.00, +0.61]$

Table 5.1: 1σ and 2σ confidence intervals for the NP scenario in Eq. (5.9) with a $\text{Pull}_{\rm SM}$ of 6.9σ and p-value=28.3%.

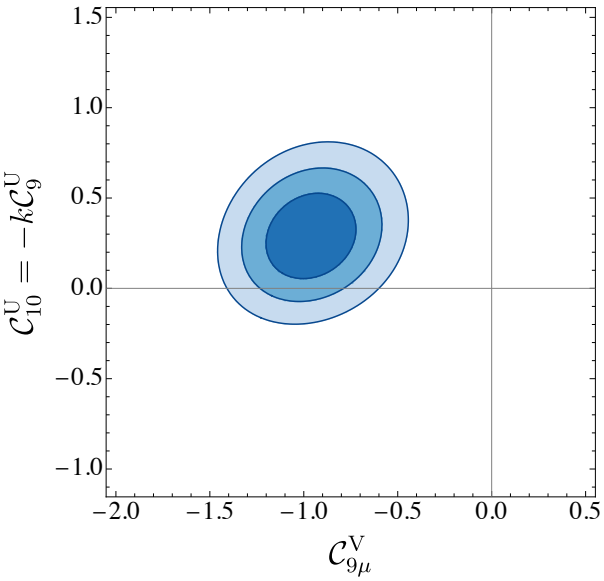

Figure 5.1: Preferred 1σ, 2σ and 3σ regions in the $(\mathcal{C}^{\rm V}_{9\mu}, \mathcal{C}^{\rm U}_{10} = -k\mathcal{C}^{\rm U}_9)$ plane for the scenario in Eq. (5.9), including all available $b \to s\ell^+\ell^-$ data and using the most updated version of ACDMN code [4]. Note that the SM case corresponds to the (0,0) point.

5.2.2 $B_s - \bar{B}_s$ Mixing

The most important constraint on $Z' - b - s$ couplings, i.e. g_{23}^{dL}, comes from $B_s - \bar{B}_s$ mixing where the contribution to the Hamiltonian $\mathcal{H}_{\text{eff}} = \mathcal{C}_1\mathcal{O}_1$, with $\mathcal{O}_1 = \left(\bar{b}\gamma^\mu P_L s\right) \times \left(\bar{b}\gamma_\mu P_L s\right)$, is given by

$$\mathcal{C}_1 = \frac{1}{2}\left(\frac{g_{23}^{dL}}{m_{Z'}}\right)^2 \left(1 + \frac{\alpha_s}{4\pi}\frac{11}{3}\right), \tag{5.10}$$

including the NLO matching corrections of Ref. [286]. Note that the effect of the mixing induced $Z - b - s$ couplings can be neglected as it corresponds to a dimension 8 contribution. Employing the 2-loop renormalization group evolution [214, 215], this leads to an effect, normalized to the SM one, of

$$\left(\frac{g_{23}^{dL}}{0.52}\frac{10\,\text{TeV}}{m_{Z'}}\right)^2 = 0.110 \pm 0.090\,, \tag{5.11}$$

using the bag factor of Ref. [216] and the global fit to NP in $\Delta F = 2$ observables of Ref. [217].

5.2.3 LFUV in tau decays

Assuming lepton flavour conservation, $Z' - W$ boxes contribute to $\tau \to \mu\,\nu_\tau\bar{\nu}_\mu$ as [233]

$$\frac{\mathcal{A}(\tau \to \mu\,\nu_\tau\bar{\nu}_\mu)}{\mathcal{A}(\tau \to \mu\,\nu_\tau\bar{\nu}_\mu)_{SM}} = 1 - \frac{3}{8\pi^2}\, g_{22}^{\ell L}\, g_{33}^{\ell L}\, \frac{\ln\left(\frac{m_W^2}{m_{Z'}^2}\right)}{1 - \frac{m_{Z'}^2}{m_W^2}}\,, \tag{5.12}$$

and analogously for $\tau \to e\,\nu_\tau\bar{\nu}_e$ and $\mu \to e\,\nu_\mu\bar{\nu}_e$. This has to be compared to the experimental results [135]

$$\begin{aligned}
\left.\frac{\mathcal{A}\left[\tau \to \mu\nu\bar{\nu}\right]}{\mathcal{A}\left[\mu \to e\nu\bar{\nu}\right]}\right|_{\text{EXP}} &= 1.0029 \pm 0.0014\,,\\
\left.\frac{\mathcal{A}\left[\tau \to \mu\nu\bar{\nu}\right]}{\mathcal{A}\left[\tau \to e\nu\bar{\nu}\right]}\right|_{\text{EXP}} &= 1.0018 \pm 0.0014\,,\\
\left.\frac{\mathcal{A}\left[\tau \to e\nu\bar{\nu}\right]}{\mathcal{A}\left[\mu \to e\nu\bar{\nu}\right]}\right|_{\text{EXP}} &= 1.0010 \pm 0.0014\,,
\end{aligned} \tag{5.13}$$

with the correlation matrix given in Ref. [135][4].

5.2.4 Electroweak fit

The EW sector of the SM has been tested with a very high precision at LEP [288, 289] but also at the Tevatron [290] and the LHC [291–293]. Since it can be parametrized by only three Lagrangian parameters, we choose as usual the set with the smallest experimental error consisting of the Fermi constant ($G_F = 1.1663787(6)\times 10^{-5}\,\text{GeV}^{-2}$ [211]), the mass of the Z boson ($m_Z = 91.1875(21)$ GeV [289]) and the fine structure constant $\alpha_{em} = 7.2973525664(17) \times 10^{-3}$ [211, 294–296].

In our model, the relation between the Lagrangian values and the measurements of G_F and m_Z is shifted with respect to the SM. While the effect in $\mu \to e\nu\bar{\nu}$ is analogous to the one in $\tau \to \mu\nu\bar{\nu}$ discussed above we have for the Z mass

$$\frac{m_Z^2}{m_{Z_0}^2} \approx 1 - \sin\xi^2 \frac{m_{Z_0'}^2}{m_{Z_0}^2}\,, \tag{5.14}$$

from Eqs. (5.4) and (5.6). However, since the Z mass is used as in input, this translates into a shift in the W mass prediction of approximately

[4] Here we neglected semileptonic tau decays as well as other probes of LFUV in the charged current which are not affected in the absence of quark coupling (see Ref. [287] for a recent review).

$$\frac{m_W^2}{m_{W_0}^2} \approx 1 + \sin\xi^2 \frac{m_{Z'_0}^2}{m_{Z_0}^2}\,. \tag{5.15}$$

Furthermore, both the $Z - Z'$ mixing and Z' vertex corrections lead to modified $Z\ell\ell$ and $Z\nu\nu$ couplings (see Appendix F for details) which are included in the global EW fit.

The set of observables given in Appendix F are implemented in HEPfit [297] taking into account the modifications induced by Eq. (5.14) and Eq. (F.4). In addition, the Higgs mass ($m_H = 125.16 \pm 0.13$ GeV [298, 299]), the top mass ($m_t = 172.80 \pm 0.40$ GeV [300–302]), the strong coupling constant ($\alpha_s(m_Z) = 0.1181 \pm 0.0011$ [211]) and the hadronic contribution to the running of $\alpha_{\rm em}$ ($\Delta\alpha_{\rm had} = 276.1(11) \times 10^{-4}$ [211]) have been used as input parameters, since they enter EW observables indirectly via loop effects.

5.2.5 Neutrino Trident Production

The production of a $\mu^+\mu^-$ pair from the scattering of a muon-neutrino off the Coulomb field of a nucleus, known as neutrino trident production, constitutes a sensitive probe of new neutral current interactions in the lepton sector [233, 303]. Generalizing the formula of Ref. [303] we find

$$\frac{\sigma_{\rm SM+NP}}{\sigma_{\rm SM}} = 1 + 8\frac{g_{22}^{\ell L}}{g_2^2}\frac{m_W^2}{m_{Z'}^2}\frac{\left(1+4s_W^2\right)\left(g_{22}^{\ell L}+g_{22}^{\ell R}\right)+\left(g_{22}^{\ell L}-g_{22}^{\ell R}\right)}{\left(1+4s_W^2\right)^2+1}\,. \tag{5.16}$$

This ratio is bounded by the weighted average

$$\frac{\sigma_{\rm exp}}{\sigma_{\rm SM}} = 0.83 \pm 0.18\,, \tag{5.17}$$

obtained from averaging the CHARM-II [304], CCFR [305] and NuTeV results [306].

5.2.6 Direct searches

LEP-II sets stringent bounds on 4-lepton operators from $e^+e^- \to \ell^+\ell^-$ (with $\ell = e, \mu, \tau$) [288] for specific chiralities. A general approach to derive the constraints for any Z' model is discussed in Refs. [307, 308] which provides the formula used in our analysis. In the limit in which the only quark couplings of the Z' are to $b - s$, LHC searches are not very constraining and assuming a lower limit of 2 TeV is not in conflict with ATLAS and CMS searches.

5.3 Phenomenology

Let us now study the combined phenomenological consequences of $Z - Z'$ mixing in $b \to s\ell^+\ell^-$ and the global EW fit. For this purpose we will focus on an illustrative simplified scenario for an $SU(2)_L$ singlet Z'. As discussed in the previous section, $b \to s\ell^+\ell^-$ data motivates vectorial couplings to leptons, i.e. $g_{ii}^{\ell L} = g_{ii}^{\ell R} = g_{ii}^{\ell V}$ which also allow for simple configurations without gauge anomalies such as $L_\mu - L_\tau$ [233, 242] or $B_3 - L_2$ [274]. We consider in this illustrative scenario only left-handed $Z' - b - s$ couplings but assume absence of sizable couplings to light quarks in order to avoid direct LHC searches. Note that such a scenario could be generated in models with vector-like quarks [99, 233],. While these assumptions are justified by the $b \to s\ell^+\ell^-$ fit, we will assume in addition $g_{11}^{\ell V} = 0$ and $g_{22}^{\ell V} = -g_{33}^{\ell V} = g'$, i.e. a $L_\mu = -L_\tau$ symmetry [309–311]. This does not only avoid the LEP II bounds on 4-lepton contact interactions but also the effect of $Z - Z'$ mixing in the total Z width will cancel to leading order such that in this scenario the largest lepton couplings are possible (see Fig. 5.2) and $\tau \to \mu\nu\nu$ receives the desired constructive contribution via $W - Z'$ box diagrams[5].

Let us now consider the impact of $Z - Z'$ mixing in this scenario. Notably, as discussed in the introduction, the current experimental average for the mass of the W boson, $m_W = 80.379(12)$ GeV [312], shows a 1.8σ discrepancy with the value predicted from the EW fit within the SM [282], before considering the impact of the new CDF measurement discussed in Section 5.4. This prediction is changed in our

[5] Note, that our analysis would to a good approximation also apply to other scenarios, such as $B_3 - L_2$.

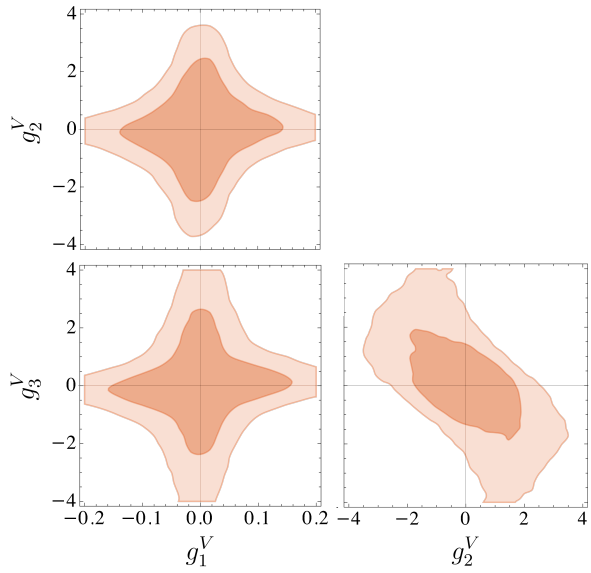

Figure 5.2: Global fit to EW data, neutrino trident production, LEP bounds on 4-lepton contact interactions and $\tau \to \mu\nu\nu$ data with vectorial flavour diagonal couplings $g^L_{ii} = g^R_{ii} = g^V_i$. Here we marginalized over the $Z - Z'$ mixing angle ξ. The 68% and 95% confidence level regions are shown for a Z' mass of 2 TeV. Note that a preference for the $L_\mu - L_\tau$ scenario emerges.

model according to Eq. (5.15) such that one accounts for data with a non-zero mixing angle of $|\sin\xi| \simeq 2.5 \times 10^{-3} \frac{1\,\text{TeV}}{m_{Z'}}$, i.e. solving this tension.

Moving to the complete EW fit (including also LFUV in tau decays, LEP bounds on 4-lepton operators and neutrino trident production) we have $m_{Z'}$, g' and $\sin\xi$ as free parameters. However, since all expressions depend on $g'^2/m^2_{Z'}$ despite logarithmic terms we set $m_{Z'} = 2\,\text{TeV}$. The resulting preferred regions from the EW fit and LFUV in tau decays are shown in Fig. 5.3. Now we include $b \to s\ell^+\ell^-$, corresponding to the scenario $\{\mathcal{C}^{\text{V}}_{9\mu}, \mathcal{C}^{\text{U}}_{10} = -k\mathcal{C}^{\text{U}}_9\}$, as well as $B_s - \bar{B}_s$ mixing. This introduces in addition g^{dL}_{23} as a free parameter. Marginalizing over g^{dL}_{23} we find the 1σ and 2σ regions shown in blue in Fig. 5.3. Note that all 1σ regions nicely overlap, showing that there is a preference for a non-zero $Z - Z'$ mixing angle which can account for the tension in the W mass prediction of the EW fit.

Observable	Scenario 1	Experiment	Pull
$R^{[1.1,6]}_{K^+}$	$+0.79 \pm 0.01$	$+0.85 \pm 0.04$	-1.3
$R^{[1.1,6]}_{K^0_S}$	$+0.79 \pm 0.01$	$+0.66 \pm 0.20$	$+0.7$
$R^{[1.1,6]}_{K^{*0}}$	$+0.87 \pm 0.08$	$+0.69 \pm 0.12$	$+1.3$
$R^{[0.045,6]}_{K^{*+}}$	$+0.84 \pm 0.04$	$+0.70 \pm 0.18$	$+0.8$
$Q^{[1.1,6]}_5$	$+0.28 \pm 0.02$	$+0.66 \pm 0.50$	-0.8
$\langle P'_5\rangle^{[4,6]}$	-0.57 ± 0.11	-0.44 ± 0.12	-0.8
$\langle P'_5\rangle^{[6,8]}$	-0.79 ± 0.11	-0.58 ± 0.09	-1.4
$10^7 \times \mathcal{B}^{[4,6]}_{B_s\to\phi\mu^+\mu^-}$	$+0.78 \pm 0.15$	$+0.62 \pm 0.06$	$+1.0$
$10^9 \times \mathcal{B}_{B_s\to\mu^+\mu^-}$	$+3.08 \pm 0.14$	$+2.85 \pm 0.34$	$+0.6$

Table 5.2: Predictions for some of the most relevant observables in the $b \to s\ell^+\ell^-$ fit within the scenario of Eq. (5.9). The pulls are given in units of standard deviations.

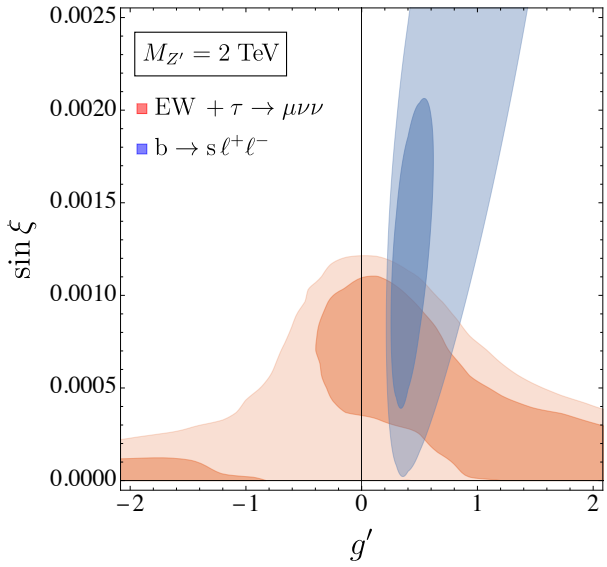

Figure 5.3: Global fit EW precision observables, neutrino trident production, LEP bounds on 4-lepton contact interactions and $\tau \to \mu\nu\nu$ data (red) and $b \to s\ell^+\ell^-$ data (blue) in the g' - $\sin\xi$ plane for $m_{Z'_0} = 2\,\text{TeV}$. One can see that both regions overlap nicely and that a non-zero value of the mixing angle is preferred.

5.4 Implications of the new measurement of m_W

Intriguingly, the CDF collaboration just released results [283] which point towards a W mass above the SM expectation [312] with a significance of $\approx 7\sigma$. Combining this new measurement with the existing ones from the LHC [291–293, 313], one finds $m_W = (80.4133 \pm 0.0080)\text{GeV}$ and $m_W = (80.413 \pm 0.015)\text{GeV}$, where in the second formula the error has been inflated to reflect the tensions between the different measurements. The SM prediction is given by $m_W^{\text{SM}} = (80.3499 \pm 0.0056)\text{GeV}$, and $m_W^{\text{SM}} = (80.3505 \pm 0.0077)$ GeV for a conservative error estimate [314]. This corresponds to a 6.5σ and 3.7σ tension for the standard and the conservative scenario, respectively.

In our model, the prediction for the W mass is modified according to Eq. (5.15).[6] We updated the phenomenological analysis for our $SU(2)_L$ singlet Z' with vectorial $L_\mu - L_\tau$ [309–311] couplings to leptons [233, 242] and left-handed $Z' - b - s$ couplings to quarks while we assume absence of sizable couplings to light quarks in order to avoid direct LHC searches.

Since the new experimental average for the mass of the W boson deviates from the SM prediction, a non-zero $Z - Z'$ mixing angle is now clearly preferred according to Eq. (5.15), i.e. $|\sin\xi| \simeq 3.5 \times 10^{-3} \times 1\text{TeV}/m_{Z'}$. Once all EW data and LFUV in tau decays are included the central value of $|\sin\xi|$ gets reduced to $\simeq 1.0 \times 10^{-3}$ and $\simeq 0.85 \times 10^{-3}$ for the 2 TeV and 3 TeV scenarios, respectively, as can be seen in Fig. 5.4. The resulting confidence level regions from the EW fit and LFUV in tau decays are shown in orange in Fig. 5.4. Importantly, the region preferred by the $b \to s\ell^+\ell^-$ fit (blue), including $B_s - \bar{B}_s$ mixing, overlaps significantly with this region when marginalizing over g_{23}^{dL} for $m_{Z'} \approx 2 - 3$ TeV.

In conclusion, the new measurement of the W mass by the CDF collaboration is consistent with the expectations from a Z' explanation of the $b \to s\ell^+\ell^-$ anomalies and strongly suggests that $SU(2)_L$ breaking and the breaking of the new $U(1)'$ symmetry are linked. In this case, one predicts, in addition to the direct LFUV contribution $\mathcal{C}_{9\mu}^{\text{V}}$, a sizable mixing induced lepton flavour universal contribution to $b \to s\ell^+\ell^-$ data with the structure $\mathcal{C}_{10}^{\text{U}} = -\mathcal{C}_9^{\text{U}}/(1 - 4s_w^2)$. This pattern can be tested by forthcoming measurement of LHCb, CMS and Belle II.

[6] In this context, Refs. [315–320] pointed out that a Z' mixing with the SM Z can explain the CDF measurement.

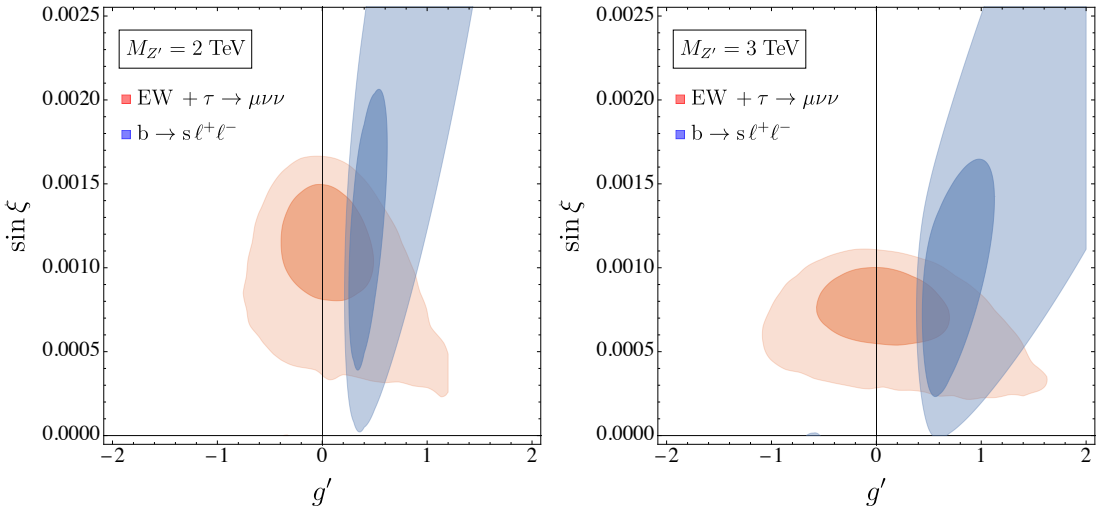

Figure 5.4: Global fit to EW precision observables, neutrino trident production, LEP bounds on 4-lepton contact interactions and $\tau \to \mu\nu\nu$ data (orange) and $b \to s\ell^+\ell^-$ data (blue) in the g' - $\sin\xi$ plane for $m_{Z'} = 2$ TeV (left) and $m_{Z'} = 3$ TeV (right). One can see that both regions (nearly) overlap at the 1σ level and that a non-zero $Z - Z'$ value of the mixing angle, as preferred by the new world average for the W mass, is compatible with $b \to s\ell^+\ell^-$ data.

5.5 Summary and Conclusions

In this chapter we systematically studied the impact of $Z - Z'$ mixing on the global fit to $b \to s\ell^+\ell^-$ data and EW precision observables. Concerning the former, we observe that a LFU effect, mainly in $\mathcal{C}_{10}$, is generated while in the latter the mixing leads to modified Z couplings and to an enhancement in the predicted W mass w.r.t. the SM which improves the agreement with data. Therefore, while in previous analyses in the literature the effect of $Z - Z'$ mixing was usually assumed to be small and was therefore neglected, we stress that the fit even prefers a small but non-zero value of the order of 10^{-3}. Note that this is in agreement with the expectation $\sin\xi \approx g_2 g' m_Z^2/M_{Z'}^2$ for a TeV scale Z' with order one couplings in case $U(1)'$ and EW symmetry breaking are related.

If $b \to s\ell^+\ell^-$ data is in fact explained by a Z' with non-vanishing $Z - Z'$ mixing, giving rise to a scenario like $\{\mathcal{C}_{9\mu}^{\mathrm{V}}, \mathcal{C}_{10}^{\mathrm{U}} = -k\mathcal{C}_9^{\mathrm{U}}\}$, one predicts a pattern for the main observables driving the anomaly as shown in Table 5.2. We observe that all tensions with experiment reduce significantly below the 1.5σ level in the scenario analyzed. Because $b \to s\ell^+\ell^-$ ratios testing LFUV depend naturally (and almost entirely) on $\mathcal{C}_{9\mu}^{\mathrm{V}}$ and thus do not carry information on $\sin\xi$, angular observables are necessary for a distinctive study of Z' models. It will therefore be important to verify with more precise LHCb data together with future Belle II analysis if this scenario gets reinforced.

Furthermore, the new measurement of the W mass by the CDF collaboration is consistent with the expectations from a Z' explanation of the $b \to s\ell^+\ell^-$ anomalies and strongly suggests, through the need of a non-zero $Z - Z'$ mixing, that $SU(2)_L$ breaking and the breaking of the new $U(1)'$ symmetry are linked, implying the existence of a field charged under both symmetries, which has important consequences for model building.

Conclusions and Outlook

In this Thesis we explored one of the most promising areas in Flavour Physics in regards to the possibility of unveiling physics beyond the SM. After several years of experimental measurements indicating clear tensions with respect to the SM predictions in different decays involving a b quark, it is of common belief that the B sector offers a great window of insight into the properties of a new theory that supersedes the SM. We mainly focused on the current status of the global analyses of the semileptonic $b \to s\ell^+\ell^-$ transitions but also the charged partner current $b \to c\ell\nu$. Furthermore, we provided interpretations for the directions in the NP Wilson coefficient space that the experimental data seems to point to, which may help setting the next steps in determining the underlying structure of NP.

For that reason, the goal of this Thesis is to provide the reader with the basic tools needed to understand the whole framework that describes the B-anomalies, specially for the case of semileptonic $b \to s\ell^+\ell^-$ transitions as they are the channel showing the largest set of coherent deviations w.r.t. the SM. Consequently, we devoted Chapter 1 to discuss the EFT framework used to describe the $b \to s\ell^+\ell^-$ transitions and to present the latest, most updated global analysis concerning this type of B decays. We found that some NP hypotheses reach high levels of significance of $\sim 7\sigma$ when compared to the SM hypothesis. While this is a remarkable achievement in terms of building consensus towards the need of a new, more general theory, it is clear that still more data is needed. For instance, there are several NP scenarios with different implications for model building that can explain data with a very similar statistical importance. Therefore, we need new modes and new observables to help us disentangle between those preferred scenarios and hence further constrain the NP parameter space. In this direction, the measurement of interesting observables that can act as a discriminator of models is fundamental, as we showed with the key observable Q_5, which together with more and more precise measurements of other essential observables such as R_K and R_{K^*} can ultimately provide us with a clear path towards the right NP scenario.

Another important aspect that can supply new information is the inclusion of S-wave observables in the analyses of the $B \to K^*(K^+\pi^-)\ell^+\ell^-$ decay. So far, given the poor theoretical knowledge on the form factors of the $K\pi$ system, this is treated as background in experimental analyses, and therefore not included in phenomenological studies. We showed in Chapter 2 that using the symmetries of the angular distribution of the decay we can define new P- and S-wave interference observables $W_{1,2}$ that give us access to additional information without having to rely on poorly known hadronic quantities by expressing S-wave observables in terms of P-wave quantities. Moreover, the relations found between the newly defined S-wave observables can be used as a crosscheck to validate the experimental methodology applied in fits to data.

To close the first part of this Thesis, devoted to semileptonic B decays, we turned our focus to the charged transition $B \to D^*\ell\nu$ in Chapter 3. Starting from the symmetries existing in the angular distribution of this process, we established a set of robust relations between the angular coefficients. These relations allowed us to define an alternative way of measuring the longitudinal polarisation $F_L^{D^*}$ involving different angular coefficients, which can be useful in future measurements to better understand the tension showed by the latest results from the Belle collaboration. On top of that, we also checked that the binned version of the observables fulfill the symmetry relations to a good degree of accuracy and tested their behaviour under the most relevant NP hypotheses from global fits.

The second main part of this Thesis shifted the attention towards a different mode of a $b \to s$ decay which does not involve leptons of any kind. Chapter 4 presents a study of the nonleptonic $B_{d,s} \to \bar{K}^{*0}K^{*0}$ decays which exhibit a remarkable 2.6σ tension between the SM prediction and data on the observable from a naive $SU(3)$ estimate concerning the observable $L_{\bar{K}^{*0}K^{*0}}$ that compares the longitudinal polarisation fractions involving a spectator s quark over a d quark in the parent B meson. We explored the possibility to reduce the observed tension with a simplified NP model, even if the conclusion turned out to be that a significant amount of fine tuning is required. However, we firmly believe that one should

pursue the enterprise of determining the interplay between different $b \to s$ modes, as it is somewhat natural to expect a common origin for the different anomalies involving a b-quark flavour.

In Part III we discussed a possible extension of the SM based on adding an extra gauge boson Z' that mixes with the usual Z boson as a source for the NP contributions with the goal to explain the $b \to s\ell^+\ell^-$ data as well as the EW precision observables. While the former see the tension with experiment reduced below 1.5σ once contributions to $\mathcal{C}_{9\mu}^{\mathrm{V}}$ and $\mathcal{C}_{10}^{\mathrm{U}}$ are generated by the modified Z couplings, the latter predicts an enhancement in the W mass compared to the SM value, which goes exactly in the direction of the recent measurements of m_W by the CDF collaboration, strengthening the hypothesis of a non-zero $Z - Z'$ mixing. If confirmed, this would imply, for instance, the breaking of the $SU(2)_L$ and $U(1)'$ symmetries, which has relevant consequences for model building.

In summary, we have discussed in this Thesis different sources of tensions with the Standard Model, as well as novel ways to establish connections among them. However, we are certainly not at the end of the road, as there are still issues that need a better understanding in order to set up a rock solid foundation for future endeavours in the field of Flavour Physics. For instance, under the current criterium to claim a discovery, we need to further refine the experimental precision, besides of course adding more statistics, in order to reach the standard 5σ deviation in a single measurement. The one observable closest to this milestone is R_K, at 3.1σ, so there is still a gap to bridge in this regard. On the other hand, one could argue that this particular indicator should be revised, given that we are studying a global set of indirect measurements instead of a single one (like in the case of a resonance), and therefore we may already be reaching a level of statistical significance to clearly discard the SM as a functional hypothesis to describe the data collected.

On a different note, increased precision in experimental measurements should be matched by increased precision in theoretical uncertainties. To achieve that, we can expect more precise theoretical computations of the main source of uncertainties, the hadronic form factors. At a certain point Lattice QCD techniques will be applied to extend ranges beyond the natural region of application (the low-recoil region) thanks to more powerful computational tools. Moreover, new and improved computations of the hadronic contributions that appear in the form of Light Cone Sum Rules and the parametrisation of the challenging charm loop contributions will reduce the space for uncontrolled uncertainties, allowing us to be even more certain of the underlying NP structure.

Finally, new analyses extending the scope to include CP-violating observables to constrain possible complex NP contributions should bring forth information that can provide a better handle on the plethora of existing anomalies. Furthermore, we should expect that more attention is paid to the study of potential connections between the B-anomalies and other flavour anomalies such as the anomalous magnetic moment of the muon $(g-2)_\mu$ or the Cabbibo Angle Anomaly, among others. Establishing links between apparently unrelated tensions w.r.t. the SM can only help us further confirm the existence of a coherent pattern of deviations and set up future guidelines to chase the ultimate goal we face as a physics community, which is none other than to determine the essence of what lies beyond the Standard Model.

Appendix A

Angular conventions

In this appendix we provide a dictionary between the different definitions of the angles θ_{K^*}, θ_ℓ and ϕ used to describe the $B \to K^*\ell^+\ell^-$ decay distribution, as the standard theory conventions [9, 11, 12] differ from the ones used by the experimental collaborations, in particular by LHCb [27].

The connection between LHCb convention and our definitions for the three angles θ_{K^*}, θ_ℓ and ϕ is the following:

$$\theta_{K^*}^{\rm LHCb} = \theta_{K^*}\,, \qquad \theta_\ell^{\rm LHCb} = \pi - \theta_\ell\,, \qquad \phi^{\rm LHCb} = -\phi \tag{A.1}$$

Therefore, concerning the definition of the optimized observables P_i in Eqs. (1.47), taking into account the different numerical factors LHCb uses to define these quantities from the whole differential distribution, we obtain the following dictionary:

$$\begin{aligned} &P_1^{\rm LHCb} = P_1, \qquad P_2^{\rm LHCb} = -\,P_2, \quad P_3^{\rm LHCb} = P_3, \\ &P_4'^{\rm LHCb} = -\,\frac{1}{2}P_4, \quad P_5'^{\rm LHCb} = P_5', \qquad P_6'^{\rm LHCb} = P_6', \quad P_8'^{\rm LHCb} = -\,\frac{1}{2}P_8'. \end{aligned} \tag{A.2}$$

Appendix B

Predictions for the observables in the Standard Model

We provide here the observables included in our Fits "All" (254 observables) and "LFUV" (24 observables, replacing $P'_{4e,\mu}, P'_{5e,\mu}$ by Q_4, Q_5, measured by Belle). In the following table, we provide all the observables considered in both types of fits with the corresponding legend: no mark for observables for the fit "All" only, ‡ for the fit "LFUV" only, and † for both fits "LFUV" and "All". The theoretical predictions of the observables in the SM as well as the individual tension with respect to the experimental value are also provided.

Our angle convention and definition of the angular observables for the $B \to K^* \ell^+ \ell^-$ decay differs from the usual LHCb convention [26, 27]. We follow the conventions given in Ref. [22] and explicitly detailed in Appendix A.

Standard Model Predictions			
$10^7 \times BR(B^+ \to K^+ \mu^+ \mu^-)$[LHCb]	Standard Model	Experiment [321]	Pull
$[0.1, 0.98]$	0.32 ± 0.10	0.29 ± 0.02	$+0.3$
$[1.1, 2]$	0.33 ± 0.10	0.21 ± 0.02	$+1.2$
$[2, 3]$	0.37 ± 0.11	0.28 ± 0.02	$+0.7$
$[3, 4]$	0.36 ± 0.12	0.25 ± 0.02	$+0.9$
$[4, 5]$	0.36 ± 0.12	0.22 ± 0.02	$+1.2$
$[5, 6]$	0.36 ± 0.12	0.23 ± 0.02	$+1.0$
$[6, 7]$	0.36 ± 0.13	0.25 ± 0.02	$+0.9$
$[7, 8]$	0.36 ± 0.13	0.23 ± 0.02	$+0.9$
$[15, 22]$	1.02 ± 0.14	0.85 ± 0.05	$+1.2$
$10^7 \times BR(B^0 \to K^0 \mu^+ \mu^-)$[LHCb]	Standard Model	Experiment [321]	Pull
$[0.1, 2]$	0.65 ± 0.20	0.23 ± 0.11	$+1.9$
$[2, 4]$	0.68 ± 0.21	0.37 ± 0.11	$+1.3$
$[4, 6]$	0.67 ± 0.22	0.35 ± 0.10	$+1.3$
$[6, 8]$	0.66 ± 0.24	0.54 ± 0.12	$+0.5$
$[15, 22]$	0.94 ± 0.13	0.67 ± 0.12	$+1.6$
$10^7 \times BR(B^0 \to K^{*0} \mu^+ \mu^-)$[LHCb]	Standard Model	Experiment [109]	Pull
$[0.1, 0.98]$	0.92 ± 0.80	0.89 ± 0.09	$+0.0$
$[1.1, 2.5]$	0.56 ± 0.35	0.46 ± 0.06	$+0.3$
$[2.5, 4]$	0.58 ± 0.40	0.50 ± 0.06	$+0.2$
$[4, 6]$	0.91 ± 0.66	0.71 ± 0.07	$+0.3$
$[6, 8]$	1.12 ± 0.89	0.86 ± 0.08	$+0.3$
$[15, 19]$	2.50 ± 0.21	1.74 ± 0.14	$+3.0$
$10^7 \times BR(B^+ \to K^{*+} \mu^+ \mu^-)$[LHCb]	Standard Model	Experiment [321]	Pull
$[0.1, 2]$	1.40 ± 1.08	1.12 ± 0.27	$+0.3$
$[2, 4]$	0.84 ± 0.56	1.12 ± 0.32	-0.4
$[4, 6]$	0.99 ± 0.72	0.50 ± 0.20	$+0.7$

$[6, 8]$	1.22 ± 0.96	0.66 ± 0.22	$+0.6$
$[15, 19]$	2.69 ± 0.23	1.60 ± 0.32	$+2.8$
$10^7 \times BR(B_s \to \phi\mu^+\mu^-)$[LHCb]	Standard Model	Experiment [75]	Pull
$[0.1, 0.98]$	1.06 ± 0.23	0.68 ± 0.06	$+1.6$
$[1.1, 2.5]$	0.71 ± 0.15	0.44 ± 0.05	$+1.7$
$[2.5, 4]$	0.71 ± 0.15	0.35 ± 0.04	$+2.3$
$[4, 6]$	1.04 ± 0.21	0.62 ± 0.06	$+1.9$
$[6, 8]$	1.21 ± 0.25	0.63 ± 0.06	$+2.2$
$[15, 19]$	2.29 ± 0.15	1.85 ± 0.13	$+1.9$
$F_L(B^0 \to K^{*0}\mu^+\mu^-)$[LHCb]	Standard Model	Experiment [110]	Pull
$[0.1, 0.98]$	0.23 ± 0.24	0.26 ± 0.03	-0.1
$[1.1, 2.5]$	0.68 ± 0.26	0.66 ± 0.05	$+0.1$
$[2.5, 4]$	0.77 ± 0.23	0.76 ± 0.05	$+0.0$
$[4, 6]$	0.71 ± 0.28	0.68 ± 0.04	$+0.1$
$[6, 8]$	0.63 ± 0.32	0.65 ± 0.03	-0.0
$[15, 19]$	0.34 ± 0.03	0.35 ± 0.02	-0.1
$P_1(B^0 \to K^{*0}\mu^+\mu^-)$[LHCb]	Standard Model	Experiment [110]	Pull
$[0.1, 0.98]$	0.03 ± 0.08	0.09 ± 0.12	-0.4
$[1.1, 2.5]$	-0.00 ± 0.05	-0.62 ± 0.30	$+2.0$
$[2.5, 4]$	0.00 ± 0.06	0.17 ± 0.37	-0.4
$[4, 6]$	0.02 ± 0.12	0.09 ± 0.24	-0.2
$[6, 8]$	0.02 ± 0.13	-0.07 ± 0.21	$+0.4$
$[15, 19]$	-0.64 ± 0.06	-0.58 ± 0.10	-0.6
$P_2(B^0 \to K^{*0}\mu^+\mu^-)$[LHCb]	Standard Model	Experiment [110]	Pull
$[0.1, 0.98]$	0.12 ± 0.02	0.00 ± 0.04	$+2.8$
$[1.1, 2.5]$	0.44 ± 0.03	0.44 ± 0.10	-0.0
$[2.5, 4]$	0.23 ± 0.13	0.19 ± 0.12	$+0.2$
$[4, 6]$	-0.19 ± 0.11	-0.11 ± 0.07	-0.6
$[6, 8]$	-0.38 ± 0.07	-0.21 ± 0.05	-2.1
$[15, 19]$	-0.36 ± 0.02	-0.36 ± 0.02	-0.1
$P_3(B^0 \to K^{*0}\mu^+\mu^-)$[LHCb]	Standard Model	Experiment [110]	Pull
$[0.1, 0.98]$	-0.00 ± 0.00	-0.07 ± 0.06	$+1.3$
$[1.1, 2.5]$	0.00 ± 0.00	-0.32 ± 0.15	$+2.2$
$[2.5, 4]$	0.00 ± 0.01	-0.05 ± 0.20	$+0.3$
$[4, 6]$	0.00 ± 0.01	0.09 ± 0.14	-0.6
$[6, 8]$	0.00 ± 0.00	0.07 ± 0.10	-0.6
$[15, 19]$	0.00 ± 0.02	-0.05 ± 0.05	$+1.0$
$P_4'(B^0 \to K^{*0}\mu^+\mu^-)$[LHCb]	Standard Model	Experiment [110]	Pull
$[0.1, 0.98]$	-0.50 ± 0.16	-0.27 ± 0.24	-0.8
$[1.1, 2.5]$	-0.07 ± 0.16	0.16 ± 0.29	-0.7
$[2.5, 4]$	0.53 ± 0.21	0.87 ± 0.35	-0.9
$[4, 6]$	0.82 ± 0.15	0.62 ± 0.23	$+0.7$
$[6, 8]$	0.93 ± 0.11	1.15 ± 0.19	-1.0
$[15, 19]$	1.28 ± 0.02	1.28 ± 0.12	$+0.0$
$P_5'(B^0 \to K^{*0}\mu^+\mu^-)$[LHCb]	Standard Model	Experiment [110]	Pull
$[0.1, 0.98]$	0.67 ± 0.13	0.52 ± 0.10	$+0.9$
$[1.1, 2.5]$	0.19 ± 0.11	0.37 ± 0.12	-1.0
$[2.5, 4]$	-0.47 ± 0.12	-0.15 ± 0.15	-1.7
$[4, 6]$	-0.82 ± 0.08	-0.44 ± 0.12	-2.7
$[6, 8]$	-0.94 ± 0.08	-0.58 ± 0.09	-2.9

$[15, 19]$	-0.57 ± 0.05	-0.67 ± 0.06	$+1.2$
$P_6'(B^0 \to K^{*0}\mu^+\mu^-)$[LHCb]	Standard Model	Experiment [110]	Pull
$[0.1, 0.98]$	-0.06 ± 0.02	0.02 ± 0.09	-0.7
$[1.1, 2.5]$	-0.07 ± 0.03	-0.23 ± 0.13	$+1.2$
$[2.5, 4]$	-0.06 ± 0.03	-0.16 ± 0.15	$+0.6$
$[4, 6]$	-0.04 ± 0.02	-0.29 ± 0.12	$+2.2$
$[6, 8]$	-0.02 ± 0.01	-0.16 ± 0.10	$+1.4$
$[15, 19]$	-0.00 ± 0.07	0.07 ± 0.07	-0.8
$P_8'(B^0 \to K^{*0}\mu^+\mu^-)$[LHCb]	Standard Model	Experiment [110]	Pull
$[0.1, 0.98]$	0.02 ± 0.02	0.01 ± 0.24	$+0.0$
$[1.1, 2.5]$	0.04 ± 0.03	0.73 ± 0.32	-2.2
$[2.5, 4]$	0.05 ± 0.03	-0.07 ± 0.34	$+0.4$
$[4, 6]$	0.03 ± 0.02	-0.33 ± 0.25	$+1.4$
$[6, 8]$	0.02 ± 0.01	0.26 ± 0.20	-1.2
$[15, 19]$	-0.00 ± 0.03	-0.02 ± 0.14	$+0.2$
$F_L(B^+ \to K^{*+}\mu^+\mu^-)$[LHCb]	Standard Model	Experiment [69]	Pull
$[0.1, 0.98]$	0.23 ± 0.24	0.34 ± 0.12	-0.4
$[1.1, 2.5]$	0.68 ± 0.26	0.54 ± 0.19	$+0.5$
$[2.5, 4]$	0.77 ± 0.23	0.17 ± 0.24	$+1.8$
$[4, 6]$	0.71 ± 0.28	0.67 ± 0.14	$+0.1$
$[6, 8]$	0.63 ± 0.32	0.39 ± 0.21	$+0.6$
$[15, 19]$	0.34 ± 0.03	0.40 ± 0.13	-0.4
$P_1(B^+ \to K^{*+}\mu^+\mu^-)$[LHCb]	Standard Model	Experiment [69]	Pull
$[0.1, 0.98]$	0.03 ± 0.08	0.44 ± 0.41	-1.0
$[1.1, 2.5]$	-0.00 ± 0.05	1.60 ± 4.93	-0.3
$[2.5, 4]$	0.00 ± 0.06	-0.29 ± 1.45	$+0.2$
$[4, 6]$	0.02 ± 0.12	-1.24 ± 1.21	$+1.0$
$[6, 8]$	0.02 ± 0.13	-0.78 ± 0.70	$+1.1$
$[15, 19]$	-0.64 ± 0.06	-0.70 ± 0.44	$+0.1$
$P_2(B^+ \to K^{*+}\mu^+\mu^-)$[LHCb]	Standard Model	Experiment [69]	Pull
$[0.1, 0.98]$	0.12 ± 0.02	0.05 ± 0.12	$+0.6$
$[1.1, 2.5]$	0.44 ± 0.03	0.28 ± 0.45	$+0.4$
$[2.5, 4]$	0.23 ± 0.13	-0.03 ± 0.28	$+0.8$
$[4, 6]$	-0.19 ± 0.11	0.15 ± 0.21	-1.5
$[6, 8]$	-0.38 ± 0.07	0.06 ± 0.14	-2.9
$[15, 19]$	-0.36 ± 0.02	-0.34 ± 0.10	-0.2
$P_3(B^+ \to K^{*+}\mu^+\mu^-)$[LHCb]	Standard Model	Experiment [69]	Pull
$[0.1, 0.98]$	-0.00 ± 0.00	0.42 ± 0.22	-2.0
$[1.1, 2.5]$	0.00 ± 0.00	0.09 ± 1.01	-0.1
$[2.5, 4]$	0.00 ± 0.01	0.45 ± 0.65	-0.7
$[4, 6]$	0.00 ± 0.01	0.52 ± 0.83	-0.6
$[6, 8]$	0.00 ± 0.00	-0.17 ± 0.34	$+0.5$
$[15, 19]$	0.00 ± 0.02	0.07 ± 0.13	-0.5
$P_4'(B^+ \to K^{*+}\mu^+\mu^-)$[LHCb]	Standard Model	Experiment [69]	Pull
$[0.1, 0.98]$	-0.50 ± 0.16	0.18 ± 0.76	-0.8
$[1.1, 2.5]$	-0.07 ± 0.16	-1.16 ± 1.26	$+0.9$
$[2.5, 4]$	0.53 ± 0.21	1.62 ± 2.20	-0.5
$[4, 6]$	0.82 ± 0.15	1.58 ± 0.96	-0.8
$[6, 8]$	0.93 ± 0.11	0.86 ± 0.91	$+0.1$

$[15, 19]$	1.28 ± 0.02	0.78 ± 0.47	$+1.1$
$P_5'(B^+ \to K^{*+}\mu^+\mu^-)$[LHCb]	Standard Model	Experiment [69]	Pull
$[0.1, 0.98]$	0.67 ± 0.13	0.51 ± 0.32	$+0.5$
$[1.1, 2.5]$	0.19 ± 0.11	0.88 ± 0.72	-1.0
$[2.5, 4]$	-0.47 ± 0.12	-0.87 ± 1.68	$+0.2$
$[4, 6]$	-0.82 ± 0.08	-0.25 ± 0.41	-1.4
$[6, 8]$	-0.94 ± 0.08	-0.15 ± 0.41	-1.9
$[15, 19]$	-0.57 ± 0.05	-0.24 ± 0.17	-1.9
$P_6'(B^+ \to K^{*+}\mu^+\mu^-)$[LHCb]	Standard Model	Experiment [69]	Pull
$[0.1, 0.98]$	-0.06 ± 0.02	-0.02 ± 0.40	-0.1
$[1.1, 2.5]$	-0.07 ± 0.03	0.25 ± 1.32	-0.2
$[2.5, 4]$	-0.06 ± 0.03	-0.37 ± 3.91	$+0.1$
$[4, 6]$	-0.04 ± 0.02	-0.09 ± 0.41	$+0.1$
$[6, 8]$	-0.02 ± 0.01	-0.74 ± 0.40	$+1.8$
$[15, 19]$	-0.00 ± 0.07	-0.28 ± 0.19	$+1.4$
$P_8'(B^+ \to K^{*+}\mu^+\mu^-)$[LHCb]	Standard Model	Experiment [69]	Pull
$[0.1, 0.98]$	0.02 ± 0.02	-0.90 ± 1.02	$+1.0$
$[1.1, 2.5]$	0.04 ± 0.03	-0.24 ± 1.52	$+0.2$
$[2.5, 4]$	0.05 ± 0.03	-0.24 ± 15.80	$+0.0$
$[4, 6]$	0.03 ± 0.02	0.30 ± 0.97	-0.3
$[6, 8]$	0.02 ± 0.01	0.78 ± 0.78	-1.0
$[15, 19]$	-0.00 ± 0.03	0.22 ± 0.38	-0.6
$P_1(B_s \to \phi\mu^+\mu^-)$[LHCb]	Standard Model	Experiment [74]	Pull
$[0.1, 0.98]$	0.11 ± 0.08	-0.01 ± 0.19	$+0.6$
$[1.1, 4]$	0.01 ± 0.06	-0.22 ± 0.42	$+0.5$
$[4, 6]$	-0.17 ± 0.11	-1.09 ± 0.47	$+1.9$
$[6, 8]$	-0.21 ± 0.11	0.07 ± 0.43	-0.6
$[15, 18.9]$	-0.69 ± 0.03	-0.77 ± 0.14	$+0.6$
$P_4'(B_s \to \phi\mu^+\mu^-)$[LHCb]	Standard Model	Experiment [74]	Pull
$[0.1, 0.98]$	-0.45 ± 0.15	-0.98 ± 0.38	$+1.3$
$[1.1, 4]$	0.44 ± 0.15	0.49 ± 0.35	-0.1
$[4, 6]$	1.01 ± 0.08	0.97 ± 0.41	$+0.1$
$[6, 8]$	1.08 ± 0.06	0.73 ± 0.32	$+1.1$
$[15, 18.9]$	1.30 ± 0.01	0.87 ± 0.20	$+2.2$
$P_6'(B_s \to \phi\mu^+\mu^-)$[LHCb]	Standard Model	Experiment [74]	Pull
$[0.1, 0.98]$	-0.07 ± 0.02	-0.41 ± 0.16	$+2.1$
$[1.1, 4]$	-0.07 ± 0.02	-0.23 ± 0.17	$+0.9$
$[4, 6]$	-0.03 ± 0.01	0.38 ± 0.20	-2.1
$[6, 8]$	-0.02 ± 0.01	0.07 ± 0.17	-0.5
$[15, 18.9]$	-0.00 ± 0.07	0.01 ± 0.10	-0.1
$F_L(B_s \to \phi\mu^+\mu^-)$[LHCb]	Standard Model	Experiment [74]	Pull
$[0.1, 0.98]$	0.28 ± 0.09	0.25 ± 0.05	$+0.3$
$[1.1, 4]$	0.77 ± 0.05	0.72 ± 0.06	$+0.6$
$[4, 6]$	0.71 ± 0.05	0.70 ± 0.05	$+0.1$
$[6, 8]$	0.60 ± 0.06	0.62 ± 0.05	-0.3
$[15, 18.9]$	0.36 ± 0.02	0.36 ± 0.04	-0.1
$B^0 \to K^{*0}e^+e^-$[LHCb]	Standard Model	Experiment [322]	Pull
$F_L[0.008, 0.257]$	0.03 ± 0.06	0.04 ± 0.03	-0.2
$P_1[0.008, 0.257]$	0.03 ± 0.08	0.11 ± 0.10	-0.6

$P_2[0.008, 0.257]$	0.01 ± 0.00	0.03 ± 0.04	-0.5
R_{K^+}[LHCb]†	Standard Model	Experiment [63]	Pull
$[1.1, 6.0]$	1.00 ± 0.01	0.85 ± 0.04	$+3.4$
R_{K^0}[LHCb]†	Standard Model	Experiment [52]	Pull
$[1.1, 6.0]$	1.00 ± 0.01	0.66 ± 0.20	$+1.7$
R_K[Belle]†	Standard Model	Experiment [323]	Pull
$[1.0, 6.0]$	1.00 ± 0.01	1.03 ± 0.28	-0.1
$[14.18, 22.90]$	1.00 ± 0.01	1.16 ± 0.30	-0.6
$R_{K^{*0}}$[LHCb]†	Standard Model	Experiment [324]	Pull
$[0.045, 1.1]$	0.91 ± 0.02	0.66 ± 0.11	$+2.2$
$[1.1, 6.0]$	1.00 ± 0.01	0.69 ± 0.12	$+2.6$
$R_{K^{*+}}$[LHCb]†	Standard Model	Experiment [52]	Pull
$[0.045, 6.0]$	0.93 ± 0.05	0.70 ± 0.18	$+1.2$
R_{K^*}[Belle]†	Standard Model	Experiment [325]	Pull
$[0.045, 1.1]$	0.92 ± 0.02	0.52 ± 0.36	$+1.1$
$[1.1, 6.0]$	1.00 ± 0.01	0.96 ± 0.46	$+0.1$
$[15, 19]$	1.00 ± 0.00	1.18 ± 0.53	-0.5
$P_4'(B \to K^* e^+ e^-)$[Belle]	Standard Model	Experiment [50]	Pull
$[0.1, 4]$	-0.09 ± 0.15	-0.68 ± 0.93	$+0.6$
$[4, 8]$	0.88 ± 0.13	1.04 ± 0.48	-0.3
$[14.18, 19]$	1.26 ± 0.03	0.30 ± 0.82	$+1.2$
$P_4'(B \to K^* \mu^+ \mu^-)$[Belle]	Standard Model	Experiment [50]	Pull
$[0.1, 4]$	-0.06 ± 0.16	0.76 ± 1.03	-0.8
$[4, 8]$	0.88 ± 0.13	0.14 ± 0.66	$+1.1$
$[14.18, 19]$	1.26 ± 0.03	0.20 ± 0.79	$+1.3$
$P_5'(B \to K^* e^+ e^-)$[Belle]	Standard Model	Experiment [50]	Pull
$[0.1, 4]$	0.18 ± 0.09	0.51 ± 0.47	-0.7
$[4, 8]$	-0.88 ± 0.07	-0.52 ± 0.28	-1.3
$[14.18, 19]$	-0.60 ± 0.05	-0.91 ± 0.36	$+0.9$
$P_5'(B \to K^* \mu^+ \mu^-)$[Belle]	Standard Model	Experiment [50]	Pull
$[0.1, 4]$	0.17 ± 0.10	0.42 ± 0.41	-0.6
$[4, 8]$	-0.89 ± 0.07	-0.03 ± 0.32	-2.7
$[14.18, 19]$	-0.60 ± 0.05	-0.13 ± 0.39	-1.3
$Q_4(B \to K^*)$[Belle]‡	Standard Model	Experiment [50]	Pull
$[0.1, 4]$	0.03 ± 0.01	1.45 ± 1.39	-1.0
$[4, 8]$	0.00 ± 0.01	-0.90 ± 0.80	$+1.1$
$[14.18, 19]$	0.00 ± 0.01	-0.08 ± 1.14	$+0.1$
$Q_5(B \to K^*)$[Belle]‡	Standard Model	Experiment [50]	Pull
$[0.1, 4]$	-0.02 ± 0.01	-0.10 ± 0.62	$+0.1$
$[4, 8]$	-0.00 ± 0.01	0.50 ± 0.42	-1.2
$[14.18, 19]$	-0.00 ± 0.01	0.78 ± 0.51	-1.5
$10^7 \times BR(B^+ \to K^+ \mu^+ \mu^-)$[Belle]	Standard Model	Experiment [323]	Pull
$[1, 6]$	1.82 ± 0.58	2.30 ± 0.40	-0.7

$[14.18, 22.9]$	1.23 ± 0.17	1.34 ± 0.23	-0.4
$10^7 \times BR(B^0 \to K^0\mu^+\mu^-)$[Belle]	Standard Model	Experiment [323]	Pull
$[1, 6]$	1.69 ± 0.54	0.62 ± 0.38	$+1.6$
$[14.18, 22.9]$	1.14 ± 0.15	0.98 ± 0.40	$+0.4$
$F_L(B^0 \to K^{*0}\mu^+\mu^-)$[ATLAS]	Standard Model	Experiment [326]	Pull
$[0.04, 2]$	0.36 ± 0.30	0.44 ± 0.11	-0.3
$[2, 4]$	0.76 ± 0.23	0.64 ± 0.12	$+0.5$
$[4, 6]$	0.71 ± 0.28	0.42 ± 0.18	$+0.9$
$P_1(B^0 \to K^{*0}\mu^+\mu^-)$[ATLAS]	Standard Model	Experiment [326]	Pull
$[0.04, 2]$	0.02 ± 0.07	-0.05 ± 0.31	$+0.2$
$[2, 4]$	-0.00 ± 0.05	-0.78 ± 0.61	$+1.3$
$[4, 6]$	0.02 ± 0.12	0.14 ± 0.50	-0.2
$P_4'(B^0 \to K^{*0}\mu^+\mu^-)$[ATLAS]	Standard Model	Experiment [326]	Pull
$[0.04, 2]$	-0.35 ± 0.14	-0.62 ± 0.89	$+0.3$
$[2, 4]$	0.43 ± 0.21	1.52 ± 0.75	-1.4
$[4, 6]$	0.82 ± 0.15	-1.28 ± 0.75	$+2.7$
$P_5'(B^0 \to K^{*0}\mu^+\mu^-)$[ATLAS]	Standard Model	Experiment [326]	Pull
$[0.04, 2]$	0.50 ± 0.10	0.67 ± 0.31	-0.5
$[2, 4]$	-0.36 ± 0.12	-0.33 ± 0.34	-0.1
$[4, 6]$	-0.82 ± 0.08	0.26 ± 0.39	-2.7
$P_6'(B^0 \to K^{*0}\mu^+\mu^-)$[ATLAS]	Standard Model	Experiment [326]	Pull
$[0.04, 2]$	-0.06 ± 0.02	-0.18 ± 0.21	$+0.6$
$[2, 4]$	-0.06 ± 0.03	0.31 ± 0.34	-1.1
$[4, 6]$	-0.04 ± 0.02	0.06 ± 0.30	-0.3
$P_8'(B^0 \to K^{*0}\mu^+\mu^-)$[ATLAS]	Standard Model	Experiment [326]	Pull
$[0.04, 2]$	0.03 ± 0.02	0.58 ± 1.03	-0.5
$[2, 4]$	0.05 ± 0.03	-2.14 ± 1.13	$+1.9$
$[4, 6]$	0.03 ± 0.02	0.48 ± 0.86	-0.5
$P_1(B^0 \to K^{*0}\mu^+\mu^-)$[CMS 8 TeV]	Standard Model	Experiment [327]	Pull
$[1, 2]$	0.00 ± 0.06	0.12 ± 0.48	-0.2
$[2, 4.3]$	0.00 ± 0.05	-0.69 ± 0.62	$+1.1$
$[4.3, 6]$	0.03 ± 0.12	0.53 ± 0.38	-1.3
$[6, 8.68]$	0.02 ± 0.14	-0.47 ± 0.31	$+1.4$
$[16, 19]$	-0.70 ± 0.05	-0.53 ± 0.25	-0.7
$P_5'(B^0 \to K^{*0}\mu^+\mu^-)$[CMS 8 TeV]	Standard Model	Experiment [327]	Pull
$[1, 2]$	0.33 ± 0.11	0.10 ± 0.33	$+0.7$
$[2, 4.3]$	-0.41 ± 0.12	-0.57 ± 0.38	$+0.4$
$[4.3, 6]$	-0.84 ± 0.08	-0.96 ± 0.33	$+0.4$
$[6, 8.68]$	-0.95 ± 0.08	-0.64 ± 0.23	-1.3
$[16, 19]$	-0.53 ± 0.04	-0.56 ± 0.14	$+0.2$
$F_L(B^0 \to K^{*0}\mu^+\mu^-)$[CMS 8 TeV]	Standard Model	Experiment [328]	Pull
$[1, 2]$	0.63 ± 0.28	0.64 ± 0.12	-0.0
$[2, 4.3]$	0.76 ± 0.23	0.80 ± 0.10	-0.2
$[4.3, 6]$	0.71 ± 0.28	0.62 ± 0.12	$+0.3$
$[6, 8.68]$	0.62 ± 0.32	0.50 ± 0.08	$+0.3$
$[16, 19]$	0.34 ± 0.03	0.38 ± 0.07	-0.6

$A_{FB}(B^0 \to K^{*0}\mu^+\mu^-)$[CMS 8 TeV]	Standard Model	Experiment [328]	Pull
$[1, 2]$	-0.20 ± 0.18	-0.27 ± 0.41	$+0.3$
$[2, 4.3]$	-0.08 ± 0.08	-0.12 ± 0.18	$+0.2$
$[4.3, 6]$	0.09 ± 0.11	0.01 ± 0.15	$+0.4$
$[6, 8.68]$	0.22 ± 0.21	0.03 ± 0.10	$+0.8$
$[16, 19]$	0.34 ± 0.03	0.35 ± 0.07	-0.2
$10^7 \times BR(B^0 \to K^{*0}\mu^+\mu^-)$[CMS 8 TeV]	Standard Model	Experiment [328]	Pull
$[1, 2]$	0.42 ± 0.26	0.46 ± 0.08	-0.1
$[2, 4.3]$	0.89 ± 0.61	0.76 ± 0.12	$+0.2$
$[4.3, 6]$	0.78 ± 0.58	0.58 ± 0.10	$+0.4$
$[6, 8.68]$	1.57 ± 1.25	1.26 ± 0.13	$+0.2$
$[16, 19]$	1.73 ± 0.14	1.26 ± 0.13	$+2.5$
$F_H(B^+ \to K^+\mu^+\mu^-)$[CMS 8 TeV]	Standard Model	Experiment [329]	Pull
$[1, 2]$	0.05 ± 0.00	0.21 ± 0.49	-0.4
$[2, 4.3]$	0.02 ± 0.00	0.85 ± 0.37	-2.4
$[4.3, 8.68]$	0.01 ± 0.00	0.01 ± 0.04	$+0.0$
$[16, 18]$	0.01 ± 0.00	0.07 ± 0.10	-0.6
$[18, 22]$	0.01 ± 0.00	0.10 ± 0.13	-0.7
$A_{FB}(B^+ \to K^+\mu^+\mu^-)$[CMS 8 TeV]	Standard Model	Experiment [329]	Pull
$[1, 2]$	0 ± 0.00	0.08 ± 0.23	-0.4
$[2, 4.3]$	0 ± 0.00	-0.04 ± 0.14	$+0.3$
$[4.3, 8.68]$	0 ± 0.00	0.00 ± 0.04	$+0.0$
$[16, 18]$	0 ± 0.00	0.04 ± 0.06	-0.8
$[18, 22]$	0 ± 0.00	0.05 ± 0.05	-1.1
$F_L(B^+ \to K^{*+}\mu^+\mu^-)$[CMS 8 TeV]	Standard Model	Experiment [70]	Pull
$[1, 8.68]$	0.67 ± 0.29	0.60 ± 0.34	$+0.2$
$[14.18, 19]$	0.35 ± 0.04	0.55 ± 0.14	-1.7
$A_{FB}(B^+ \to K^{*+}\mu^+\mu^-)$[CMS 8 TeV]	Standard Model	Experiment [70]	Pull
$[1, 8.68]$	0.08 ± 0.09	-0.14 ± 0.39	$+0.6$
$[14.18, 19]$	0.37 ± 0.03	0.33 ± 0.12	$+0.3$
$F_L(B^0 \to K^{*0}\mu^+\mu^-)$[CMS 7 TeV]	Standard Model	Experiment [330]	Pull
$[1, 2]$	0.63 ± 0.28	0.60 ± 0.34	$+0.1$
$[2, 4.3]$	0.76 ± 0.23	0.65 ± 0.17	$+0.4$
$[4.3, 8.68]$	0.65 ± 0.31	0.81 ± 0.14	-0.5
$[16, 19]$	0.34 ± 0.03	0.44 ± 0.08	-1.3
$A_{FB}(B^0 \to K^{*0}\mu^+\mu^-)$[CMS 7 TeV]	Standard Model	Experiment [330]	Pull
$[1, 2]$	-0.20 ± 0.18	-0.29 ± 0.41	$+0.2$
$[2, 4.3]$	-0.08 ± 0.08	-0.07 ± 0.20	-0.0
$[4.3, 8.68]$	0.18 ± 0.18	-0.01 ± 0.11	$+0.9$
$[16, 19]$	0.34 ± 0.03	0.41 ± 0.06	-1.1
$10^7 \times BR(B^0 \to K^{*0}\mu^+\mu^-)$[CMS 7 TeV]	Standard Model	Experiment [330]	Pull
$[1, 2]$	0.42 ± 0.26	0.48 ± 0.15	-0.2
$[2, 4.3]$	0.89 ± 0.61	0.87 ± 0.18	$+0.0$
$[4.3, 8.68]$	2.35 ± 1.82	1.62 ± 0.35	$+0.4$
$[16, 19]$	1.73 ± 0.14	1.56 ± 0.23	$+0.6$
$10^5 \times BR(B^0 \to K^{*0}\gamma)$[PDG]†	Standard Model	Experiment [312]	Pull

	4.57 ± 5.27	4.18 ± 0.25	$+0.1$
$10^5 \times BR(B^+ \to K^{*+}\gamma)$[PDG]†	Standard Model	Experiment [312]	Pull
	4.61 ± 5.49	3.92 ± 0.22	$+0.1$
$10^5 \times BR(B_s \to \phi\gamma)$[PDG]†	Standard Model	Experiment [312]	Pull
	4.86 ± 1.35	3.40 ± 0.40	$+1.0$
$10^4 \times BR(B \to X_s\gamma)$[HFLAV]†	Standard Model [209]	Experiment [100]	Pull
	3.32 ± 0.15	3.40 ± 0.17	-0.4
$S(B \to K^*\gamma)$[BaBar+Belle]†	Standard Model [25]	Experiment [100]	Pull
	-0.03 ± 0.01	-0.16 ± 0.22	$+0.6$
$AI(B \to K^*\gamma)$[BaBar+Belle]†	Standard Model [25]	Experiment [100]	Pull
	0.041 ± 0.025	0.063 ± 0.017	-0.7
$10^9 \times BR(B_s \to \mu^+\mu^-)$[LHCb+CMS+ATLAS]†	Standard Model [48]	Experiment [68]	Pull
	3.64 ± 0.14	2.85 ± 0.34	$+2.2$
$10^6 \times BR(B \to X_s\mu^+\mu^-)$[BaBar]†	Standard Model [331]	Experiment [332]	Pull
$[1, 6]$	1.73 ± 0.13	0.66 ± 0.88	$+1.2$
$10^6 \times BR(B \to X_s e^+e^-)$[BaBar]†	Standard Model [331]	Experiment [332]	Pull
$[1, 6]$	1.78 ± 0.13	1.93 ± 0.55	-0.3

Appendix C

The 7th massive relation

In this Appendix we will provide the necessary steps to determine the last of the relations described in Chapter 2. This relation vanishes in the massless limit and is particularly lengthy. For both reasons, specially the latter, is of limited practical use. Therefore we will present here the steps to derive this relation but will not write it out explicitly. The derivation is based on five steps:

Step 1: Our starting point will be a particular combination of the 2D vectors that will allow us to introduce the structure of the observable M_1 for the first time.

$$\begin{aligned} & (n_\parallel^\dagger n_S + n_\parallel^\dagger n'_S) \times (n_\parallel^\dagger n_S - n_\parallel^\dagger n'_S) \\ + \quad & (n_\perp^\dagger n_S + n_\perp^\dagger n'_S) \times (n_\perp^\dagger n'_S - n_\perp^\dagger n_S) = +4(A_\parallel^{L*} A_\parallel^R + A_\perp^{L*} A_\perp^R) A_0'^L A_0'^{R*} \end{aligned} \tag{C.1}$$

In order to avoid repeating the coefficient $4m_\ell^2/q^2$ of M_1, we introduce a reduced version, that we will call m_1 defined by

$$m_1 = \frac{q^2}{4m_\ell^2 \beta_\ell^2}(\beta_\ell^2 J_{1s} - (2+\beta_\ell^2) J_{2s}) = \mathrm{Re}(A_\perp^L A_\perp^{R*} + A_\parallel^L A_\parallel^{R*})\,. \tag{C.2}$$

We will use the freedom given by the symmetry (see section 2.2) to choose the phase such that $A_0'^L$ has only a real component. Then we solve Eq. (C.1) for m_1 and its imaginary counterpart:

$$m_1 = \frac{-b\,\mathrm{Im}[A_0'^R] + a\,\mathrm{Re}[A_0'^R]}{4|A_0'^R|^2 \mathrm{Re}[A_0'^L]} \tag{C.3}$$

$$\mathrm{Im}[A_\parallel^{L*} A_\parallel^R + A_\perp^{L*} A_\perp^R] = \frac{a\,\mathrm{Im}[A_0'^R] + b\,\mathrm{Re}[A_0'^R]}{4|A_0'^R|^2 \mathrm{Re}[A_0'^L]} \tag{C.4}$$

where

$$\begin{aligned} a = \quad & + \quad \frac{1}{6\beta^4}\left(\frac{4\Gamma'}{3}\right)^2 \left(-\beta^2[(S_{S3}^i)^2 + (S_{S3}^r)^2 + (S_{S4}^i)^2 + (S_{S4}^r)^2] \right. \\ & + \quad \left. 4[(S_{S2}^i)^2 + (S_{S2}^r)^2 + (S_{S5}^i)^2 + (S_{S5}^r)^2]\right) \\ b = \quad & + \quad \frac{2}{3\beta^3}\left(\frac{4\Gamma'}{3}\right)^2 \left(S_{S2}^r S_{S4}^i - S_{S2}^i S_{S4}^r - S_{S3}^r S_{S5}^i + S_{S3}^i S_{S5}^r\right) \end{aligned} \tag{C.5}$$

Step 2: Using $n_0 = e n_S + f n'_S$ and multiplying this equation by $\sigma.n_S$, $\sigma.n'_S$ and $\sigma.n_0$, where $\sigma = ((0,1),(1,0))$ one can show that all terms $A_0^{(\prime)L} A_0^{(\prime)R}$ can be written in terms of $A_0'^L A_0'^{R*}$.

$$\begin{aligned} A_0^L A_0'^{R*} + A_0'^L A_0^{R*} &= 2e A_0'^L A_0'^{R*} \\ -A_0^L A_0'^{R*} + A_0'^L A_0^{R*} &= -2f A_0'^L A_0'^{R*} \\ A_0^L A_0^{R*} &= (e^2 - f^2) A_0'^L A_0'^{R*} \end{aligned} \tag{C.6}$$

where

$$\begin{aligned} e &= \frac{(n_\parallel^\dagger n'_S)(n_\perp^\dagger n_0) - (n_\parallel^\dagger n_0)(n_\perp^\dagger n'_S)}{(n_\parallel^\dagger n'_S)(n_\perp^\dagger n_S) - (n_\parallel^\dagger n_S)(n_\perp^\dagger n'_S)} \\ f &= \frac{(n_\parallel^\dagger n_S)(n_\perp^\dagger n_0) - (n_\parallel^\dagger n_0)(n_\perp^\dagger n_S)}{(n_\parallel^\dagger n_S)(n_\perp^\dagger n'_S) - (n_\parallel^\dagger n'_S)(n_\perp^\dagger n_S)} \end{aligned} \tag{C.7}$$

Both coefficients e and f can be trivially rewritten in terms of P- and S-wave observables, as in Eq. (C.5).

Step 3: We define a set of reduced observables related to the corresponding remaining massive observables:

$$\begin{aligned} m_2 &= |A_t|^2 + 2\mathrm{Re}(A_0^L A_0^{R*}) \\ m'_3 &= |A'_t|^2 + 2\mathrm{Re}(A_0'^L A_0'^{R*}) \\ m'_4 &= \mathrm{Re}(A'_t A_t^*) + \mathrm{Re}(A_0'^L A_0^{R*} + A_0^L A_0'^{R*}) \\ m'_5 &= \mathrm{Im}(A'_t A_t^*) + \mathrm{Im}(A_0'^L A_0^{R*} + A_0^L A_0'^{R*}) \end{aligned} \tag{C.8}$$

We can combine them in one single equation cancelling the dependence on $A_t^{(\prime)}$:

$$\begin{aligned} (m_2 - 2\mathrm{Re}[A_0^L A_0^{R*}])(m'_3 - 2\mathrm{Re}[A_0'^L A_0'^{R*}]) = &+ (m'_4 - \mathrm{Re}[A_0^L A_0'^{R*} + A_0'^L A_0^{R*}])^2 \\ &+ (m'_5 - \mathrm{Im}[A_0^L A_0'^{R*} + A_0'^L A_0^{R*}])^2 \end{aligned} \tag{C.9}$$

and using Eqs.(C.6) we can rewrite this equation in terms of only $A_0'^L A_0'^{R*}$:

$$\begin{aligned} (m_2 - 2\mathrm{Re}[(e^2 - f^2) A_0'^L A_0'^{R*}])(m'_3 - 2\mathrm{Re}[A_0'^L A_0'^{R*}]) = &+ (m'_4 - \mathrm{Re}[2e A_0'^L A_0'^{R*}])^2 \\ &+ (m'_5 - \mathrm{Im}[2e A_0'^L A_0'^{R*}])^2 , \end{aligned} \tag{C.10}$$

giving the desired relation but involving $A_0'^L$ and $A_0'^R$ amplitudes that still need to be expressed in terms of observables.

Step 4: Using the decomposition $n_\perp = g n_S + h n'_S$ and after determining g and h by multiplying by $n_\perp$ and $n_\parallel$, we find the following relation:

$$(h^{*2} - g^{*2}) n_S'^\dagger n_S = h^* n_\perp^\dagger n_S - g^* n_\perp^\dagger n'_S , \tag{C.11}$$

where

$$\begin{aligned} g &= \frac{|n_\perp|^2 (n_\parallel^\dagger n'_S) - (n_\parallel^\dagger n_\perp)(n_\perp^\dagger n'_S)}{(n_\parallel^\dagger n'_S)(n_\perp^\dagger n_S) - (n_\parallel^\dagger n_S)(n_\perp^\dagger n'_S)} , \\ h &= \frac{|n_\perp|^2 (n_\parallel^\dagger n_S) - (n_\parallel^\dagger n_\perp)(n_\perp^\dagger n_S)}{(n_\parallel^\dagger n_S)(n_\perp^\dagger n'_S) - (n_\parallel^\dagger n'_S)(n_\perp^\dagger n_S)} . \end{aligned} \tag{C.12}$$

Then combining the previous equation with the observable F_S, one can determine $|A_0'^L|^2$ and $|A_0'^R|^2$ (remember that $A_0^{L\prime}$ is taken to be real using the symmetry properties) by solving the system:

$$|A_0'^L|^2 - |A_0'^R|^2 = \frac{h^* n_\perp^\dagger n_S - g^* n_\perp^\dagger n'_S}{h^{*2} - g^{*2}} = \Delta , \tag{C.13}$$

$$|A_0'^L|^2 + |A_0'^R|^2 \equiv F_S \Gamma' . \tag{C.14}$$

Now we have all the necessary ingredients to arrive at the relation. If we define

$$\begin{aligned} x &= \mathrm{Re}[A_0'^L]\mathrm{Re}[A_0'^R] , \\ y &= \mathrm{Re}[A_0'^L]\mathrm{Im}[A_0'^R] , \end{aligned} \tag{C.15}$$

we have two equations in terms of x and y (using Eq. (C.3) and Eqs. (C.13) and (C.14)):

$$\begin{aligned} m_1 &= \frac{-by + ax}{4(x^2+y^2)} \\ x^2 + y^2 &= \frac{1}{4}\left((F_S\Gamma')^2 - \Delta^2\right) \end{aligned} \tag{C.16}$$

These two equations can be solved to determine x and y in terms of observables.

Step 5: Finally, the last step consists of trivially expressing $A_0'^L$, $A_0'^R$ in Eq. (C.10) in terms of x and y (all other quantities like the m_i and the coefficients e and f are already direct functions of observables). Then after solving the system for x and y using Eq. (C.16) insert the result in Eq. (C.10) to get a final lengthly expression written entirely in terms of observables.

Notice that in order to relate the reduced observables to the measured massive observables $M_{1,2,3',4',5'}$ one needs to multiply the previous relations involving the m_i's on both sides by factors of $4m_\ell^2/q^2$. For this reason in particular Eq. (C.10) vanishes exactly in the massless limit.

Appendix D

A hitchhiker's guide to the symmetry relations in $B \to D^* \ell \nu$

This appendix details the steps needed to derive the relations among observables of the transition $B \to D^* \ell \nu$ discussed in Chapter 3, as well as the effect of binning the polarisation fraction $\tilde{F}_T^{D^*}$ under different relevant NP scenarios.

D.1 Massive relations among angular coefficients of $B \to D^* \ell \nu$

Below we describe the methodology followed and the full expressions of the dependencies among the angular coefficients in the massive case with no tensor contributions. It is useful to define the following four combinations in order to obtain compact expressions:

$$R_{s,d} = \mathrm{Re}(H_+) \pm \mathrm{Re}(H_-)\,, \quad I_{s,d} = \mathrm{Im}(H_+) \pm \mathrm{Im}(H_-) \tag{D.1}$$

One can solve the system of equations in terms of the variables defined above and find a twofold solution:

$$R_s = \frac{1}{H_0}\frac{I_4 q^2}{q^2 - m_\ell^2} \tag{D.2}$$

$$I_d = \frac{1}{H_0}\frac{I_8 q^2}{q^2 - m_\ell^2} \tag{D.3}$$

$$R_d = (-1)^n \frac{q^2\left(I_4 I_8 q^2 + H_0^2 I_9 (q^2 - m_\ell^2)\right)}{\sqrt{H_0^2 (q^2 - m_\ell^2)^2}\sqrt{-I_4^2 q^4 + H_0^2 (m_\ell^2 - q^2)\left[(|H_-|^2 + |H_+|^2)(m_\ell^2 - q^2) + I_3 q^2)\right]}} \tag{D.4}$$

$$I_s = (-1)^n \frac{\sqrt{-I_4^2 q^4 + H_0^2 (m_\ell^2 - q^2)\left[(|H_-|^2 + |H_+|^2)(m_\ell^2 - q^2) + I_3 q^2)\right]}}{\sqrt{H_0^2 (q^2 - m_\ell^2)^2}} \tag{D.5}$$

with $n = 0, 1$. However, this sign ambiguity product of the twofold nature of the solution can be fixed, since physical combinations prevent interference terms that could be problematic. This set of solutions can be used to determine the square of the four amplitudes once H_0 is fixed to be real and positive through the symmetry of the angular distribution. One can also rewrite the real and imaginary parts of H_t in terms of the variables in Eq. (D.1) and H_0:

$$\mathrm{Re}(H_t) = -\frac{q^2\left[I_7\, I_s + I_5 R_d - 2H_0 (I_s^2 + R_d^2)\right]}{2m_\ell^2\,(I_d I_s + R_s R_d)} \tag{D.6}$$

$$\mathrm{Im}(H_t) = \frac{q^2\left[-I_5 I_d + I_7 R_s + 2H_0 (I_d R_d - R_s I_s)\right]}{2m_\ell^2\,(I_d I_s + R_s R_d)} \tag{D.7}$$

With these definitions, one can find the whole set of dependencies among angular coefficients. Besides the trivial dependency Eq. (3.57), there are four more relations which are obtained by taking combinations of the modulus of H_+, H_- and $\mathrm{Re}(H_t)$, $\mathrm{Im}(H_t)$.

The first non-trivial relation can be derived from the sum $|H_+|^2 + |H_-|^2$:

$$\begin{aligned} 0 &= \frac{m_\ell^2 - q^2}{2a}\Big\{ -4I_{1s}^2 I_{2c}(m_\ell^2 - q^2)^2 + 4I_{1s}(I_4^2 + I_8^2)(m_\ell^2 - q^2)(m_\ell^2 + 3q^2) \\ &+ \left[-2I_3 I_4^2 + 2I_3 I_8^2 - 4I_4 I_8 I_9 + I_{2c}(I_3^2 + I_9^2)\right](m_\ell^2 + 3q^2)^2 \Big\} \end{aligned} \tag{D.8}$$

where

$$a = (m_\ell^2 - q^2)^2(m_\ell^2 + 3q^2)\left[2I_{1s}I_{2c}(m_\ell^2 - q^2) + (I_{2c}I_3 - 2I_4^2)(m_\ell^2 + 3q^2)\right] \tag{D.9}$$

From $|H_+|^2|H_-|^2$ one can obtain the second dependency:

$$0 = -I_3^2 - I_9^2 + \left(1 - \frac{m_\ell^2}{q^2}\right)^2 \left[\left(\frac{2I_{1s}}{3 + m_\ell^2/q^2}\right)^2 - \frac{I_{6s}^2}{4}\right] \tag{D.10}$$

The third one follows from $[\mathrm{Re}(H_t)]^2$:

$$\begin{aligned} 0 &= \frac{8q^4}{a}\left[2I_{1s}I_{2c}I_7(m_\ell^2 - q^2) + (I_{2c}I_3I_7 - 2I_4^2I_7 + 2I_4I_5I_8 - I_{2c}I_5I_9)(m_\ell^2 + 3q^2)\right]^2 \\ &- \left[\frac{I_{6s}I_{6c}}{2} - \frac{4q^4}{a}\Big(4I_{1s}^2I_{2c}^2(m_\ell^2 - q^2)^2 + 4I_{1s}I_{2c}(I_{2c}I_3 - 2I_4^2)(m_\ell^2 - q^2)(m_\ell^2 + 3q^2) \right. \\ &+ \left.(4I_4^2(I_4^2 + I_8^2) - 4I_{2c}I_4(I_3I_4 + I_8I_9) + I_{2c}^2(I_3^2 + I_9^2))(m_\ell^2 + 3q^2)^2\Big)\right]^2 \end{aligned} \tag{D.11}$$

with a defined in Eq. (D.9).

Finally, the last dependency is related to $[\mathrm{Im}(H_t)]^2$:

$$\begin{aligned} 0 &= 256I_{6s}^2(I_4I_7 - I_5I_8)^2(m_\ell^2 - q^2)^4 q^{12} \\ &\quad \times\left[I_{6c}^2(m_\ell^2 - q^2)^2 + 8I_{1c}I_{2c}m_\ell^2(-m_\ell^2 + q^2) + 8I_{2c}^2m_\ell^2(m_\ell^2 + q^2)\right] \\ &+\left[64b - 64(I_4I_7 - I_5I_8)^2(m_\ell^2 - q^2)^2q^8 + I_{6s}^2(m_\ell^2 - q^2)^2q^4(I_{6c}^2(m_\ell^2 - q^2)^2\right. \\ &\quad \left.+8I_{1c}I_{2c}m_\ell^2(-m_\ell^2 + q^2) + 8I_{2c}^2m_\ell^2(m_\ell^2 + q^2))\right]^2 \end{aligned} \tag{D.12}$$

with

$$b = \frac{2q^{12}(2I_{1s}I_{2c}I_4(m_\ell^2 - q^2) + (-2I_4(I_4^2 + I_8^2) + I_{2c}(I_3I_4 + I_8I_9))(m_\ell^2 + 3q^2))^2}{(m_\ell^2 + 3q^2)(2I_{1s}I_{2c}(m_\ell^2 - q^2) + (I_{2c}I_3 - 2I_4^2)(m_\ell^2 + 3q^2))} \tag{D.13}$$

As a final comment, notice that these dependencies among angular coefficients yield Eqs. (3.58)-(3.61) when one considers only real Wilson coefficients, so that all imaginary contributions and $I_{7,8,9}$ can be neglected.

D.2 Comparison of binned expressions for $\tilde{F}_T^{D^*}$ in benchmark NP scenarios

Following the setup of Section 3.3.5, we illustrate in Fig. D.1 to Fig. D.6 the errors induced on the binning by the approximation Eq. (3.78) on relations derived using the amplitude symmetries under various assumptions on the NP scenario in the τ lepton case. We follow same convention as in Fig. 3.1.

We provide the relative errors for selected scenarios in Tables D.1 and D.2.

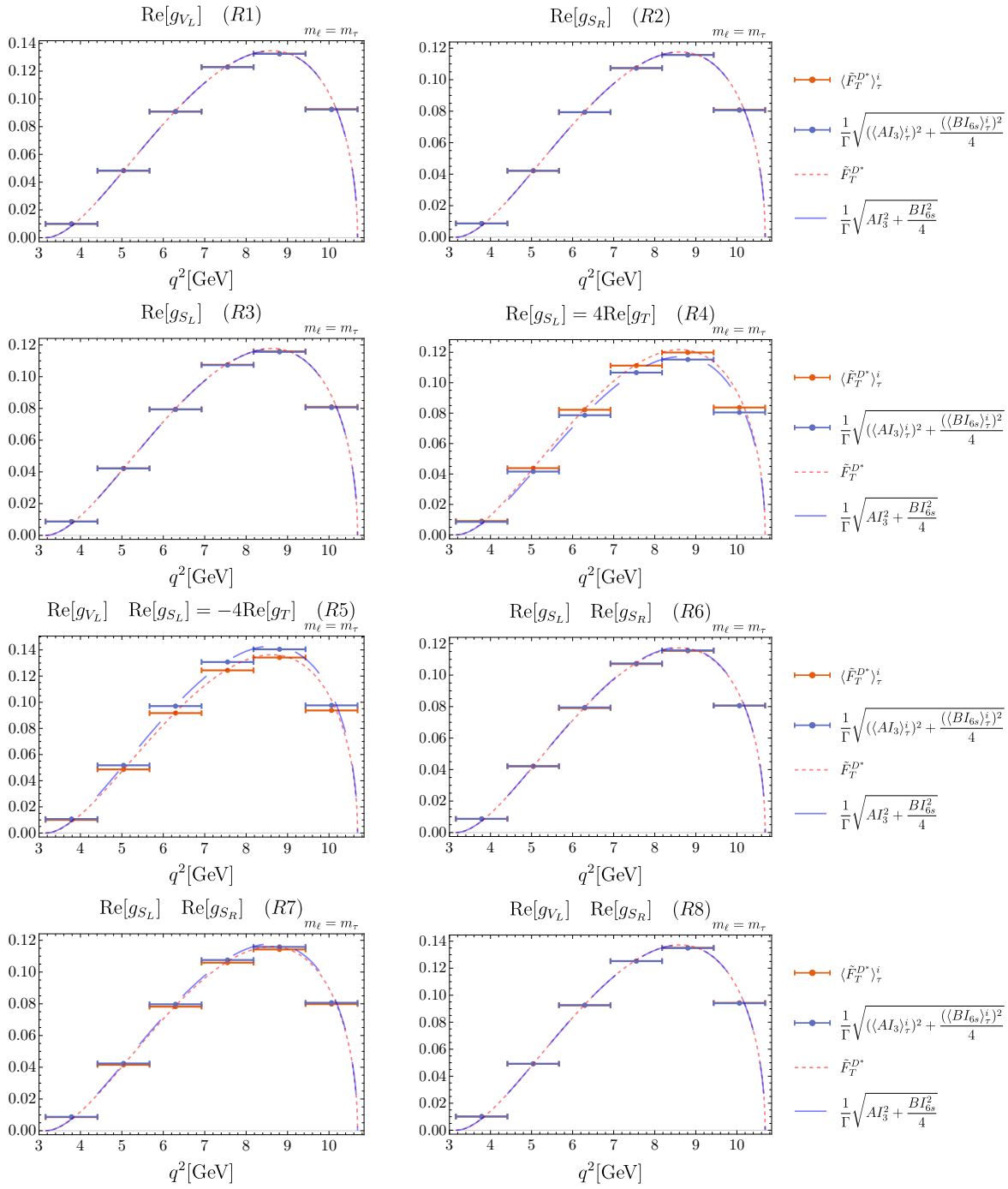

Figure D.1: Study of binning effects for Eq. (3.81) for benchmark NP scenarios with real contributions.

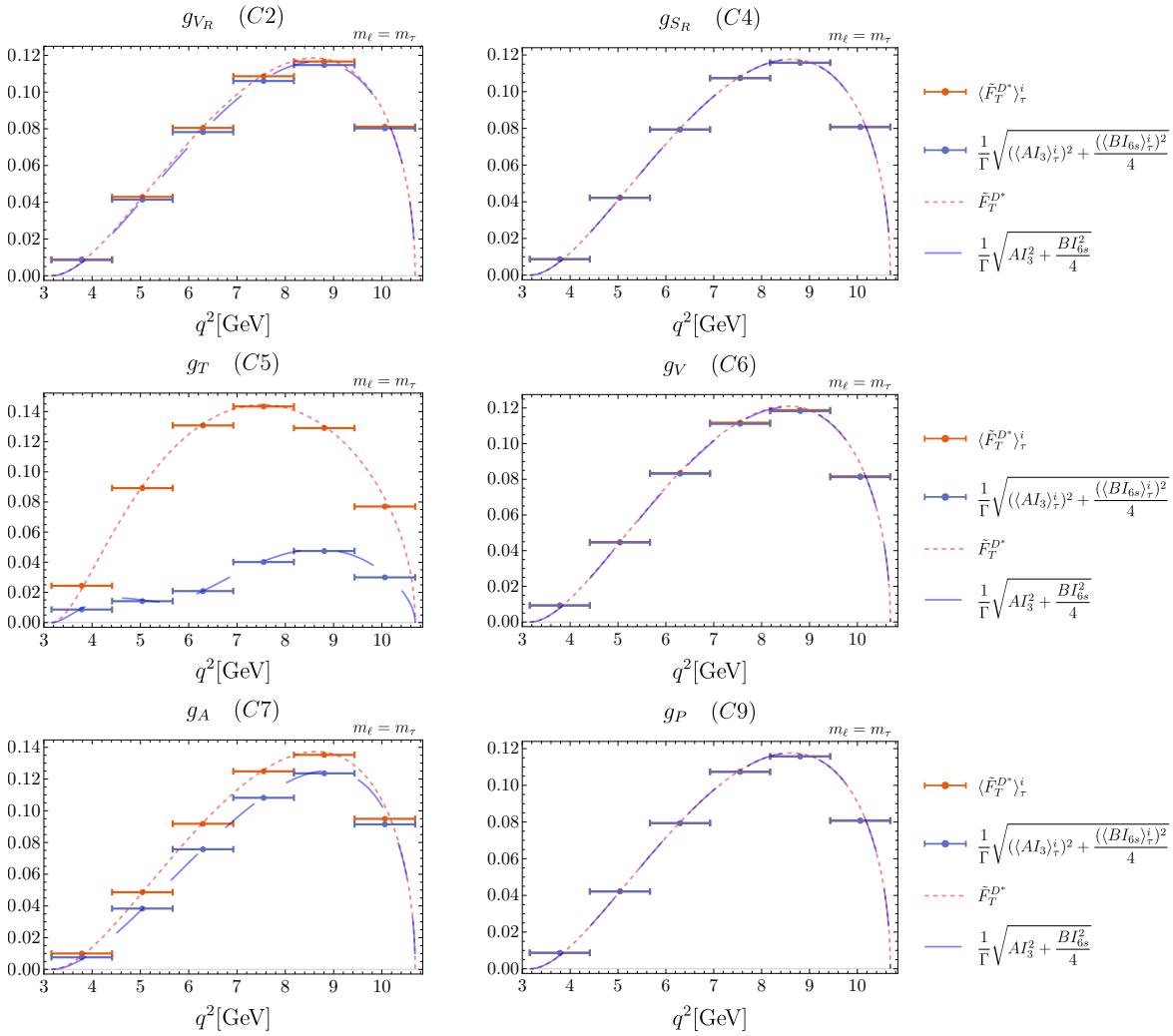

Figure D.2: Study of binning effects for Eq. (3.81) for benchmark NP scenarios with complex contributions.

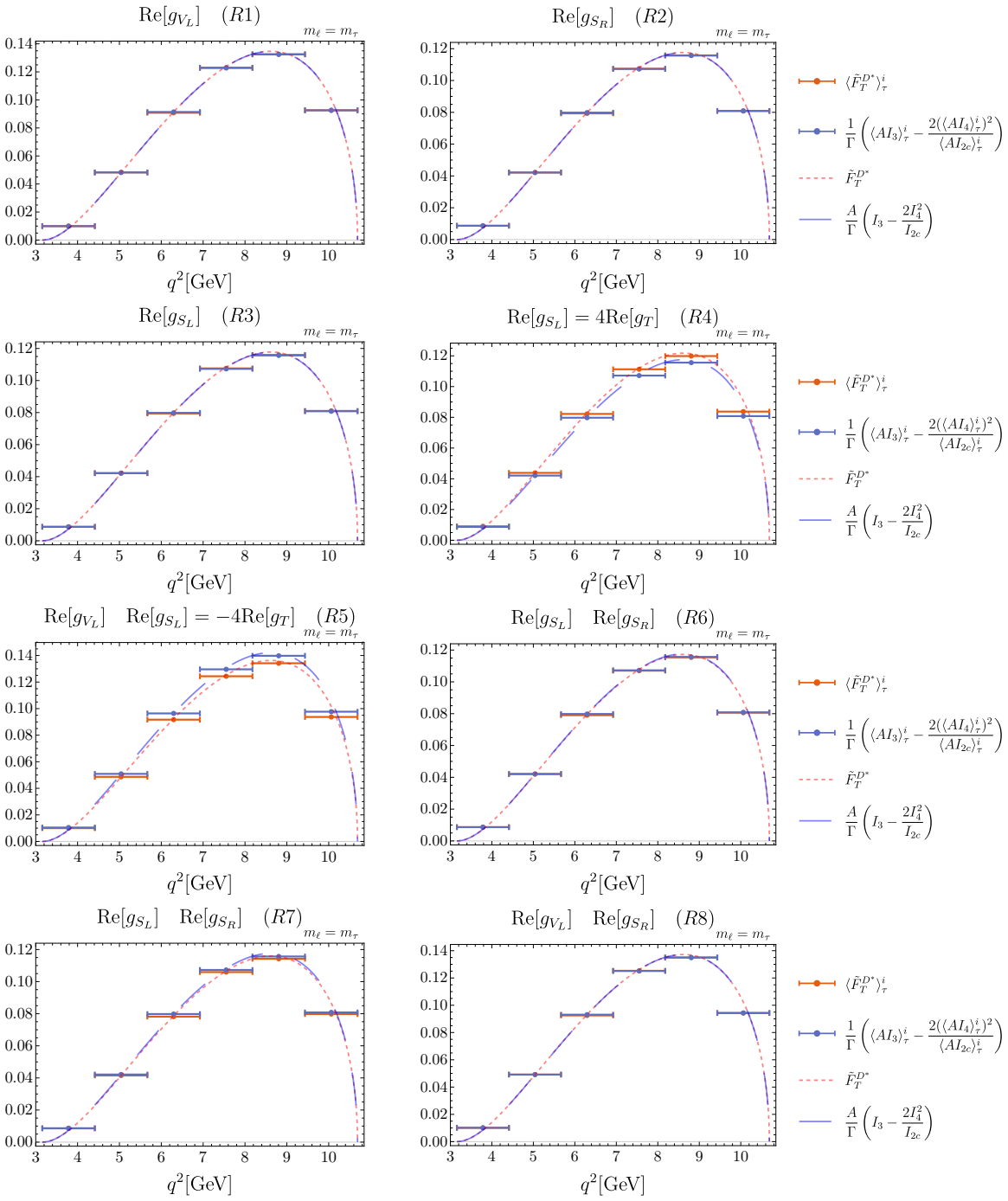

Figure D.3: Study of binning effects for Eq. (3.82) for benchmark NP scenarios with real contributions.

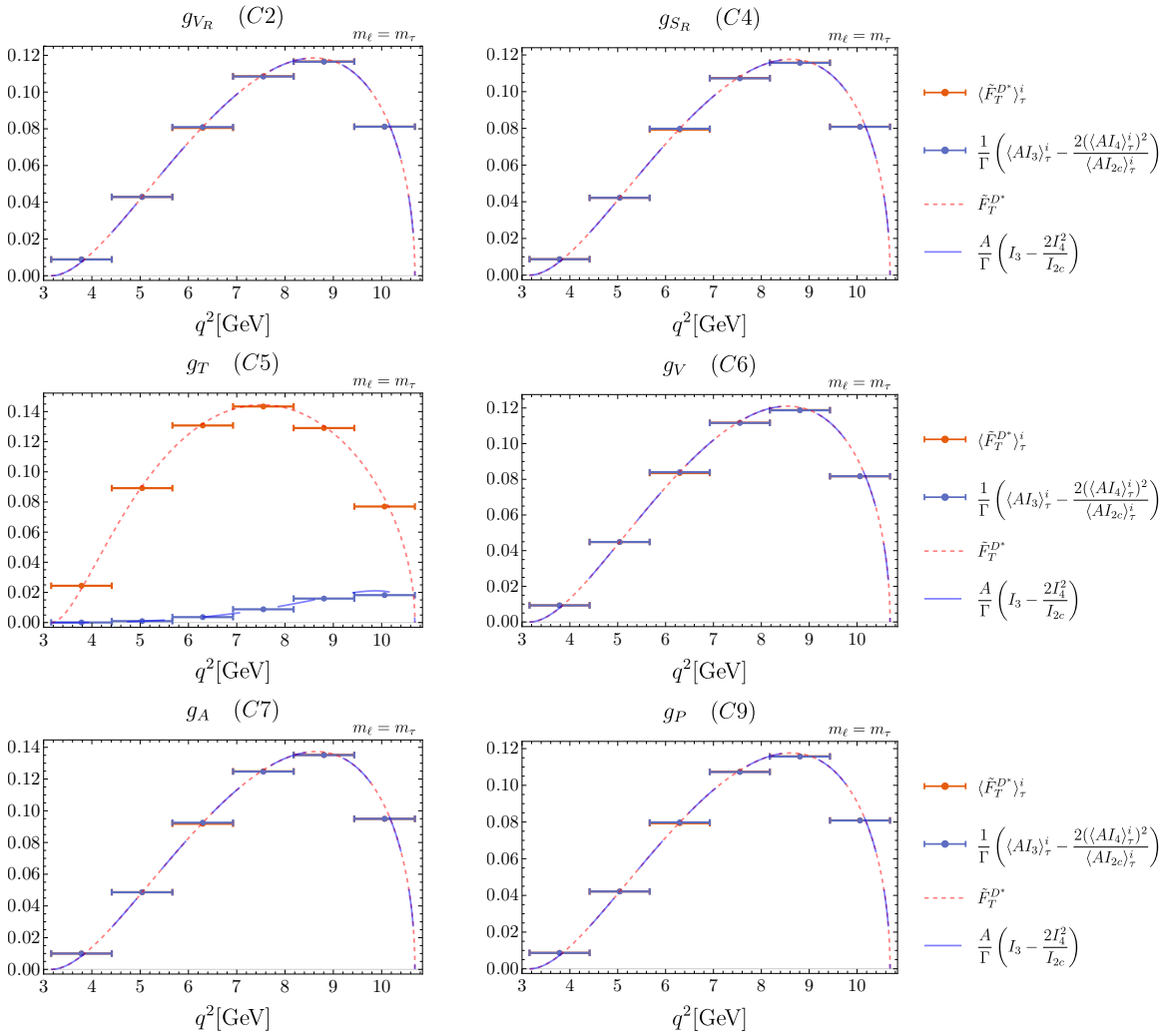

Figure D.4: Study of binning effects for Eq. (3.82) for benchmark NP scenarios with complex contributions.

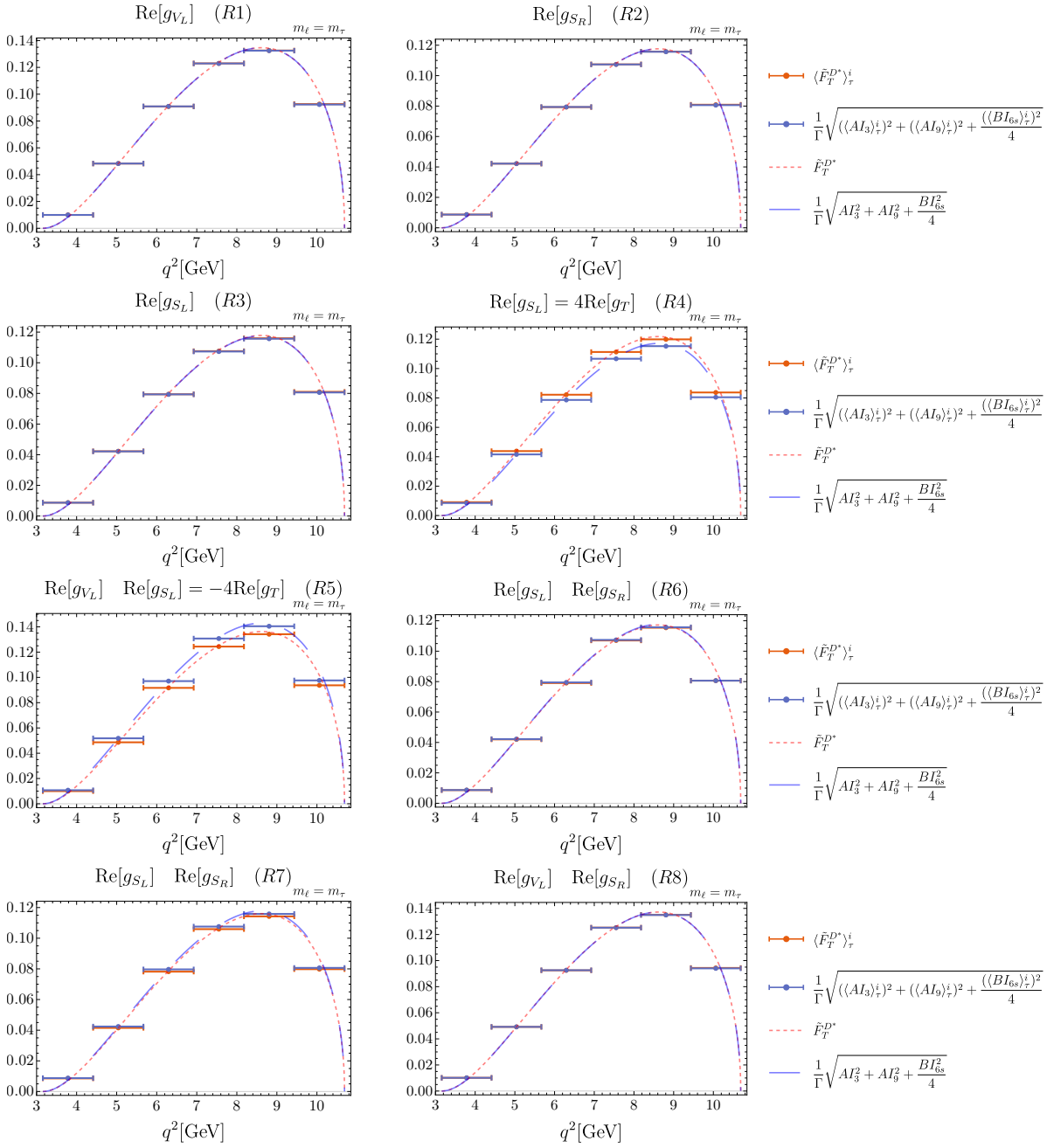

Figure D.5: Study of binning effects for Eq. (3.80) for benchmark NP scenarios with real contributions.

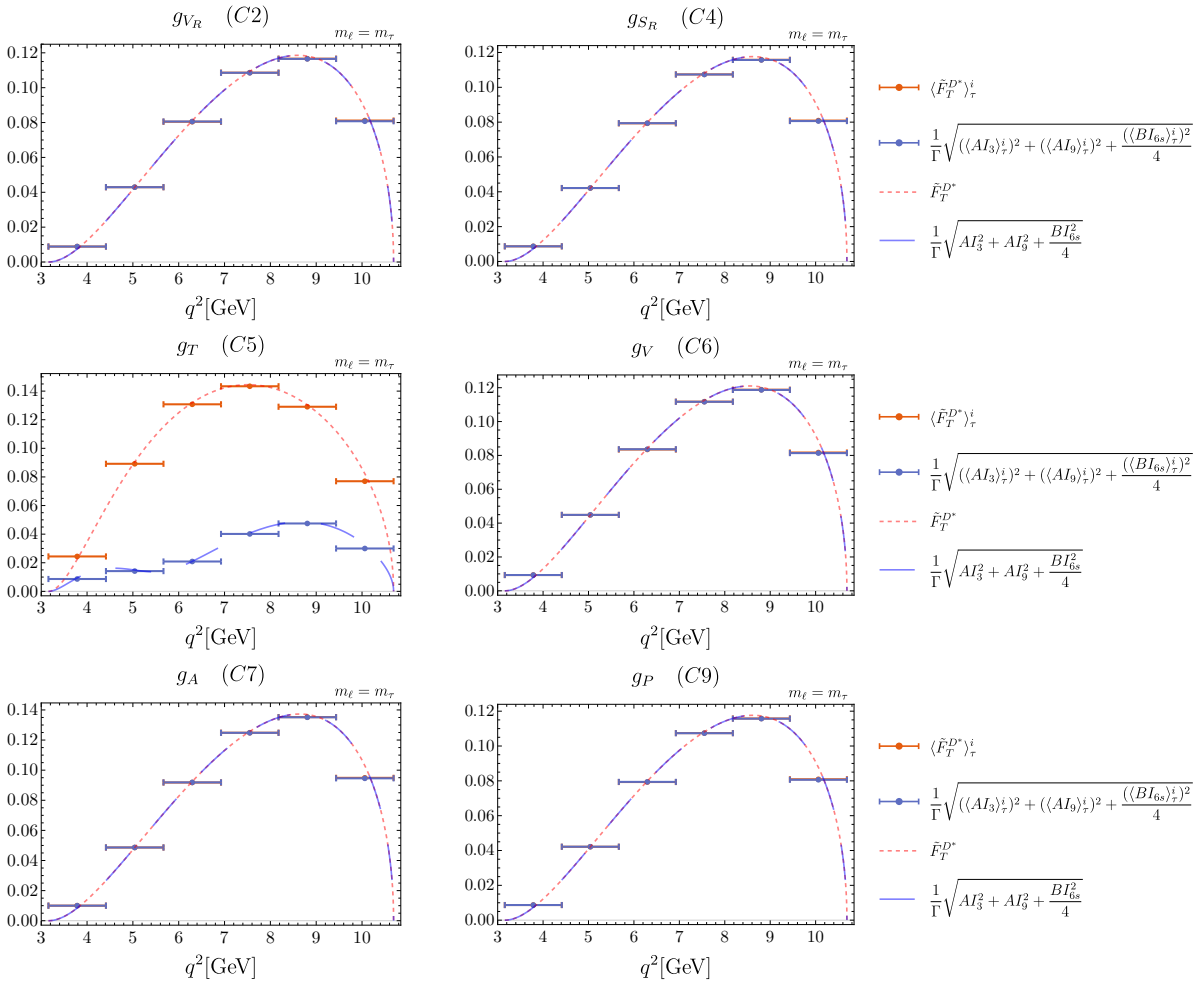

Figure D.6: Study of binning effects for Eq. (3.80) for benchmark NP scenarios with complex contributions.

Scenario \ Bin	$[3.2, 4.4]$	$[4.4, 5.7]$	$[5.7, 6.9]$	$[6.9, 8.2]$	$[8.2, 9.4]$	$[9.4, 10.7]$	$[m_\tau^2, (m_B - m_{D^*})^2]$
SM	0.03%	0.03%	0.1%	0.04%	0.09%	0.4%	1%
C1	0.03%	0.03%	0.1%	0.04%	0.09%	0.4%	1%
C0	40%	30%	30%	20%	20%	20%	20%
C3	0.03%	0.03%	0.1%	0.04%	0.09%	0.4%	1%

Table D.1: Relative difference in percent of the approximate binned expression of $\langle \tilde{F}_T^{D^* \text{alt}} \rangle_\tau$ with respect to the "standard" $\langle \tilde{F}_T^{D^*} \rangle_\tau$ for the SM and different NP scenarios. It corresponds to the relative difference in between the orange and blue bins displayed in Fig. 3.1 (normalized by the "standard" $\langle \tilde{F}_T^{D^*} \rangle_\tau$ i.e. the orange bins). The bins in the first 6 columns correspond to the division of the kinematic range ($[m_\tau^2, (m_B - m_{D^*})^2]$) in 6 equally sized intervals. The last column corresponds to the whole kinematic range (not displayed in Fig. 3.1). Notice that, as expected, this approximation works better for smaller bins. The scenario $C0$ is displayed as an example of a scenario with tensor contributions where, as expected, the two determinations should yield different results.

Scenario \ Bin	$[0, 1.8]$	$[1.8, 3.6]$	$[3.6, 5.3]$	$[5.3, 7.1]$	$[7.1, 8.9]$	$[8.9, 10.7]$	$[0, (m_B - m_{D^*})^2]$
SM	0.08%	0.04%	0.1%	0.05%	0.1%	0.4 %	2%

Table D.2: Relative difference in percent of the approximate binned expression of $\langle \tilde{F}_T^{D^* \text{alt}} \rangle_0$ with respect to the "standard" $\langle \tilde{F}_T^{D^*} \rangle_0$ for the SM. It corresponds to the relative difference in between the orange and blue bins displayed in Fig. 3.1 (normalized by the "standard" $\langle \tilde{F}_T^{D^*} \rangle_0$ i.e. the orange bins). The bins in the first 6 columns correspond to the division of the kinematic range ($[m_\tau^2, (m_B - m_{D^*})^2]$) in 6 equally sized intervals. The last column corresponds to the whole kinematic range (not displayed in Fig. 3.1). Notice that, as expected, this approximation works better for smaller bins. The scenario $C0$ is displayed as an example of a scenario with tensor contributions where, as expected, the two determinations should yield different results.

Appendix E

Theoretical framework for $B_{d,s} \to K^{*0}\bar{K}^{*0}$ decays

In this appendix we present some additional definitions and discussion concerning the observable related to the non-leptonic B decay discussed in Chapter 4. We will first detail the structure of the Weak Effective Hamiltonian used to describe such transitions, as well as the elements needed to obtain a semi-analytical expressions of the observable $L_{K^*\bar{K}^*}$ in Eq. (4.14). In the following section we show the sensitivity of the observable $L_{K^*\bar{K}^*}$ to NP contributions from different Wilson coefficients.

E.1 Weak effective theory and QCD factorization framework

The separation between short and long distances at the scale $\mu_b = m_b$ is performed in the weak effective theory to compute b-quark decays within the SM:

$$H_{\text{eff}} = \frac{G_F}{\sqrt{2}} \sum_{p=c,u} \lambda_p^{(q)} \Big(\mathcal{C}_{1s}^p Q_{1s}^p + \mathcal{C}_{2s}^p Q_{2s}^p + \sum_{i=3\ldots10} \mathcal{C}_{is} Q_{is} + \mathcal{C}_{7\gamma s} Q_{7\gamma s} + \mathcal{C}_{8gs} Q_{8gs} \Big) . \tag{E.1}$$

This effective Hamiltonian describes the quark transitions $b \to u\bar{u}s$, $b \to c\bar{c}s$, $b \to sq'\bar{q}'$ with $q' = u, d, s, c, b$, and $b \to sg$, $b \to s\gamma$. $Q_{1s,2s}^p$ are the left-handed current-current operators arising from W-boson exchange, $Q_{3s\ldots6s}$ and $Q_{7s\ldots10s}$ are QCD and electroweak penguin operators, and $Q_{7\gamma s}$ and Q_{8gs} are the electromagnetic and chromomagnetic dipole operators. They are given by [197]:

$$\begin{aligned}
Q_{1s}^p &= (\bar{p}b)_{V-A}(\bar{s}p)_{V-A}\,, & Q_{7s} &= (\bar{s}b)_{V-A} \sum_q \frac{3}{2} e_q (\bar{q}q)_{V+A}\,,\\
Q_{2s}^p &= (\bar{p}_i b_j)_{V-A}(\bar{s}_j p_i)_{V-A}\,, & Q_{8s} &= (\bar{s}_i b_j)_{V-A} \sum_q \frac{3}{2} e_q (\bar{q}_j q_i)_{V+A}\,,\\
Q_{3s} &= (\bar{s}b)_{V-A} \sum_q (\bar{q}q)_{V-A}\,, & Q_{9s} &= (\bar{s}b)_{V-A} \sum_q \frac{3}{2} e_q (\bar{q}q)_{V-A}\,,\\
Q_{4s} &= (\bar{s}_i b_j)_{V-A} \sum_q (\bar{q}_j q_i)_{V-A}\,, & Q_{10s} &= (\bar{s}_i b_j)_{V-A} \sum_q \frac{3}{2} e_q (\bar{q}_j q_i)_{V-A}\,,\\
Q_{5s} &= (\bar{s}b)_{V-A} \sum_q (\bar{q}q)_{V+A}\,, & Q_{7\gamma s} &= \frac{-e}{8\pi^2}\, m_b \bar{s}\sigma_{\mu\nu}(1+\gamma_5)F^{\mu\nu}b\,,\\
Q_{6s} &= (\bar{s}_i b_j)_{V-A} \sum_q (\bar{q}_j q_i)_{V+A}\,, & Q_{8gs} &= \frac{-g_s}{8\pi^2}\, m_b\, \bar{s}\sigma_{\mu\nu}(1+\gamma_5)G^{\mu\nu}b\,,
\end{aligned} \tag{E.2}$$

where $(\bar{q}_1 q_2)_{V\pm A} = \bar{q}_1\gamma_\mu(1\pm\gamma_5)q_2$, i, j are color indices, e_q are the electric charges of the quarks in units of $|e|$, and a summation over $q = u, d, s, c, b$ is implied. The NLO Wilson coefficients at the scale $\mu = 4.2$ GeV are given in Table E.1.

A similar weak effective theory can be written for the $b \to d$ transition by performing the trivial replacement $s \to d$. Neglecting the difference of mass between the d and s quarks, the SM values of the Wilson coefficients are identical in both cases, and we omit the d or s subscript in Table E.1.

In the SM, $\mathcal{C}_1^c = \mathcal{C}_1^u$ is the largest coefficient and it corresponds to the color-allowed tree-level contribution from the W exchange, whereas $\mathcal{C}_2^c = \mathcal{C}_2^u$ is color suppressed. QCD-penguin operators are numerically suppressed, and the electroweak operators even more so. It proves convenient to define the effective coefficients $\mathcal{C}_{7\gamma}^{\rm eff}$ and $\mathcal{C}_{8g}^{\rm eff}$ which are given in the scheme of Ref. [197] as

$$\mathcal{C}_{7\gamma}^{\rm eff} = \mathcal{C}_{7\gamma} - \frac{1}{3}\mathcal{C}_5 - \mathcal{C}_6\,, \tag{E.3}$$

$$\mathcal{C}_{8g}^{\rm eff} = \mathcal{C}_{8g} + \mathcal{C}_5\,. \tag{E.4}$$

QCD factorization relies on this weak effective theory to compute non-leptonic B-decay hadronic matrix elements, by performing a further separation of scales between m_b and the typical QCD scale, later reinterpreted in terms of a Soft-Collinear Effective Theory (SCET). Following Refs. [190, 205] and using the same notation as in this reference, we have for the vector modes for a given polarisation:

$$\begin{aligned}
T(\bar{B}_d \to \bar{K}^{*0}K^{*0}) &= A_{\bar{K}^*K^*}[\alpha_4^u - \frac{1}{2}\alpha_{4,EW}^u + \beta_3^u + \beta_4^u - \frac{1}{2}\beta_{3,EW}^u - \frac{1}{2}\beta_{4,EW}^u] \\
&\quad + A_{K^*\bar{K}^*}[\beta_4^u - \frac{1}{2}\beta_{4,EW}^u]\,, \\
P(\bar{B}_d \to \bar{K}^{*0}K^{*0}) &= A_{\bar{K}^*K^*}[\alpha_4^c - \frac{1}{2}\alpha_{4,EW}^c + \beta_3^c + \beta_4^c - \frac{1}{2}\beta_{3,EW}^c - \frac{1}{2}\beta_{4,EW}^c] \\
&\quad + A_{K^*\bar{K}^*}[\beta_4^c - \frac{1}{2}\beta_{4,EW}^c]\,, \\
T(\bar{B}_s \to \bar{K}^{*0}K^{*0}) &= A_{\bar{K}^*K^*}[\beta_4^u - \frac{1}{2}\beta_{4,EW}^u] \\
&\quad + A_{K^*\bar{K}^*}[\alpha_4^u - \frac{1}{2}\alpha_{4,EW}^u + \beta_3^u + \beta_4^u - \frac{1}{2}\beta_{3,EW}^u - \frac{1}{2}\beta_{4,EW}^u]\,, \\
P(\bar{B}_s \to \bar{K}^{*0}K^{*0}) &= A_{\bar{K}^*K^*}[\beta_4^c - \frac{1}{2}\beta_{4,EW}^c] \\
&\quad + A_{K^*\bar{K}^*}[\alpha_4^c - \frac{1}{2}\alpha_{4,EW}^c + \beta_3^c + \beta_4^c - \frac{1}{2}\beta_{3,EW}^c - \frac{1}{2}\beta_{4,EW}^c]\,.
\end{aligned} \tag{E.5}$$

The coefficients α and β involve form factors and convolutions of perturbative kernels with light-cone distribution amplitudes multiplied by the Wilson coefficients of the weak effective Hamiltonian. The difference between α_i^u and α_i^c occurs from the $\mathcal{O}(\alpha_s)$ penguin contractions in P_4^p and P_6^p, and specifically from the loops with u or c quarks and a W exchange (so that these contributions come with factors $\alpha_s/(4\pi)$ and $\mathcal{C}_1^c$). This comes from the fact that the effective Hamiltonian has a specific structure in the SM: only two types of four-fermion operators O_1^p and O_2^p ($p = u, c$) involve explicitly different $\lambda_p^{(q)}$, whereas the other operators treat all quarks on the same footing, they come from top loops and are accompanied with a CKM term $\lambda_t^{(q)} = -\lambda_u^{(q)} - \lambda_c^{(q)}$ leading to an identical contribution to T and P.

As discussed in Refs. [193–195], this explains why the quantity Δ defined in Eq. (4.2) can be computed safely within QCD factorization for penguin mediated decays because of the cancellation of long-distance contributions. As a consequence of this cancellation, only penguin contractions contribute to Δ, as can be seen by inspection of the formulae above, leading to the following very simple expression within QCD factorization:

$$\Delta = A_{M_1M_2}^Q \frac{C_F\alpha_s}{4\pi N}\mathcal{C}_1[\bar{G}_{M_2}(m_c^2/m_b^2) - \bar{G}_{M_2}(0)]\,, \tag{E.6}$$

where the normalization $A_{M_1M_2}^Q$ is defined as:

$$A_{M_1M_2}^Q = \frac{G_F}{\sqrt{2}} m_{B_q}^2 f_{M_2} A^{B_q\to M_1}(0)\,, \tag{E.7}$$

and $\bar{G}_{M_2}$ is the penguin function defined in Ref. [194].

$B_{d,s}$ Distribution Amplitudes (at $\mu = 1$ GeV) [32, 333]		
λ_{B_d} [GeV]	$\lambda_{B_s}/\lambda_{B_d}$	σ_B
0.383 ± 0.153	1.19 ± 0.14	1.4 ± 0.4

K^* Distribution Amplitudes (at $\mu = 2$ GeV) [334]			
$\alpha_1^{K^*}$	$\alpha_{1,\perp}^{K^*}$	$\alpha_2^{K^*}$	$\alpha_{2,\perp}^{K^*}$
0.02 ± 0.02	0.03 ± 0.03	0.08 ± 0.06	0.08 ± 0.06

Decay Constants (at $\mu = 2$ GeV) [128, 216, 335]			
f_{B_d}	f_{B_s}/f_{B_d}	f_{K^*}	$f_{K^*}^{\perp}/f_{K^*}$
0.190 ± 0.0013	1.209 ± 0.005	0.204 ± 0.007	0.712 ± 0.012

$B_{d,s} \to K^*$ form factors [128] and B-meson lifetimes (ps)			
$A_0^{B_s}(q^2 = 0)$	$A_0^{B_d}(q^2 = 0)$	τ_{B_d}	τ_{B_s}
0.314 ± 0.048	0.356 ± 0.046	1.519 ± 0.004	1.515 ± 0.004

Wolfenstein parameters [202]			
A	λ	$\bar{\rho}$	$\bar{\eta}$
$0.8235^{+0.0056}_{-0.0145}$	$0.22484^{+0.00025}_{-0.00006}$	$0.1569^{+0.0102}_{-0.0061}$	$0.3499^{+0.0079}_{-0.0065}$

QCD scale and masses [GeV]					
$\bar{m}_b(\bar{m}_b)$	m_b/m_c	m_{B_d}	m_{B_s}	m_{K^*}	$\Lambda_{\rm QCD}$
4.2	4.577 ± 0.008	5.280	5.367	0.892	0.225

SM Wilson Coefficients (at $\mu = 4.2$ GeV)					
$\mathcal{C}_1$	$\mathcal{C}_2$	$\mathcal{C}_3$	$\mathcal{C}_4$	$\mathcal{C}_5$	$\mathcal{C}_6$
1.082	-0.191	0.013	-0.036	0.009	-0.042
$\mathcal{C}_7/\alpha_{em}$	$\mathcal{C}_8/\alpha_{em}$	$\mathcal{C}_9/\alpha_{em}$	$\mathcal{C}_{10}/\alpha_{em}$	$\mathcal{C}_{7\gamma}^{\rm eff}$	$\mathcal{C}_{8g}^{\rm eff}$
-0.011	0.058	-1.254	0.223	-0.318	-0.151

Table E.1: Input parameters used to determine the SM predictions.

E.2 Semi-analytical expressions

In the following we provide the key elements to construct a semi-analytical expression of $L_{K^*\bar{K}^*}$. Specifically we give P_s and P_d in terms of Wilson coefficients and the parameters X_H and X_A. κ is given in Eq. (4.22) and the last bracket in Eq. (4.19) has a negligible impact and can be taken to be conservative 0.99 ± 0.01. We have followed the corrected expression of Ref. [336] for the modelling of the weak annihilation in terms of X_A.

$$
\begin{aligned}
10^7 \times P_d = {} & i0.076\mathcal{C}_{7\gamma}^{\text{eff}} - i8.8\mathcal{C}_{8g}^{\text{eff}} + ((2.6 - i1.8) + i0.13X_A - i0.041X_A^2 - i0.025X_H)\mathcal{C}_1^c \\
& + ((-0.045 + i0.39) - i0.61X_A + i0.16X_A^2 + i0.035X_H)\mathcal{C}_2^c \\
& + ((15.5 + i38.9) + i0.31X_A + i0.25X_A^2 + i3.8X_H)\mathcal{C}_3 \\
& + ((11.0 + i156.9) + i0.25X_A + i0.96X_A^2 - i0.54X_H)\mathcal{C}_4 \\
& + ((-7.4 - i7.2) + i9.2X_A - i3.3X_A^2 + i0.11X_H)\mathcal{C}_5 \\
& + ((11.0 - i19.9) + i27.7X_A - 8.9X_A^2 + i0.24X_H)\mathcal{C}_6 \\
& + ((3.7 + i3.8) - i4.7X_A + i1.7X_A^2 + i0.00042X_H)\mathcal{C}_7 \\
& + ((i6.9) - i15.7X_A + i5.0X_A^2 - i0.008X_H)\mathcal{C}_8 \\
& + ((-6.4 - i19.4) - i0.55X_A - i0.041X_A^2 - i1.9X_H)\mathcal{C}_9 \\
& + (-i81.9 - 1.4X_A - i0.15X_A^2 + i0.32X_H)\mathcal{C}_{10}\,,
\end{aligned} \tag{E.8}
$$

$$
\begin{aligned}
10^7 \times P_s = {} & i0.069\mathcal{C}_{7\gamma}^{\text{eff}} - i8.0\mathcal{C}_{8g}^{\text{eff}} + ((2.4 - i1.7) + i0.16X_A - i0.049X_A^2 - i0.026X_H)\mathcal{C}_1^c \\
& + ((-0.041 + i0.45) - i0.74X_A + i0.1X_A^2 + i0.037X_H)\mathcal{C}_2^c \\
& + ((14.2 + i36.4) + i0.37X_A + i0.3X_A^2 + i3.9X_H)\mathcal{C}_3 \\
& + ((10.0 + i142.7) + i0.31X_A + i1.2X_A^2 - i0.56X_H)\mathcal{C}_4 \\
& + ((-6.7 - i7.7) + i11.1X_A - i3.9X_A^2 + i0.11X_H)\mathcal{C}_5 \\
& + ((10.0 - i21.7) + i33.5X_A - 10.8X_A^2 + i0.25X_H)\mathcal{C}_6 \\
& + ((3.4 + i4.0) - i5.7X_A + i2.0X_A^2 + i0.00043X_H)\mathcal{C}_7 \\
& + ((i8.3) - i19.0X_A + i6.0X_A^2 - i0.008X_H)\mathcal{C}_8 \\
& + ((-5.8 - i18.1) - i0.66X_A - i0.049X_A^2 - i2.0X_H)\mathcal{C}_9 \\
& + (-i74.3 - 1.7X_A - i0.18X_A^2 + i0.33X_H)\mathcal{C}_{10}\,.
\end{aligned} \tag{E.9}
$$

E.3 Sensitivity to New Physics

We show how NP contributions can help to reduce the tension between theory and experiment for $L_{K^*\bar{K}^*}$, completing the results shown in Fig. 4.1 discussed in Section 4.3. In Fig. E.1 we show the 1σ-range for the NP contribution to each Wilson coefficient that is able to explain the experimental value of $L_{K^*\bar{K}^*}$, normalized to its SM value.

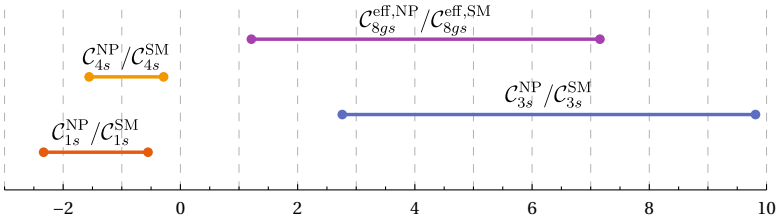

Figure E.1: 1σ intervals for the NP contribution to Wilson coefficients needed to explain $L_{K^*\bar{K}^*}$, normalized to their SM value.

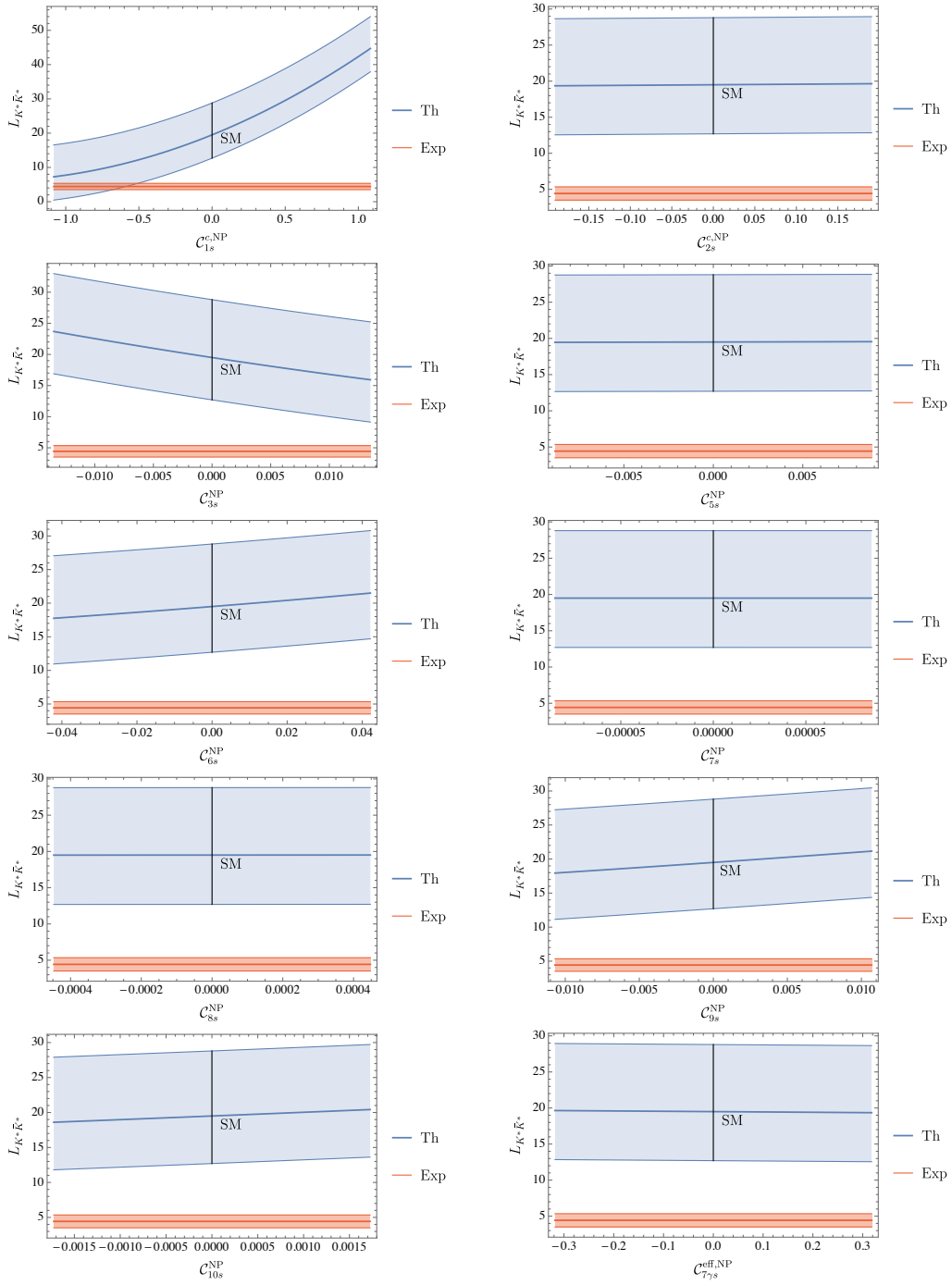

Figure E.2: Sensitivity of $L_{K^*\bar{K}^*}$ to individual contributions of NP in all different $\mathcal{C}_{is}^{\mathrm{NP}}$. For each coefficient, the range of variation considered for the NP contribution corresponds to 100% of its SM value.

Appendix F

Electroweak observables and interaction Lagrangian

This appendix provides the list of Electroweak observables included in the fit described in Chapter 5, as well as the detailed expressions of the interactions between the Z boson and fermions.

Observable	Experimental value
m_W [GeV]	80.379(12)
Γ_W [GeV]	2.085(42)
$\mathcal{B}(W \to \text{had})$	0.6741(27)
$\mathcal{B}(W \to \text{lep})$	0.1086(9)
$\sin^2\theta^{\text{CDF}}_{\text{eff, e}}$	0.23248(52)
$\sin^2\theta^{\text{D0}}_{\text{eff, e}}$	0.23146(47)
$\sin^2\theta^{\text{CDF}}_{\text{eff, }\mu}$	0.2315(10)
$\sin^2\theta^{\text{CMS}}_{\text{eff, }\mu}$	0.2287(32)
$\sin^2\theta^{\text{LHCb}}_{\text{eff, }\mu}$	0.2314(11)
P_τ^{pol}	0.1465(33)
A_e	0.1516(21)
A_μ	0.142(15)
A_τ	0.136(15)
Γ_Z [GeV]	2.4952(23)
σ_h^0 [nb]	41.541(37)
R_e^0	20.804(50)
R_μ^0	20.785(33)
R_τ^0	20.764(45)
$A_{\text{FB}}^{0,e}$	0.0145(25)
$A_{\text{FB}}^{0,\mu}$	0.0169(13)
$A_{\text{FB}}^{0,\tau}$	0.0188(17)
R_b^0	0.21629(66)
R_c^0	0.1721(30)
$A_{\text{FB}}^{0,b}$	0.0992(16)
$A_{\text{FB}}^{0,c}$	0.0707(35)
A_b	0.923(20)
A_c	0.670(27)

Table F.1: Electroweak observables [211, 289] used in our fit performed using HEPfit [297] with m_{Z_0}, α and G_F as input.

We write the interactions of the SM Z with fermions as

$$\begin{aligned}\mathcal{L}_{Zff} = &\,\bar{\ell}_j\gamma_\mu\left(\Delta_{ji}^{\ell L}P_L + \Delta_{ji}^{\ell R}P_R\right)\ell_i Z^\mu + \bar{\nu}_j\gamma_\mu\Delta_{ji}^{\nu L}P_L\nu_i Z^\mu \\ &+ \bar{u}_j\,\gamma_\mu\left(\Delta_{ji}^{uL}P_L + \Delta_{ji}^{uR}P_R\right)u_i\,Z^\mu \\ &+ \bar{d}_j\,\gamma_\mu\left(\Delta_{ji}^{dL}P_L + \Delta_{ji}^{dR}P_R\right)d_i\,Z^\mu\,,\end{aligned} \tag{F.1}$$

with $i,j = 1,2,3$ and

$$\begin{aligned}\Delta_{ji}^{\ell L(R)} &\simeq \sin\xi\, g_{ji}^{\ell L(R)} + g_{\rm SM}^{\ell L(R)}\delta_{ji}\,,\\ \Delta_{ji}^{\nu L} &\simeq \sin\xi\, g_{ji}^{\ell L} + g_{\rm SM}^{\nu L}\delta_{ji}\,,\\ \Delta_{ji}^{uL} &\simeq \sin\xi\, V_{jk}g_{kk'}^{q}V_{ik'}^{*} + g_{\rm SM}^{uL}\delta_{ji}\,,\\ \Delta_{ji}^{uR} &\simeq \sin\xi\, g_{ji}^{u} + g_{\rm SM}^{uR}\delta_{ji}\,,\\ \Delta_{ji}^{dL(R)} &\simeq \sin\xi\, g_{ji}^{q(d)} + g_{\rm SM}^{dL(R)}\delta_{ji}\,,\end{aligned} \tag{F.2}$$

where $g_{\rm SM}^{iL(R)}$ are the SM couplings given by

$$\begin{aligned}g_{\rm SM}^{\nu L} &= -\frac{e}{2s_W c_W}\,,\\ g_{\rm SM}^{\ell L} &= \frac{e}{2s_W c_W}\left(1-2s_W^2\right)\,, \qquad g_{\rm SM}^{\ell R} = -\frac{e\,s_W}{c_W}\,,\\ g_{\rm SM}^{uL} &= -\frac{e}{s_W c_W}\left(\frac{1}{2}-\frac{2}{3}s_W^2\right)\,, \qquad g_{\rm SM}^{uR} = \frac{2}{3}\frac{e\,s_W}{c_W}\,,\\ g_{\rm SM}^{dL} &= \frac{e}{s_W c_W}\left(\frac{1}{2}-\frac{1}{3}s_W^2\right)\,, \qquad g_{\rm SM}^{dR} = -\frac{1}{3}\frac{e\,s_W}{c_W}\,,\end{aligned} \tag{F.3}$$

with $e = g_1g_2/\sqrt{g_1^2+g_2^2} = g_1c_W = g_2s_W$ being the electric charge. Moreover, taking into account the $Z-Z'$ mixing in Eq. (F.2) and the vertex corrections [233, 337], we have the following modified Z couplings to leptons

$$\begin{aligned}\Delta_{ij}^{\ell L} &= g_{\rm SM}^{\ell L}\left(\delta_{ij} + \sin\xi\frac{g_{ij}^{\ell L}}{g_{\rm SM}^{\ell L}} + \sum_k \frac{g_{ik}^{\ell L}g_{kj}^{\ell L}}{(4\pi)^2}K_F\left(\frac{m_Z^2}{m_{Z'}^2}\right)\right)\,,\\ \Delta_{ij}^{\nu L} &= g_{\rm SM}^{\nu L}\left(\delta_{ij} + \sin\xi\frac{g_{ij}^{\ell L}}{g_{\rm SM}^{\nu L}} + \sum_k \frac{g_{ik}^{\ell L}g_{kj}^{\ell L}}{(4\pi)^2}K_F\left(\frac{m_Z^2}{m_{Z'}^2}\right)\right)\,,\\ \Delta_{ij}^{\ell R} &= g_{\rm SM}^{\ell R}\left(\delta_{ij} + \sin\xi\frac{g_{ij}^{\ell R}}{g_{\rm SM}^{\ell R}} + \sum_k \frac{g_{ik}^{\ell R}g_{kj}^{\ell R}}{(4\pi)^2}K_F\left(\frac{m_Z^2}{m_{Z'}^2}\right)\right)\,,\end{aligned} \tag{F.4}$$

at the Z pole with

$$\begin{aligned}K_F(x) = &-\frac{2(x+1)^2(\mathrm{Li}_2(-x)+\ln(x)\ln(x+1))}{x^2}\\ &-\frac{7x+4}{2x}+\frac{(3x+2)\ln(x)}{x}.\end{aligned} \tag{F.5}$$

Bibliography

[1] Simone Bifani et al. "Review of Lepton Universality tests in B decays". In: *J. Phys. G* 46.2 (2019), p. 023001. DOI: 10.1088/1361-6471/aaf5de. arXiv: 1809.06229 [hep-ex].

[2] Johannes Albrecht, Danny van Dyk, and Christoph Langenbruch. "Flavour anomalies in heavy quark decays". In: *Prog. Part. Nucl. Phys.* 120 (2021), p. 103885. DOI: 10.1016/j.ppnp.2021.103885. arXiv: 2107.04822 [hep-ex].

[3] David London and Joaquim Matias. "B Flavour Anomalies: 2021 Theoretical Status Report". In: (Oct. 2021). DOI: 10.1146/annurev-nucl-102020-090209. arXiv: 2110.13270 [hep-ph].

[4] Marcel Algueró et al. "$b \to s\ell^+\ell^-$ global fits after R_{K_S} and $R_{K^{*+}}$". In: *Eur. Phys. J. C* 82.4 (2022), p. 326. DOI: 10.1140/epjc/s10052-022-10231-1. arXiv: 2104.08921 [hep-ph].

[5] Benjamin Grinstein, Roxanne P. Springer, and Mark B. Wise. "Effective Hamiltonian for Weak Radiative B Meson Decay". In: *Phys. Lett. B* 202 (1988), pp. 138–144. DOI: 10.1016/0370-2693(88)90868-4.

[6] Gerhard Buchalla, Andrzej J. Buras, and Markus E. Lautenbacher. "Weak decays beyond leading logarithms". In: *Rev. Mod. Phys.* 68 (1996), pp. 1125–1144. DOI: 10.1103/RevModPhys.68.1125. arXiv: hep-ph/9512380.

[7] Andrzej J. Buras. "Weak Hamiltonian, CP violation and rare decays". In: *Les Houches Summer School in Theoretical Physics, Session 68: Probing the Standard Model of Particle Interactions*. June 1998, pp. 281–539. arXiv: hep-ph/9806471.

[8] F. Kruger and E. Lunghi. "Looking for novel CP violating effects in $\bar{B} \to K^*\ell^+\ell^-$". In: *Phys. Rev. D* 63 (2001), p. 014013. DOI: 10.1103/PhysRevD.63.014013. arXiv: hep-ph/0008210.

[9] Wolfgang Altmannshofer et al. "Symmetries and Asymmetries of $B \to K^*\mu^+\mu^-$ Decays in the Standard Model and Beyond". In: *JHEP* 01 (2009), p. 019. DOI: 10.1088/1126-6708/2009/01/019. arXiv: 0811.1214 [hep-ph].

[10] M. Beneke, Th. Feldmann, and D. Seidel. "Exclusive radiative and electroweak $b \to d$ and $b \to s$ penguin decays at NLO". In: *Eur. Phys. J. C* 41 (2005), pp. 173–188. DOI: 10.1140/epjc/s2005-02181-5. arXiv: hep-ph/0412400.

[11] Joaquim Matias et al. "Complete Anatomy of $\bar{B}_d -> \bar{K}^{*0}(-> K\pi)l^+l^-$ and its angular distribution". In: *JHEP* 04 (2012), p. 104. DOI: 10.1007/JHEP04(2012)104. arXiv: 1202.4266 [hep-ph].

[12] Sebastien Descotes-Genon et al. "Optimizing the basis of $B \to K^*ll$ observables in the full kinematic range". In: *JHEP* 05 (2013), p. 137. DOI: 10.1007/JHEP05(2013)137. arXiv: 1303.5794 [hep-ph].

[13] M. Beneke et al. "QCD factorization for exclusive, nonleptonic B meson decays: General arguments and the case of heavy light final states". In: *Nucl. Phys. B* 591 (2000), pp. 313–418. DOI: 10.1016/S0550-3213(00)00559-9. arXiv: hep-ph/0006124.

[14] M. Beneke, T. Feldmann, and D. Seidel. "Systematic approach to exclusive $B \to V\ell^+\ell^-$, $V\gamma$ decays". In: *Nucl. Phys. B* 612 (2001), pp. 25–58. DOI: 10.1016/S0550-3213(01)00366-2. arXiv: hep-ph/0106067.

[15] Andrzej J. Buras and Manfred Munz. "Effective Hamiltonian for B —> X(s) e+ e- beyond leading logarithms in the NDR and HV schemes". In: *Phys. Rev. D* 52 (1995), pp. 186–195. DOI: 10.1103/PhysRevD.52.186. arXiv: hep-ph/9501281.

[16] Christoph Greub, Volker Pilipp, and Christof Schupbach. "Analytic calculation of two-loop QCD corrections to $b \to sl^+l^-$ in the high q^2 region". In: *JHEP* 12 (2008), p. 040. DOI: 10.1088/1126-6708/2008/12/040. arXiv: 0810.4077 [hep-ph].

[17] Thomas Blake et al. "An empirical model to determine the hadronic resonance contributions to $\bar{B}^0 \to \bar{K}^{*0}\mu^+\mu^-$ transitions". In: *Eur. Phys. J. C* 78.6 (2018), p. 453. DOI: 10.1140/epjc/s10052-018-5937-3. arXiv: 1709.03921 [hep-ph].

[18] Marco Ciuchini et al. "On flavourful easter eggs for new physics hunger and lepton flavour universality violation". In: *Eur. Phys. J.* C77.10 (2017), p. 688. DOI: 10.1140/epjc/s10052-017-5270-2. arXiv: 1704.05447 [hep-ph].

[19] Christoph Bobeth et al. "Long-distance effects in $B \to K^*\ell\ell$ from analyticity". In: *Eur. Phys. J.* C78.6 (2018), p. 451. DOI: 10.1140/epjc/s10052-018-5918-6. arXiv: 1707.07305 [hep-ph].

[20] Bernat Capdevila et al. "Hadronic uncertainties in $B \to K^*\mu^+\mu^-$: a state-of-the-art analysis". In: *JHEP* 04 (2017), p. 016. DOI: 10.1007/JHEP04(2017)016. arXiv: 1701.08672 [hep-ph].

[21] A. Arbey et al. "Hadronic and New Physics Contributions to $b \to s$ Transitions". In: *Phys. Rev. D* 98.9 (2018), p. 095027. DOI: 10.1103/PhysRevD.98.095027. arXiv: 1806.02791 [hep-ph].

[22] Sébastien Descotes-Genon et al. "Global analysis of $b \to s\ell\ell$ anomalies". In: *JHEP* 06 (2016), p. 092. DOI: 10.1007/JHEP06(2016)092. arXiv: 1510.04239 [hep-ph].

[23] A. Khodjamirian et al. "Charm-loop effect in $B \to K^{(*)}\ell^+\ell^-$ and $B \to K^*\gamma$". In: *JHEP* 09 (2010), p. 089. DOI: 10.1007/JHEP09(2010)089. arXiv: 1006.4945 [hep-ph].

[24] Konstantin G. Chetyrkin, Mikolaj Misiak, and Manfred Munz. "Weak radiative B meson decay beyond leading logarithms". In: *Phys. Lett. B* 400 (1997). [Erratum: Phys.Lett.B 425, 414 (1998)], pp. 206–219. DOI: 10.1016/S0370-2693(97)00324-9. arXiv: hep-ph/9612313.

[25] Sebastien Descotes-Genon et al. "Exploring New Physics in the $C7-C7'$ plane". In: *JHEP* 06 (2011), p. 099. DOI: 10.1007/JHEP06(2011)099. arXiv: 1104.3342 [hep-ph].

[26] Roel Aaij et al. "Angular analysis of the $B^0 \to K^{*0}\mu^+\mu^-$ decay using 3 fb^{-1} of integrated luminosity". In: *JHEP* 02 (2016), p. 104. DOI: 10.1007/JHEP02(2016)104. arXiv: 1512.04442 [hep-ex].

[27] R. Aaij et al. "Differential branching fraction and angular analysis of the decay $B^0 \to K^{*0}\mu^+\mu^-$". In: *JHEP* 08 (2013), p. 131. DOI: 10.1007/JHEP08(2013)131. arXiv: 1304.6325 [hep-ex].

[28] Ulrik Egede et al. "New physics reach of the decay mode $\bar{B} \to \bar{K}^{*0}\ell^+\ell^-$". In: *JHEP* 10 (2010), p. 056. DOI: 10.1007/JHEP10(2010)056. arXiv: 1005.0571 [hep-ph].

[29] M. Beneke and T. Feldmann. "Symmetry breaking corrections to heavy to light B meson form-factors at large recoil". In: *Nucl. Phys. B* 592 (2001), pp. 3–34. DOI: 10.1016/S0550-3213(00)00585-X. arXiv: hep-ph/0008255.

[30] Sébastien Descotes-Genon et al. "On the impact of power corrections in the prediction of $B \to K^* \mu^+ \mu^-$ observables". In: *JHEP* 12 (2014), p. 125. DOI: 10.1007/JHEP12(2014)125. arXiv: 1407.8526 [hep-ph].

[31] Sebastien Descotes-Genon, Joaquim Matias, and Javier Virto. "Understanding the $B \to K^* \mu^+ \mu^-$ Anomaly". In: *Phys. Rev. D* 88 (2013), p. 074002. DOI: 10.1103/PhysRevD.88.074002. arXiv: 1307.5683 [hep-ph].

[32] Patricia Ball and Roman Zwicky. "$|V_{td}/V_{ts}|$ from $B \to V\gamma$". In: *JHEP* 04 (2006), p. 046. DOI: 10.1088/1126-6708/2006/04/046. arXiv: hep-ph/0603232.

[33] Aoife Bharucha, David M. Straub, and Roman Zwicky. "$B \to V\ell^+\ell^-$ in the Standard Model from light-cone sum rules". In: *JHEP* 08 (2016), p. 098. DOI: 10.1007/JHEP08(2016)098. arXiv: 1503.05534 [hep-ph].

[34] Nico Gubernari, Ahmet Kokulu, and Danny van Dyk. "$B \to P$ and $B \to V$ Form Factors from B-Meson Light-Cone Sum Rules beyond Leading Twist". In: *JHEP* 01 (2019), p. 150. DOI: 10.1007/JHEP01(2019)150. arXiv: 1811.00983 [hep-ph].

[35] Chris Bouchard et al. "Rare decay $B \to K\ell^+\ell^-$ form factors from lattice QCD". In: *Phys. Rev. D* 88.5 (2013). [Erratum: Phys.Rev.D 88, 079901 (2013)], p. 054509. DOI: 10.1103/PhysRevD.88.054509. arXiv: 1306.2384 [hep-lat].

[36] Matthias Neubert. "Effective field theory and heavy quark physics". In: *Theoretical Advanced Study Institute in Elementary Particle Physics: Physics in $D \geqq 4$*. Dec. 2005, pp. 149–194. DOI: 10.1142/9789812773579_0004. arXiv: hep-ph/0512222.

[37] Gerhard Buchalla. "Heavy quark theory". In: *55th Scottish Universities Summer School in Physics: Heavy Flavor Physics (SUSSP 2001)*. Feb. 2002, pp. 57–104. arXiv: hep-ph/0202092.

[38] Michael J. Dugan and Benjamín Grinstein. "QCD basis for factorization in decays of heavy mesons". In: *Physics Letters B* 255.4 (1991), pp. 583–588. ISSN: 0370-2693. DOI: https://doi.org/10.1016/0370-2693(91)90271-Q. URL: https://www.sciencedirect.com/science/article/pii/037026939190271Q.

[39] J. Charles et al. "Heavy to light form-factors in the heavy mass to large energy limit of QCD". In: *Phys. Rev. D* 60 (1999), p. 014001. DOI: 10.1103/PhysRevD.60.014001. arXiv: hep-ph/9812358.

[40] Frank Kruger and Joaquim Matias. "Probing new physics via the transverse amplitudes of $B^0 \to K^{*0}(\to K^-\pi^+)l^+l^-$ at large recoil". In: *Phys. Rev. D* 71 (2005), p. 094009. DOI: 10.1103/PhysRevD.71.094009. arXiv: hep-ph/0502060.

[41] Sebastien Descotes-Genon et al. "Implications from clean observables for the binned analysis of $B \to K^* \mu^+ \mu^-$ at large recoil". In: *JHEP* 01 (2013), p. 048. DOI: 10.1007/JHEP01(2013)048. arXiv: 1207.2753 [hep-ph].

[42] Sébastien Descotes-Genon and Javier Virto. "Time dependence in $B \to V\ell\ell$ decays". In: *JHEP* 04 (2015). [Erratum: JHEP 07, 049 (2015)], p. 045. DOI: 10.1007/JHEP04(2015)045. arXiv: 1502.05509 [hep-ph].

[43] Christoph Bobeth, Gudrun Hiller, and Giorgi Piranishvili. "CP Asymmetries in bar $B \to \bar{K}^*(\to \bar{K}\pi)\bar{\ell}\ell$ and Untagged $\bar{B}_s$, $B_s \to \phi(\to K^+K^-)\bar{\ell}\ell$ Decays at NLO". In: *JHEP* 07 (2008), p. 106. DOI: 10.1088/1126-6708/2008/07/106. arXiv: 0805.2525 [hep-ph].

[44] C. Bobeth et al. "Analysis of neutral Higgs boson contributions to the decays $\bar{B}(\ s^{)} \to \ell^+\ell^-$ and $\bar{B} \to K\ell^+\ell^-$". In: *Phys. Rev. D* 64 (2001), p. 074014. DOI: 10.1103/PhysRevD.64.074014. arXiv: hep-ph/0104284.

[45] Christoph Bobeth, Gudrun Hiller, and Giorgi Piranishvili. "Angular distributions of $\bar{B} \to K\bar{\ell}\ell$ decays". In: *JHEP* 07.12 (2007), p. 040. DOI: 10.1088/1126-6708/2007/12/040. arXiv: 0709.4174 [hep-ph].

[46] Christoph Bobeth et al. "$B_{s,d} \to l^+l^-$ in the Standard Model with Reduced Theoretical Uncertainty". In: *Phys. Rev. Lett.* 112 (2014), p. 101801. DOI: 10.1103/PhysRevLett.112.101801. arXiv: 1311.0903 [hep-ph].

[47] Martin Beneke, Christoph Bobeth, and Robert Szafron. "Enhanced electromagnetic correction to the rare B-meson decay $B_{s,d} \to \mu^+\mu^-$". In: *Phys. Rev. Lett.* 120.1 (2018), p. 011801. DOI: 10.1103/PhysRevLett.120.011801. arXiv: 1708.09152 [hep-ph].

[48] Mikolaj Misiak. Talk given at the workshop "New physics at the low-energy precision frontier", Orsay (https://indico.cern.ch/event/815529/) and private communication. 2019.

[49] Bernat Capdevila et al. "Assessing lepton-flavour non-universality from $B \to K^*\ell\ell$ angular analyses". In: *JHEP* 10 (2016), p. 075. DOI: 10.1007/JHEP10(2016)075. arXiv: 1605.03156 [hep-ph].

[50] S. Wehle et al. "Lepton-Flavor-Dependent Angular Analysis of $B \to K^*\ell^+\ell^-$". In: *Phys. Rev. Lett.* 118.11 (2017), p. 111801. DOI: 10.1103/PhysRevLett.118.111801. arXiv: 1612.05014 [hep-ex].

[51] Roel Aaij et al. "Test of lepton universality in beauty-quark decays". Mar. 2021. arXiv: 2103.11769 [hep-ex].

[52] Roel Aaij et al. "Tests of lepton universality using $B^0 \to K^0_S\ell^+\ell^-$ and $B^+ \to K^{*+}\ell^+\ell^-$ decays". In: (Oct. 2021). arXiv: 2110.09501 [hep-ex].

[53] Bernat Capdevila et al. "Patterns of New Physics in $b \to s\ell^+\ell^-$ transitions in the light of recent data". In: *JHEP* 01 (2018), p. 093. DOI: 10.1007/JHEP01(2018)093. arXiv: 1704.05340 [hep-ph].

[54] Marcel Algueró et al. "Are we overlooking lepton flavour universal new physics in $b \to s\ell\ell$?" In: *Phys. Rev. D* 99.7 (2019), p. 075017. DOI: 10.1103/PhysRevD.99.075017. arXiv: 1809.08447 [hep-ph].

[55] Marcel Algueró et al. "Emerging patterns of New Physics with and without Lepton Flavour Universal contributions". In: *Eur. Phys. J. C* 79.8 (2019), p. 714. DOI: 10.1140/epjc/s10052-019-7216-3. arXiv: 1903.09578 [hep-ph].

[56] Li-Sheng Geng et al. "Implications of new evidence for lepton-universality violation in $b \to s\ell^+\ell^-$ decays". Mar. 2021. arXiv: 2103.12738 [hep-ph].

[57] Wolfgang Altmannshofer and Peter Stangl. "New Physics in Rare B Decays after Moriond 2021". Mar. 2021. arXiv: 2103.13370 [hep-ph].

[58] T. Hurth, F. Mahmoudi, and S. Neshatpour. "Model independent analysis of the angular observables in $B^0 \to K^{*0}\mu^+\mu^-$ and $B^+ \to K^{*+}\mu^+\mu^-$". Dec. 2020. arXiv: 2012.12207 [hep-ph].

[59] Ashutosh Kumar Alok et al. "Continuing search for new physics in $b \to s\mu\mu$ decays: two operators at a time". In: *JHEP* 06 (2019), p. 089. DOI: 10.1007/JHEP06(2019)089. arXiv: 1903.09617 [hep-ph].

[60] Marco Ciuchini et al. "Lessons from the $B^{0,+} \to K^{*0,+}\mu^+\mu^-$ angular analysis". In: (Nov. 2020). arXiv: 2011.01212 [hep-ph].

[61] Alakabha Datta, Jacky Kumar, and David London. "The B anomalies and new physics in $b \to se^+e^-$". In: *Phys. Lett. B* 797 (2019), p. 134858. DOI: 10.1016/j.physletb.2019.134858. arXiv: 1903.10086 [hep-ph].

[62] T. Hurth, F. Mahmoudi, and S. Neshatpour. "Implications of the new LHCb angular analysis of $B \to K^* \mu^+ \mu^-$: Hadronic effects or new physics?" In: *Phys. Rev. D* 102.5 (2020), p. 055001. DOI: 10.1103/PhysRevD.102.055001. arXiv: 2006.04213 [hep-ph].

[63] Roel Aaij et al. "Test of lepton universality in beauty-quark decays". In: (Mar. 2021). arXiv: 2103.11769 [hep-ex].

[64] S. Choudhury et al. "Test of lepton flavor universality and search for lepton flavor violation in $B \to K\ell\ell$ decays". In: *JHEP* 03 (2021), p. 105. DOI: 10.1007/JHEP03(2021)105. arXiv: 1908.01848 [hep-ex].

[65] Roel Aaij et al. "Analysis of neutral B-meson decays into two muons". Aug. 2021. arXiv: 2108.09284 [hep-ex].

[66] Albert M Sirunyan et al. "Measurement of properties of $\mathrm{B}_\mathrm{s}^0 \to \mu^+\mu^-$ decays and search for $\mathrm{B}^0 \to \mu^+\mu^-$ with the CMS experiment". In: *JHEP* 04 (2020), p. 188. DOI: 10.1007/JHEP04(2020)188. arXiv: 1910.12127 [hep-ex].

[67] Morad Aaboud et al. "Study of the rare decays of B_s^0 and B^0 mesons into muon pairs using data collected during 2015 and 2016 with the ATLAS detector". In: *JHEP* 04 (2019), p. 098. DOI: 10.1007/JHEP04(2019)098. arXiv: 1812.03017 [hep-ex].

[68] T. Hurth et al. "More Indications for Lepton Nonuniversality in $b \to s\ell^+\ell^-$". In: *Phys. Lett. B* 824 (2022), p. 136838. DOI: 10.1016/j.physletb.2021.136838. arXiv: 2104.10058 [hep-ph].

[69] Roel Aaij et al. "Angular Analysis of the $B^+ \to K^{*+}\mu^+\mu^-$ Decay". In: *Phys. Rev. Lett.* 126.16 (2021), p. 161802. DOI: 10.1103/PhysRevLett.126.161802. arXiv: 2012.13241 [hep-ex].

[70] Albert M Sirunyan et al. "Angular analysis of the decay $\mathrm{B}^+ \to \mathrm{K}^*(892)^+\mu^+\mu^-$ in proton-proton collisions at $\sqrt{s} = 8$ TeV". In: *JHEP* 04 (2021), p. 124. DOI: 10.1007/JHEP04(2021)124. arXiv: 2010.13968 [hep-ex].

[71] Albert M Sirunyan et al. "Angular analysis of the decay $\mathrm{B}^+ \to \mathrm{K}^+\mu^+\mu^-$ in proton-proton collisions at $\sqrt{s} = 8$ TeV". In: *Phys. Rev. D* 98.11 (2018), p. 112011. DOI: 10.1103/PhysRevD.98.112011. arXiv: 1806.00636 [hep-ex].

[72] Roel Aaij et al. "Strong constraints on the $b \to s\gamma$ photon polarisation from $B^0 \to K^{*0}e^+e^-$ decays". In: *JHEP* 12 (2020), p. 081. DOI: 10.1007/JHEP12(2020)081. arXiv: 2010.06011 [hep-ex].

[73] Roel Aaij et al. "Angular analysis of the $B^0 \to K^{*0}e^+e^-$ decay in the low-q^2 region". In: *JHEP* 04 (2015), p. 064. DOI: 10.1007/JHEP04(2015)064. arXiv: 1501.03038 [hep-ex].

[74] Roel Aaij et al. "Angular analysis of the rare decay $B_s^0 \to \phi\mu^+\mu^-$". July 2021. arXiv: 2107.13428 [hep-ex].

[75] Roel Aaij et al. "Branching fraction measurements of the rare $B_s^0 \to \phi\mu^+\mu^-$ and $B_s^0 \to f_2'(1525)\mu^+\mu^-$ decays". May 2021. arXiv: 2105.14007 [hep-ex].

[76] Roel Aaij et al. "Angular analysis and differential branching fraction of the decay $B_s^0 \to \phi\mu^+\mu^-$". In: *JHEP* 09 (2015), p. 179. DOI: 10.1007/JHEP09(2015)179. arXiv: 1506.08777 [hep-ex].

[77] Roel Aaij et al. "Angular moments of the decay $\Lambda_b^0 \to \Lambda\mu^+\mu^-$ at low hadronic recoil". In: *JHEP* 09 (2018), p. 146. DOI: 10.1007/JHEP09(2018)146. arXiv: 1808.00264 [hep-ex].

[78] Thomas Blake, Stefan Meinel, and Danny van Dyk. "Bayesian Analysis of $b \to s\mu^+\mu^-$ Wilson Coefficients using the Full Angular Distribution of $\Lambda_b \to \Lambda(\to p\,\pi^-)\mu^+\mu^-$ Decays". In: *Phys. Rev. D* 101.3 (2020), p. 035023. DOI: 10.1103/PhysRevD.101.035023. arXiv: 1912.05811 [hep-ph].

[79] S. Jäger and J. Martin Camalich. "On $B \to V\ell\ell$ at small dilepton invariant mass, power corrections, and new physics". In: *JHEP* 05 (2013), p. 043. DOI: 10.1007/JHEP05(2013)043. arXiv: 1212.2263 [hep-ph].

[80] Sebastian Jäger and Jorge Martin Camalich. "Reassessing the discovery potential of the $B \to K^*\ell^+\ell^-$ decays in the large-recoil region: SM challenges and BSM opportunities". In: *Phys. Rev.* D93.1 (2016), p. 014028. DOI: 10.1103/PhysRevD.93.014028. arXiv: 1412.3183 [hep-ph].

[81] Marco Ciuchini et al. "$B \to K^*\ell^+\ell^-$ decays at large recoil in the Standard Model: a theoretical reappraisal". In: *JHEP* 06 (2016), p. 116. DOI: 10.1007/JHEP06(2016)116. arXiv: 1512.07157 [hep-ph].

[82] Patricia Ball and Roman Zwicky. "$B_{d,s} \to \rho, \omega, K^*, \phi$ decay form-factors from light-cone sum rules revisited". In: *Phys. Rev. D* 71 (2005), p. 014029. DOI: 10.1103/PhysRevD.71.014029. arXiv: hep-ph/0412079.

[83] A. Khodjamirian, Th. Mannel, and Y. M. Wang. "$B \to K\ell^+\ell^-$ decay at large hadronic recoil". In: *JHEP* 02 (2013), p. 010. DOI: 10.1007/JHEP02(2013)010. arXiv: 1211.0234 [hep-ph].

[84] Nico Gubernari, Danny Van Dyk, and Javier Virto. "Non-local matrix elements in $B_{(s)} \to \{K^{(*)}, \phi\}\ell^+\ell^-$". In: *JHEP* 02 (2021), p. 088. DOI: 10.1007/JHEP02(2021)088. arXiv: 2011.09813 [hep-ph].

[85] Ronald R. Horgan et al. "Lattice QCD calculation of form factors describing the rare decays $B \to K^*\ell^+\ell^-$ and $B_s \to \phi\ell^+\ell^-$". In: *Phys. Rev. D* 89.9 (2014), p. 094501. DOI: 10.1103/PhysRevD.89.094501. arXiv: 1310.3722 [hep-lat].

[86] Benjamin Grinstein and Dan Pirjol. "Subleading corrections to the |V(ub)| determination from exclusive B decays". In: *Phys. Lett. B* 549 (2002), pp. 314–320. DOI: 10.1016/S0370-2693(02)02929-5. arXiv: hep-ph/0209211.

[87] Christoph Bobeth, Gudrun Hiller, and Danny van Dyk. "The Benefits of $\bar{B} -> \bar{K}^* l^+ l^-$ Decays at Low Recoil". In: *JHEP* 07 (2010), p. 098. DOI: 10.1007/JHEP07(2010)098. arXiv: 1006.5013 [hep-ph].

[88] M. Beylich, G. Buchalla, and T. Feldmann. "Theory of $B \to K^{(*)}\ell^+\ell^-$ decays at high q^2: OPE and quark-hadron duality". In: *Eur. Phys. J. C* 71 (2011), p. 1635. DOI: 10.1140/epjc/s10052-011-1635-0. arXiv: 1101.5118 [hep-ph].

[89] Christoph Bobeth, Gudrun Hiller, and Danny van Dyk. "General analysis of $\bar{B} \to \bar{K}^{(*)}\ell^+\ell^-$ decays at low recoil". In: *Phys. Rev. D* 87.3 (2013), p. 034016. DOI: 10.1103/PhysRevD.87.034016. arXiv: 1212.2321 [hep-ph].

[90] Marco Ciuchini et al. "New Physics without bias: Charming Penguins and Lepton Universality Violation in $b \to s\ell^+\ell^-$ decays". In: (Oct. 2021). arXiv: 2110.10126 [hep-ph].

[91] Hans Dembinski and Piti Ongmongkolkul et al. "scikit-hep/iminuit". In: (2020). DOI: 10.5281/zenodo.3949207. URL: https://doi.org/10.5281/zenodo.3949207.

[92] J. Bhom et al. "A model-independent analysis of $b \to s\mu^+\mu^-$ transitions with GAMBIT's FlavBit". In: (June 2020). arXiv: 2006.03489 [hep-ph].

[93] S. S. Wilks. "The Large-Sample Distribution of the Likelihood Ratio for Testing Composite Hypotheses". In: *Annals Math. Statist.* 9.1 (1938), pp. 60–62. DOI: 10.1214/aoms/1177732360.

[94] Gino Isidori et al. "On the significance of new physics in b→sℓ+ℓ− decays". In: *Phys. Lett. B* 822 (2021), p. 136644. DOI: 10.1016/j.physletb.2021.136644. arXiv: 2104.05631 [hep-ph].

[95] Gino Isidori et al. "A general effective field theory description of $b \to s l^+ l^-$ lepton universality ratios". In: (Oct. 2021). arXiv: 2110.09882 [hep-ph].

[96] Tobias Hurth et al. "New global fits to $b \to s$ data with all relevant parameters". In: *Nucl. Part. Phys. Proc.* 303-305 (2018). Ed. by Giulia Ricciardi et al., pp. 2–7. DOI: 10.1016/j.nuclphysbps.2019.03.002. arXiv: 1812.07602 [hep-ph].

[97] Marcel Algueró et al. "What R_K and Q_5 can tell us about New Physics in $b \to s\ell\ell$ transitions?" In: *JHEP* 07 (2019), p. 096. DOI: 10.1007/JHEP07(2019)096. arXiv: 1902.04900 [hep-ph].

[98] Andreas Crivellin, Dario Müller, and Christoph Wiegand. "$b \to s\ell^+\ell^-$ transitions in two-Higgs-doublet models". In: *JHEP* 06 (2019), p. 119. DOI: 10.1007/JHEP06(2019)119. arXiv: 1903.10440 [hep-ph].

[99] Christoph Bobeth et al. "Patterns of Flavour Violation in Models with Vector-Like Quarks". In: *JHEP* 04 (2017), p. 079. DOI: 10.1007/JHEP04(2017)079. arXiv: 1609.04783 [hep-ph].

[100] Yasmine Sara Amhis et al. "Averages of b-hadron, c-hadron, and τ-lepton properties as of 2018". In: *Eur. Phys. J. C* 81.3 (2021), p. 226. DOI: 10.1140/epjc/s10052-020-8156-7. arXiv: 1909.12524 [hep-ex].

[101] B. Grzadkowski et al. "Dimension-Six Terms in the Standard Model Lagrangian". In: *JHEP* 10 (2010), p. 085. DOI: 10.1007/JHEP10(2010)085. arXiv: 1008.4884 [hep-ph].

[102] Bernat Capdevila et al. "Searching for New Physics with $b \to s\tau^+\tau^-$ processes". In: *Phys. Rev. Lett.* 120.18 (2018), p. 181802. DOI: 10.1103/PhysRevLett.120.181802. arXiv: 1712.01919 [hep-ph].

[103] Andreas Crivellin et al. "Importance of Loop Effects in Explaining the Accumulated Evidence for New Physics in B Decays with a Vector Leptoquark". In: *Phys. Rev. Lett.* 122.1 (2019), p. 011805. DOI: 10.1103/PhysRevLett.122.011805. arXiv: 1807.02068 [hep-ph].

[104] Sébastien Descotes-Genon, Alexander Khodjamirian, and Javier Virto. "Light-cone sum rules for $B \to K\pi$ form factors and applications to rare decays". In: *JHEP* 12 (2019), p. 083. DOI: 10.1007/JHEP12(2019)083. arXiv: 1908.02267 [hep-ph].

[105] T. Abe et al. "Belle II Technical Design Report". Nov. 2010. arXiv: 1011.0352 [physics.ins-det].

[106] S. Descotes-Genon and Martín Novoa-Brunet. "Angular analysis of the rare decay $\Lambda_b \to \Lambda(1520)(\to NK)\ell^+\ell^-$". In: *JHEP* 06 (2019). [Erratum: JHEP 06, 102 (2020)], p. 136. DOI: 10.1007/JHEP06(2019)136. arXiv: 1903.00448 [hep-ph].

[107] Sébastien Descotes-Genon, Martín Novoa-Brunet, and K. Keri Vos. "The time-dependent angular analysis of $B_d \to K_S\ell\ell$, a new benchmark for new physics". In: *JHEP* 02 (2021), p. 129. DOI: 10.1007/JHEP02(2021)129. arXiv: 2008.08000 [hep-ph].

[108] Marcel Algueró et al. "A complete description of P- and S-wave contributions to the $B^0 \to K^+\pi^-\ell^+\ell^-$ decay". In: (July 2021). arXiv: 2107.05301 [hep-ph].

[109] Roel Aaij et al. "Measurements of the S-wave fraction in $B^0 \to K^+\pi^-\mu^+\mu^-$ decays and the $B^0 \to K^*(892)^0\mu^+\mu^-$ differential branching fraction". In: *JHEP* 11 (2016). [Erratum: JHEP 04, 142 (2017)], p. 047. DOI: 10.1007/JHEP11(2016)047. arXiv: 1606.04731 [hep-ex].

[110] Roel Aaij et al. "Measurement of CP-Averaged Observables in the $B^0 \to K^{*0}\mu^+\mu^-$ Decay". In: *Phys. Rev. Lett.* 125.1 (2020), p. 011802. DOI: 10.1103/PhysRevLett.125.011802. arXiv: 2003.04831 [hep-ex].

[111] Damir Becirevic and Andrey Tayduganov. "Impact of $B \to K_0^* \ell^+ \ell^-$ on the New Physics search in $B \to K^* \ell^+ \ell^-$ decay". In: *Nucl. Phys. B* 868 (2013), pp. 368–382. DOI: 10.1016/j.nuclphysb.2012.11.016. arXiv: 1207.4004 [hep-ph].

[112] Joaquim Matias. "On the S-wave pollution of $B \to K^* \ell^+ \ell^-$ observables". In: *Phys. Rev. D* 86 (2012), p. 094024. DOI: 10.1103/PhysRevD.86.094024. arXiv: 1209.1525 [hep-ph].

[113] Diganta Das et al. "The $\bar{B} \to \bar{K} \pi \ell\ell$ and $\bar{B}_s \to \bar{K} K \ell\ell$ distributions at low hadronic recoil". In: *JHEP* 09 (2014), p. 109. DOI: 10.1007/JHEP09(2014)109. arXiv: 1406.6681 [hep-ph].

[114] Diganta Das, Gudrun Hiller, and Martin Jung. "$B \to K \pi \ell\ell$ in and outside the K^* window". In: (June 2015). arXiv: 1506.06699 [hep-ph].

[115] Thomas Blake, Ulrik Egede, and Alex Shires. "The effect of S-wave interference on the $B^0 \to K^{*0} \ell^+ \ell^-$ angular observables". In: *JHEP* 03 (2013), p. 027. DOI: 10.1007/JHEP03(2013)027. arXiv: 1210.5279 [hep-ph].

[116] Ulf-G. Meißner and Wei Wang. "Generalized Heavy-to-Light Form Factors in Light-Cone Sum Rules". In: *Phys. Lett. B* 730 (2014), pp. 336–341. DOI: 10.1016/j.physletb.2014.02.009. arXiv: 1312.3087 [hep-ph].

[117] Ulf-G. Meißner and Wei Wang. "$\mathbf{B_s \to K^{(*)} \ell \bar{\nu}}$, Angular Analysis, S-wave Contributions and $|\mathbf{V_{ub}}|$". In: *JHEP* 01 (2014), p. 107. DOI: 10.1007/JHEP01(2014)107. arXiv: 1311.5420 [hep-ph].

[118] Yu-Ji Shi and Wei Wang. "Chiral Dynamics and S-wave contributions in Semileptonic D_s/B_s decays into $\pi^+\pi^-$". In: *Phys. Rev. D* 92.7 (2015), p. 074038. DOI: 10.1103/PhysRevD.92.074038. arXiv: 1507.07692 [hep-ph].

[119] D. Aston et al. "A study of $K^-\pi^+$ scattering in the reaction $K^-p \to K^-\pi^+n$ at 11 GeV/c". In: *Nuclear Physics B* 296.3 (1988), pp. 493–526. ISSN: 0550-3213. DOI: https://doi.org/10.1016/0550-3213(88)90028-4. URL: https://www.sciencedirect.com/science/article/pii/0550321388900284.

[120] Zhou Rui and Wen-Fei Wang. "S-wave $K\pi$ contributions to the hadronic charmonium B decays in the perturbative QCD approach". In: *Phys. Rev. D* 97.3 (2018), p. 033006. DOI: 10.1103/PhysRevD.97.033006. arXiv: 1711.08959 [hep-ph].

[121] Cai-Dian Lu and Wei Wang. "Analysis of $B \to K_J^*(\to K\pi)\mu^+\mu^-$ in the higher kaon resonance region". In: *Phys. Rev. D* 85 (2012), p. 034014. DOI: 10.1103/PhysRevD.85.034014. arXiv: 1111.1513 [hep-ph].

[122] Lars Hofer and Joaquim Matias. "Exploiting the symmetries of P and S wave for $B \to K^*\mu^+\mu^-$". In: *JHEP* 09 (2015), p. 104. DOI: 10.1007/JHEP09(2015)104. arXiv: 1502.00920 [hep-ph].

[123] Robert Fleischer, Ruben Jaarsma, and Gilberto Tetlalmatzi-Xolocotzi. "In Pursuit of New Physics with $B^0_{s,d} \to \ell^+\ell^-$". In: *JHEP* 05 (2017), p. 156. DOI: 10.1007/JHEP05(2017)156. arXiv: 1703.10160 [hep-ph].

[124] Marcel Algueró et al. "Symmetries in $B \to D^* \ell \nu$ angular observables". In: *JHEP* 06 (2020), p. 156. DOI: 10.1007/JHEP06(2020)156. arXiv: 2003.02533 [hep-ph].

[125] Joaquim Matias and Nicola Serra. "Symmetry relations between angular observables in $B^0 \to K^*\mu^+\mu^-$ and the LHCb P_5' anomaly". In: *Phys. Rev. D* 90.3 (2014), p. 034002. DOI: 10.1103/PhysRevD.90.034002. arXiv: 1402.6855 [hep-ph].

[126] *Framework TDR for the LHCb Upgrade: Technical Design Report*. Tech. rep. CERN-LHCC-2012-007. Geneva: CERN, 2012.

[127] "Physics case for an LHCb Upgrade II — Opportunities in flavour physics, and beyond, in the HL-LHC era". In: CERN-LHCC-2018-027 LHCb-PUB-2018-009 (2018). arXiv: 1808.08865 [hep-ex].

[128] Aoife Bharucha, David M. Straub, and Roman Zwicky. "$B \to V\ell^+\ell^-$ in the Standard Model from light-cone sum rules". In: *JHEP* 08 (2016), p. 098. DOI: 10.1007/JHEP08(2016)098. arXiv: 1503.05534 [hep-ph].

[129] J. P. Lees et al. "Evidence for an excess of $\bar{B} \to D^{(*)}\tau^-\bar{\nu}_\tau$ decays". In: *Phys. Rev. Lett.* 109 (2012), p. 101802. DOI: 10.1103/PhysRevLett.109.101802. arXiv: 1205.5442 [hep-ex].

[130] J. P. Lees et al. "Measurement of an Excess of $\bar{B} \to D^{(*)}\tau^-\bar{\nu}_\tau$ Decays and Implications for Charged Higgs Bosons". In: *Phys. Rev. D* 88.7 (2013), p. 072012. DOI: 10.1103/PhysRevD.88.072012. arXiv: 1303.0571 [hep-ex].

[131] M. Huschle et al. "Measurement of the branching ratio of $\bar{B} \to D^{(*)}\tau^-\bar{\nu}_\tau$ relative to $\bar{B} \to D^{(*)}\ell^-\bar{\nu}_\ell$ decays with hadronic tagging at Belle". In: *Phys. Rev. D* 92.7 (2015), p. 072014. DOI: 10.1103/PhysRevD.92.072014. arXiv: 1507.03233 [hep-ex].

[132] Roel Aaij et al. "Measurement of the ratio of branching fractions $\mathcal{B}(\bar{B}^0 \to D^{*+}\tau^-\bar{\nu}_\tau)/\mathcal{B}(\bar{B}^0 \to D^{*+}\mu^-\bar{\nu}_\mu)$". In: *Phys. Rev. Lett.* 115.11 (2015). [Erratum: Phys.Rev.Lett. 115, 159901 (2015)], p. 111803. DOI: 10.1103/PhysRevLett.115.111803. arXiv: 1506.08614 [hep-ex].

[133] R. Aaij et al. "Measurement of the ratio of the $B^0 \to D^{*-}\tau^+\nu_\tau$ and $B^0 \to D^{*-}\mu^+\nu_\mu$ branching fractions using three-prong τ-lepton decays". In: *Phys. Rev. Lett.* 120.17 (2018), p. 171802. DOI: 10.1103/PhysRevLett.120.171802. arXiv: 1708.08856 [hep-ex].

[134] A. Abdesselam et al. "Measurement of $\mathcal{R}(D)$ and $\mathcal{R}(D^*)$ with a semileptonic tagging method". In: (Apr. 2019). arXiv: 1904.08794 [hep-ex].

[135] Yasmine Sara Amhis et al. "Averages of b-hadron, c-hadron, and τ-lepton properties as of 2018". In: *Eur. Phys. J. C* 81.3 (2021), p. 226. DOI: 10.1140/epjc/s10052-020-8156-7. arXiv: 1909.12524 [hep-ex].

[136] A. Abdesselam et al. "Measurement of the D^{*-} polarization in the decay $B^0 \to D^{*-}\tau^+\nu_\tau$". In: *10th International Workshop on the CKM Unitarity Triangle*. Mar. 2019. arXiv: 1903.03102 [hep-ex].

[137] S. Hirose et al. "Measurement of the τ lepton polarization and $R(D^*)$ in the decay $\bar{B} \to D^*\tau^-\bar{\nu}_\tau$". In: *Phys. Rev. Lett.* 118.21 (2017), p. 211801. DOI: 10.1103/PhysRevLett.118.211801. arXiv: 1612.00529 [hep-ex].

[138] S. Hirose et al. "Measurement of the τ lepton polarization and $R(D^*)$ in the decay $\bar{B} \to D^*\tau^-\bar{\nu}_\tau$ with one-prong hadronic τ decays at Belle". In: *Phys. Rev. D* 97.1 (2018), p. 012004. DOI: 10.1103/PhysRevD.97.012004. arXiv: 1709.00129 [hep-ex].

[139] Monika Blanke et al. "Impact of polarization observables and $B_c \to \tau\nu$ on new physics explanations of the $b \to c\tau\nu$ anomaly". In: *Phys. Rev. D* 99.7 (2019), p. 075006. DOI: 10.1103/PhysRevD.99.075006. arXiv: 1811.09603 [hep-ph].

[140] Monika Blanke et al. "Addendum to "Impact of polarization observables and $B_c \to \tau\nu$ on new physics explanations of the $b \to c\tau\nu$ anomaly"". In: (May 2019). [Addendum: Phys.Rev.D 100, 035035 (2019)]. DOI: 10.1103/PhysRevD.100.035035. arXiv: 1905.08253 [hep-ph].

[141] Damir Bečirević et al. "Lepton Flavor Universality tests through angular observables of $\overline{B} \to D^{(*)}\ell\overline{\nu}$ decay modes". In: (July 2019). arXiv: 1907.02257 [hep-ph].

[142] Clara Murgui et al. "Global fit to $b \to c\tau\nu$ transitions". In: *JHEP* 09 (2019), p. 103. DOI: 10.1007/JHEP09(2019)103. arXiv: 1904.09311 [hep-ph].

[143] Pouya Asadi and David Shih. "Maximizing the Impact of New Physics in $b \to c\tau\nu$ Anomalies". In: *Phys. Rev. D* 100.11 (2019), p. 115013. DOI: 10.1103/PhysRevD.100.115013. arXiv: 1905.03311 [hep-ph].

[144] Rui-Xiang Shi et al. "Revisiting the new-physics interpretation of the $b \to c\tau\nu$ data". In: *JHEP* 12 (2019), p. 065. DOI: 10.1007/JHEP12(2019)065. arXiv: 1905.08498 [hep-ph].

[145] P. Colangelo, F. De Fazio, and F. Loparco. "Probing New Physics with $\bar{B} \to \rho(770)\,\ell^-\bar{\nu}_\ell$ and $\bar{B} \to a_1(1260)\,\ell^-\bar{\nu}_\ell$". In: *Phys. Rev. D* 100.7 (2019), p. 075037. DOI: 10.1103/PhysRevD.100.075037. arXiv: 1906.07068 [hep-ph].

[146] "Measurement of the P_1 and P_5' angular parameters of the decay $B^0 \to K^{*0}\mu^+\mu^-$ in proton-proton collisions at $\sqrt{s} = 8$ TeV". In: (2017).

[147] Pietro Biancofiore, Pietro Colangelo, and Fulvia De Fazio. "On the anomalous enhancement observed in $B \to D^{(*)}\tau\bar{\nu}_\tau$ decays". In: *Phys. Rev. D* 87.7 (2013), p. 074010. DOI: 10.1103/PhysRevD.87.074010. arXiv: 1302.1042 [hep-ph].

[148] Murugeswaran Duraisamy and Alakabha Datta. "The Full $B \to D^*\tau^-\bar{\nu}_\tau$ Angular Distribution and CP violating Triple Products". In: *JHEP* 09 (2013), p. 059. DOI: 10.1007/JHEP09(2013)059. arXiv: 1302.7031 [hep-ph].

[149] Murugeswaran Duraisamy, Preet Sharma, and Alakabha Datta. "Azimuthal $B \to D^*\tau^-\bar{\nu}_\tau$ angular distribution with tensor operators". In: *Phys. Rev. D* 90.7 (2014), p. 074013. DOI: 10.1103/PhysRevD.90.074013. arXiv: 1405.3719 [hep-ph].

[150] Damir Becirevic et al. "Angular distributions of $\bar{B} \to D^{(*)}\ell\bar{\nu}_\ell$ decays and search of New Physics". In: *Nucl. Phys. B* 946 (2019), p. 114707. DOI: 10.1016/j.nuclphysb.2019.114707. arXiv: 1602.03030 [hep-ph].

[151] Rodrigo Alonso, Andrew Kobach, and Jorge Martin Camalich. "New physics in the kinematic distributions of $\bar{B} \to D^{(*)}\tau^-(\to \ell^-\bar{\nu}_\ell\nu_\tau)\bar{\nu}_\tau$". In: *Phys. Rev. D* 94.9 (2016), p. 094021. DOI: 10.1103/PhysRevD.94.094021. arXiv: 1602.07671 [hep-ph].

[152] Zoltan Ligeti, Michele Papucci, and Dean J. Robinson. "New Physics in the Visible Final States of $B \to D^{(*)}\tau\nu$". In: *JHEP* 01 (2017), p. 083. DOI: 10.1007/JHEP01(2017)083. arXiv: 1610.02045 [hep-ph].

[153] Donal Hill et al. "Model-independent method for measuring the angular coefficients of $B^0 \to D^{*-}\tau^+\nu_\tau$ decays". In: *JHEP* 11 (2019), p. 133. DOI: 10.1007/JHEP11(2019)133. arXiv: 1908.04643 [hep-ph].

[154] Jason Aebischer, Thomas Kuhr, and Kilian Lieret. "Clustering of $\bar{B} \to D^{(*)}\tau^-\bar{\nu}_\tau$ kinematic distributions with ClusterKinG". In: *JHEP* 04 (2020). [Erratum: JHEP 05, 147 (2021)], p. 007. DOI: 10.1007/JHEP04(2020)007. arXiv: 1909.11088 [hep-ph].

[155] Bhubanjyoti Bhattacharya et al. "CP Violation in $\bar{B}^0 \to D^{*+}\mu^-\bar{\nu}_\mu$". In: *JHEP* 05 (2019), p. 191. DOI: 10.1007/JHEP05(2019)191. arXiv: 1903.02567 [hep-ph].

[156] Pietro Colangelo and Fulvia De Fazio. "Scrutinizing $\overline{B} \to D^*\,(D\pi)\,\ell^-\bar{\nu}_\ell$ and $\overline{B} \to D^*\,(D\gamma)\,\ell^-\bar{\nu}_\ell$ in search of new physics footprints". In: *JHEP* 06 (2018), p. 082. DOI: 10.1007/JHEP06(2018)082. arXiv: 1801.10468 [hep-ph].

[157] Sebastien Descotes-Genon et al. "Implications from clean observables for the binned analysis of $B- > K*\mu^+\mu^-$ at large recoil". In: *JHEP* 01 (2013), p. 048. DOI: 10.1007/JHEP01(2013)048. arXiv: 1207.2753 [hep-ph].

[158] Xin-Qiang Li, Ya-Dong Yang, and Xin Zhang. "Revisiting the one leptoquark solution to the R($D^{()}$) anomalies and its phenomenological implications". In: *JHEP* 08 (2016), p. 054. DOI: 10.1007/JHEP08(2016)054. arXiv: 1605.09308 [hep-ph].

[159] Rodrigo Alonso, Benjamín Grinstein, and Jorge Martin Camalich. "Lifetime of B_c^- Constrains Explanations for Anomalies in $B \to D^{(*)}\tau\nu$". In: *Phys. Rev. Lett.* 118.8 (2017), p. 081802. DOI: 10.1103/PhysRevLett.118.081802. arXiv: 1611.06676 [hep-ph].

[160] A. G. Akeroyd and Chuan-Hung Chen. "Constraint on the branching ratio of $B_c \to \tau\bar{\nu}$ from LEP1 and consequences for $R(D^{(*)})$ anomaly". In: *Phys. Rev. D* 96.7 (2017), p. 075011. DOI: 10.1103/PhysRevD.96.075011. arXiv: 1708.04072 [hep-ph].

[161] Admir Greljo, Jorge Martin Camalich, and José David Ruiz-Álvarez. "Mono-τ Signatures at the LHC Constrain Explanations of B-decay Anomalies". In: *Phys. Rev. Lett.* 122.13 (2019), p. 131803. DOI: 10.1103/PhysRevLett.122.131803. arXiv: 1811.07920 [hep-ph].

[162] Damir Bečirević et al. "Scalar leptoquarks from grand unified theories to accommodate the B-physics anomalies". In: *Phys. Rev. D* 98.5 (2018), p. 055003. DOI: 10.1103/PhysRevD.98.055003. arXiv: 1806.05689 [hep-ph].

[163] Minoru Tanaka and Ryoutaro Watanabe. "New physics in the weak interaction of $\bar{B} \to D^{(*)}\tau\bar{\nu}$". In: *Phys. Rev. D* 87.3 (2013), p. 034028. DOI: 10.1103/PhysRevD.87.034028. arXiv: 1212.1878 [hep-ph].

[164] Ulrik Egede, Mitesh Patel, and Konstantinos A. Petridis. "Method for an unbinned measurement of the q^2 dependent decay amplitudes of $\overline{B}^0 \to K^{*0}\mu^+\mu^-$ decays". In: *JHEP* 06 (2015), p. 084. DOI: 10.1007/JHEP06(2015)084. arXiv: 1504.00574 [hep-ph].

[165] Martín González-Alonso, Jorge Martin Camalich, and Kin Mimouni. "Renormalization-group evolution of new physics contributions to (semi)leptonic meson decays". In: *Phys. Lett. B* 772 (2017), pp. 777–785. DOI: 10.1016/j.physletb.2017.07.003. arXiv: 1706.00410 [hep-ph].

[166] Nathan Isgur and Mark B. Wise. "Weak Decays of Heavy Mesons in the Static Quark Approximation". In: *Phys. Lett. B* 232 (1989), pp. 113–117. DOI: 10.1016/0370-2693(89)90566-2.

[167] Nathan Isgur and Mark B. Wise. "WEAK TRANSITION FORM-FACTORS BETWEEN HEAVY MESONS". In: *Phys. Lett. B* 237 (1990), pp. 527–530. DOI: 10.1016/0370-2693(90)91219-2.

[168] Adam F. Falk and Matthias Neubert. "Second order power corrections in the heavy quark effective theory. 1. Formalism and meson form-factors". In: *Phys. Rev. D* 47 (1993), pp. 2965–2981. DOI: 10.1103/PhysRevD.47.2965. arXiv: hep-ph/9209268.

[169] Benjamin Grinstein and Zoltan Ligeti. "Heavy quark symmetry in $_{B\to D(*)l\overline{\nu}}$ spectra". In: *Phys. Lett. B* 526 (2002). [Erratum: Phys.Lett.B 601, 236–237 (2004)], pp. 345–354. DOI: 10.1016/S0370-2693(01)01517-9. arXiv: hep-ph/0111392.

[170] C. Glenn Boyd, Benjamin Grinstein, and Richard F. Lebed. "Model independent extraction of |V(cb)| using dispersion relations". In: *Phys. Lett. B* 353 (1995), pp. 306–312. DOI: 10.1016/0370-2693(95)00480-9. arXiv: hep-ph/9504235.

[171] Irinel Caprini, Laurent Lellouch, and Matthias Neubert. "Dispersive bounds on the shape of anti-B —> D(*) lepton anti-neutrino form-factors". In: *Nucl. Phys. B* 530 (1998), pp. 153–181. DOI: 10.1016/S0550-3213(98)00350-2. arXiv: hep-ph/9712417.

[172] Paolo Gambino, Thomas Mannel, and Nikolai Uraltsev. "B -> D* at zero recoil revisited". In: *Phys. Rev. D* 81 (2010), p. 113002. DOI: 10.1103/PhysRevD.81.113002. arXiv: 1004.2859 [hep-ph].

[173] Paolo Gambino, Thomas Mannel, and Nikolai Uraltsev. "B-> D* Zero-Recoil Formfactor and the Heavy Quark Expansion in QCD: A Systematic Study". In: *JHEP* 10 (2012), p. 169. DOI: 10.1007/JHEP10(2012)169. arXiv: 1206.2296 [hep-ph].

[174] C. Bernard et al. "The $\bar{B} \to D^* \ell \bar{\nu}$ form factor at zero recoil from three-flavor lattice QCD: A Model independent determination of $|V_{cb}|$". In: *Phys. Rev. D* 79 (2009), p. 014506. DOI: 10.1103/PhysRevD.79.014506. arXiv: 0808.2519 [hep-lat].

[175] Jon A. Bailey et al. "Update of $|V_{cb}|$ from the $\bar{B} \to D^* \ell \bar{\nu}$ form factor at zero recoil with three-flavor lattice QCD". In: *Phys. Rev. D* 89.11 (2014), p. 114504. DOI: 10.1103/PhysRevD.89.114504. arXiv: 1403.0635 [hep-lat].

[176] Judd Harrison, Christine Davies, and Matthew Wingate. "$|V_{cb}|$ from the $\bar{B}^0 \to D^{*+} \ell^- \bar{\nu}$ zero-recoil form factor using $2+1+1$ flavour HISQ and NRQCD". In: *PoS* LATTICE2016 (2017), p. 287. DOI: 10.22323/1.256.0287. arXiv: 1612.06716 [hep-lat].

[177] Florian U. Bernlochner et al. "Combined analysis of semileptonic B decays to D and D^*: $R(D^{(*)})$, $|V_{cb}|$, and new physics". In: *Phys. Rev. D* 95.11 (2017). [Erratum: Phys.Rev.D 97, 059902 (2018)], p. 115008. DOI: 10.1103/PhysRevD.95.115008. arXiv: 1703.05330 [hep-ph].

[178] D. Melikhov and B. Stech. "Weak form-factors for heavy meson decays: An Update". In: *Phys. Rev. D* 62 (2000), p. 014006. DOI: 10.1103/PhysRevD.62.014006. arXiv: hep-ph/0001113.

[179] Pouya Asadi, Matthew R. Buckley, and David Shih. "It's all right(-handed neutrinos): a new W model for the $R_{D^{(*)}}$ anomaly". In: *JHEP* 09 (2018), p. 010. DOI: 10.1007/JHEP09(2018)010. arXiv: 1804.04135 [hep-ph].

[180] Admir Greljo et al. "R(D$^{()}$) from W and right-handed neutrinos". In: *JHEP* 09 (2018), p. 169. DOI: 10.1007/JHEP09(2018)169. arXiv: 1804.04642 [hep-ph].

[181] Dean J. Robinson, Bibhushan Shakya, and Jure Zupan. "Right-handed neutrinos and R(D$^{()}$)". In: *JHEP* 02 (2019), p. 119. DOI: 10.1007/JHEP02(2019)119. arXiv: 1807.04753 [hep-ph].

[182] Aleksandr Azatov et al. "Combined explanations of B-physics anomalies: the sterile neutrino solution". In: *JHEP* 10 (2018), p. 092. DOI: 10.1007/JHEP10(2018)092. arXiv: 1807.10745 [hep-ph].

[183] Julian Heeck and Daniele Teresi. "Pati-Salam explanations of the B-meson anomalies". In: *JHEP* 12 (2018), p. 103. DOI: 10.1007/JHEP12(2018)103. arXiv: 1808.07492 [hep-ph].

[184] Pouya Asadi, Matthew R. Buckley, and David Shih. "Asymmetry Observables and the Origin of $R_{D^{(*)}}$ Anomalies". In: *Phys. Rev. D* 99.3 (2019), p. 035015. DOI: 10.1103/PhysRevD.99.035015. arXiv: 1810.06597 [hep-ph].

[185] K. S. Babu, Bhaskar Dutta, and Rabindra N. Mohapatra. "A theory of R(D*, D) anomaly with right-handed currents". In: *JHEP* 01 (2019), p. 168. DOI: 10.1007/JHEP01(2019)168. arXiv: 1811.04496 [hep-ph].

[186] Debjyoti Bardhan and Diptimoy Ghosh. "B -meson charged current anomalies: The post-Moriond 2019 status". In: *Phys. Rev. D* 100.1 (2019), p. 011701. DOI: 10.1103/PhysRevD.100.011701. arXiv: 1904.10432 [hep-ph].

[187] John D. Gómez, Néstor Quintero, and Eduardo Rojas. "Charged current $b \to c\tau\bar{\nu}_\tau$ anomalies in a general W' boson scenario". In: *Phys. Rev. D* 100.9 (2019), p. 093003. DOI: 10.1103/PhysRevD.100.093003. arXiv: 1907.08357 [hep-ph].

[188] Rusa Mandal et al. "The role of right-handed neutrinos in $b \to c\tau\bar{\nu}$ anomalies". In: *JHEP* 08.08 (2020), p. 022. DOI: 10.1007/JHEP08(2020)022. arXiv: 2004.06726 [hep-ph].

[189] Alexander L. Kagan. "Polarization in B —> VV decays". In: *Phys. Lett. B* 601 (2004), pp. 151–163. DOI: 10.1016/j.physletb.2004.09.030. arXiv: hep-ph/0405134.

[190] Martin Beneke, Johannes Rohrer, and Deshan Yang. "Branching fractions, polarisation and asymmetries of B —> VV decays". In: *Nucl. Phys. B* 774 (2007), pp. 64–101. DOI: 10.1016/j.nuclphysb.2007.03.020. arXiv: hep-ph/0612290.

[191] Marcel Algueró et al. "A new B-flavour anomaly in $B_{d,s} \to K^{*0}\bar{K}^{*0}$: anatomy and interpretation". In: *JHEP* 04 (2021), p. 066. DOI: 10.1007/JHEP04(2021)066. arXiv: 2011.07867 [hep-ph].

[192] Gudrun Hiller and Frank Kruger. "More model-independent analysis of $b \to s$ processes". In: *Phys. Rev. D* 69 (2004), p. 074020. DOI: 10.1103/PhysRevD.69.074020. arXiv: hep-ph/0310219.

[193] Sebastien Descotes-Genon, Joaquim Matias, and Javier Virto. "An analysis of $B_{d,s}$ mixing angles in presence of New Physics and an update of $B_s \to \bar{K}^{0*}anti - K^{0*}$". In: *Phys. Rev. D* 85 (2012), p. 034010. DOI: 10.1103/PhysRevD.85.034010. arXiv: 1111.4882 [hep-ph].

[194] Sebastien Descotes-Genon, Joaquim Matias, and Javier Virto. "Exploring B(d,s) —> KK decays through flavour symmetries and QCD-factorisation". In: *Phys. Rev. Lett.* 97 (2006), p. 061801. DOI: 10.1103/PhysRevLett.97.061801. arXiv: hep-ph/0603239.

[195] Sebastien Descotes-Genon, Joaquim Matias, and Javier Virto. "Penguin-mediated $B_{d,s} \to VV$ decays and the $B_s - \bar{B}_s$ mixing angle". In: *Phys. Rev. D* 76 (2007). [Erratum: Phys.Rev.D 84, 039901 (2011)], p. 074005. DOI: 10.1103/PhysRevD.76.074005. arXiv: 0705.0477 [hep-ph].

[196] Alexander L. Kagan. "Right-handed currents, CP violation, and B —> VV". In: (July 2004). arXiv: hep-ph/0407076.

[197] M. Beneke et al. "QCD factorization in B —> pi K, pi pi decays and extraction of Wolfenstein parameters". In: *Nucl. Phys. B* 606 (2001), pp. 245–321. DOI: 10.1016/S0550-3213(01)00251-6. arXiv: hep-ph/0104110.

[198] Roel Aaij et al. "Amplitude analysis of the $B^0_{(s)} \to K^{*0}\overline{K}^{*0}$ decays and measurement of the branching fraction of the $B^0 \to K^{*0}\overline{K}^{*0}$ decay". In: *JHEP* 07 (2019), p. 032. DOI: 10.1007/JHEP07(2019)032. arXiv: 1905.06662 [hep-ex].

[199] Bernard Aubert et al. "Observation of $B^0 \to$ K*0 $\bar{K}$* 0 and search for $B^0 \to$ K*0 K*0". In: *Phys. Rev. Lett.* 100 (2008), p. 081801. DOI: 10.1103/PhysRevLett.100.081801. arXiv: 0708.2248 [hep-ex].

[200] Roel Aaij et al. "First measurement of the CP-violating phase $\phi_s^{d\bar{d}}$ in $B_s^0 \to (K^+\pi^-)(K^-\pi^+)$ decays". In: *JHEP* 03 (2018), p. 140. DOI: 10.1007/JHEP03(2018)140. arXiv: 1712.08683 [hep-ex].

[201] Kristof De Bruyn et al. "Branching Ratio Measurements of B_s Decays". In: *Phys. Rev. D* 86 (2012), p. 014027. DOI: 10.1103/PhysRevD.86.014027. arXiv: 1204.1735 [hep-ph].

[202] J. Charles et al. "CP violation and the CKM matrix: Assessing the impact of the asymmetric B factories". In: *Eur.Phys.J.* C41 (2005). updated results and plots available at: http://ckmfitter.in2p3.fr, pp. 1–131. DOI: 10.1140/epjc/s2005-02169-1. arXiv: hep-ph/0406184 [hep-ph].

[203] Jérôme Charles et al. "Modeling theoretical uncertainties in phenomenological analyses for particle physics". In: *Eur. Phys. J. C* 77.4 (2017), p. 214. DOI: 10.1140/epjc/s10052-017-4767-z. arXiv: 1611.04768 [hep-ph].

[204] Sebastien Descotes-Genon and Patrick Koppenburg. "The CKM Parameters". In: *Ann. Rev. Nucl. Part. Sci.* 67 (2017), pp. 97–127. DOI: 10.1146/annurev-nucl-101916-123109. arXiv: 1702.08834 [hep-ex].

[205] Martin Beneke and Matthias Neubert. "QCD factorization for B —> PP and B —> PV decays". In: *Nucl. Phys. B* 675 (2003), pp. 333–415. DOI: 10.1016/j.nuclphysb.2003.09.026. arXiv: hep-ph/0308039.

[206] Yuval Grossman, Matthias Neubert, and Alexander L. Kagan. "Trojan penguins and isospin violation in hadronic B decays". In: *JHEP* 10 (1999), p. 029. DOI: 10.1088/1126-6708/1999/10/029. arXiv: hep-ph/9909297.

[207] Alexander Lenz and Gilberto Tetlalmatzi-Xolocotzi. "Model-independent bounds on new physics effects in non-leptonic tree-level decays of B-mesons". In: *JHEP* 07 (2020), p. 177. DOI: 10.1007/JHEP07(2020)177. arXiv: 1912.07621 [hep-ph].

[208] Albert M Sirunyan et al. "Search for new physics in dijet angular distributions using proton–proton collisions at $\sqrt{s} = 13$ TeV and constraints on dark matter and other models". In: *Eur. Phys. J. C* 78.9 (2018), p. 789. DOI: 10.1140/epjc/s10052-018-6242-x. arXiv: 1803.08030 [hep-ex].

[209] M. Misiak, Abdur Rehman, and Matthias Steinhauser. "Towards $\overline{B} \to X_s\gamma$ at the NNLO in QCD without interpolation in m_c". In: *JHEP* 06 (2020), p. 175. DOI: 10.1007/JHEP06(2020)175. arXiv: 2002.01548 [hep-ph].

[210] Andreas Crivellin and Lorenzo Mercolli. "$B- > X_d\gamma$ and constraints on new physics". In: *Phys. Rev. D* 84 (2011), p. 114005. DOI: 10.1103/PhysRevD.84.114005. arXiv: 1106.5499 [hep-ph].

[211] P.A. Zyla et al. "Review of Particle Physics". In: *PTEP* 2020.8 (2020), p. 083C01. DOI: 10.1093/ptep/ptaa104.

[212] Christoph Greub and Patrick Liniger. "Calculation of next-to-leading QCD corrections to b —> sg". In: *Phys. Rev. D* 63 (2001), p. 054025. DOI: 10.1103/PhysRevD.63.054025. arXiv: hep-ph/0009144.

[213] D. Becirevic et al. "$B_d - \bar{B}_d$ mixing and the $B_d \to J/\psi K_s$ asymmetry in general SUSY models". In: *Nucl. Phys. B* 634 (2002), pp. 105–119. DOI: 10.1016/S0550-3213(02)00291-2. arXiv: hep-ph/0112303.

[214] Marco Ciuchini et al. "Next-to-leading order QCD corrections to Delta F = 2 effective Hamiltonians". In: *Nucl.Phys.* B523 (1998), pp. 501–525. DOI: 10.1016/S0550-3213(98)00161-8. arXiv: hep-ph/9711402 [hep-ph].

[215] Andrzej J. Buras, Mikolaj Misiak, and Jorg Urban. "Two loop QCD anomalous dimensions of flavor changing four quark operators within and beyond the standard model". In: *Nucl.Phys.* B586 (2000), pp. 397–426. DOI: 10.1016/S0550-3213(00)00437-5. arXiv: hep-ph/0005183 [hep-ph].

[216] S. Aoki et al. "FLAG Review 2019: Flavour Lattice Averaging Group (FLAG)". In: *Eur. Phys. J. C* 80.2 (2020), p. 113. DOI: 10.1140/epjc/s10052-019-7354-7. arXiv: 1902.08191 [hep-lat].

[217] M. Bona et al. "Model-independent constraints on $\Delta F = 2$ operators and the scale of new physics". In: *JHEP* 0803 (2008), p. 049. DOI: 10.1088/1126-6708/2008/03/049. arXiv: 0707.0636 [hep-ph].

[218] Jérôme Charles et al. "New physics in B meson mixing: future sensitivity and limitations". In: *Phys. Rev. D* 102.5 (2020), p. 056023. DOI: 10.1103/PhysRevD.102.056023. arXiv: 2006.04824 [hep-ph].

[219] Lorenzo Calibbi et al. "Z' models with less-minimal flavour violation". In: *Phys. Rev.* D101.9 (2020), p. 095003. DOI: 10.1103/PhysRevD.101.095003. arXiv: 1910.00014 [hep-ph].

[220] Albert M Sirunyan et al. "Search for new physics with dijet angular distributions in proton-proton collisions at $\sqrt{s} = 13$ TeV". In: *JHEP* 07 (2017), p. 013. DOI: 10.1007/JHEP07(2017)013. arXiv: 1703.09986 [hep-ex].

[221] Pere Arnan et al. "Generic loop effects of new scalars and fermions in $b \to s\ell^+\ell^-$ and a vector-like 4^{th} generation". In: *JHEP* 06 (2019), p. 118. DOI: 10.1007/JHEP06(2019)118. arXiv: 1904.05890 [hep-ph].

[222] Georges Aad et al. "Search for new non-resonant phenomena in high-mass dilepton final states with the ATLAS detector". In: (June 2020). arXiv: 2006.12946 [hep-ex].

[223] Roberto Contino et al. "Warped/composite phenomenology simplified". In: *JHEP* 05 (2007), p. 074. DOI: 10.1088/1126-6708/2007/05/074. arXiv: hep-ph/0612180.

[224] Kamila Kowalska, Dinesh Kumar, and Enrico Maria Sessolo. "Implications for new physics in $b \to s\mu\mu$ transitions after recent measurements by Belle and LHCb". In: *Eur. Phys. J. C* 79.10 (2019), p. 840. DOI: 10.1140/epjc/s10052-019-7330-2. arXiv: 1903.10932 [hep-ph].

[225] Marco Ciuchini et al. "New Physics in $b \to s\ell^+\ell^-$ confronts new data on Lepton Universality". In: *Eur. Phys. J. C* 79.8 (2019), p. 719. DOI: 10.1140/epjc/s10052-019-7210-9. arXiv: 1903.09632 [hep-ph].

[226] Andreas Crivellin, Dario Müller, and Francesco Saturnino. "Flavor Phenomenology of the Leptoquark Singlet-Triplet Model". In: *JHEP* 06 (2020), p. 020. DOI: 10.1007/JHEP06(2020)020. arXiv: 1912.04224 [hep-ph].

[227] Bernat Capdevila et al. "Explaining $b \to s\ell^+\ell^-$ and the Cabibbo angle anomaly with a vector triplet". In: *Phys. Rev. D* 103.1 (2021), p. 015032. DOI: 10.1103/PhysRevD.103.015032. arXiv: 2005.13542 [hep-ph].

[228] Andreas Crivellin et al. "Combined Explanation of the $Z \to b\bar{b}$ Forward-Backward Asymmetry, the Cabibbo Angle Anomaly, and $\tau \to \mu\nu\nu$ and $b \to s\ell^+\ell^-$ Data". In: *Phys. Rev. Lett.* 127.1 (2021), p. 011801. DOI: 10.1103/PhysRevLett.127.011801. arXiv: 2010.14504 [hep-ph].

[229] Marcel Algueró et al. "Importance of $Z - Z'$ Mixing in $b \to s\ell^+\ell^-$ and the W mass". In: (Jan. 2022). arXiv: 2201.08170 [hep-ph].

[230] Andrzej J. Buras and Jennifer Girrbach. "Left-handed Z' and Z FCNC quark couplings facing new $b \to s\mu^+\mu^-$ data". In: *JHEP* 12 (2013), p. 009. DOI: 10.1007/JHEP12(2013)009. arXiv: 1309.2466 [hep-ph].

[231] Rhorry Gauld, Florian Goertz, and Ulrich Haisch. "On minimal Z' explanations of the $B \to K^*\mu^+\mu^-$ anomaly". In: *Phys. Rev. D* 89 (2014), p. 015005. DOI: 10.1103/PhysRevD.89.015005. arXiv: 1308.1959 [hep-ph].

[232] Rhorry Gauld, Florian Goertz, and Ulrich Haisch. "An explicit Z'-boson explanation of the $B \to K^*\mu^+\mu^-$ anomaly". In: *JHEP* 01 (2014), p. 069. DOI: 10.1007/JHEP01(2014)069. arXiv: 1310.1082 [hep-ph].

[233] Wolfgang Altmannshofer et al. "Quark flavor transitions in $L_\mu - L_\tau$ models". In: *Phys. Rev. D* 89 (2014), p. 095033. DOI: 10.1103/PhysRevD.89.095033. arXiv: 1403.1269 [hep-ph].

[234] Andreas Crivellin, Giancarlo D'Ambrosio, and Julian Heeck. "Explaining $h \to \mu^{\pm}\tau^{\mp}$, $B \to K^*\mu^+\mu^-$ and $B \to K\mu^+\mu^-/B \to Ke^+e^-$ in a two-Higgs-doublet model with gauged $L_\mu - L_\tau$". In: *Phys. Rev. Lett.* 114 (2015), p. 151801. DOI: 10.1103/PhysRevLett.114.151801. arXiv: 1501.00993 [hep-ph].

[235] Andreas Crivellin, Giancarlo D'Ambrosio, and Julian Heeck. "Addressing the LHC flavor anomalies with horizontal gauge symmetries". In: *Phys. Rev. D* 91.7 (2015), p. 075006. DOI: 10.1103/PhysRevD.91.075006. arXiv: 1503.03477 [hep-ph].

[236] Christoph Niehoff, Peter Stangl, and David M. Straub. "Violation of lepton flavour universality in composite Higgs models". In: *Phys. Lett. B* 747 (2015), pp. 182–186. DOI: 10.1016/j.physletb.2015.05.063. arXiv: 1503.03865 [hep-ph].

[237] D. Aristizabal Sierra, Florian Staub, and Avelino Vicente. "Shedding light on the $b \to s$ anomalies with a dark sector". In: *Phys. Rev. D* 92.1 (2015), p. 015001. DOI: 10.1103/PhysRevD.92.015001. arXiv: 1503.06077 [hep-ph].

[238] Adrian Carmona and Florian Goertz. "Lepton Flavor and Nonuniversality from Minimal Composite Higgs Setups". In: *Phys. Rev. Lett.* 116.25 (2016), p. 251801. DOI: 10.1103/PhysRevLett.116.251801. arXiv: 1510.07658 [hep-ph].

[239] Adam Falkowski, Marco Nardecchia, and Robert Ziegler. "Lepton Flavor Non-Universality in B-meson Decays from a U(2) Flavor Model". In: *JHEP* 11 (2015), p. 173. DOI: 10.1007/JHEP11(2015)173. arXiv: 1509.01249 [hep-ph].

[240] Alejandro Celis, Wan-Zhe Feng, and Dieter Lüst. "Stringy explanation of $b \to s\ell^+\ell^-$ anomalies". In: *JHEP* 02 (2016), p. 007. DOI: 10.1007/JHEP02(2016)007. arXiv: 1512.02218 [hep-ph].

[241] Alejandro Celis et al. "Family nonuniversal Z' models with protected flavor-changing interactions". In: *Phys. Rev. D* 92.1 (2015), p. 015007. DOI: 10.1103/PhysRevD.92.015007. arXiv: 1505.03079 [hep-ph].

[242] Andreas Crivellin et al. "Lepton-flavour violating B decays in generic Z' models". In: *Phys. Rev. D* 92.5 (2015), p. 054013. DOI: 10.1103/PhysRevD.92.054013. arXiv: 1504.07928 [hep-ph].

[243] Sofiane M. Boucenna et al. "Non-abelian gauge extensions for B-decay anomalies". In: *Phys. Lett. B* 760 (2016), pp. 214–219. DOI: 10.1016/j.physletb.2016.06.067. arXiv: 1604.03088 [hep-ph].

[244] Wolfgang Altmannshofer, Marcela Carena, and Andreas Crivellin. "$L_\mu - L_\tau$ theory of Higgs flavor violation and $(g-2)_\mu$". In: *Phys. Rev. D* 94.9 (2016), p. 095026. DOI: 10.1103/PhysRevD.94.095026. arXiv: 1604.08221 [hep-ph].

[245] Sofiane M. Boucenna et al. "Phenomenology of an $SU(2) \times SU(2) \times U(1)$ model with lepton-flavour non-universality". In: *JHEP* 12 (2016), p. 059. DOI: 10.1007/JHEP12(2016)059. arXiv: 1608.01349 [hep-ph].

[246] Andreas Crivellin et al. "Lepton Flavor Non-Universality in B decays from Dynamical Yukawas". In: *Phys. Lett. B* 766 (2017), pp. 77–85. DOI: 10.1016/j.physletb.2016.12.057. arXiv: 1611.02703 [hep-ph].

[247] Isabel Garcia Garcia. "LHCb anomalies from a natural perspective". In: *JHEP* 03 (2017), p. 040. DOI: 10.1007/JHEP03(2017)040. arXiv: 1611.03507 [hep-ph].

[248] Gaber Faisel and Jusak Tandean. "Connecting $b \to s\ell\bar{\ell}$ anomalies to enhanced rare nonleptonic $\overline{B}{}^0_s$ decays in Z' model". In: *JHEP* 02 (2018), p. 074. DOI: 10.1007/JHEP02(2018)074. arXiv: 1710.11102 [hep-ph].

[249] Stephen F. King. "Flavourful Z' models for $R_{K^{(*)}}$". In: *JHEP* 08 (2017), p. 019. DOI: 10.1007/JHEP08(2017)019. arXiv: 1706.06100 [hep-ph].

[250] Cheng-Wei Chiang et al. "$R_{K^{(*)}}$ and related $b \to s\ell^+\ell^-$ anomalies in minimal flavor violation framework with Z' boson". In: *Phys. Rev. D* 96.11 (2017), p. 115022. DOI: 10.1103/PhysRevD.96.115022. arXiv: 1706.02696 [hep-ph].

[251] Stefano Di Chiara et al. "Minimal flavor-changing Z' models and muon $g-2$ after the R_{K^*} measurement". In: *Nucl. Phys. B* 923 (2017), pp. 245–257. DOI: 10.1016/j.nuclphysb.2017.08.003. arXiv: 1704.06200 [hep-ph].

[252] P. Ko et al. "LHCb anomaly and B physics in flavored Z' models with flavored Higgs doublets". In: *Phys. Rev. D* 95.11 (2017), p. 115040. DOI: 10.1103/PhysRevD.95.115040. arXiv: 1702.08666 [hep-ph].

[253] Francesco Sannino et al. "Flavor Physics and Flavor Anomalies in Minimal Fundamental Partial Compositeness". In: *Phys. Rev. D* 97.11 (2018), p. 115046. DOI: 10.1103/PhysRevD.97.115046. arXiv: 1712.07646 [hep-ph].

[254] Stuart Raby and Andreas Trautner. "Vectorlike chiral fourth family to explain muon anomalies". In: *Phys. Rev. D* 97.9 (2018), p. 095006. DOI: 10.1103/PhysRevD.97.095006. arXiv: 1712.09360 [hep-ph].

[255] Adam Falkowski et al. "Flavourful Z' portal for vector-like neutrino Dark Matter and $R_{K^{(*)}}$". In: *JHEP* 08 (2018), p. 061. DOI: 10.1007/JHEP08(2018)061. arXiv: 1803.04430 [hep-ph].

[256] Richard H. Benavides et al. "Minimal Z' models for flavor anomalies". In: *J. Phys. G* 47.7 (2020), p. 075003. DOI: 10.1088/1361-6471/ab8d8d. arXiv: 1812.05077 [hep-ph].

[257] P. Maji, P. Nayek, and S. Sahoo. "Implication of family non-universal Z' model to rare exclusive $b \to s(\ell\bar{\ell}, \nu\bar{\nu})$ transitions". In: *PTEP* 2019.3 (2019), 033B06. DOI: 10.1093/ptep/ptz010. arXiv: 1811.03869 [hep-ph].

[258] Shivaramakrishna Singirala, Suchismita Sahoo, and Rukmani Mohanta. "Exploring dark matter, neutrino mass and $R_{K^{(*)},\phi}$ anomalies in $L_\mu - L_\tau$ model". In: *Phys. Rev. D* 99.3 (2019), p. 035042. DOI: 10.1103/PhysRevD.99.035042. arXiv: 1809.03213 [hep-ph].

[259] Diego Guadagnoli, Méril Reboud, and Olcyr Sumensari. "A gauged horizontal $SU(2)$ symmetry and $R_{K^{(*)}}$". In: *JHEP* 11 (2018), p. 163. DOI: 10.1007/JHEP11(2018)163. arXiv: 1807.03285 [hep-ph].

[260] B. C. Allanach and Joe Davighi. "Third family hypercharge model for $R_{K^{(*)}}$ and aspects of the fermion mass problem". In: *JHEP* 12 (2018), p. 075. DOI: 10.1007/JHEP12(2018)075. arXiv: 1809.01158 [hep-ph].

[261] Masaya Kohda, Tanmoy Modak, and Abner Soffer. "Identifying a Z' behind $b \to s\ell\ell$ anomalies at the LHC". In: *Phys. Rev. D* 97.11 (2018), p. 115019. DOI: 10.1103/PhysRevD.97.115019. arXiv: 1803.07492 [hep-ph].

[262] Stephen F. King. "$R_{K^{(*)}}$ and the origin of Yukawa couplings". In: *JHEP* 09 (2018), p. 069. DOI: 10.1007/JHEP09(2018)069. arXiv: 1806.06780 [hep-ph].

[263] Guang Hua Duan et al. "A minimal $U(1)'$ extension of MSSM in light of the B decay anomaly". In: *Phys. Lett. B* 789 (2019), pp. 54–58. DOI: 10.1016/j.physletb.2018.12.005. arXiv: 1808.04116 [hep-ph].

[264] Paulina Rocha-Moran and Avelino Vicente. "Lepton flavor violation in a Z' model for the $b \to s$ anomalies". In: *Phys. Rev. D* 99.3 (2019), p. 035016. DOI: 10.1103/PhysRevD.99.035016. arXiv: 1810.02135 [hep-ph].

[265] Siddharth Dwivedi et al. "Associated Z' production in the flavorful $U(1)$ scenario for $R_{K^{(*)}}$". In: *Eur. Phys. J. C* 80.3 (2020), p. 263. DOI: 10.1140/epjc/s10052-020-7810-4. arXiv: 1908.03031 [hep-ph].

[266] Patrick Foldenauer. "Phenomenology of Extra Abelian Gauge Symmetries". PhD thesis. U. Heidelberg (main), July 2019. DOI: 10.11588/heidok.00026777.

[267] P. Ko, Takaaki Nomura, and Chaehyun Yu. "$b \to s\mu^+\mu^-$ anomalies and related phenomenology in $U(1)_{B_3-x_\mu L_\mu - x_\tau L_\tau}$ flavor gauge models". In: *JHEP* 04 (2019), p. 102. DOI: 10.1007/JHEP04(2019)102. arXiv: 1902.06107 [hep-ph].

[268] B. C. Allanach and Joe Davighi. "Naturalising the third family hypercharge model for neutral current B-anomalies". In: *Eur. Phys. J. C* 79.11 (2019), p. 908. DOI: 10.1140/epjc/s10052-019-7414-z. arXiv: 1905.10327 [hep-ph].

[269] Junichiro Kawamura, Stuart Raby, and Andreas Trautner. "Complete vectorlike fourth family and new $U(1)'$ for muon anomalies". In: *Phys. Rev. D* 100.5 (2019), p. 055030. DOI: 10.1103/PhysRevD.100.055030. arXiv: 1906.11297 [hep-ph].

[270] Wolfgang Altmannshofer, Joe Davighi, and Marco Nardecchia. "Gauging the accidental symmetries of the standard model, and implications for the flavor anomalies". In: *Phys. Rev. D* 101.1 (2020), p. 015004. DOI: 10.1103/PhysRevD.101.015004. arXiv: 1909.02021 [hep-ph].

[271] Lorenzo Calibbi et al. "Z' models with less-minimal flavour violation". In: *Phys. Rev. D* 101.9 (2020), p. 095003. DOI: 10.1103/PhysRevD.101.095003. arXiv: 1910.00014 [hep-ph].

[272] Jason Aebischer et al. "Quark-lepton connections in Z' mediated FCNC processes: gauge anomaly cancellations at work". In: *JHEP* 02 (2020), p. 183. DOI: 10.1007/JHEP02(2020)183. arXiv: 1912.09308 [hep-ph].

[273] Junichiro Kawamura, Stuart Raby, and Andreas Trautner. "Complete vectorlike fourth family with $U(1)'$: A global analysis". In: *Phys. Rev. D* 101.3 (2020), p. 035026. DOI: 10.1103/PhysRevD.101.035026. arXiv: 1911.11075 [hep-ph].

[274] B. C. Allanach. "$U(1)_{B_3-L_2}$ explanation of the neutral current $B-$anomalies". In: *Eur. Phys. J. C* 81.1 (2021). [Erratum: Eur.Phys.J.C 81, 321 (2021)], p. 56. DOI: 10.1140/epjc/s10052-021-08855-w. arXiv: 2009.02197 [hep-ph].

[275] Admir Greljo, Peter Stangl, and Anders Eller Thomsen. "A model of muon anomalies". In: *Phys. Lett. B* 820 (2021), p. 136554. DOI: 10.1016/j.physletb.2021.136554. arXiv: 2103.13991 [hep-ph].

[276] Joe Davighi. "Anomalous Z' bosons for anomalous B decays". In: *JHEP* 08 (2021), p. 101. DOI: 10.1007/JHEP08(2021)101. arXiv: 2105.06918 [hep-ph].

[277] Rigo Bause et al. "B-anomalies from flavorful U(1)$'$ extensions, safely". In: *Eur. Phys. J. C* 82.1 (2022), p. 42. DOI: 10.1140/epjc/s10052-021-09957-1. arXiv: 2109.06201 [hep-ph].

[278] B. C. Allanach, J. Eliel Camargo-Molina, and Joe Davighi. "Global fits of third family hypercharge models to neutral current B-anomalies and electroweak precision observables". In: *Eur. Phys. J. C* 81.8 (2021), p. 721. DOI: 10.1140/epjc/s10052-021-09377-1. arXiv: 2103.12056 [hep-ph].

[279] Mario Fernández Navarro and Stephen F. King. "Fermiophobic Z' model for simultaneously explaining the muon anomalies $R_{K^{(*)}}$ and $(g-2)_\mu$". In: (Sept. 2021). arXiv: 2109.08729 [hep-ph].

[280] P. Ko, Takaaki Nomura, and Hiroshi Okada. "Muon $g-2$, $B \to K^{(*)}\mu^+\mu^-$ anomalies, and leptophilic dark matter in $U(1)_{\mu-\tau}$ gauge symmetry". In: (Oct. 2021). arXiv: 2110.10513 [hep-ph].

[281] B. C. Allanach, J. M. Butterworth, and Tyler Corbett. "Large hadron collider constraints on some simple Z' models for $b \to s\mu^+\mu^-$ anomalies". In: *Eur. Phys. J. C* 81.12 (2021), p. 1126. DOI: 10.1140/epjc/s10052-021-09919-7. arXiv: 2110.13518 [hep-ph].

[282] J. de Blas et al. "Global analysis of electroweak data in the Standard Model". In: (Dec. 2021). arXiv: 2112.07274 [hep-ph].

[283] T. Aaltonen et al. "High-precision measurement of the W boson mass with the CDF II detector". In: *Science* 376.6589 (2022), pp. 170–176. DOI: 10.1126/science.abk1781.

[284] F. del Aguila, J. de Blas, and M. Perez-Victoria. "Electroweak Limits on General New Vector Bosons". In: *JHEP* 09 (2010), p. 033. DOI: 10.1007/JHEP09(2010)033. arXiv: 1005.3998 [hep-ph].

[285] J. de Blas, J. M. Lizana, and M. Perez-Victoria. "Combining searches of Z' and W' bosons". In: *JHEP* 01 (2013), p. 166. DOI: 10.1007/JHEP01(2013)166. arXiv: 1211.2229 [hep-ph].

[286] Andrzej J. Buras and Jennifer Girrbach. "Complete NLO QCD Corrections for Tree Level Delta F = 2 FCNC Processes". In: *JHEP* 03 (2012), p. 052. DOI: 10.1007/JHEP03(2012)052. arXiv: 1201.1302 [hep-ph].

[287] Douglas Bryman et al. "Testing Lepton Flavor Universality with Pion, Kaon, Tau, and Beta Decays". In: (Nov. 2021). arXiv: 2111.05338 [hep-ph].

[288] S. Schael et al. "Electroweak Measurements in Electron-Positron Collisions at W-Boson-Pair Energies at LEP". In: *Phys. Rept.* 532 (2013), pp. 119–244. DOI: 10.1016/j.physrep.2013.07.004. arXiv: 1302.3415 [hep-ex].

[289] S. Schael et al. "Precision electroweak measurements on the Z resonance". In: *Phys. Rept.* 427 (2006), pp. 257–454. DOI: 10.1016/j.physrep.2005.12.006. arXiv: hep-ex/0509008.

[290] Timo Antero Aaltonen et al. "Combination of CDF and D0 W-Boson Mass Measurements". In: *Phys. Rev. D* 88.5 (2013), p. 052018. DOI: 10.1103/PhysRevD.88.052018. arXiv: 1307.7627 [hep-ex].

[291] Morad Aaboud et al. "Measurement of the W-boson mass in pp collisions at $\sqrt{s} = 7$ TeV with the ATLAS detector". In: *Eur. Phys. J. C* 78.2 (2018). [Erratum: Eur.Phys.J.C 78, 898 (2018)], p. 110. DOI: 10.1140/epjc/s10052-017-5475-4. arXiv: 1701.07240 [hep-ex].

[292] Serguei Chatrchyan et al. "Measurement of the weak mixing angle with the Drell-Yan process in proton-proton collisions at the LHC". In: *Phys. Rev. D* 84 (2011), p. 112002. DOI: 10.1103/PhysRevD.84.112002. arXiv: 1110.2682 [hep-ex].

[293] Roel Aaij et al. "Measurement of the forward-backward asymmetry in $Z/\gamma^* \to \mu^+\mu^-$ decays and determination of the effective weak mixing angle". In: *JHEP* 11 (2015), p. 190. DOI: 10.1007/JHEP11(2015)190. arXiv: 1509.07645 [hep-ex].

[294] Peter J. Mohr, David B. Newell, and Barry N. Taylor. "CODATA Recommended Values of the Fundamental Physical Constants: 2014". In: *Rev. Mod. Phys.* 88.3 (2016), p. 035009. DOI: 10.1103/RevModPhys.88.035009. arXiv: 1507.07956 [physics.atom-ph].

[295] Rym Bouchendira et al. "New determination of the fine structure constant and test of the quantum electrodynamics". In: *Phys. Rev. Lett.* 106 (2011), p. 080801. DOI: 10.1103/PhysRevLett.106.080801. arXiv: 1012.3627 [physics.atom-ph].

[296] Richard H. Parker et al. "Measurement of the fine-structure constant as a test of the Standard Model". In: *Science* 360 (2018), p. 191. DOI: 10.1126/science.aap7706. arXiv: 1812.04130 [physics.atom-ph].

[297] J. De Blas et al. "HEPfit: a code for the combination of indirect and direct constraints on high energy physics models". In: *Eur. Phys. J. C* 80.5 (2020), p. 456. DOI: 10.1140/epjc/s10052-020-7904-z. arXiv: 1910.14012 [hep-ph].

[298] Morad Aaboud et al. "Measurement of the Higgs boson mass in the $H \to ZZ^* \to 4\ell$ and $H \to \gamma\gamma$ channels with $\sqrt{s} = 13$ TeV pp collisions using the ATLAS detector". In: *Phys. Lett. B* 784 (2018), pp. 345–366. DOI: 10.1016/j.physletb.2018.07.050. arXiv: 1806.00242 [hep-ex].

[299] Albert M Sirunyan et al. "A measurement of the Higgs boson mass in the diphoton decay channel". In: *Phys. Lett. B* 805 (2020), p. 135425. DOI: 10.1016/j.physletb.2020.135425. arXiv: 2002.06398 [hep-ex].

[300] "Combination of CDF and D0 results on the mass of the top quark using up 9.7 fb^{-1} at the Tevatron". In: (Aug. 2016). arXiv: 1608.01881 [hep-ex].

[301] Morad Aaboud et al. "Measurement of the top quark mass in the $t\bar{t} \to$ lepton+jets channel from $\sqrt{s} = 8$ TeV ATLAS data and combination with previous results". In: *Eur. Phys. J. C* 79.4 (2019), p. 290. DOI: 10.1140/epjc/s10052-019-6757-9. arXiv: 1810.01772 [hep-ex].

[302] Albert M Sirunyan et al. "Measurement of the top quark mass in the all-jets final state at $\sqrt{s} = 13$ TeV and combination with the lepton+jets channel". In: *Eur. Phys. J. C* 79.4 (2019), p. 313. DOI: 10.1140/epjc/s10052-019-6788-2. arXiv: 1812.10534 [hep-ex].

[303] Wolfgang Altmannshofer et al. "Neutrino Trident Production: A Powerful Probe of New Physics with Neutrino Beams". In: *Phys. Rev. Lett.* 113 (2014), p. 091801. DOI: 10.1103/PhysRevLett.113.091801. arXiv: 1406.2332 [hep-ph].

[304] D. Geiregat et al. "First observation of neutrino trident production". In: *Phys. Lett. B* 245 (1990), pp. 271–275. DOI: 10.1016/0370-2693(90)90146-W.

[305] S. R. Mishra et al. "Neutrino tridents and $W - Z$ interference". In: *Phys. Rev. Lett.* 66 (1991), pp. 3117–3120. DOI: 10.1103/PhysRevLett.66.3117.

[306] T. Adams et al. "Neutrino trident production from NuTeV". In: *29th International Conference on High-Energy Physics*. July 1998, pp. 631–634. arXiv: hep-ex/9811012.

[307] Adam Falkowski and Kin Mimouni. "Model independent constraints on four-lepton operators". In: *JHEP* 02 (2016), p. 086. DOI: 10.1007/JHEP02(2016)086. arXiv: 1511.07434 [hep-ph].

[308] Andrzej J. Buras et al. "Global analysis of leptophilic Z' bosons". In: *JHEP* 06 (2021), p. 068. DOI: 10.1007/JHEP06(2021)068. arXiv: 2104.07680 [hep-ph].

[309] X. G. He et al. "New Z' phenomenology". In: *Phys. Rev. D* 43 (1991), pp. 22–24. DOI: 10.1103/PhysRevD.43.R22.

[310] Robert Foot. "New Physics From Electric Charge Quantization?" In: *Mod. Phys. Lett. A* 6 (1991), pp. 527–530. DOI: 10.1142/S0217732391000543.

[311] Xiao-Gang He et al. "Simplest Z-prime model". In: *Phys. Rev. D* 44 (1991), pp. 2118–2132. DOI: 10.1103/PhysRevD.44.2118.

[312] P. A. Zyla et al. "Review of Particle Physics". In: *PTEP* 2020.8 (2020), p. 083C01. DOI: 10.1093/ptep/ptaa104.

[313] Roel Aaij et al. "Measurement of the W boson mass". In: *JHEP* 01 (2022), p. 036. DOI: 10.1007/JHEP01(2022)036. arXiv: 2109.01113 [hep-ex].

[314] J. de Blas et al. "Impact of the recent measurements of the top-quark and W-boson masses on electroweak precision fits". In: (Apr. 2022). arXiv: 2204.04204 [hep-ph].

[315] Reuven Balkin et al. "On the implications of positive W mass shift". In: (Apr. 2022). arXiv: 2204.05992 [hep-ph].

[316] Motoi Endo and Satoshi Mishima. "New physics interpretation of W-boson mass anomaly". In: (Apr. 2022). arXiv: 2204.05965 [hep-ph].

[317] Luca Di Luzio, Ramona Gröber, and Paride Paradisi. "Higgs physics confronts the M_W anomaly". In: (Apr. 2022). arXiv: 2204.05284 [hep-ph].

[318] Jiayin Gu et al. "Speculations on the W-Mass Measurement at CDF". In: (Apr. 2022). arXiv: 2204.05296 [hep-ph].

[319] Yu-Pan Zeng et al. "Extra boson mix with Z boson explaining the mass of W boson". In: (Apr. 2022). arXiv: 2204.09487 [hep-ph].

[320] Mingxuan Du, Zuowei Liu, and Pran Nath. "CDF W mass anomaly in a Stueckelberg extended standard model". In: (Apr. 2022). arXiv: 2204.09024 [hep-ph].

[321] R. Aaij et al. "Differential branching fractions and isospin asymmetries of $B \to K^{(*)}\mu^+\mu^-$ decays". In: *JHEP* 06 (2014), p. 133. DOI: 10.1007/JHEP06(2014)133. arXiv: 1403.8044 [hep-ex].

[322] Roel Aaij et al. "Strong constraints on the $b \to s\gamma$ photon polarisation from $B^0 \to K^{*0}e^+e^-$ decays". In: *JHEP* 12 (2020), p. 081. DOI: 10.1007/JHEP12(2020)081. arXiv: 2010.06011 [hep-ex].

[323] S. Choudhury et al. "Test of lepton flavor universality and search for lepton flavor violation in $B \to K\ell\ell$ decays". In: *JHEP* 03 (2021), p. 105. DOI: 10.1007/JHEP03(2021)105. arXiv: 1908.01848 [hep-ex].

[324] R. Aaij et al. "Test of lepton universality with $B^0 \to K^{*0}\ell^+\ell^-$ decays". In: *JHEP* 08 (2017), p. 055. DOI: 10.1007/JHEP08(2017)055. arXiv: 1705.05802 [hep-ex].

[325] A. Abdesselam et al. "Test of Lepton-Flavor Universality in $B \to K^*\ell^+\ell^-$ Decays at Belle". In: *Phys. Rev. Lett.* 126.16 (2021), p. 161801. DOI: 10.1103/PhysRevLett.126.161801. arXiv: 1904.02440 [hep-ex].

[326] Morad Aaboud et al. "Angular analysis of $B_d^0 \to K^*\mu^+\mu^-$ decays in pp collisions at $\sqrt{s} = 8$ TeV with the ATLAS detector". In: *JHEP* 10 (2018), p. 047. DOI: 10.1007/JHEP10(2018)047. arXiv: 1805.04000 [hep-ex].

[327] Albert M Sirunyan et al. "Measurement of angular parameters from the decay $\mathrm{B}^0 \to \mathrm{K}^{*0}\mu^+\mu^-$ in proton-proton collisions at $\sqrt{s} = 8$ TeV". In: *Phys. Lett. B* 781 (2018), pp. 517–541. DOI: 10.1016/j.physletb.2018.04.030. arXiv: 1710.02846 [hep-ex].

[328] Vardan Khachatryan et al. "Angular analysis of the decay $B^0 \to K^{*0}\mu^+\mu^-$ from pp collisions at $\sqrt{s} = 8$ TeV". In: *Phys. Lett. B* 753 (2016), pp. 424–448. DOI: 10.1016/j.physletb.2015.12.020. arXiv: 1507.08126 [hep-ex].

[329] Albert M Sirunyan et al. "Angular analysis of the decay $\mathrm{B}^+ \to \mathrm{K}^+\mu^+\mu^-$ in proton-proton collisions at $\sqrt{s} = 8$ TeV". In: *Phys. Rev. D* 98.11 (2018), p. 112011. DOI: 10.1103/PhysRevD.98.112011. arXiv: 1806.00636 [hep-ex].

[330] Serguei Chatrchyan et al. "Angular Analysis and Branching Fraction Measurement of the Decay $B^0 \to K^{*0}\mu^+\mu^-$". In: *Phys. Lett. B* 727 (2013), pp. 77–100. DOI: 10.1016/j.physletb.2013.10.017. arXiv: 1308.3409 [hep-ex].

[331] Tobias Huber et al. "Phenomenology of inclusive $\overline{B} \to X_s \ell^+ \ell^-$ for the Belle II era". In: *JHEP* 10 (2020), p. 088. DOI: 10.1007/JHEP10(2020)088. arXiv: 2007.04191 [hep-ph].

[332] J. P. Lees et al. "Measurement of the $B \to X_s l^+ l^-$ branching fraction and search for direct CP violation from a sum of exclusive final states". In: *Phys. Rev. Lett.* 112 (2014), p. 211802. DOI: 10.1103/PhysRevLett.112.211802. arXiv: 1312.5364 [hep-ex].

[333] Alexander Khodjamirian, Rusa Mandal, and Thomas Mannel. "Inverse moment of the B_s-meson distribution amplitude from QCD sum rule". In: *JHEP* 10 (2020), p. 043. DOI: 10.1007/JHEP10(2020)043. arXiv: 2008.03935 [hep-ph].

[334] Patricia Ball and G.W. Jones. "Twist-3 distribution amplitudes of K* and phi mesons". In: *JHEP* 03 (2007), p. 069. DOI: 10.1088/1126-6708/2007/03/069. arXiv: hep-ph/0702100.

[335] C. Allton et al. "Physical Results from 2+1 Flavor Domain Wall QCD and SU(2) Chiral Perturbation Theory". In: *Phys. Rev. D* 78 (2008), p. 114509. DOI: 10.1103/PhysRevD.78.114509. arXiv: 0804.0473 [hep-lat].

[336] Matthaus Bartsch, Gerhard Buchalla, and Christina Kraus. "B —> V(L) V(L) Decays at Next-to-Leading Order in QCD". In: (Oct. 2008). arXiv: 0810.0249 [hep-ph].

[337] Ulrich Haisch and Susanne Westhoff. "Massive Color-Octet Bosons: Bounds on Effects in Top-Quark Pair Production". In: *JHEP* 08 (2011), p. 088. DOI: 10.1007/JHEP08(2011)088. arXiv: 1106.0529 [hep-ph].